DEVELOPING REGIONAL EQUATIONS OF SEDIMENT YIELD ESTIMATION

Manaye Getu Tsige

Vollständiger Abdruck der von der Fakultät für Bauingenieurwesen und Umweltwissenschaften der Universität der Bundeswehr München zur Erlangung des akademischen Grades eines

Doktor-Ingenieurs (Dr.-Ing.)

angenommenen Dissertation.

Gutachter/Gutachterin:

1. Univ.-Prof. Dr.-Ing. Andreas Malcherek
2. Univ.-Prof. Dr. Yilma Seleshi

Die Dissertation wurde am 15.05.2023 bei der Universität der Bundeswehr München eingereicht und durch die Fakultät für Bauingenieurwesen und Umweltwissenschaften am 18.09.2023 angenommen. Die mündliche Prüfung fand am 09.10.2023 statt.

DECLARATION OF AUTHORSHIP

I hereby declare that this PhD dissertation is my original work and has not been presented for a degree in any other University, and all sources of material used for this dissertation have been duly acknowledged.

ACKNOWLEDGMENT

I would like to acknowledge financial support from German Academic Exchange Service: EECBP Home Grown PhD Scholarship Programme, and Universität der Bundeswehr: Scholarship and Support Program for Foreign Students and Doctoral Candidates (STIBET III) Matching Funds Scholarship, and Universität der Bundeswehr.

Then, I would like to thank my supervisor Prof. Dr.-Ing. Andreas Malcherek for the resources, fund-raising, training, brainstorming seminars, comments and suggestions, and guidance that helped me to successfully complete my PhD dissertation. I would like also to thank doctorate committee members Prof. Dr.-Ing. Andreas Malcherek, Prof. Dr. Yilma Seleshi and Prof. Dr.-Ing. Steffen Krause.

My thank also goes to Dr.-Ing. Ivo Baselt for reviewing a part of this dissertation work, and for constructive comments. I also thank Julia Adamski who helped me to draw a three-dimensional figure showing the main variables affecting soil erosion.

Finally, I thank Sebastian Müller, Johanna Schmidt, Alexander Britz, Katrin Mueller, Susanna Nofal, and the laboratory staff for all support that they gave me during my PhD research stays at Universität der Bundeswehr.

CONTENTS

LIST OF FIGURES

LIST OF TABLES

ABSTRACT

Soil erosion and sediment transport are quite complex processes as they depend on physical, biological, mechanical, and chemical processes within a particular catchment. Different soil erosion and sediment transport models have been developed while taking into account site-specific conditions. In Ethiopia, there is no commonly adopted soil erosion and sediment transport model. This may be because of limited land use management and hydro-climatic data. Therefore, it is highly essential to better explain engaged physical processes and means of accounting for site-specific conditions, for soil loss and sediment yield estimation.

The objective of this Ph.D. dissertation is to propose regional equations of sediment yield estimation. The specific tasks of this study include data preparation, review, and analysis; regionalizing and improving the MUSLE; deriving a soil loss equation for sediment yield estimation; improving the accuracy of a model, checking the performance of the original SWAT+ model; modifying the SWAT+ model for sediment yield estimation, and proposing a method for deriving and solving an accurate sediment rating equation.

The main reason behind regionalizing the MUSLE was the effect of the topographic factor of the MUSLE on soil erosion and sediment yield is not clear. Except for the coefficient, soil erodibility, cover, and conservation practice factors of the MUSLE, an individual effect of the exponent and topographic factor of the MUSLE on soil erosion and sediment yield can be seen by applying the model at different watersheds. Therefore, to regionalize the MUSLE we estimate the best exponent and topographic factor of the MUSLE under the hydro-climatic conditions of Ethiopia. For the sake of the evaluation procedure, the main factors of the MUSLE that directly affect the soil erosion process, such as the cover, conservation practice, soil erodibility, and topographic factors, are estimated based on past experiences from the literature and comparative approaches, whereas the parameters that do not directly affect the erosion process or that have no direct physical meaning (i.e., coefficient a and exponent b) are estimated through calibration. The main reason behind improving the MUSLE was our need to change the input data requirement of the MUSLE for the calculation of its runoff factor for possible application in data-scarce areas. Basically, the MUSLE was developed for a small agricultural watershed, where the extent of erosion is from sheet to rill erosion, but we cannot exactly tell whether it considers gully erosion or not. The underlying physical assumption to improve the MUSLE is that the amount of potential energy of runoff is proportional to the shear stress for sediment transport from a slope field and the kinetic energy of the runoff at the bottom of the slope field for gully formation. As the MUSLE or improved MUSLE does not consider sediment deposition, deriving Soil Loss Equations for Sediment Yield Estimation based on the improved MUSLE becomes important to explain sediment transport and deposition processes. To derive the Soil Loss Equations for Sediment Yield Estimation, we mainly considered physical concepts such as shear force, energy, and work done. To modify the SWAT+ model for sediment yield estimation, we replace the best exponent and the best equation of the topographic factor of the MUSLE in the source code, and also we replace the improved MUSLE or the first revised version of the Soil Loss Equation for Sediment Yield Estimation in place of the MUSLE in the source code.

The Soil Loss Equation for Sediment Yield Estimation and its revised versions showed the best performance over the regionalized MUSLE or improved MUSLE. All types of the modified SWAT+ models showed better performance than the original SWAT+ model. This dissertation also presents an iterative approach for deriving and solving an accurate sediment rating equation.

Keywords: USLE, RUSLE, MUSLE, SWAT+ model, potential energy, kinetic energy, work done, shear force, regression equation, sediment rating curve, Ethiopia

Kurzfassung

Bodenerosion und Sedimenttransport sind recht komplexe Prozesse, da sie von physikalischen, biologischen, mechanischen und chemischen Vorgängen in einem bestimmten Einzugsgebiet abhängen. Es wurden verschiedene Modelle für die Bodenerosion und den Sedimenttransport entwickelt, die die standortspezifischen Bedingungen berücksichtigen. In Äthiopien gibt es kein allgemein angewandtes Bodenerosions- und Sedimenttransportmodell. Der Grund dafür könnte in der begrenzten Landnutzung und dem geringen Umfang hydroklimatischer Daten liegen. Daher ist es äußerst wichtig, die beteiligten physikalischen Prozesse besser zu erklären und Mittel zur Berücksichtigung standortspezifischer Bedingungen für die Abschätzung von Bodenverlust und Sedimentabtrag zu finden.

Ziel dieser Dissertation ist es, regionale Gleichungen für die Abschätzung des Sedimentabtrags vorzuschlagen. Zu den spezifischen Aufgaben dieser Studie gehören die Vorbereitung, Überprüfung und Analyse von Daten, die Regionalisierung und Verbesserung von MUSLE, die Ableitung einer Gleichung für den Bodenverlust zur Schätzung der Sedimentmenge, die Verbesserung der Genauigkeit eines Modells, die Überprüfung der Leistung des ursprünglichen SWAT+-Modells, die Modifizierung des SWAT+-Modells zur Schätzung der Sedimentmenge und der Vorschlag einer Methode zur Ableitung und Lösung einer genauen Gleichung zur Sedimentbewertung.

Der Hauptgrund für die Regionalisierung des MUSLE-Modells war, dass die Auswirkung des topografischen Faktors des MUSLE-Modells auf die Bodenerosion und den Sedimentabtrag nicht eindeutig ist. Abgesehen von den Koeffizienten der Bodenerodierbarkeit, Bedeckung und Erhaltungsmaßnahmen des MUSLE-Modells lässt sich bei Anwendung des Modells in verschiedenen Wassereinzugsgebieten eine individuelle Wirkung des Exponenten und des topografischen Faktors des MUSLE-Modells auf die Bodenerosion und den Sedimentabtrag feststellen. Zur Regionalisierung des MUSLE-Modells schätzen wir daher den besten Exponenten und topographischen Faktor des MUSLE-Modells unter den hydroklimatischen Bedingungen Äthiopiens. Für das Bewertungsverfahren werden die wichtigsten Faktoren des MUSLE-Modells, die sich direkt auf den Bodenerosionsprozess auswirken, wie z.B. die Bodenbedeckung, die Schutzmaßnahmen, die Erodierbarkeit des Bodens und die topographischen Faktoren, auf der Grundlage von Erfahrungen aus der Literatur und vergleichenden Ansätzen geschätzt, während die Parameter, die sich nicht direkt auf den Erosionsprozess auswirken oder die keine direkte physikalische Bedeutung haben (d.h. Koeffizient a und Exponent b) durch Kalibrierung ermittelt werden. Der Hauptgrund für die Verbesserung des MUSLE-Modells war die Notwendigkeit, die Anforderungen an die Eingabedaten für die Berechnung des Abflussfaktors des MUSLE-Modells zu ändern, um eine Anwendung in Gebieten mit geringer Datendichte zu ermöglichen. Grundsätzlich wurde das MUSLE-Modell für kleine landwirtschaftliche Einzugsgebiete entwickelt, in dem das Ausmaß der Erosion von der Blatterosion bis zur Rillenerosion reicht, aber wir können nicht genau sagen, ob es die Gullyerosion berücksichtigt oder nicht. Die zugrundeliegende physikalische Annahme zur Verbesserung des MUSLE-Modells ist, dass der Betrag der potenziellen Energie des Abflusses proportional zur Schubspannung für den Sedimenttransport aus einem Hangfeld und zur kinetischen Energie des Abflusses am Boden des Hangfeldes für die Rinnenbildung

ist. Da das MUSLE-Modell bzw. das verbesserte MUSLE-Modell die Sedimentablagerung nicht berücksichtigt, ist die Ableitung von Bodenverlustgleichungen für die Abschätzung des Sedimentabtrags auf der Grundlage des verbesserten MUSLE-Modells wichtig, um Sedimenttransport- und Ablagerungsprozesse zu erklären. Bei der Ableitung der Gleichungen für Bodenverluste zur Schätzung des Sedimentabtrags haben wir hauptsächlich physikalische Konzepte wie Scherkraft, Energie und geleistete Arbeit berücksichtigt. Um das SWAT+-Modell für die Abschätzung des Sedimentabtrags zu modifizieren, ersetzen wir den besten Exponenten und die beste Gleichung des topografischen Faktors des MUSLE-Modells im Quellcode, und wir ersetzen auch die des verbesserten MUSLE-Modells oder die erste überarbeitete Version der Bodenverlustgleichung für die Abschätzung des Sedimentabtrags anstelle des MUSLE-Modells im Quellcode.

Die Bodenverlustgleichung für die Abschätzung des Sedimentabtrags und ihre überarbeiteten Versionen zeigten die beste Leistung gegenüber des regionalisierten MUSLE-Modells oder des verbesserten MUSLE-Modells. Alle Typen der modifizierten SWAT+-Modelle zeigten eine bessere Leistung als das ursprüngliche SWAT+-Modell. In dieser Dissertation wird auch ein iterativer Ansatz zur Ableitung und Lösung einer genauen Sedimentbewertungsgleichung vorgestellt.

ABBREVIATIONS AND ACRONYMS

AGNPS	Agricultural Non-Point Source Pollution model
ANSWERS	Areal Nonpoint Source Watershed Environment Response Simulation
APEX	Agricultural Policy/Environmental eXtender Model
ArcSWAT	ArcGIS-ArcView extension and interface for SWAT model
CREAMS	Chemicals, Runoff, and Erosion from the Agricultural Management Systems
CSLE	Chinese Soil Loss Equation
DEM	Digital Elevation Model
ET	Evapotranspiration
EUROSEM	European Soil Erosion Model
GIS	Geographic Information System
GSSHA	Gridded Surface/Subsurface Hydrologic Analysis
GUEST	Griffith University Erosion System Template
HEC-RAS	Hydrologic Engineering Center-River Analysis system
HRU	Hydrologic response Unit
HSPF	Hydrological Simulation Program-Fortran
IPEAT+	Integrated Parameter Estimation and Uncertainty Analysis Tool Plus
LISEM	LImburg Soil Erosion Model
MAE	Mean absolute error
MIKE SHE	European Hydrological System Model
MIKE-11	One-dimensional river model
M-M-F-SEM	Morgan-Morgan-Finney Soil Erosion Model
MUSLE	Modified Universal Soil Loss Equation
NDVI	Normalized difference Vegetation Index
NSE	Nash-Sutcliffe efficiency
PBIAS	Percentage of bias
PSR	Root mean square to standard deviation ratio
QGIS	Quantum Geographic Information System
QSWAT	QGIS interface for SWAT model
RMSE	Root mean square error
RUSLE	Revised Universal Soil Loss Equation
SCS CN or CN	Soil Conservation Service Curve Number or simply curve number

SOBEK	Hydraulic numerical model
SSE	Sum of square error
SWAT	Soil and Water Assessment Tool
SWAT-HS	SWAT-hillslope model
SWATplus-CUP	Calibration Uncertainty Program for the SWAT+ model
SWAT-VSA	SWAT-Variable-Source-Area model
SWAT-WB	SWAT-Water-Balance model
SWAT-wil	SWAT-with-impermeable layer model
SWRRB	Simulator for Water Resources in Rural Basins
tRIBS-Erosion	Triangulated Irregular Network-based Real-time Integrated Basin Simulator Soil Erosion Model
USLE	Universal Soil Loss Equation
VE	Volume error
WATEM/SEDEM	Water and Tillage Erosion Model and Sediment Delivery Model
WEPP	Water Erosion Prediction Project
R^2	Coefficient of determination

1. INTRODUCTION

1.1 Background

The fate of soil erosion and sediment transport can be seen in different ways. Sediment affects the water quantity and quality in rivers, lakes, and reservoirs (Msadala and Basson, 2017). This is because, quantity issues of sediment dynamics concern morphological aspects along with prevailing hydraulics to affect the aquatic habitats as well as the maintenance of flood control, navigable waterways, and harbors, as well as coastal protection (Noack et al., 2015). In addition, quality issues relate to nutrients and hydrophobic pollutants associated with fine sediments to influence water quality, freshwater ecosystem services, human health, and management options such as dredging or dumping sediments (Noack et al., 2015). Soil erosion and sediment transport can have a negative impact on poverty reduction and sustainable development. For example, it results in crop yield reduction in Sub-Saharan Africa (Tully et al., 2015). If we particularly consider Ethiopia, soil erosion and sediment transport are some of the key problems for the sustainable development of the country. For example, it results in the sedimentation of water supply, irrigation, and hydroelectric power reservoirs. Some of these sediment affected reservoirs are Koka Hydroelectric Power Reservoir (Tadesse and Dai, 2019), Gilgel Gibe 1 Hydroelectric Power Reservoir (Devi et al., 2008), Angereb Water Supply Reservoir (Haregeweyn et al., 2012), Selamko and Shina Irrigation Reservoirs (Moges et al., 2018) and many more (Haregeweyn et al., 2006; Tamene et al., 2006). Furthermore, soil erosion leads to crop production reduction (Hurni et al., 2015), lowers groundwater table (Tilahun et al., 2016), natural lake sedimentation (Aga et al., 2018; Degife et al., 2021; Lemma et al., 2020) and economic loss (Hurni et al., 2015; World Bank Group, 2007) in Ethiopia.

Sediment yield can be determined by direct measurements from reservoir sediment deposit surveys or river-suspended sediment sampling. We can also estimate sediment yield using indirect methods such as statistical or probabilistic, and empirical or physically based models, which take different approaches in modeling the process. For example, shear stress, concentration, stream power, mass, energy, and momentum balance are some physical approaches to modeling sediment yield. Some models which have been used to estimate soil erosion or sediment transport in a catchment are the USLE, RUSLE, MUSLE, SWAT model, AGNPS (Young et al., 1987), HSPF (Donigian et al., 1995), SWRRB (Williams et al., 1985), ANSWERS (Beasley et al., 1980), CREAMS (Knisel, 1980), MIKE SHE (Refsgaard and Storm, 1995), WEPP (Flanagan and Nearing, 1995), GUEST (Hairsine and Rose, 1992a, 1992b; Rose et al., 1983) as cited by Tan et al. (2018), M-M-F-SEM (Morgan and Duzant, 2008), tRIBS-Erosion model (Francipane et al., 2012), Pelletier's model (Pelletier, 2012), Patil's model (Patil et al., 2012), WATEM/SEDEM, EUROSEM (Morgan et al., 1998), LISEM (Ad et al., 1998), GSSHA (Ogden et al., 2003), and APEX. Some models for the study of sediment transport in river channels are the HEC-RAS, MIKE-11, SOBEK, and other Hydromorphodynamic models. The advantage and/or limitations of some above models are discussed by Adu and Kumarasamy (2018); Betrie et al. (2011); Devi et al. (2015); Tan et al. (2018).

The suitability of these and other models for a particular location, and their accuracy level of estimation depend on the limitations of the models and the basic assumptions they follow. In addition, model calibration, and validation depend on observed data quantity and quality.

1.2 Statement of Problems

Most of the tropical countries in the Eastern, Central, and Southern Africa have no appropriate and accurate soil erosion models as reviewed and pointed out by Ndomba (2010). In Ethiopia, there is no commonly adopted soil erosion and sediment transport model (Fenta et al., 2021; Haregeweyn et al., 2017; Tamene et al., 2006). This may be because of limited hydro-climatic and watershed management data.

However, soil erosion, sediment transport, deposition, consolidation, and re-suspension are quite complex processes as they depend on physical, biological, mechanical, and chemical processes within a particular catchment. Thus, the sedimentation processes are affected by weather and hydrological conditions, the temporal and spatial distribution of rainfall, rainfall intensity, hydraulics of flow, topography, density and patterns of land cover, the impact of land use change (Jeloudar et al., 2018), stream network, type and extent of soil conservation and flood protection works, the temporal and spatial variation of soil physical properties, chemical properties, and mineralogical constituents, biological properties and constituents, and soil mechanical properties. Some of these properties and constituents that affect soil erosion and sediment transport are soil texture (Li et al., 2020; Wischmeier and Smith, 1978), soil structure (Wischmeier and Smith, 1978), particle density and volume fraction (Razavian et al., 1997), pore size distribution (Dlapa et al., 2020), viscosity (Lee et al., 2016), bulk density (Jepsen et al., 1997), settling velocity (Jing et al., 2018), consistence (Boekel and Peerlkamp, 1956), permeability (Wischmeier and Smith, 1978), particle size distribution (Razavian et al., 1997), soil moisture (Wei et al., 2007), gravel content (Li et al., 2020), bed roughness (Torri et al., 2012), history of sediment bed formation and consolidation (Sanford, 2008), cohesion (Jain and Kothyari, 2009), soil shear strength (Brunori et al., 1989), compaction (Rousseva et al., 2002), gypsum content (Kuttah and Sato, 2015), calcium carbonate content (Rimmeri and Greenland, 1976), soil salinity (Neave and Rayburg, 2006), organic carbon content (Blanco-Canqui and Benjamin, 2013), soil hydrogen ion concentration (pH) (Matsumoto et al., 2018), cation exchange capacity (Fang et al., 2017), soil base saturation (Kaba£a and £ABAZ, 2018), potassium, nitrogen and phosphorus fertilizers (Belay et al., 2002), organic matter content (Ekwue, 1990), Bioturbation (Gabet et al., 2003), presence of micro-organisms like microphytobenthos (Hope et al., 2020), soil microbial biomass (Powlson et al., 2001), macrofaunal species (Sofo et al., 2020), biofilm formation (Cai et al., 2019), biochar (Jien and Wang, 2013), glomalin (Vaidya et al., 2011), antibiotics in soil (Cyco n et al., 2019), soil management (Stanchi et al., 2021), etc.

Therefore, it is highly essential to better explain engaged physical processes and means of accounting for site-specific conditions, and the best accurate representation of the processes, for soil loss and sediment yield estimation. Therefore, we propose regional equations of sediment yield under constrain of site-specific conditions and the quite complex nature of soil erosion and sediment transport. To propose the equations, we mainly

focus on commonly used soil erosion models such as the USLE, RUSLE, MUSLE, and SWAT model. We also focus on regression techniques to propose a regression method for sediment rating.

1.3 Objective of Studies

1.3.1 General Objective

The general objective of this study is to propose regional equations of sediment yield estimation.

1.3.2 Specific Objectives

The specific objectives of this study are:

1. Data preparation, review, and analysis
2. Regionalizing the MUSLE under the hydro-climatic conditions of Ethiopia
3. Improving the MUSLE by physical interpretation of its factors
4. Deriving soil loss equations for sediment yield estimation
5. Improving the accuracy of a model by modifying its mathematical form
6. Checking the performance of the original SWAT+ model
7. Modifying the SWAT+ model in three different types for sediment yield estimation, and compiling the SWAT+ Editor
8. Proposing a method for deriving and solving an accurate sediment rating equation

2. LITERATURE REVIEW

2.1 Erosion Models

Commonly used soil erosion models are the USLE (Wischmeier and Smith, 1978), RUSLE (Renard et al., 1997) and MUSLE. In connection to these models, similar erosion models are the RUSLE1, RUSLE2 (`http://www.ars.usda.gov/Research/docs.htm?docid=6010` accessed on 20.01.2020) and CSLE (Baoyuan et al., 2002).

2.1.1 The USLE and RUSLE

The USLE is the foundation for others; it is used to estimate the annual soil loss from a field area, where the extent of erosion from sheet to rill erosion. However, it does not consider gully erosion, streambank erosion, streambed erosion, mudflow, massive land movement due to landslides or slumps. In fact, the USLE is an empirical soil loss model, is given by Wischmeier and Smith (1978):

$$A = RKLSCP \tag{2.1}$$

where, where A is soil loss in tons per acre per year, R is the rainfall erosivity factor in hundreds of foot-tons inches per acre per hour, K is the soil erodibility factor (in $0.01 * tons * acre * hour/acre * year * foot * tons * inch$), L is the slope length factor, S is the slope steepness factor or LS is the topographic factor, C is the cover factor, and P is the soil conservation practice factor. The USLE was originally developed at the plot scale (unit plot of 72.6 ft long, with a uniform lengthwise slope of 9 percent, in continuous fallow, tilled up and down the slope (Wischmeier and Smith, 1978). As a consequence of this, the USLE model operates mathematically in two steps; the first step is to predict soil loss from the unit plot (A_1), $A_1 = R * K$ where L, S, C, and P all have values of 1.0, and the second step modifies that value to take account of the conditions that vary from the unit plot; $A_2 = A_1 * L * S * C * P$ (Kinnell, 2019).

An updated form of USLE (RUSLE) was published to include new rainfall erosivity maps for the United States of America and improvements to the method of calculating the different USLE factors (Renard et al., 1997) as cited by Benavidez et al. (2018). The RUSLE added changes in soil erodibility due to freeze–thaw and soil moisture, a method for calculating cover and management factors, changes to how the influence of topography is incorporated into the model, and updated values to represent soil conservation practices (Renard and Freimund, 1994) as cited by Benavidez et al. (2018).

The USLE or RUSLE is widely used with a combined sediment delivery ratio to calculate sediment yield at the outlet of a watershed. It has been observed that the delivery ratios to determine the sediment yield from the USLE can be predicted accurately but varies considerably (Pandey et al., 2009). The sediment delivery ratio varies with storms; the assumption of a constant sediment delivery ratio adds another source of error to the estimates as reviewed and reported by Sadeghi et al. (2014). The reason for this may be due to the variation in rainfall distribution over time, from year to year (Pandey et al., 2009). The USLE is more accurate for soils with medium texture and slopes

of less than 400 ft in length with a gradient ranging between 3% and 18%, and it is managed with consistent cropping practices that are well represented in a plot scale erosion studies (Wischmeier and Smith, 1978). It is also warned that the farther these limits are exceeded, the greater will be the probability of significant extrapolation error (Wischmeier and Smith, 1978). For further reference, other problems connected to the USLE or RUSLE are discussed by Kinnell (2005).

As part of evaluations of the models, some important considerations are the physical explanation behind the models, the physical connection between factors, the suitability of the models toward a specific location, and the experiences of some other authors about the behavior of the models.

Regards to the physical explanation behind the USLE or RUSLE, they depend on rainfall impact energy, and we expect soil detachment due to the rainfall impact. However, the rainfall impact or hammering also contributes to subsoil compaction, and it may reduce subsoil erosion. Yes, of course, we expect soil detachment due to the rainfall impact, however, we can not exactly tell in which direction a soil particle jumps or moves, where it reaches, or where measurement can be taken. Furthermore, the rainfall impact does not tell us how much energy is required to detach soil particles (soil strength or resistance against the rainfall impact energy). If the particle jumping due to the rainfall impact is not considered, it is the combined action of rainfall and runoff that causes soil erosion and sediment transport from a slope field, therefore, it is based on this principle that the amount of soil loss from the field can be measured at the bottom of the slope field. This is because, in the beginning of rain, more soil erosion due to the impact of rainfall and less sediment transport is expected. At the latter time, less soil erosion due to compaction but more sediment transport by runoff is expected. This can be a case particularly in the tropics where heavy rainfall compacts soil, infiltration decreases, runoff dominates quickly, and subsequently, more erosion in the beginning of rain is expected. As we said above the USLE/RUSLE/RUSLE2/CSLE considers the rainfall impact energy for soil detachment but it does not consider energy for sediment transport. The rainfall impact leads to sheet to rill erosion which mainly erodes topsoil. However, runoff concentration leads to gully formation (which erodes subsoil), riverbank erosion, and bedload transport.

Regards to the physical connection between factors, as far as we are talking about the rainfall impact energy for soil detachment; the physical connection between the rainfall erosivity, soil erodibility, topographic, cover, and conservation practice factors of the USLE or RUSLE is not convincing. One evidence for this is that, for instance, the soil cover factor reduces rainfall impact energy but the soil conservation practice factor does not reduce the impact energy of the rainfall.

Regards to the suitability of the models toward specific conditions or locations, in tropical Africa, the USLE and RUSLE are difficult to apply. This may be because unrealistic values were obtained for tropical soils from the equation's erodibility nomograph (Mulengera and Payton, 1999; Ndomba, 2007) as cited by Adegede and Mbajiorgu (2019). It has also been observed that the table that was developed for estimating crop and soil management factors in the USA is inconsistent with farming practices in tropical Africa (Mulengera and Payton, 1999) as cited by Adegede and Mbajiorgu (2019).

Regards to the data requirement and data availability, the USLE/RUSLE requires less

than 30 minutes maximum rainfall intensity for its rainfall erosivity factor. We have daily rainfall data but we do not have 30 min rainfall data to test the USLE/RUSLE using its original data requirement; therefore, we can not minimize uncertainty. It is also required that the temporal and spatial distributions of rainfall should be captured at different points in a large watershed. This leads us to check whether the existing gauging stations are enough or not to capture the rainfall distributions of the watersheds under our consideration. In addition to several missing climatic data, the spatial distribution and density of the gauging stations are in question for the large watersheds of Ethiopia. Practically, it is not easy to test the USLE/RUSLE/ at the large watersheds in Ethiopia. However, the USLE/RUSLE was applied at different parts of Ethiopia following similar or different approaches to estimate any of its factors (e.g, Balabathina et al. (2020); Bekele and Gemi (2021); Degife et al. (2021); Gashaw et al. (2017); Gelagay and Minale (2016); Haile and Fetene (2012); Haregeweyn et al. (2017); Kidane et al. (2019); Moges et al. (2018); Tadesse et al. (2017); Tessema et al. (2020); Wagari and Tamiru (2021); Wolka et al. (2015); Yesuph and Dagnew (2019)).

2.1.2 The MUSLE

In the same family of the USLE or RUSLE, another type of soil erosion model is the MUSLE. Williams (1975) developed the MUSLE using 778 storm-runoff events collected from 18 small watersheds (Williams, 1977, 1975), with areas varying from 15 to 1500 ha, slopes from 0.9 to 5.9%, and slope lengths of 78.64 to 173.74 m (Hann et al.1994) as cited by Sadeghi et al. (2014). The MUSLE is given by.

$$y = a(Qq)^b KLSCP \tag{2.2}$$

where y is the sediment yield in metric tons, a is the coefficient and b is the exponent ($a = 11.8$ and $b = 0.56$ for USA, where the MUSLE was originally developed), Q is the runoff volume in m^3,q is the peak runoff rate in $\mathrm{m^3 s^{-1}}$, K is the soil erodibility factor in $0.01 * tons * acre * hour * acre^{-1} * year^{-1} * foot^{-1} * tons^{-1} * inch^{-1}$, L is the slope length factor, S is the slope steepness factor, C is the cover factor, P is the soil conservation practice factor. Essentially, the MUSLE was developed for a small agricultural watershed, where the extent of erosion is from sheet to rill erosion.

However, we cannot exactly tell whether it considers gully erosion or not. To apply the MUSLE for a large watershed, one approach that was proposed is using the MUSLE in the SWAT model environment.

This may be because the sediment yield can be more accurately estimated if the large watershed is divided into subwatersheds (area $<$ 2590 ha) to compensate for nonuniformly distributed sediment sources; the effect of watershed hydraulics and sediment particle size can be included by routing the sediment yield from subwatersheds to the large watershed (Williams, 1975). As part of the evaluation of the model, we considered the specific behavior of the MUSLE, the experiences of other authors, the physical connection between factors of the MUSLE, and the suitability of the model toward a specific location.

If we consider the specific behavior of the MUSLE, we found that the MUSLE showed better performance in the case of directly measured flow data rather than indirectly obtained flow data using indirect methods (Sadeghi et al., 2014). The model also provides

appropriate estimates at a watershed rather than an experimental plot as was reviewed and reported by Sadeghi et al. (2014). In this connection, if we consider the SWAT model, the SWAT model uses an indirect method (such as the Soil Conservation Service Curve Number) to generate runoff, then it uses the MUSLE to estimate the soil loss from a HRU (which is similar to a plot scale), then the SWAT model routes sediment output in channels to the outlet of a large watershed. However, this also leads to accumulative error at the end due to uncertainty in the definition of a channel, channel depth, and width in the SWAT model environment.

If we consider the experiences of some other authors, the MUSLE is unsuitable for the prediction of the sediment yield for small storms (Sadeghi et al., 2007). However, the slight variation in hydrological response of a watershed in terms of the sediment yield might be changing in the antecedent hydrological conditions, the spatial and temporal distribution of rainfall, availability of eroded sediment throughout the watershed, which is not taken into account by the MUSLE as for many other lumped models (Sadeghi et al., 2007).

If we consider the physical connection between factors of the MUSLE, as far as the runoff energy for soil detachment and sediment transport is concerned; the physical connection between the runoff, soil erodibility, topographic, cover, and soil conservation practice factors is convincing; however, further refining the physical connection between the factors may become necessary.

For instance, the cover and soil conservation factors play a role to break runoff energy so as to protect soil loss due to runoff. As the slope length becomes increasingly larger, there is a possibility that erosion from the upper part of the slope becomes deposited at the lower part of the slope (for instance, if we consider the last runoff from the slope-field after the end of rainfall). This is because, depending on the magnitude of the runoff and its sediment transport capacity, the runoff takes up more soil particles and becomes concentrated on its way to the bottom of the slope. In other words, the energy of the runoff decreases as resistance against flow increases along the length of the slope, and its shear force decreases.

If we consider the suitability of the model toward a specific location, the MUSLE has been observed to give good results in various applications in some parts of tropical Africa (Ndomba, 2007) as cited by Adegede and Mbajiorgu (2019), and it has been successfully demonstrated in sub-Saharan Africa (Adegede and Mbajiorgu, 2019). As per the experimental plot result of sheet erosion at Enerta study site in Ethiopia, the MUSLE was better at estimating soil loss from a cultivated field than the USLE (Muche et al., 2013).

2.1.2.1 The Factors of the MUSLE

The factors of the MUSLE are the runoff factor, soil erodibility factor, soil cover factor, soil conservation practice factor, and topographic factors. The descriptions of each of these factors are given below.

a) The Runoff factor

In the MUSLE, the runoff factor is the product of the total runoff volume and peak runoff rate. Pongsai et al. (2010) reviewed that the runoff factor represents the energy used in transporting as well as in detaching sediment, which acts as the best indicator

for predicting sediment yield for the individual storm event.

b) The Soil Erodibility Factor (K-Factor)

Wischmeier and Smith (1978) defined the soil erodibility factor as the soil loss rate per erosion index unit for a specified soil as measured on a unit plot; the unit plot is defined as a 72.6 ft length of uniform 9% slope continuously in clean-tilled fallow; it is the continuous fallow tilled up and down the slope. The soil erodibility factor is given by (Wischmeier and Smith, 1978):

$$K = \frac{\sum_{n=1}^{N} (A)_n}{\sum_{n=1}^{N} (EI_{30})_n} \tag{2.3}$$

where A is the event soil loss from the unit plot in tons/acre/year, E is the storm kinetic energy in 100 foot-tons/acre, I_{30} is the maximum 30 min intensity in inch per hour, and K is the soil erodibility factor in $0.01 * tons * acre * hour * acre^{-1} * year^{-1} * foot^{-1} * tons^{-1} * inch^{-1}$. It is important to note that the soil erodibility factor represents the worst or the maximum possible erosion from the unit plot with the specified field slope and length.

At the same rainfall impact pressure, less soil erosion condition that is different from the worst condition considers the soil cover and conservation practices on the same field slope and length. On the unit plot, or any unit plot for that matter, the temporal and spatial variation of the soil erodibility depend on the types of soil; the quite complex interaction of physical, biological, chemical, and mechanical processes.

From the soil erodibility table and equations (see figure 3.28), we can reveal that the soil erodibility factor varies from 0 to 1, where 0 indicates the soil that is hard to erode, whereas 1 represents easily erodible soil by the same rainfall impact pressure under otherwise similar soil erosion conditions. From this range of the soil erodibility factor, we can conclude that soil erodibility refers to the degree of being easy to erode a given soil.

The soil erodibility factor (K-factor) can be estimated by direct field measurement or by using different empirical equations or a soil erodibility nomograph.

1. The K-factor that was originally developed for the soil conditions of the USA (Wischmeier and Smith, 1978):

$$K = \frac{\left\{\left[2.1M^{1.14}(12-a) * 10^{-4}\right] + 3.25(b-2) + 2.5(c-3)\right\}}{100} \tag{2.4}$$

where K = the soil erodibility in $0.01 * tons * acre * hour/acre * year * foot * tons * inch$; M = (%silt + %very fine sand) * (100 − %clay), M =Particle-size parameter, silt (%) = percentage of silt, % very fine sand = percentage of very fine sand (0.1 to 0.05 mm), clay (%) = percentage of clay, a = percentage of organic matter, b = soil structure code used in soil classification, and c = profile permeability class. For soils containing less than 70 percent silt and very fine sand, the nomograph (Wischmeier and Smith, 1978) is used to solve the above equation.

Some comments on this equation: we do not have a percentage of very fine sand in our database to test the equation. Our source of data is the harmonized world soil data, which includes the texture, reference soil depth, drainage class, available water capacity, sand, silt and clay fraction, bulk density, gravel content, organic carbon

content, pH, cation exchange capacity, base saturation, total exchangeable bases, calcium carbonate content, gypsum content, sodicity, and salinity content. As land tillage and mechanical compaction (due to rainfall impact) change the structure of the soil; the structure of tilled, bare, or compacted soil varies at temporal and spatial scales. As soil permeability depends on soil texture and organic matter, their relationship should be explicitly shown. Unrealistic values were obtained for tropical soils from the equation's erodibility nomograph (Mulengera and Payton, 1999; Ndomba, 2007) as cited by Adegede and Mbajiorgu (2019).

2. The K-factor (Williams and Renard, 1983) as cited by Chen et al. (2011) and similar equation is shown by Cole et al. (1990); Kruk (2021).

$$K = \left(0.2 + 0.3\exp\left(-0.0256S_a * (1 - \frac{S_i}{100})\right)\right) * \left(\frac{S_i}{c_L + S_i}\right)^{0.3} * \left(1 - \frac{0.25c}{c + \exp(3.72 - 2.95c)}\right) * \left(1 - \frac{0.7S_N}{S_N + \exp(-5.51 + 22.9S_N)}\right) \tag{2.5}$$

where S_a = sand (%); S_i = silt (%); C_L = clay (%); $S_N = 1 - (S_a/100)$; C = organic carbon

3. The K-factor that was tested in the soil conditions of the Philippines (David, 1988):

$$K = \left[0.043 * pH + \frac{0.62}{OM} + 0.0082S - 0.0062C\right] * Si \tag{2.6}$$

where pH = pH of the soil, OM = organic matter (%), S = sand content (%), C = clay ratio =% clay / (% sand + % silt), and Si = silt content = % silt /100.

4. The K-factor that was originally developed for the volcanic soil of Hawaii, USA (El-Swaify and Dangler, 1976) as cited by Renard et al. (1997):

$$K = -0.03970 + 0.00311x_1 + 0.00043x_2 + 0.00185x_3 + 0.00258x_4 - 0.00823x_5 \tag{2.7}$$

where x_1 = unstable aggregate size fraction (< 0.250 mm)(%), x_2 = modified silt (0.002–0.1 mm) (%) * modified sand (0.1–2 mm) (%), x_3: % base saturation, x_4 = silt fraction (0.002–0.050 mm) (%), and x_5 = modified sand fraction (0.1–2 mm) (%).
We do not have unstable aggregate size fraction or modified silt and sand data in our database to test the equation.

5. Williams (1995) proposed the following K-factor as cited by Wawer et al. (2005):

$$K = f_{csand} * f_{cl-si} * f_{orgC} * f_{hisand} \tag{2.8}$$

$$f_{csand} = 0.2 + 0.3\exp[-0.256m_s(1 - \frac{m_{silt}}{100})] \tag{2.9}$$

$$f_{cl-si} = (\frac{m_{silt}}{m_c - m_{silt}})^{0.3} \tag{2.10}$$

$$forgC = 1 - \frac{0.25 * orgC}{orgC + \exp[3.72 - 2.95 * orgC]} \tag{2.11}$$

$$f_{hisand} = 1 - \frac{0.7(1 - \frac{m_s}{100})}{1 - \frac{m_s}{100} + \exp[-5.51 + 22.9(1 - \frac{m_s}{100})]} \tag{2.12}$$

where m_s is the percent sand content; m_{silt} is the percent silt content; m_c is the percent clay content; $orgC$ is the percent carbon content

6. Other soil erodibility equations are mentioned by Kruk (2021); Liu et al. (2020); Panagos et al. (2014); Renard et al. (1997); van der Knijff et al. (2000); Wang et al. (2016); Wawer et al. (2005); Wischmeier and Mannering (1969).

c) The Slope Steepness and Slope Length Factors

The slope steepness factor (S) is the ratio of soil loss from a field slope gradient to soil loss from the 9% slope under otherwise identical conditions (Ganasri and Ramesh, 2016). A high rate of soil loss is associated with steep slopes (Gwapedza et al., 2018; Renard et al., 2011), and soil-loss prediction is more sensitive to the slope steepness than slope length (Moore and Wilson, 1992). Slope length is defined as the distance from the point of origin of overland flow to the point where either the slope gradient decreases enough that deposition begins or the runoff water enters a well-defined channel that may be part of a drainage network or a constructed channel (Wischmeier and Smith, 1978). It is important to note that the definition of the slope length relies on the conditions at which the unit plot was constructed by Wischmeier and Smith (1978); the unit plot represents the worst condition for the maximum soil erosion case.

Therefore, for the worst condition for the maximum erosion case, the slope length is the shortest distance from the origin of overland flow to the point where deposition takes place or enters stream channels. The slope lengths would rarely have a constant gradient along their entire length, and the slope irregularities would affect the amount of soil movement to the foot of the slope (Wischmeier and Smith, 1978). The slope length factor is given by (Wischmeier and Smith, 1978):

$$L = \left(\frac{\lambda}{\lambda_o}\right)^m \tag{2.13}$$

where λ is the slope length, and λ_0 is the unit plot length = 72.6 ft = 22.13 m. λ_0 is also defined as the horizontal projection of the slope length (e.g., Fagbohun et al. (2016); Kinnell (2010); Mitasova et al. (1996); Renard et al. (2011)). In one term, the slope steepness factor (S) and slope length factor (L) together are called the topographic factor (LS-factor). The topographic factor is the ratio of soil loss per unit area from a field slope length and gradient to that from the 22.1 m length of uniform 9% slope under otherwise identical conditions (Wischmeier and Smith, 1978). Different equations have been suggested at different locations to estimate the topographic factor while taking into account site-specific conditions.

1. The topographic factor that was proposed at the topographic condition of USA (Wischmeier and Smith, 1978):

$$LS = \left(\frac{\lambda}{72.6}\right)^m \left(65.41sin^2\theta + 4.56sin\theta + 0.065\right) \tag{2.14}$$

where λ = slope length in feet, θ = angle of the slope, and m = dependent on the slope (0.5 if the slope $>$ 5%, 0.4 if the slope is between 3.5% and 4.5% , 0.3 if the slope is between 1% and 3%, and 0.2 if the slope is less than 1%).

2. McCool et al. (1987) improved the LS-factor from classic USLE for use in terrain

with steeper slopes as cited by Pongsai et al. (2010) for use in RUSLE (Renard et al., 2011):

$$L = \left(\frac{\lambda}{22.13}\right)^{m} \tag{2.15}$$

$$m = \frac{\sin\theta}{\sin\theta + 0.269\,(\sin\theta)^{0.8} + 0.05} \tag{2.16}$$

$$S = 3.0\,(\sin\theta)^{0.8} + 0.56 \text{ for } \lambda < 4\text{m} \tag{2.17}$$

$$S = 10.8 * \sin\theta + 0.03 \text{ for } \lambda > \text{ 4m and } s < 9\% \tag{2.18}$$

$$S = 16.8\sin\theta - 0.50 \text{ for } \lambda > \text{ 4m and } s > 9\% \tag{2.19}$$

where λ is the slope length in meters, m is the dimensionless parameter, θ is the angle of field slope in degrees $= tan^{-1}$ (s/100), and s is the field slope as a percentage.

3. Foster et al., (1977) and McCool et al., (1987, 1989) proposed the following equations for the calculation of the LS-factors as cited by Renard et al. (1997):

$$L = \left(\frac{\lambda}{22.13}\right)^{m} \tag{2.20}$$

$$m = \frac{\beta}{1+\beta} \tag{2.21}$$

$$\beta = \frac{\frac{\sin\theta}{0.0896}}{3\,(\sin\theta)^{0.8} + 0.56} \tag{2.22}$$

$$S = 10.8\sin\theta + 0.03 \text{ if the slope (s) is less than } 9\% \tag{2.23}$$

$$S = 16.8 sin\theta - 0.5 \text{ if the slope is greater than or equal to } 9\% \tag{2.24}$$

$$S = 3\,(\sin\theta)^{0.8} + 0.56 \text{ if the slope length is shorter than 4.6 m} \tag{2.25}$$

where θ is the angle of the slope, s and θ are defined above
Equation 2.21 was given by Foster et al., 1977 as cited in (Renard et al., 1997). Equations 2.22 – 2.25 were given by McCool et al., 1989 as cited in (Renard et al., 1997). Equation 2.25 was given for the condition where water drains freely from slope end, and it is assumed that inter-rill erosion is insignificant on slopes shorter than 4.6 m (Renard et al., 2011).

As a remark, when conditions favor more inter-rill and less rill erosion, as in cases of consolidated soils, such as those found in no-till agriculture, m should be decreased by halving the β value, where a low rill to inter-rill erosion ratio is typical of the conditions on rangelands (Renard et al., 2011). With thawing, and cultivated soils dominated by surface flow, a constant value of 0.5 should be used (McCool et al., 1989, 1993) as cited by Renard et al. (2011). When freshly tilled soil is thawing, in a weakened state and primarily subjected to surface flow, we use the following equation (McCool et al., 1993) as cited by Renard et al. (2011).

$$S = 10.8 \sin\theta + 0.03 \text{ if } s < 9\% \tag{2.26}$$

$$S = \left(\frac{\sin\theta}{0.0896}\right)^{0.6} \text{ if } s > 9\% \tag{2.27}$$

where s is the slope steepness in percent

4. The slope factor that is approximately equal to the LS-factor at the topographic condition of the Philippines (David, 1988):

$$S = a + b * {S_L}^{4/3} \tag{2.28}$$

where S is the slope factor, a = 0.1, and b = 0.21; S_L is the slope in percent.

5. The LS-factor was developed for the the topographic condition of Britain (Morgan, 2005):

$$LS = \left(\frac{\lambda}{22}\right)^{0.50} * \left(0.065 + 0.045s + 0.0065s^2\right) \tag{2.29}$$

where λ is the slope length (m), and s is the slope steepness (%). Apart from the LS-factor of the USLE or RUSLE, the CSLE (Baoyuan et al., 2002) was developed while taking into consideration the Chinese soil environment and topographic conditions (including the modified equation that can calculate LS-factor in >10° conditions) (Zhang et al., 2017). In the CSLE, the LS-factor is calculated by (Zhang et al., 2017):

$$L = \left(\frac{\lambda}{22.1}\right)^{m} \tag{2.30}$$

$$m = 0.2 \text{ for } \theta \leq 1.7\% \tag{2.31}$$

$$m = 0.3 \text{ for } 1.7\% < \theta \leq 5.2\% \tag{2.32}$$

$$m = 0.4 \text{ for } 5.2\% < \theta \leq 9\% \tag{2.33}$$

$$m = 0.5 \text{ for } \theta > 9\% \tag{2.34}$$

$$S = 10.8 \sin\theta + 0.03 \text{ for } \theta < 9\% \tag{2.35}$$

$$S = 16.8 \sin\theta - 0.05 \text{ for } 9\% \leq \theta < 17.6\% \tag{2.36}$$

$$S = 21.9 \sin\theta - 0.96 \text{ for } \theta \geq 17.6\% \tag{2.37}$$

where λ is the slope length (m), m is the variable slope-length exponent, and θ is the slope angle (°).

6. Other equations of the slope or slope length factor are mentioned by Baoyuan et al. (2002); Benavidez et al. (2018); Moore and Wilson (1992); Pongsai et al. (2010); Schmidt et al. (2019); Wang and Liu (2014); Zhang et al. (2017).

USLE and RUSLE were originally developed for gently sloping cropland and the topography factor (LS) was one dimension (Zhang et al., 2017). In other word, the USLE/RUSLE is primarily designed to predict erosion on straight slope sections. When applying USLE or RUSLE equation to calculate the average annual sheet and rill erosion per unit area at

watershed or even larger scales, however, topography becomes two-dimensional and LS is more difficult to estimate than other terms in the equation (Van Remortel et al., 2004) as cited in (Zhang et al., 2017).

Foster and Wischmeier (1974) were the first to develop a procedure to calculate the average soil loss on complex slope profiles by dividing an irregular slope into a limited number of uniform segments as cited by Desmet and Govers (1996). According to literature review report by Desmet and Govers (1996), slope length was replaced by a unit contributing area for a two-dimensional situation. The unit contributing area is to mean an upslope drainage area per unit of contour length, where contour length is length of line through the grid cell center and perpendicular to the aspect direction. In a grid-based DEM (meaning; DEM in grid data format but it can be presented in different data format like contour or triangular irregular network (TIN), the unit contributing area is contributing area of cell divided by effective contour length (Desmet and Govers, 1996). The unit contributing area may differ considerably from slope length, as it is affected by flow convergence and/or divergence (Desmet and Govers, 1996).

According to literature review report by Benavidez et al. (2018), the following LS factor was provided based on the contributing area at topographic condition of USA.

$$LS = (m+1)\left(\frac{U}{L_o}\right)^m \left(\frac{\sin\theta}{S_0}\right)^n \tag{2.38}$$

where U is the upslope contributing area per unit width as a proxy for discharge; U = flow accumulation * cell size; L_0 is the length of the unit plot (22.1); S_0 is the slope of unit plot (0.09); θ is the slope; m (sheet) and n (rill) depend on the prevailing type of erosion (m = 0.4 to 0.6) and n (1.0 to 1.3).

Moore and Wilson (1992) presented a simplified equation using unit contributing area (UCA) to calculate LS for three-dimensional terrain.

$$LS = \left(\frac{A_s}{22.13}\right)^m \left(\frac{\sin\theta}{0.0896}\right)^n \tag{2.39}$$

where A_s is the unit contributing area (m) (Zhang et al., 2017), θ is the slope in radians, and m (0.4–0.56) and n (1.2–1.3) are exponents.

With support of GIS, the concept of unit contributing can be applied to calculate the topographic factor of the USLE (Gwapedza et al., 2018; Zhang et al., 2017).

d) The Cover Factor (C-Factor)

The C-factor is the ratio of soil loss from a field with specified cropping to that from clean-tilled, continuous fallow under otherwise similar conditions. These similar conditions are no soil conservation works (land is tilled up and down the slope), soil, slope steepness, slope length, and the rainfall impact pressure is the same for both cropped field and fallow area. The C-factor is related to the land use and land cover, and it is the reduction factor for soil erosion vulnerability (Arekhi et al., 2012).

Therefore, the C-factor lies between 0 and 1, which describes the extent of vegetation cover to protect soil from erosion in a given catchment. Its value closer to 0 indicates dense vegetation cover, whereas its value closer to 1 indicates poor vegetation cover.

Essentially, surface cover or canopy protects soil erosion by decreasing rainfall impact energy; however, it may have less importance to protect sediment transport from a field.

To some extent, we can say that surface cover affects soil erosion by reducing the transport capacity of the runoff water (Foster, 1982) and by causing deposition in ponded areas (Laflen, 1983) as cited by Renard et al. (1997) and also by decreasing the surface area susceptible to raindrop impact (Renard et al., 1997).

In addition, the plant-root depth and distribution and porosity increase the infiltration rate of rainfall water into the soil, and thus they play a role in reducing soil loss (Jeong et al. 2012) as cited by Jang et al. (2015).

Although the C-factor value can be taken from the literature or determined in situ, an extensive literature review compiling the potential soil loss rates of different crop and forest covers compared to likely soil loss rates of bare soil can be used to determine likely C-factor values of a particular site (Benavidez et al., 2018). The published guidelines (Renard et al., 2011; Wischmeier and Smith, 1978), the revised C-factor (Cai et al., 2000) as cited by Luo et al. (2016) and the Normalized Difference Vegetation Index (Liu et al., 2020; van der Knijff et al., 2000) can be used to compute the C-factor.

e) The Soil Conservation or Erosion Control Practice Factor (P-Factor)

The P-factor is the ratio of soil loss associated with a specific support practice to the corresponding soil loss when cultivation is done up and down the slope (Renard et al., 1997) under otherwise similar conditions. The P-factor describes the effects of practices, such as contouring, strip cropping, concave slopes, terraces, grass hedges, silt fences, straw bales, and subsurface drainage (Arekhi et al., 2012).

These conservation practices change the direction and speed of runoff (Renard et al., 2011); it mainly reduces the transport of soil particles by blocking runoff and breaking its speed; however, it does not reduce rainfall impact energy to reduce soil erosion. Therefore, the P-factor ranges from 0 to 1, where 0 represents the strong conservation practice (no soil loss from a field is expected), whereas 1 represents the worst condition for the maximum erosion due to lack of conservation practice and when land is tilled up and down the slope, and runoff takes the shortest well-defined channel or route in the field.

The difficulty of accurately mapping support practice factors or not observing support practices leads to many studies ignoring it by giving their P-factor a value of 1.0 (Benavidez et al., 2018). Some P-factors can be ignored if some C- factors already account for the presence of a support factor, such as intercropping or contouring (Benavidez et al., 2018). All non-agricultural lands were also assigned a value of 1 if no feasible conservation measures were applied (Gwapedza et al., 2018; Jang et al., 2015; Luo et al., 2016).

At suitably detailed scales and with enough knowledge of farming practices, using the P-factor may lead to a more accurate estimation of soil loss (Benavidez et al., 2018). Sadeghi et al. (2014) reviewed that considering the temporal variation of the P-factor could significantly improve the performance of the MUSLE, although it has been rarely taken into account.

2.2 Description of the SWAT Model

The SWAT model is a continuous-time, semi-distributed, process-based river basin model. The model is called the semi-distributed model because it subdivides the entire basin spatially into sub-basins, then further divides each sub-basin into several smaller heterogeneous, lumped, non-spatial sub-units (HRU) based on the land use, soil type, and slope. The model does so to simulate sediment, water flow, nutrient, or pesticides at the HRU and routes it to channels, then to an outlet of a large watershed. The model is called the continuous-time (long period) model because it gives us daily sediment yield, flow and nutrients at the outlet of the watershed, but it does not give us an instantaneous sediment yield or flow from the watershed. The model is called the process-based model because it relies on water balance for the simulation of the hydrological processes. The water balance equation of the model is given by

$$SW_t = SW_o + \sum_{i=1}^{t} (R_{day} - Q_{surf} - E_a - W_{seep} - Q_{gw}) \tag{2.40}$$

where, SW_t is the final soil water content (mm), SW_o is the initial soil water content (mm) on day i (mm), t is the time (days), R_{day} is the amount of precipitation on day i (mm), Q_{surf} is the amount of surface runoff on day i (mm), E_a is the amount of evapotransportation on day i (mm), W_{seep} is the amount of water entering the vadose zone from the soil profile on day i (mm), Q_{gw} is the amount of return flow on day i (mm).

Subsequent revisions of the SWAT model have been made from the first version SWAT94.2 (Arnold et al., 2012) to the latest SWAT+. Commonly known versions are the ArcSWAT and QSWAT models. The QSWAT model performs similar functions to the ArcSWAT model with additional enhanced features such as merging small sub-basins and static and dynamic visualization of outputs (Dile et al., 2016). Another version of the SWAT model is the MWSWAT model (SWAT2012 interface for version 4.8.8 of MapWindow), which was not updated and has been replaced by the QSWAT model (`https://swat.tamu.edu/software/` accessed on 2 December 2019).

The QSWAT+ or simply the SWAT+ model is a completely revised version of the SWAT model. It provides a more flexible spatial representation of interactions and processes within a watershed (`https://swat.tamu.edu/software/plus` accessed on 3 December 2019). In the SWAT+ model, the HRU can be categorized into two landscape units such as upslope and floodplain. This may facilitate making a distinction between upslope and floodplain processes. The basic algorithms used to calculate the processes in the model have not changed, and the structure and organization of both the code (object-based) and the input files (relational-based) have undergone considerable modification (`https://swat.tamu.edu/software/plus` accessed on 3 December 2019).

The primary contribution of the SWAT+ model is that the model has been reconstructed as independent modules (objects) so that it's a lot easier in terms of model maintenance and the corresponding development as well (Yen et al., 2019). In addition to modularization, there are also some key developments to enhance the performance of the model (for example, new functionalities of aquifers and reservoir operation rules are available in the SWAT+ model) (Yen et al., 2019).

Both the QSWAT and QSWAT+ models were demonstrated at Robit watershed in the Lake Tana basin of Ethiopia. As compared with the SWAT model, the SWAT+ model is more versatile than the SWAT model in modeling in hilly watersheds (Steenhuis et al., 2019). The other advantages of the SWAT+ model over the SWAT model are discussed by Bieger et al. (2017); Yen et al. (2019).

2.2.1 Modeling Approaches, Limitations and Improvements of the SWAT Model

The estimation of soil loss depends on other interrelated hydrological processes such as infiltration, evapotranspiration, and surface runoff. The SWAT model uses empirical equations to estimate each of these processes. For example, the model uses the Modified Universal Soil Loss Equation in the following form to estimate soil loss from a catchment.

$$y = 11.8(QqA)^{0.56}KCPLSf \tag{2.41}$$

where y is the sediment yield on a given day (metric tons), Q is the surface runoff volume ($mm\ ha^{-1}$), q is the peak runoff rate (m^3s^{-1}), A is the area of the HRU (ha), K is the soil erodibility factor, C is the soil cover factor, P is the support practice factor, L is the slope length factor, S is the slope steepness factor, and f is the rock or coarse fragment factor. The rock or coarse fragment factor is calculated by

$$f = e^{-0.053*rock} \tag{2.42}$$

where $rock$ is the percent rock in the first soil layer

In connection to the soil loss or sediment yield estimation, the limitations and improvement of the SWAT modelling approaches which directly or indirectly linked to the soil loss or sediment yield are presented below.

As the SWAT model is the continuous (i.e., long-term) model with limited applicability toward simulating instantaneous hydrologic responses, Yu et al. (2018) improved the SWAT model for event-based flood simulation on a sub-daily timescale.

To provide necessary variability in land use and land cover, the entire simulation period can be divided into two or more parts and can be performed interval simulations using the corresponding land use and land cover data. This may complicate the simulation processes and fail to reflect year-to-year changes in land use and land cover (Jin et al., 2019). To address this problem, Jin et al. (2019) developed the modified SWAT model (LU-SWAT) that incorporates annual land use and land cover data to simulate land use and land cover change effects on hydrological processes under different climatic conditions.

The SWAT model uses the SCS CN method to generate overland flow when the saturated hydraulic conductivity is less than rainfall intensity. A series of modified SWAT models that simulate saturation excess overload flow with some progress of improvement (Steenhuis et al., 2019) are SWAT-VSA model (Easton et al., 2008), SWAT-WB model (White et al., 2011), SWAT-HS model (Hoang et al., 2017) and SWAT-wil model (Steenhuis et al., 2019). The SWAT-WB and SWAT-VSA models increased the surface runoff, but since the SWAT model subsurface flow component was not changed, the increased runoff

resulted in less water being available for evapotranspiration (Steenhuis et al., 2019). Although the SWAT-HS model represented the hillslope processes more realistically than the SWAT-2012 model, major modifications in the SWAT model code were required, making wider application difficult (Steenhuis et al., 2019). In the SWAT-wil model, the saturation levels in the valley bottom areas were increased by restricting both the lateral flow and percolation (Steenhuis et al., 2019). The SWAT-wil model can be used with the SWAT+ model which has the functionality to group HRU into laterally connected landscape elements that can pass water along various pathways (overland, lateral, groundwater) from upslope to downslope (Steenhuis et al., 2019).

The different versions of the original SWAT models have been modified for sediment yield estimations. The modified SWAT (SWAT-TUSLE) uses Taiwan Universal Soil Loss Equation (Chen et al., 2009), which calculates the Cover factor based on NDVI and slope length factor based on slope (Lu and Chiang, 2019). The modified SWAT664 (SWAT-Twn) (Lu and Chiang, 2019) uses Taiwan Universal Soil Loss Equation (Chen et al., 2009) and landslide volume. The sediment transport capacity algorithm was included in the source code of the SWAT model (version 2009) (Bonumá et al., 2014). Since in some instances, SWAT-simulated results are greatly affected by the watershed delineation and DEM cell size (Kim et al., 2009), the SWAT ArcView GIS Patch II was developed for steep sloping watersheds, and its performance was evaluated for various threshold values and DEM cell size scenarios when delineating subwatersheds using the SWAT model (Kim et al., 2009).

2.2.2 Overview of the SWAT Model Calibration

The SWAT model requires a large number of input parameters, which complicates the model parameterization and calibration (Arnold et al., 2012). Like the SWAT model, the SWAT+ model has a lot of calibration parameters (i.e., more than one hundred eighty six calibration parameters). The calibration parameters of the SWAT+ model are stored in cal_parms.cal file. Not all parameters of the SWAT+ model are clearly defined. The SWAT+ Editor 2.1.4, SWAT+ Toolbox v1.0, and open source code of the SWAT+ rev.60.5.4 model define some of the calibration parameters.

Table 2.1: Flow calibration parameters.

Parameters	Symbol in cal_parms.cal file	Recommended range	Units
Leaf area index at which no evaporation occurs from water surface	evlai	0 – 10	m^2/m^2
Calibration coefficient used to control impact of the storage time constant for low flow (where low flow is when river is at 0.1 bankfull depth) upon the km value calculated for the reach	msk_co2	0 – 10	null

Weighting factor control relative importance of inflow rate and outflow rate in determining storage on reach	msk_x	0 – 0.3	null
Calibration coefficient to control impact of the storage time constant for the reach at bankfull depth	msk_co1	0 – 10	null
Surface runoff lag coefficient	surlag	1 – 24	hrs
Soil evaporation compensation factor	esco	0 – 1	null
Plant water uptake compensation factor	epco	0 – 1	null
Soil water at CN3: 0=fc, 0.99=near saturation	cn3_swf	0 – 1	null
Percolation coefficient; adjusts soil moisture for perc to occur (1.0 = fc)	perco	0 – 1	null
Plant ET curve number coefficient	latq_co	0 – 1	null
Slope length for lateral subsurface flow	lat_len	1 – 150	m
Maximum canopy storage	canmx	0 – 100	mm/H20
Reach evaporation adjustment factor	evrch	0.5 – 1	null
Initial soil water storage expressed as a fraction of field capacity water content	ffcb	0 – 1	mm
The SCS curve number	cn2	35 – 95	null
Manning coefficient for overland flow	ovn	0.01 – 30	$m^{1/3}s$
Available water capacity of the soil layer	awc	0.01 – 1	mm_H20/mm
Baseflow alpha factor	alpha	0 – 1	null
Minimum aquifer storage to allow return flow	flo_min	0 – 50	m
Saturated hydraulic conductivity of soil layer	k	0 – 2000	mm/hr
Channel slope	chs	-0.001 – 10	m/m
Manning coefficient in channel	chn	-0.01 – 0.3	$s/m^{1/3}$
Channel hydraulic conductivity	chk	-0.01 – 500	mm/hr
Floodplain slope	fps	1.1 – 1.9	m/m

Floodplain Manning's n	fpn	0.01 – 0.5	$s/m^{1/3}$
Equilibrium channel slope	–	–	m/m
Channel side slope	–	–	m/m
Channel width	chw	0 – 1000	m
Channel depth	chd	0 – 30	m
Channel length	chl	-0.05 – 500	km
Width-depth ratio	wd_rto	0.5 – 20	m/m
Concentration coefficient for tile flow and leach from bottom layer	–	0 – 1	–
Channel storage coefficient	–	0 – 1	null
Parameter for frozen soil adjustment on infiltration/runoff	–	–	–
Maximum initial abstraction for urban areas when using Green and Ampt	–	0 – 1	mm
PET adjustment fraction for Penman-Montieth and Priestly-Taylor methods	–	0 – 1	null
Exponential coefficient for overland flow	–	1 – 3	null
Coefficient related to radiation used in Hargreaves equation	–	–	null

Table 2.2: Sediment calibration parameters.

Parameters	Symbol in cal_parms.cal file	Recommended range	Units
Sediment concentration in lateral flow	lat_sed	0 – 5000	g/L
Average slope steepness in HRU	slope	0.0001 – 0.9	m/m
Average slope length for erosion	slope_len	10 – 150	m
Average distance to stream	dis_stream	0 – 100000	m
Median particle diameter of main channel	d50	0.00001 – 1000	mm
Linear parameter for calculating the maximum amount of sediment that can be reentrained during channel sediment routing	spcon	0.0001 – 0.01	null

Exponent parameter for calculating sediment reentrained in channel sediment routing	spexp	1 – 1.5	null
Peak rate adjustment factor for sediment routing in the main channel	prf	0 – 2	null
Peak rate adjustment factor for sediment routing in the subbasin (tributary channels)	adj_pkr	0.5 – 2	null
USLE support practice factor	usle_p	0 – 1	null
USLE soil erodibility factor	usle_k	0 – 0.65	$0.01 * tons * acre * hour/acre * year * foot * tons * inch$
Clay content	clay	0 – 100	%
Silt content	silt	0 – 100	%
Sand content	sand	0 – 100	%
Rock fragment content	rock	0 – 100	%
Soil bulk density	bd	0.9 – 2.5	mg/m^3
Organic carbon content	cbn	0.05 – 10	%
Median sediment size	d50	0.00001 – 1000	mm
Clay percent of bank and bed	ch_clay	0 – 100	%
Carbon percent of bank and bed	carbon	0 – 50	%
Dry bulk density	ch_bd	0.9 – 1.9	g/cm^3
Percent of sediment entering the channel that is bed material	bedldcoef	0 – 1	%
Erodibility factor (0=non-erosive channel; 1=no resistance to erosion)	–	–	$0.01 * tons * acre * hour/acre * year * foot * tons * inch$
Cover factor (0=channel is completely protected from erosion by cover; 1=no vegetative cover on channel)	–	–	null
days of lateral soil flow across the hillslope	lat_ttime	0.5 – 180	days

lateral soil flow coefficient - linear adjustment to daily lat flow	latq_co	0 – 1	null
Residue cover factor for computing fraction of cover	–	0.1 – 0.5	null
Splash erosion coefficient	–	0.9 – 3.1	null
Rill erosion coefficient	–	0.5 – 2	null
Scaling parameter for cover and management factor for overland flow erosion	–	0.001 – 0.45	–
Deposition coefficient	–	–	null

If data are available for each process (evapotranspiration, surface runoff, etc), the process should be calibrated individually (Arnold et al., 2012). Streamflow, sediment, and nutrient transport should be calibrated sequentially (in that order); this is because of the interdependencies between constituents due to shared transport processes (Arnold et al., 2012). For the calibration of surface runoff, separating the baseflow and surface runoff from the observed total daily streamflow is recommended.

The process-based calibration should be done at a subwatershed or landscape level. This is to ensure that variability in the predominant processes for each of the subwatershed is captured instead of determining the global (watershed-wide) processes (Arnold et al., 2012).

Users should check the water balance components (precipitation, evapotranspiration, percolation, surface runoff and lateral flow) during the calibration process. This is to make sure the predictions are reasonable for a study region or watershed (Arnold et al., 2012).

The temporal and spatial coverage of climate data used for both calibration and validation should not be substantially different, i.e., wet, moderate, and dry years occur in both periods (Arnold et al., 2012). Some of the poorer testing results reported in the previous SWAT model studies can be partially attributed to the inadequate spatial coverage of precipitation inputs (Arnold et al., 2012). This is because an inadequate number of rain gauges in simulated watershed configurations fails to capture the spatial detail of available rainfall data.

Manual or partial calibration techniques may be used to calibrate the SWAT+ model. No automatic calibration procedure can substitute for actual physical knowledge of watershed processes (Arnold et al., 2012). To manually calibrate the SWAT+ model, we can use the calibration.cal file, where we define calibration parameters. The potential automatic calibration tools for the SWAT+ model are IPEAT+ (Yen et al., 2019), SWATplusR, R-SWAT (Nguyen et al., 2022), SWATplus-CUP (licensed program), and SWAT+ Toolbox.

2.3 Regression Analysis

The relationship between independent and dependent variables is governed by accepted scientific laws (Seber and Wild, 2003) or it is expressed by mathematical, statistical, empirical, analytical, or numerical models. To find the best fit model to the measured

data, parameters of the model can be estimated either through calibration or by regression analysis. The performance of the model is evaluated by using different statistical indicators.

Regression analysis, a technique for finding the relation among variables, is important to all scientific work where interpretations need to be drawn from measured data sets (Wu and Yen., 1992). Barnes (1998); Finney (1996); Seal (1967); Stanton (2001) highlighted the history related to the regression analysis, and Fernandez-Delgado et al. (2019) provided an extensive experimental survey of regression methods.

If the relationship between dependent and independent variables is known or their relationship is defined by a chosen model, parameters of the model can be determined by the parametric regression method. The results of analyzing data using a parametric model may heavily depend on the chosen model for regression and variance functions, moreover also on a possibly underlying preliminary transformation of the variables (Bunke et al., 1999). Non-parametric regression methods, on the other hand, have in general a slower rate of convergence, but need no explicit specification of the form of the regression function (Glad, 1998); the resulting curve is hence completely determined by the data themselves (Glad, 1998). Different types of parametric or non-parametric regression methods, and their descriptions or applications are given by Fernandez-Delgado et al. (2019); Li and Yin (2009); Linnet (1998); Lolli and Gasperini (2012); Özsoy and Örkçü (2016); Qian and Reckhow (2005); Seber and Wild (2003); Wang and Du (2014); Yong (2014).

The regression methods which can be used for both parametric and non-parametric regression analysis are artificial neural network (Specht, 1991; Wu and Yen., 1992; Zhang et al., 1998) and fuzzy regression method (Bárdossy et al., 1993; Hao and Chiang, 2008; Yang and Lin, 2002). Compared to other regression approaches, the artificial neural network is more appropriate than other approaches (Pao, 2008; Rahman and Asadujjaman, 2021; Wiese and Schaper, 1993). The artificial neural network was designed to study the behavior of real, nonlinear, complex systems, and they are particularly effective in solving problems where the correlations between the dependent and independent variables are well-known (Kopal et al., 2022). However, their precise description by classical mathematical methods is too complicated, too simplified, or impossible (Du and Swamy, 2014; Kopal et al., 2022) and they also embody much uncertainty and difficulty (Masters and Land, 1997; Morala et al., 2021; Tomandl and Schober, 2001; Zhang et al., 1998). The neural network model could be a more useful nonlinear regression tool if it successfully incorporates human knowledge (heuristics) and other regression techniques (Wang, 1999).

2.4 Statistical Measures for the Evaluation of Model Performance

We use different statistical measures to judge model predictions. Some of these statistical measures are correlation coefficient, coefficient of determination, Nash-Sutcliffe efficiency, root mean square error, volume error, a sum of square error, mean absolute error, percentage of bias, root mean square to standard deviation ratio, nonparametric tests, t-test, sign test, median objective functions, auto-correlation, cross-correlation, and others.

a) Coefficient of determination

$$R^2 = \frac{\left(\sum_{i=1}^{N}\left((S_i - \bar{S})(M_i - \bar{M})\right)\right)^2}{\sum_{i=1}^{N}(S_i - \bar{S})^2 \sum_{i=1}^{N}(M_i - \bar{M})^2} \tag{2.43}$$

where, n is the number of observations, M_i is the i-th measured value, $\bar{M}$ is the mean observed value, S_i is the i-th model-simulated value and $\bar{S}$ is the mean model-simulated value.

According to this measure, a correlation between observed and simulated data sets shows $0 \leq R^2 \leq 1$. For the best model prediction, the value of R^2 is equal to one. For the poorest model prediction, the value of R^2 is zero.

b) Nash-Sutcliffe efficiency

$$NSE = 1 - \frac{\sum_{i=1}^{N}(S_i - M_i)^2}{\sum_{i=1}^{N}(M_i - \bar{M})^2} \tag{2.44}$$

According to this measure, a correlation between observed and simulated data sets shows $NSE \leq 1$. For the best model prediction, the value of NSE is equal to one. For the poorest model prediction, the value of NSE is below zero.

c) Root mean square error

$$RMSE = \sqrt{\frac{1}{N}\sum_{i=1}^{N}(S_i - M_i)^2} \tag{2.45}$$

According to this measure, a correlation between observed and simulated data sets shows $RMSE \geq 0$. For the best model prediction, the value of $RMSE$ is equal to zero.

d) Sum of square error

$$SSE = \sum_{i=1}^{N}(S_i - M_i)^2 \tag{2.46}$$

According to this measure, a correlation between observed and simulated data sets shows $SSE \geq 0$. For the best model prediction, the value of SSE is equal to zero.

e) Mean absolute error

$$MAE = \frac{1}{N}\sum_{i=1}^{N} \mid S_i - M_i \mid \tag{2.47}$$

According to this measure, a correlation between observed and simulated data sets shows $MAE \geq 0$. For the best model prediction, the value of MAE is equal to zero.

f) Volume error

$$VE = \frac{\sum_{i=1}^{N} S_i}{\sum_{i=1}^{N} M_i} \tag{2.48}$$

According to this measure, a correlation between observed and simulated data sets shows $VE \geq 0$. For the best model prediction, the value of VE is equal to one. If the value of

VE is greater than one, it shows an overprediction of the model. Whereas, if the value of VE is less than one, it shows an underprediction of the model.

g) Percentage of bias

$$PBIAS = \frac{\sum_{i=1}^{n}(M_i - S_i) * 100}{\sum_{i=1}^{n} M_i} \tag{2.49}$$

The percentage of bias measures the average tendency of the simulated data to be larger or smaller than their observed counterparts (Gupta et al., 1999). According to this measure, a correlation between observed and simulated data sets shows $PBIAS \leq 1$. For the optimal model prediction, the value of $PBIAS$ is equal to zero.

h) Root mean square to standard deviation ratio

$$PSR = \frac{\sum_{i=1}^{n}(M_i - S_i)^2}{\sqrt{\sum_{i=1}^{n}(M_i - \bar{M})^2}} \tag{2.50}$$

According to this measure, a correlation between observed and simulated data sets shows $PSR \geq 0$. For the best model prediction, the value of PSR is equal to zero.

In general, both NSE and R^2 are biased toward high flows (Arnold et al., 2012). Coffey et al. (2004) recommended R^2 and NSE for analyzing the monthly output. The median objective functions, sign test, auto-correlation, and cross-correlation for assessing daily output (Coffey et al., 2004). To date, no absolute criteria for judging model performance have been firmly established in the literature, and for a good reason: the criteria for judgment of model performance should be tied to the intended use of the model (Arnold et al., 2012; Engel et al., 2007).

3. METHODOLOGY

3.1 Descriptions of Study Areas

To begin our work, we considered four watersheds such as Gumera Watershed in Abbay River Basin, Gilgel Gibe 1 Watershed (at Assendabo) in Omo-Gibe River Basin, and Hombole and Mojo Watersheds in Upper Awash River Basin, in Ethiopia, as shown in figure 3.1.

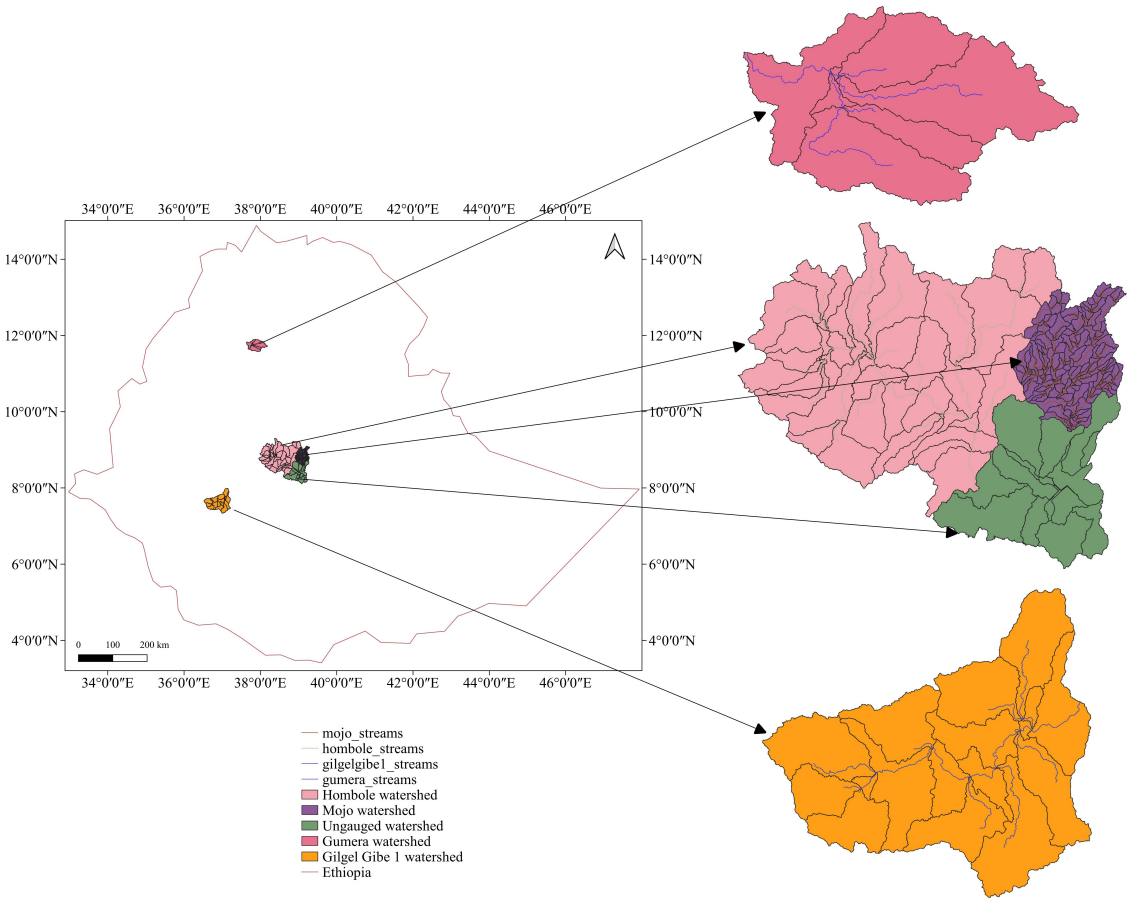

Figure 3.1: The geographical location of study areas

We describe the topography, hydro-climate, land use, and soil of the study areas based on data prepared or obtained from different sources. Therefore, the descriptions of the study areas are based on the DEM which were downloaded from the US Geological Survey; climatic data which were obtained from the National Meteorology Agency of Ethiopia; flow and sediment data which were obtained from the River Basin Authority of Ethiopia; soil and land use maps which were prepared from different sources by comparative and logical approaches. To identify the boundary of the river basin or watershed, streams are generated by delineating DEM in the SWATplus-QGIS plugin, and then the streams' shapefile is exported to the Google Earth Pro as Keyhole Markup Language to identify the outlet point of the watershed, and then the watershed is delineated by using its outlet

point, and its shapefile is exported to the Google Earth Pro as Keyhole Markup Language to identify its geographic boundary(it is important to note that the delineated watershed should be surrounded by the streams that were generated at the previous step).

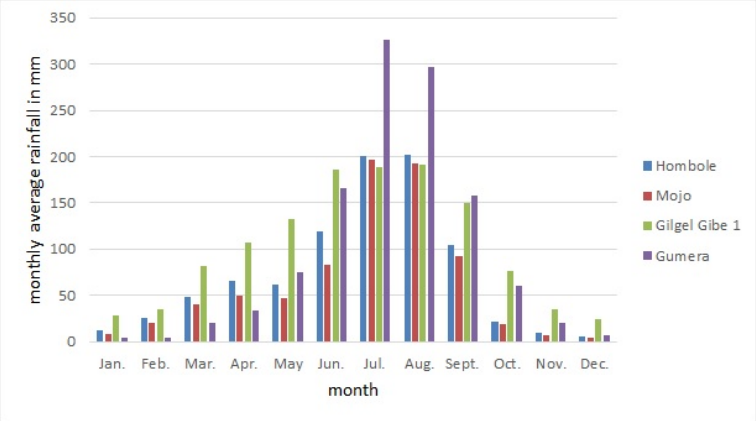

Figure 3.2: The monthly average rainfall of each watershed under our consideration.

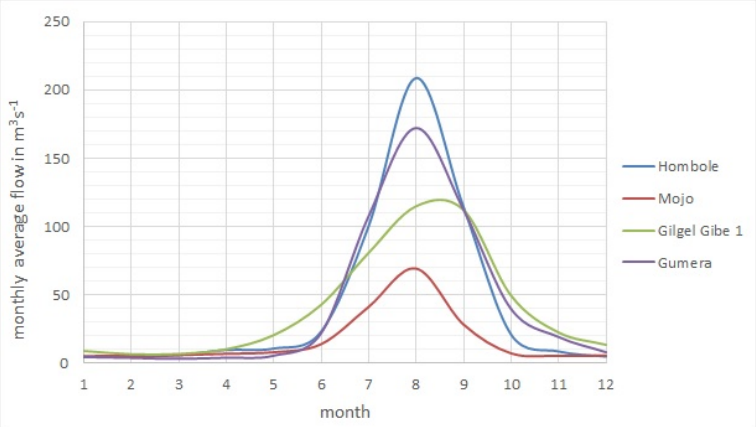

Figure 3.3: The monthly average outflow at the main outlet point of each watershed under our consideration.

3.1.1 Upper Awash River Basin

Upper Awash River Basin drains into Koka hydroelectric power reservoir. Its geographic boundary lies between latitude 8.1036°N – 9.305°N and longitude 37.950°E – 39.295°E, and its main outlet point lies at latitude 8.468521°N and longitude 39.156143°E. The basin comprises two main gauged watersheds: Hombole and Mojo Watersheds which cover 65.26% and 12.87% of the total area of the basin respectively, and the basin also includes the ungauged watershed which covers 21.87% of the total area of the basin. The total drainage area of the basin is estimated to be 11,680 km^2.

In the basin, there are active socio-economic activities like agricultural, industrial, and commercial activities. On the other angle, the basin experienced catastrophic flooding, and land degradation problems due to severe gully erosion. The gully erosion assessment

in the basin was reported by Kropaček et al. (2016). Just to report average and extreme events in the basin based on the available records (it is important to note that missing records are not considered), the maximum daily rainfall had been recorded over twenty-seven gauging stations within the record period from 1986 – 2020 is 5,039 mm, and the average of the records is 71.6 mm. The list of these stations is given in the appendix (see table A1). The daily maximum and minimum temperatures had been recorded over thirteen stations within the record period from 1986 – 2020 are 43.40°C and – 8.40°C, and the average of the maximum and minimum temperature records are 26.54°C and 10.90°C respectively. The list of these stations is given in the appendix (see table A1). The maximum and minimum relative humidity had been recorded at either of the Addis Ababa (lat. 9.01891°N and log. 38.7475°E) or Debre Zeit stations (lat. 8.733333°N and log. 38.95°E) within the record period from 1986 – 2012 are 100% and 1% respectively, and the average of the records is 58.23%. The maximum wind speed and the maximum sun hours duration had been recorded at the Debre Zeit(AF) station within the record period from 1994 – 2005 and 1994 – 2013 are 8.30 m/s and 12.60 hrs, and the average of the wind speed and sun hours duration records are 1.40 m/s and 7.98 hrs respectively.

For the Hombole Watershed, the average, maximum and minimum elevations are 2,354 m, 3,565 m, and 1,699 m above sea level respectively. The daily maximum and minimum outflow had been recorded at the main outlet of the watershed within the record period from 1990 – 2016 are 803.10 m^3/s and 0.402 m^3/s respectively, and the average of the records is 43.20 m^3/s provided that the missing records are not considered. The monthly average rainfall, and monthly average outflow at the main outlet point of the watershed are given in the figures 3.2 and 3.3 respectively (note: rainfall stations that lie inside and near the watershed, and those stations which have the record length from 15 to 35 years are considered to calculate a simple arithmetic average for the sake of comparison purpose). The maximum and minimum suspended sediment concentrations had been recorded at the main outlet of the watershed within the record period from 1989 to 2015 are 18.530 kg/m^3 and 0.136 kg/m^3 respectively, and the average of the records is 1.5 kg/m^3 provided that only available records are considered. The dominant soil types are Eutric Vertisols and Haplic Nitisols which cover 57.30% and 17.77% of the total area of the watershed respectively. Land-use changes had been observed in the watershed at four time periods, the dominant land use class is agricultural land; it covers 85.70% of the total watershed area in the time period from 1989 to 2000, 88.25% in the time period from 2001 to 2008, 86.52% in the time period from 2009 to 2012, and 86.26% in the time period from 2013 to 2015.

For the Mojo Watershed, the average, maximum and minimum elevations are 2,140.4 m, 2,932 m, and 1,739.86 m above sea level respectively. The daily maximum and minimum outflow had been recorded at the main outlet of the watershed within the record period from 1990 – 2016 are 511.189 m^3/s and 0 m^3/s respectively, and the average of the records is 17.21 m^3/s provided that the missing records are not considered. The monthly average rainfall, and monthly average outflow at the main point of the watershed are given in the figure 3.2 and 3.3 respectively (note: rainfall stations that lie inside the watershed, and those stations which have the record length from 15 to 35 years are considered to calculate the simple arithmetic average). The maximum and minimum suspended sediment concentrations had been recorded at the main outlet point within the record

period from 1989 to 2015 are 37.66 kg/m^3 and 0.16 kg/m^3 respectively provided that only available records are considered. The dominant soil types are Vertic Cambisols and Eutric Vertisols which cover 46.80% and 45.06% of the total area of the watershed respectively. Land-use changes had been observed in the watershed at four time periods; the dominant land use class is agricultural land; it covers 95.18% of the total watershed area in the time period from 1989 to 2000, 95.39% in the time period from 2001 to 2008, 93.85% in the time period from 2009 to 2012, and 93.82% in the time period from 2013 to 2015.

3.1.2 Gumera Watershed

Gumera Watershed drains into Lake Tana. Its geographic boundary lies between latitude 11.574°N – 11.9052°N and longitude 37.6308°E – 38.1852°E , and its main outlet point lies at latitude 11.83°N and longitude 37.6299°E. The total drainage area of the watershed is estimated to be 1,278 km^2. The average, maximum and minimum elevations are 2,260 m, 3,654 m, and 1,796 m above sea level respectively.

Just to report average and extreme events in the watershed based on available records (it is important to note that missing records are not considered), the maximum daily rainfall had been recorded over seven gauging stations within the record period from 1986 – 2020 is 3,736 mm, and the average of the records is 100 mm. These stations are listed in the appendix (see table A2). The daily maximum and minimum temperatures had been recorded over five stations within the record period from 1986 – 2019 are 39.7°C and -6.3°C , and the average of the maximum and minimum temperature records are 25.38°C and 10.02°C respectively. These stations are listed in the appendix (see table A2). The maximum and minimum relative humidity had been recorded at Debre Tabor station (lat. 11.8666°N and log. 37.9954°E) within the record period from 1988 to 2019 are 100% and 4% respectively, and the average of the records is 64.19%. The maximum wind speed and the maximum sun hours duration had been recorded at the Debre Tabor station within the record period from 1988 – 2018 and 1993 – 2019 are 18.3 m/s and 11.7 hrs, and the average of the wind speed and sun hours records are 1.1 m/s and 7.01 hrs respectively. The daily maximum and minimum outflow had been recorded at the main outlet of the watershed within the record period from 2000 – 2017 are 307.937 m^3/s and 0 m^3/s respectively, and the average of the records is 44.97 m^3/s. The maximum and minimum suspended sediment concentrations had been recorded within the record period from 1990 – 2017 are 10.07 kg/m^3 and 0.17 kg/m^3 respectively, and the average of the records is 3.43kg/m^3. The monthly average rainfall, and monthly average outflow at the main outlet point of the watershed are given in the figure 3.2 and 3.3 respectively (it is to note that rainfall stations that lie inside and near the watershed, and those stations which have the record length from 15 to 35 years are considered to calculate a simple arithmetic average). The dominant soil type is Haplic Luvisols which covers 69.50% of the total area of the watershed. Land-use changes had been observed in the watershed at two time periods, the dominant land use class is agricultural land; it covers 84.33% of the total watershed area in the time period from 1989 to 2009, and 88.34% in the time period from 2010 to 2015.

3.1.3 Gilgel Gibe 1 Watershed

Gilgel Gibe 1 Watershed drains into Gilgel Gibe 1 hydroelectric power reservoir. Its geographic boundary lies between latitude 7.3332°N – 7.995°N and longitude 36.515°E – 37.215°E, and its main outlet point lies at latitude 7.75°N and longitude 37.18299°E. The total drainage area of the watershed is estimated to be 2928 km^2. The average, maximum and minimum elevations are 1,973 m, 3,141 m, and 80 m above sea level respectively.

Just to report average and extreme records in the watershed based on available records (it is to note that missing records are not considered), the maximum daily rainfall had been recorded over nine gauging stations within the record period from 1986 – 2020 is 6,317 mm, and the average of the records is 111 mm. These nine gauging stations are listed in the appendix (see table A3). The daily minimum temperature had been recorded over five stations within the record period from 1986 – 2020 is 0°C, and the average of the maximum and minimum temperature records are 26.1°C and 12.47°C respectively. These five gauging stations are listed in the appendix (see table A3). The daily maximum and minimum outflow had been recorded at the main outlet of the watershed within the record period from 2000 – 2015 are 269.54 m^3/s and 1.67 m^3/s respectively, and the average of the records is 40.97 m^3/s. The maximum and minimum suspended sediment concentrations had been recorded within the record period from 1990 – 2017 are 0.90 kg/m^3 and 0.12 kg/m^3 respectively, and the average of the records is 0.43 kg/m^3. Monthly average rainfall, and monthly average outflow at the main outlet point of the watershed are given in the figures 3.2 and 3.3 respectively (it is to note that rainfall stations that lie inside and near the watershed, and those stations which have the record length from 15 to 34 years are considered to calculate a simple arithmetic average). The dominant soil types are Humic Nitisols and Mollic Fluvisols which cover 52.86% and 25% of the total area of the watershed. Land-use changes had been observed in the watershed at two time periods; the dominant land use class is agricultural land; it covers 90.23% and 91.953% of the total watershed area in the time period from 1989 – 2009 and 2010 – 2015 respectively.

3.2 Data Preparation, Review and Analysis

Some of the input data for our research works are soil, land use, stream network, climate, flow, and sediment data. We prepare soil, land use, and stream network data; we review the interdependence between climate, flow, sediment, and land use change for the data quality check, and we prepare sediment rating curves.

3.2.1 Preparation of Soil Maps

Soil data is required to estimate the soil erodibility factor of the MUSLE. The necessities of preparing soil maps are to assign a specific type of soil from a general category of the soil and to maintain the spatial variability of soil. For all our watersheds, national soil maps of Ethiopia, which we obtained recently from the River Basin Authority of Ethiopia, show the general category of soil. To assign a specific type of soil, we locate the shapefile of each watershed on a harmonized world soil data map, and we clip the harmonized world soil data map to the size of our watersheds in the QGIS environment.

Then, we compare the national soil maps of Ethiopia, the harmonized world soil map, and the field observation report from the International Soil Reference and Information Centre on QGIS. Particularly for the Upper Awash River Basin, we have two soil maps that were prepared at different times from the River Basin Authority of Ethiopia. Based on these two soil maps, we maintain the spatial variability of soil right after the specific type of soil was assigned by locating an areal coverage of the specific type of soil on the old map that completely lies inside a large area of another specific type of soil on the current soil map. Therefore, the soil maps of each watershed, which are finally prepared, are given in figures 3.4 – 3.6.

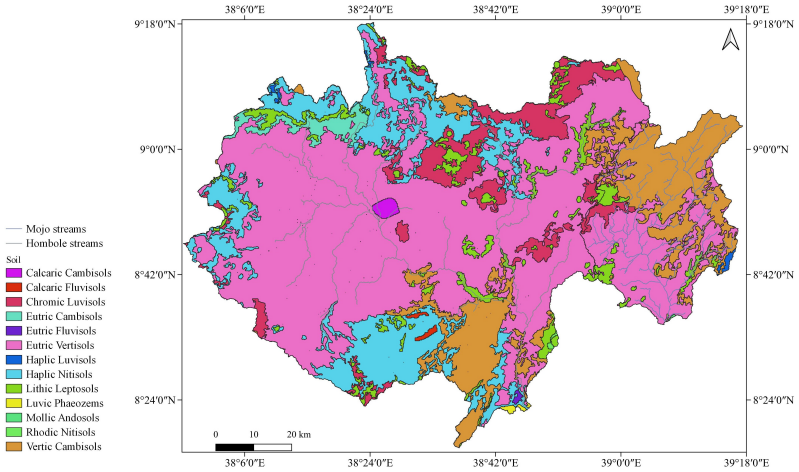

Figure 3.4: Soil maps of the Hombole and Mojo Watersheds.

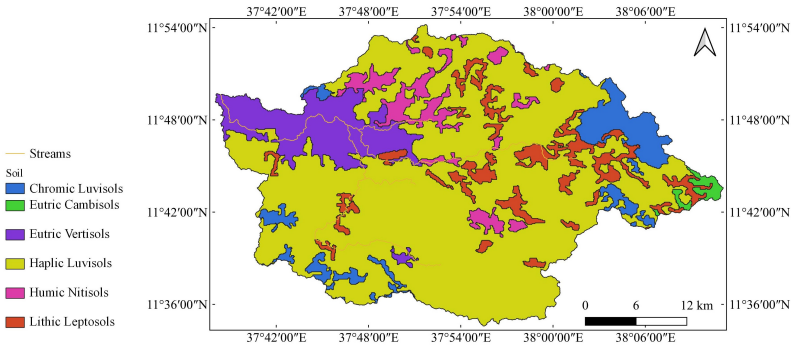

Figure 3.5: Soil map of the Gumera Watershed .

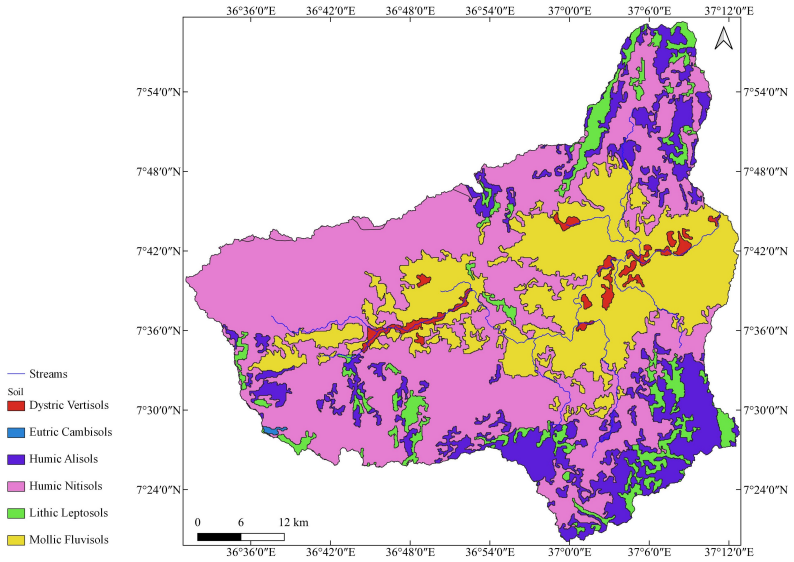

Figure 3.6: Soil map of the Gilgel Gibe 1 Watershed.

3.2.2 Preparation of Land Use Maps

Preparation of land use data is necessary to estimate the cover and conservation practice factors of the MUSLE. Based on our assessment of land use and land cover by the support of Google Earth Pro, Planet Explorer, literature review (e.g., Bogale (2020); Shawul et al. (2019); Tadese et al. (2020)), and land use maps from the River Basin Authority of Ethiopia, land-use change has been observed in the study areas. As the basis of classification of land use maps, dominant land use classes are categorized at 30 m spatial resolution. This is an acceptable level of spatial dimension to consider the spatial variability of land use at a tolerable level of accuracy. As a result, land use maps of each watershed are prepared based on a comparative approach and logical sequence.

To prepare land use maps by the comparative approach, sample geographic coordinate points with defined land use classes are collected from the Global land service map; forest and agricultural land on historical imagery in the Google Earth Pro at different acquisition dates are digitized. A time demarcation of the land-use change classification depends on a number of available baseline land use maps per watershed, the time boundary of the Global land service maps, and historical imagery in the Google Earth Pro. As a result, the time demarcations of land-use changes for the Hombole and Mojo Watersheds are 1989 – 2000, 2001 – 2008, 2009 – 2012, and 2013 – 2015 and for the Gumera and Gilgel Gibe 1 Watersheds are 1989 – 2009 and 2010 – 2015.

During the comparison of the above land use data files with the baseline national land use maps of Ethiopia on QGIS and Google Earth Pro; the vector data files are converted from the shapefile to the Keyhole Markup Language (KML) and vice versa. To prepare a land use map by the logical sequence, we check whether a change in land-use from one class to another is possible or not (for example, is the change from urban to agriculture possible?) such as the comparison of different land use data files that were prepared or acquired from different sources at the specified time demarcation.

Particularly for the Upper Awash River Basin, land use classes, found on the previous

baseline map but not on the latter map, are included on the latter map based on the logical sequence, and vice versa. Furthermore, also missing land use classes, such as water bodies, are added on either of the maps during the comparison of the maps with other sources, such as historical imagery in Google Earth Pro, while following these procedures, the land use maps that are finally prepared for each watershed are given in figures 3.7 – 3.14.

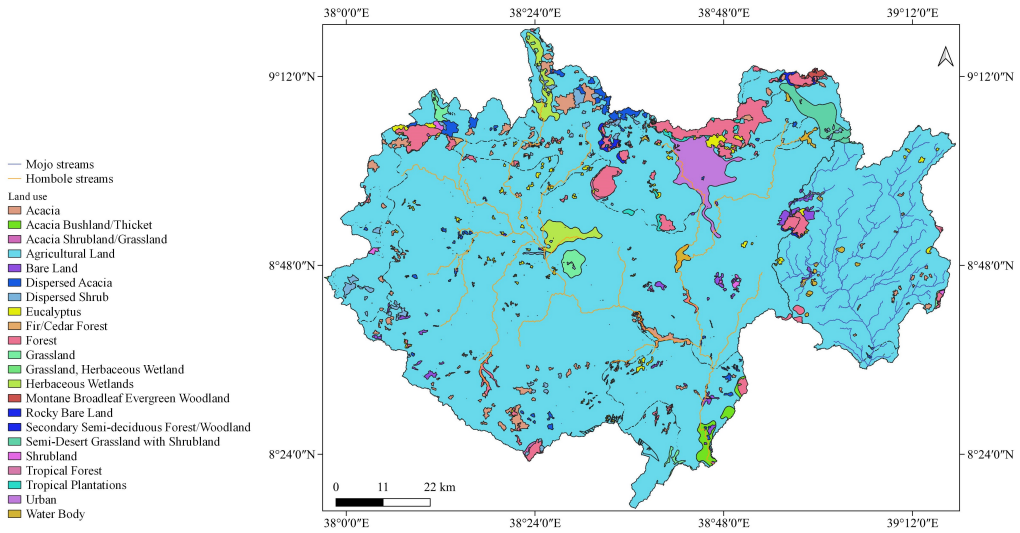

Figure 3.7: Land use map of the Hombole and Mojo Watersheds from 1989 to 2000.

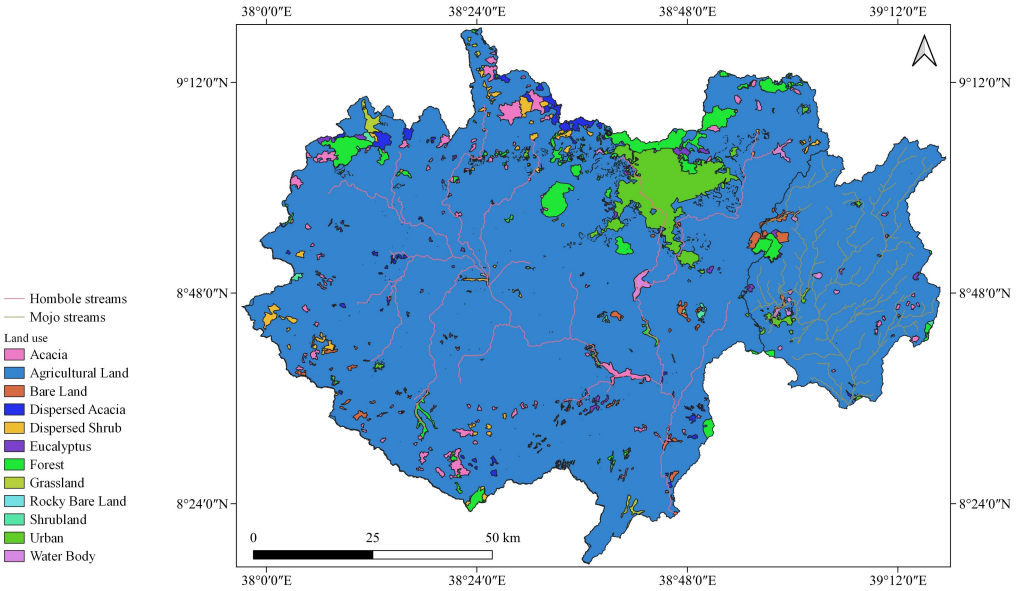

Figure 3.8: Land use map of the Hombole and Mojo Watersheds from 2001 to 2008.

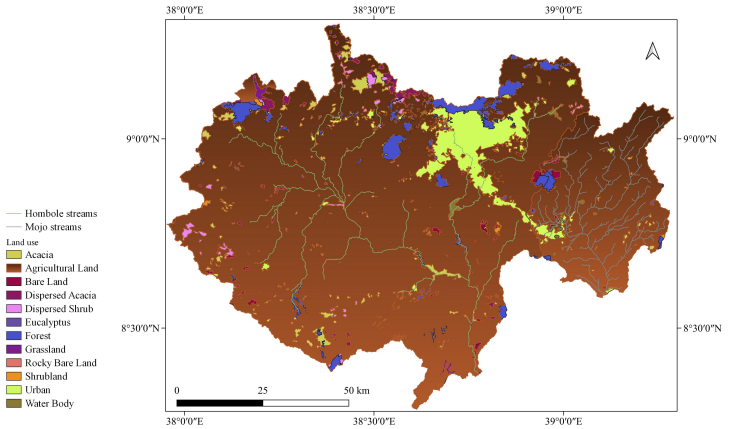

Figure 3.9: Land use map of the Hombole and Mojo Watersheds from 2009 to 2012.

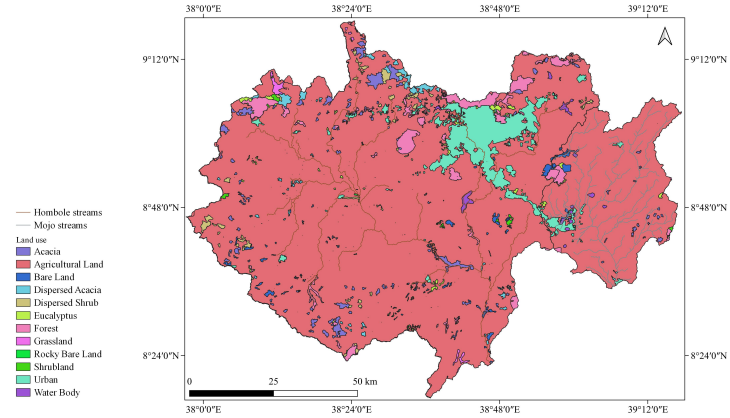

Figure 3.10: Land use map of the Hombole and Mojo Watersheds from 2013 to 2015.

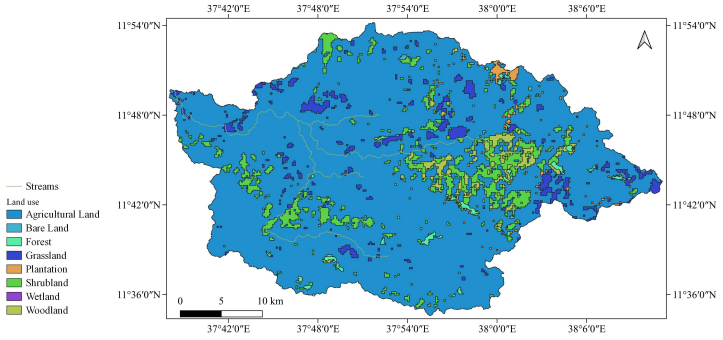

Figure 3.11: Land use map of the Gumera Watershed from 1989 to 2009.

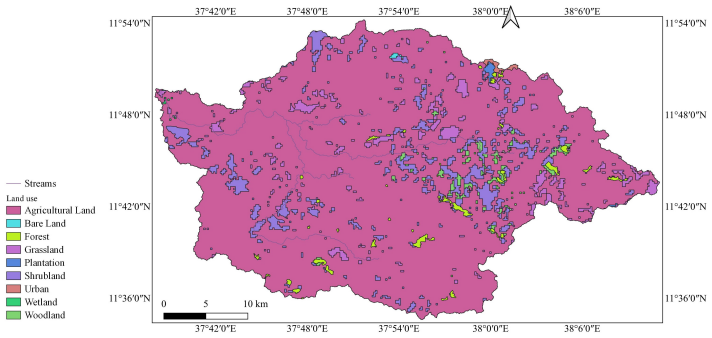

Figure 3.12: Land use map of the Gumera Watershed from 2010 to 2015.

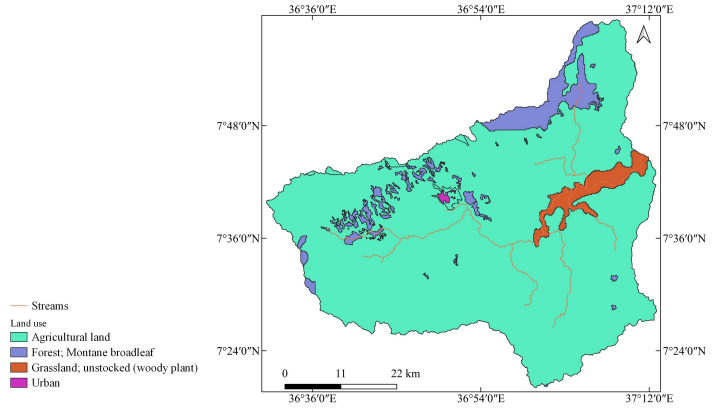

Figure 3.13: Land use map of the Gilgel Gibe 1 Watershed from 1989 to 2009.

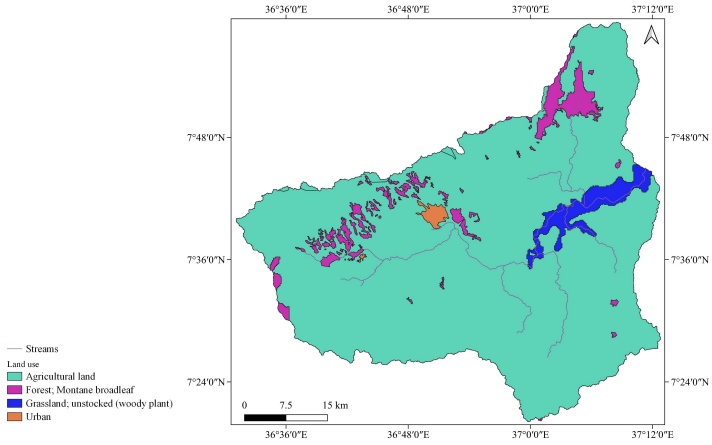

Figure 3.14: Land use map of the Gilgel Gibe 1 Watershed from 2010 to 2015.

3.2.3 Preparation of Stream Networks

We use the DEM to delineate a watershed and to generate streams. Based on the DEM alone, generating a proper stream direction in a flood plain is difficulty. In real situations, meandering in an alluvial area and construction of diversion structures change the normal course of a river or stream direction that may not be addressed by delineating the DEM alone. Therefore, to guide the stream direction during the delineation of the watershed, we should include a separate streams shape file. We need this file as input data during the

application of the SWAT+ model (see section 3.8.2). The stream networks of the Hombole Watershed are given in figure 3.15. For other watersheds under our consideration, we do not need to prepare stream networks (see section 3.8.1).

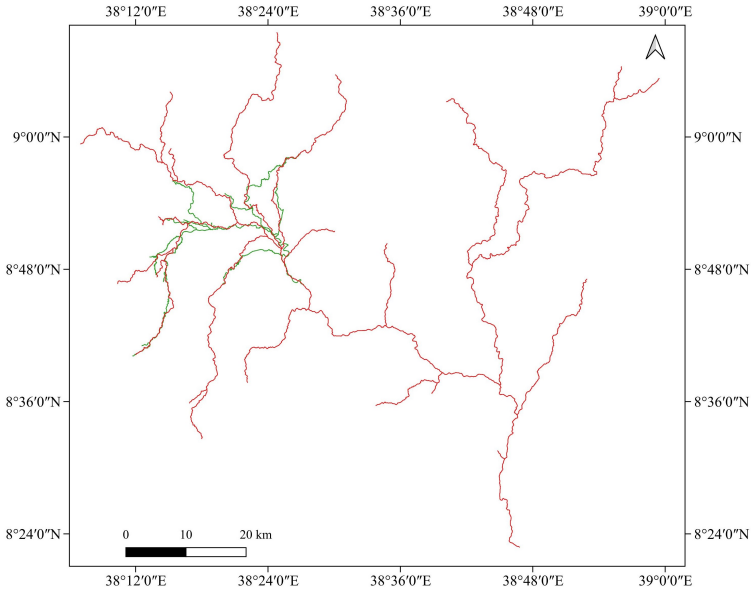

Figure 3.15: Streams networks of the Hombole Watershed.

In figure 3.15, the red color indicates the stream networks that were generated from the DEM whereas the green color indicates the stream networks that we prepared by digitizing the satellite image of the Google Earth Pro.

3.2.4 Data Review

It is essential to review data based on both quality and quantity perspectives for the selection or definition of an appropriate modeling approach. From this perspective, we assess the distribution and density of climatic stations and the relationship between rainfall, flow, sediment, and land use change. We use the Thiessen polygon to represent the area coverage of each climatic station. The distributions of the climatic stations of each watershed are given in figures 3.16 – 3.18.

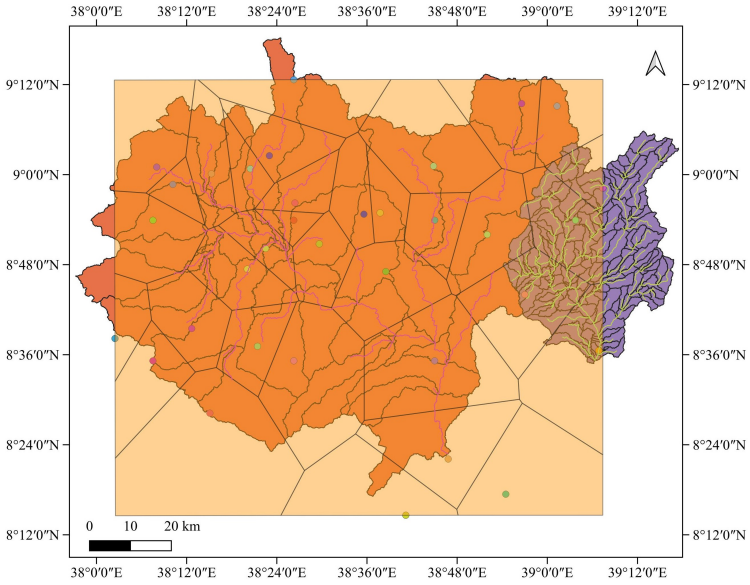

Figure 3.16: Distributions of climatic stations for the Hombole and Mojo Watersheds

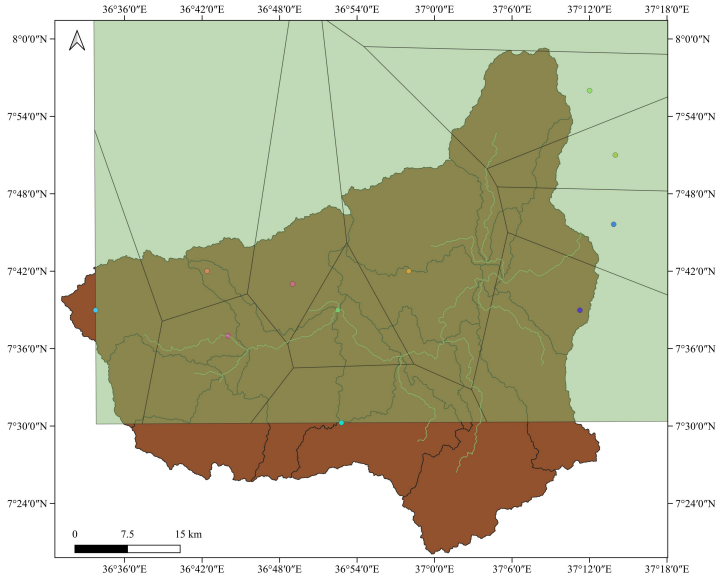

Figure 3.17: Distribution of climatic stations for the Gilgel Gibe 1 Watershed

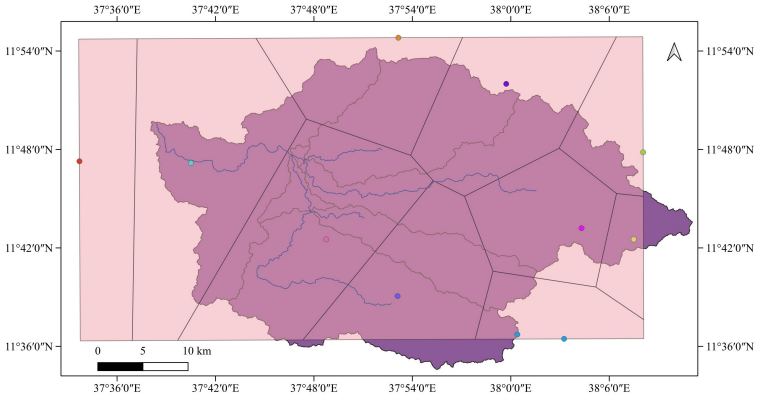

Figure 3.18: Distribution of climatic stations for the Gumera Watershed

From figures 3.16 – 3.18, we can see that the parts of the watersheds which fall outside the Thiessen polygon. According to the Thiessen polygon, the existing climatic stations particularly for the Mojo and Gilgel Gibe 1 Watersheds are not enough to cover all areas.

Since rainfall, flow, sediment, and land use change are interrelated processes, we use graphs to study a logical relationship between monthly or daily average rainfall, flow, suspended sediment concentration data, and land use change.

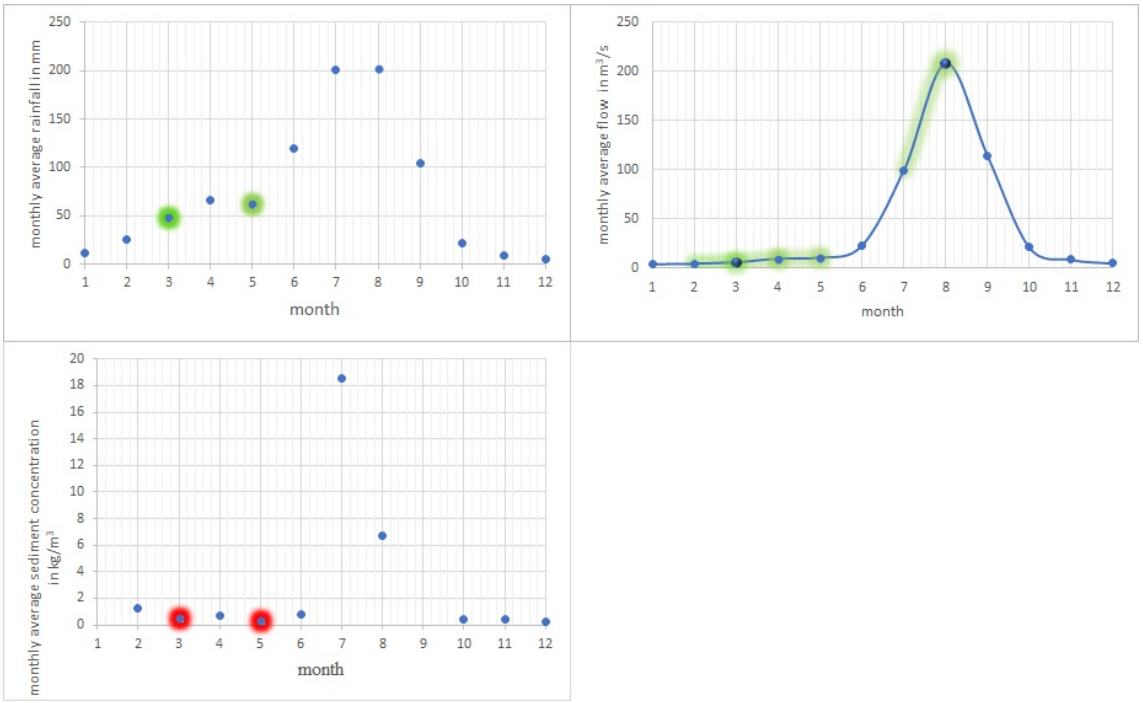

Figure 3.19: The relationship between monthly average rainfall, flow and suspended sediment concentration for the Hombole Watershed

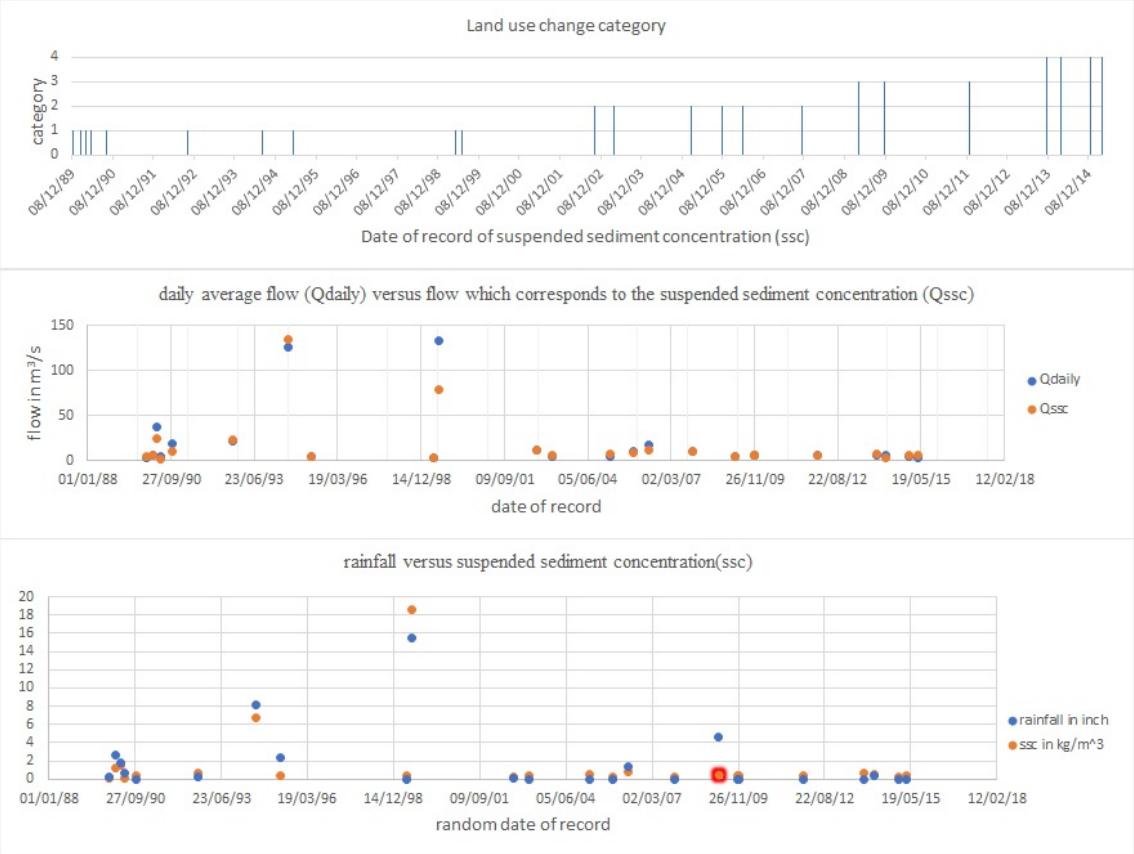

Figure 3.20: The relationship between daily average rainfall, flow and suspended sediment concentration and land use change for the Hombole Watershed.

From figure 3.19, we can see that there is a significant direct relationship between monthly average rainfall and flow. From figure 3.20, we can see that there is a significant direct relationship between daily rainfall and daily average flow regardless of land use change. In the figure, there is an insignificant difference between the daily average flow and the average flow corresponding to the suspended sediment concentration; there is also a significant direct relationship between the daily rainfall, the average flow and sediment in the period between 1989 – 2000. Based on figure A1, we do not see land use change in this period (i.e., between 1989 – 2000). There is insignificant indirect relationship between the monthly average rainfall/flow and sediment (see the highlighted data points in figure 3.19). But, there is a significant indirect relationship between the daily rainfall/flow and sediment in the record period between 2007 – 2009 (see the highlighted data points in figure 3.20). This may be because of land use change (i.e., we see less agricultural and more urban areas in the period between 2007 – 2009 as compared with an agricultural and urban land areal coverage in the period between 1989 – 2000 (see figure A1).

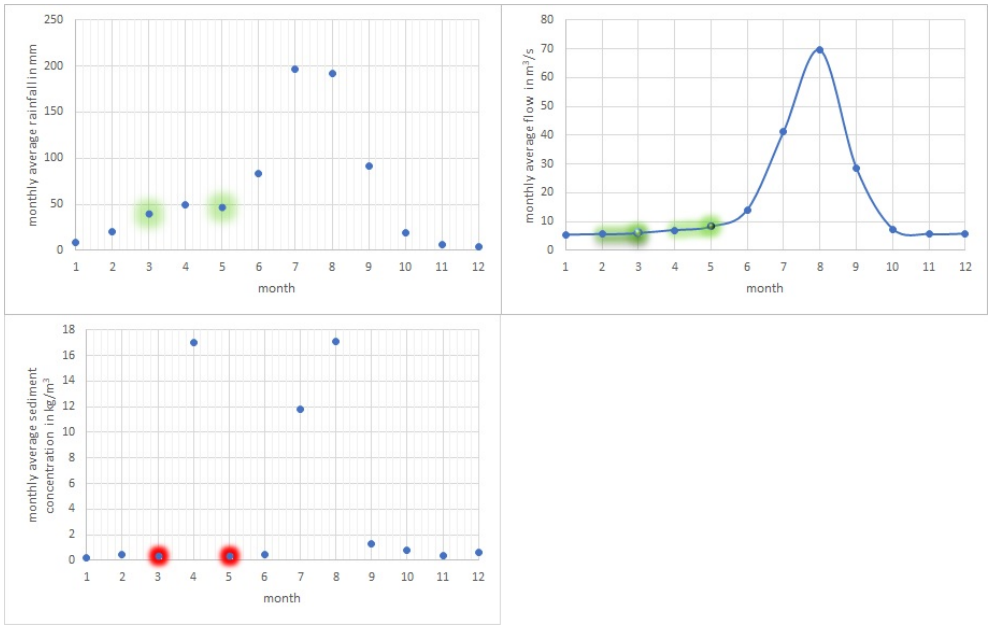

Figure 3.21: The relationship between monthly average rainfall, flow and suspended sediment concentration for the Mojo Watershed

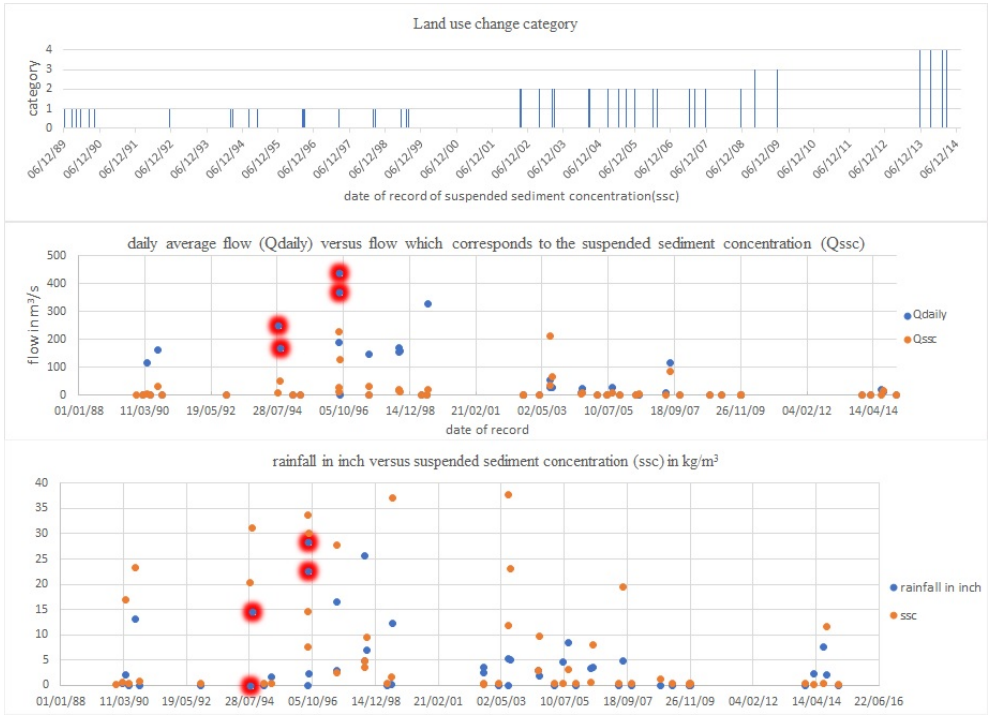

Figure 3.22: The relationship between daily average rainfall, flow and suspended sediment concentration and land use change for the Mojo Watershed

From figures 3.21, we can see that there is a direct relationship between monthly average rainfall and flow; there is a significant irregular relationship between the monthly rainfall/flow and sediment. From figure 3.22, there is a significant difference between

daily rainfall, daily average flow, and the average flow corresponding to the suspended sediment concentration. For example, if we consider two record periods August 5, 1994, and August 30, 1994, the daily rainfall increased; the daily average flow decreased; the flow corresponding to the suspended sediment concentration increased; there is a significant difference between the daily average flow and the average flow corresponding to the suspended sediment concentration; there is a significant change in the daily rainfall from 0 to 381 mm. Based on figure A2, we do not see land use change in the period between August 5 and 30, 1994. If we consider two record periods August 7 and 15, 1996, the daily rainfall decreased; the daily average flow increased; the average flow corresponding to the suspended sediment concentration decreased; there is a significant difference between the daily average flow and the average flow corresponding to the suspended sediment concentration; there is a significant decrease in the daily rainfall. Based on figure A2, we do not see land use change in the period between August 7 and 15, 1996. In general, there is an irregular relationship between the daily rainfall/flow and sediment.

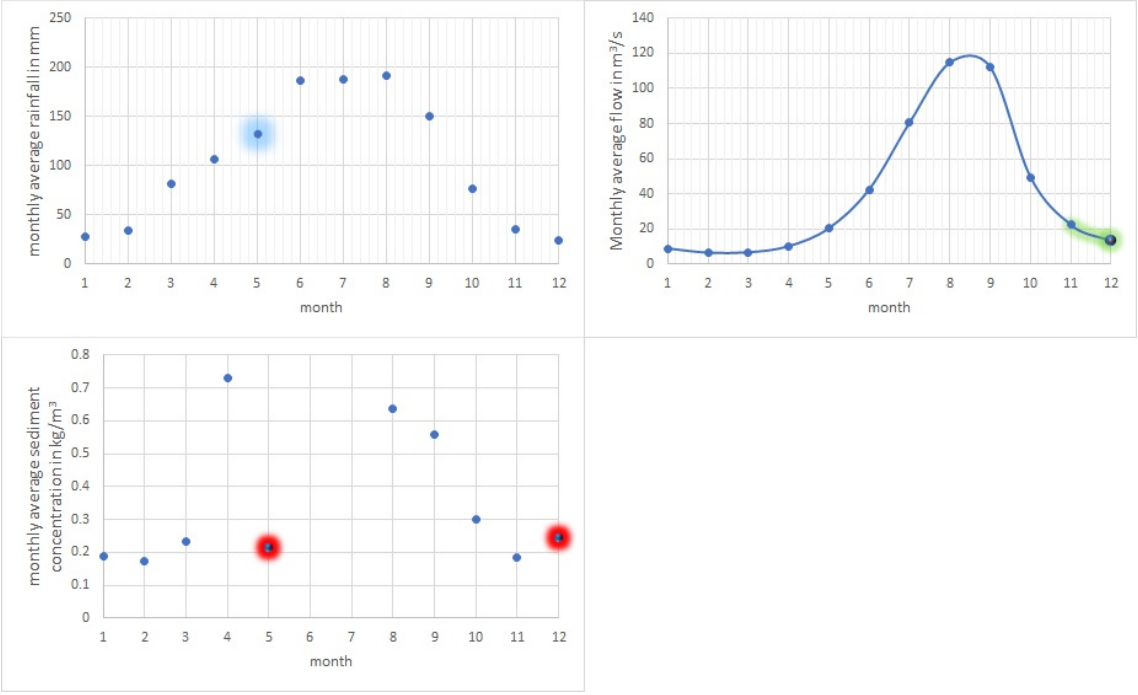

Figure 3.23: The relationship between monthly average rainfall, flow and suspended sediment concentration for the Gilgel Gibe 1 Watershed

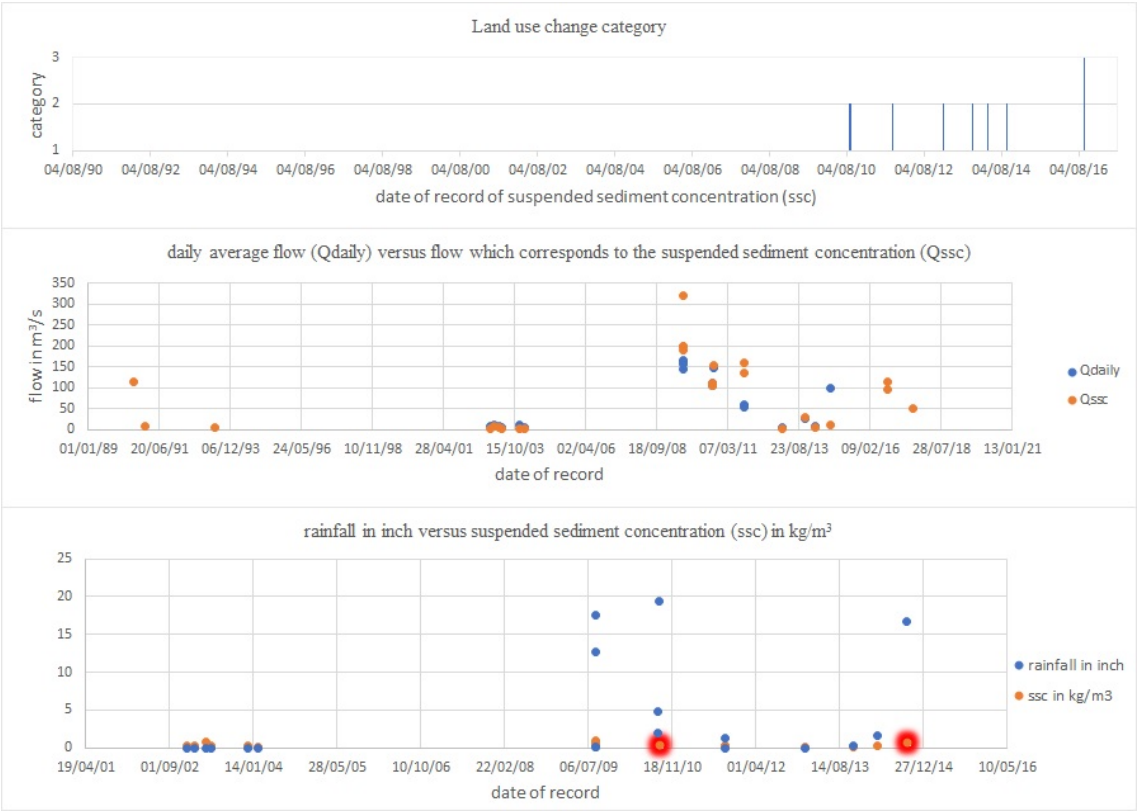

Figure 3.24: The relationship between daily average rainfall, flow and suspended sediment concentration and land use change for the Gilgel Gibe 1 Watershed

From figures 3.23, there is a direct relationship between monthly average rainfall and flow. From figures 3.24 and 3.23, there is an irregular relationship between daily or the monthly average rainfall/flow and sediment. There is a significant difference between the daily average flow and the average flow corresponding to the suspended sediment concentration.

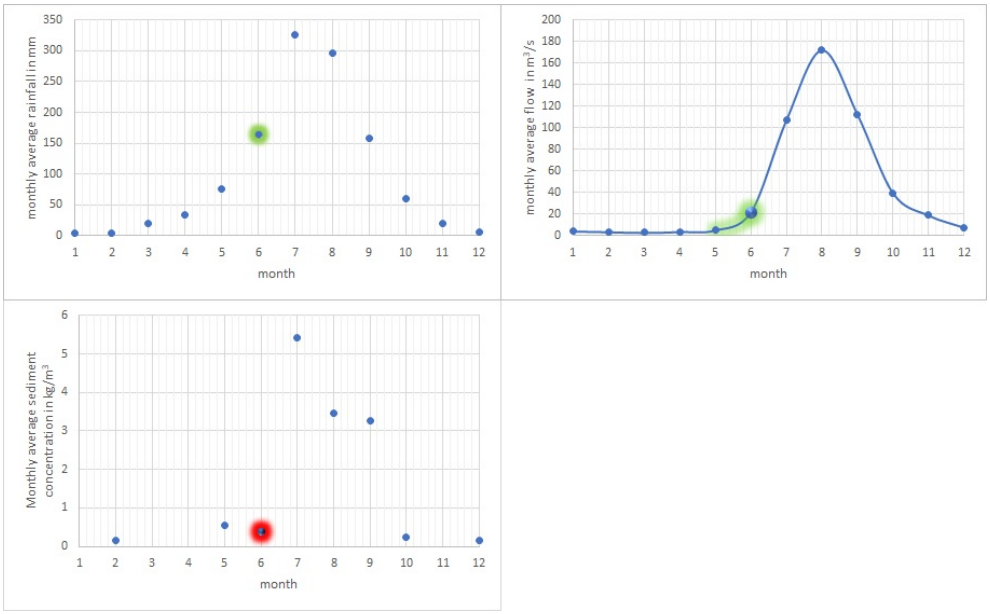

Figure 3.25: The relationship between monthly average rainfall, flow and suspended sediment concentration for the Gumera Watershed

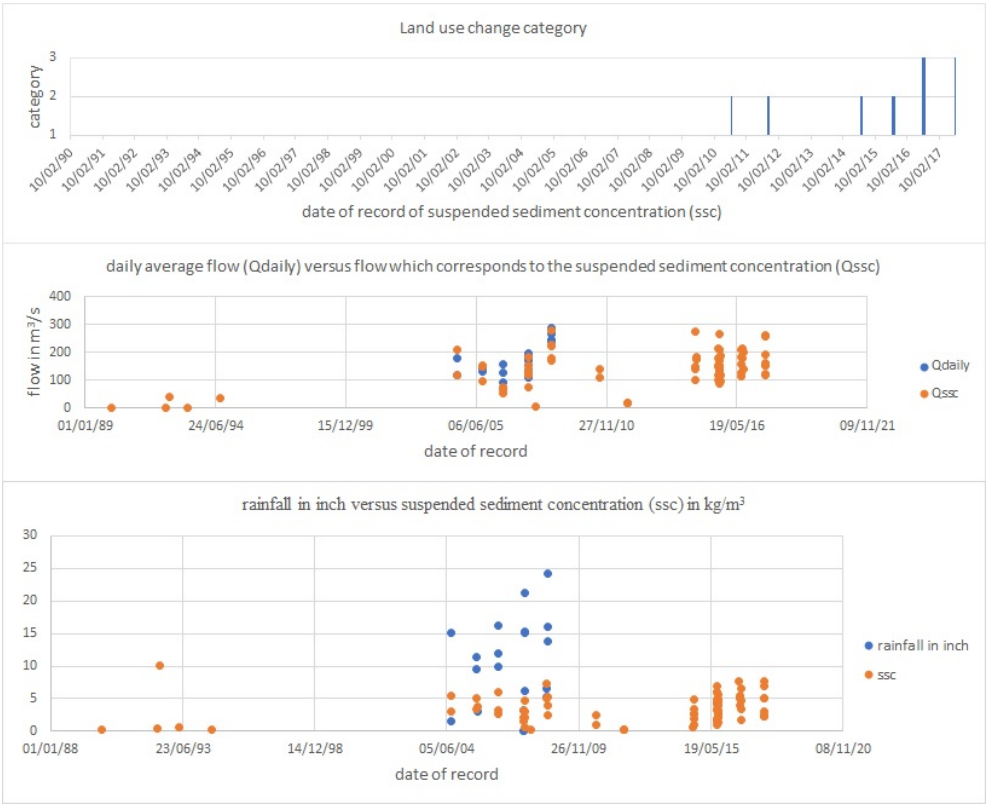

Figure 3.26: The relationship between daily average rainfall, flow and suspended sediment concentration and land use change for the Gumera Watershed

From figure 3.25, there is a direct relationship between monthly rainfall and flow. There is an insignificant indirect relationship between the monthly average rainfall/flow and

sediment (see the highlighted data points in figure 3.25). From figure 3.26, there is an irregular relationship between daily rainfall/flow and sediment. There is a significant difference between the daily average flow and the average flow corresponding to the suspended sediment concentration.

From the above relationships (for all watersheds), the irregular relationship between the daily or monthly rainfall/flow and sediment may be linked to the temporal and spatial variation of flood or erosion control works, the temporal and spatial scale of the land use change, and very limited suspended sediment concentration data for the calculation of the monthly average suspended sediment concentration. The direct relationship between the monthly average rainfall and flow, and the irregular relationship between the daily average rainfall and flow may be linked to the data manipulation. For instance, in a daily data record, over and underestimation is common; if the daily data is expressed in terms of monthly or yearly data, over and underestimation may balance each other. Therefore, in terms of data point of view (i.e., both quality and quantity perspective), sediment yield estimation at monthly time step is preferred.

3.2.5 Preparation of Sediment Rating Curves

A sediment rating curve is required to generate sediment data from corresponding flow data. The linear regression equation and nonlinear regression equations, such as power function, the second and third-order polynomial function can be used to model the sediment rating curve (e.g., Horowitz (2003)). Different authors indicate that the power function is a commonly used nonlinear regression approach to model the sediment rating curve (e.g., Asselman (2000); Hapsari et al. (2019); Heng and Suetsugi (2014)). The power function is given by:

$$C = aQ^b \tag{3.1}$$

where C is the suspended sediment load or concentration, Q is the discharge, a is the coefficient, and b is the exponent. Different authors reviewed physical meanings associated with the coefficient a, and the exponent b (e.g., Efthimiou (2019); Heng and Suetsugi (2014); Talebia et al. (2015)). Accordingly, the coefficient a represents an index of soil erodibility, whereas the exponent b is considered as an index of erosivity and transport capacity of a river. Thus, the power function can be derived by interpreting or deducting the MUSLE, where its topographic, soil erodibility, cover, and conservation practice factors describe a site-specific condition of a given watershed, and these factors affect the coefficient a of the power function at defined hydro-climatic conditions.

For the sake of simplicity of regression analysis, the nonlinear regression equation (in our case, the power function) can be transformed to the simple linear regression equation by log-transform of both sides of the nonlinear equation. Accordingly,

$$log(C) = log(a) + blog(Q) \tag{3.2}$$

$$\text{If } y = log(C), d = log(a) \text{ and } x = log(Q) \text{ then, } y = bx + d \tag{3.3}$$

The Least Squares, Reduced Major Axis Line (R.M.A.L) or other regression methods can be applied to find the best-fit regression line on logarithms of the suspended sediment load or concentration and discharge data, and back transform of the linear equation results

in the power function. Despite that there are no generally accepted procedures to model the sediment rating curve, we proceed with the Least Squares regression method, which is based on the minimum sum of squared errors to estimate the coefficient b and the constant d of the best-fit linear regression equation on logarithms of suspended sediment concentration and discharge data.

$$b = \frac{\sum_{i=1}^{n}(x_i - \bar{x})(y_i - \bar{y})}{\sum_{i=1}^{n}(x_i - \bar{x})^2} \tag{3.4}$$

$$d = \bar{y} - b\bar{x} \tag{3.5}$$

Apart from choosing sediment load–discharge (Balamurugan, 1989), logged mean loads within discharge classes (Talebia et al., 2015) or sediment concentration–discharge (Horowitz, 2003) approaches, correction factors ($y = CF * aQ^b$) (e.g., Asselman (2000); Talebia et al. (2015)) and power function with some additive constant (Asselman, 2000; Doomen et al., 2008) can be used to improve the sediment rating curve. Furthermore, to improve the sediment rating curve, we may use the data consistency or homogeneity test in order to determine the data classes at specific hydro-climatic conditions.

While considering the above advantages and limitations to model the sediment rating curve, the relationship between discharge and the suspended sediment concentration rate is checked against land-use changes, seasonal weather variations or rainfall patterns, and period of land tillage. Accordingly, the sediment rating curve that is drawn while considering the rainfall and discharge relationship for the Gilgel Gibe 1 Watershed, shows some improvement provided that one extreme discharge 319.65 m^3s^{-1} on 23 August 2009 (no similar record in the daily average discharge from 1990 to 2015), which corresponds to the suspended sediment concentration 0.53 kgm^{-3}, is removed from the records as part of the data quality check.

In addition, some data replication was possible for improving the sediment rating curve due to the assumption that two measurements that were taken at very small time differences were almost the same, as we only considered a pattern of the record rather than a period of the record, and the data record also did not show watershed information. Accordingly, the sediment rating curve is drawn for the Gumera Watershed, showing some improvement (the change in the coefficient of determination is from $R^2 = 0.324$ to $R^2 = 0.5091$).

For the Hombole and Mojo Watersheds, the sediment rating curves are drawn without any pre-conditions. This is because the above pre-conditions do not work for these two watersheds. For the Mojo Watershed, two inconsistent records of the rainfall (extremely large and small), flow and sediment on 7 August 1996 and 6 August 2003, are removed from the records as part of the data quality check. The sediment rating curves of all watersheds are given in figure 3.27.

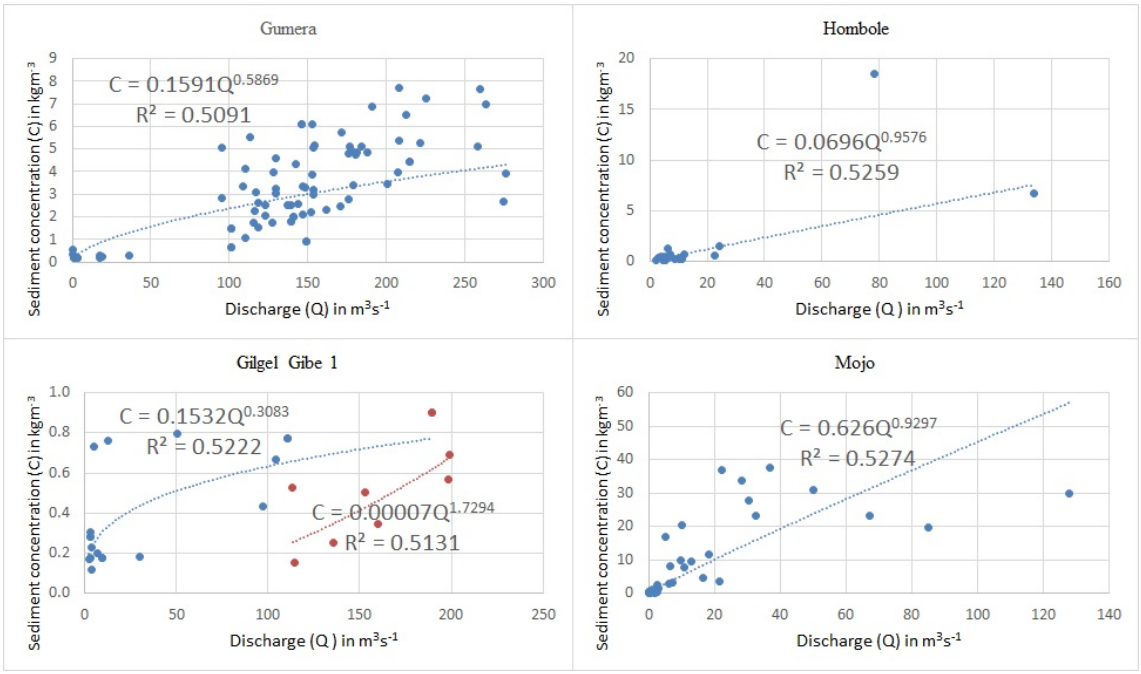

Figure 3.27: Sediment rating curves for each watershed under our consideration.

3.3 General Considerations for Regionalizing or Improving the MUSLE

We take into account the simulation time step, HRU, and calibration parameters to regionalize or improve the MUSLE.

a) Consideration of the simulation time step

Daily sediment yield may not reflect daily watershed information such as land cover, soil erodibility, and conservation activities. The reason for this can be soil erosion, sediment transport, deposition, consolidation, and re-suspension are quite complex processes, which depend on physical, biological, mechanical, and chemical activities within a large heterogeneous watershed. Due to these complex processes, the soil that was eroded at an unknown last time can be transported, deposited, consolidated, re-suspended, and reached an outlet at a different time. Therefore, measured sediment at the outlet at the current time may not reflect the current information about the watershed; it rather reflects the unknown last time. This may be because sediment that was deposited along the length and the bottom of the slope by small runoff energy at a previous time, can be transported by high runoff energy at the current time. In the original development of the USLE, the annual soil erodibility factor was taken to compute the annual soil loss from the unit plot. Based on Wischmeier and Smith (1978) formulation, we can conclude that the annual soil erodibility is the average of soil erodibility ranging from loose to compacted soil due to rainfall impact. As the soil erodibility factor of the USLE and MUSLE is the same, the annual time step is preferred over the daily time step (in the case of SWAT model). The annual simulation time step enables us to take into account gully erosion (gully erosion is usually estimated on an annual basis (Soil Conservation

Service, 1966); it is important to note here that gully erosion is a common problem in Ethiopia (eg.,Amare et al. (2021); Frankl et al. (2014); Haregeweyn et al. (2015, 2017); Krop aček et al. (2016))); to take into account gradual soil erosion process, and gradual changing activities like cyclic behavior of agricultural activities, conservation practice, flood protection activities, plant growth and harvest with respect to rainfall pattern and extreme events in a one-year full cycle.

b) Consideration of the HRU

If we consider the HRU in the SWAT model environment, as the number of HRUs becomes larger and larger, we better take into account spatial variability of land use, soil, and slope all over the watershed. To test the MUSLE at a watershed scale, sediment or flow routing in stream channels of SWAT model is not considered (it is important to note here that there is uncertainty in the definition of a channel, channel width, and depth in the SWAT model environment). Therefore, we only considered HRU to calculate the areal weighted average to capture the spatial variation of soil, cover, conservation practice, and topography.

c) Consideration of the calibration parameters

All parameters $(a, b, Q, q, K, L, S, C, P)$ of the MUSLE can potentially be used for calibration and validation (Pongsai et al., 2010). An et al. (2016) conducted global sensitivity analysis (Monte Carlo sampling) of the parameters of the MUSLE by using the extended Fourier amplitude sensitivity test (EFAST) method. Accordingly, the exponent **b** is the most sensitive parameter to predict the amount of soil loss, followed by **P**, **a**, **LS**, **C** and **q**, and **K's** influencing variables such as organic matter, soil structure class, and soil permeability class. In addition, Odongo et al. (2013) used Sobol's sensitivity analysis and found that the coefficient **a** and the exponent **b** are the most sensitive parameters of the MUSLE model contributing about 66% of the variability in the output sediment yield, at upper Malewa catchment in Kenya. On a storm event basis, Adegede and Mbajiorgu (2019) estimated the location parameters ($a = 12.4$ and $b = 0.51$) of the MUSLE for Ofuloko Watershed in Nigeria. In some studies, only the exponent of the model was calibrated, which is logically more acceptable as reviewed and reported by Sadeghi et al. (2014). The calibrated sediment does not reflect the actual soil erodibility and conservation practice factors on the ground unless otherwise they are measured. To accept our calibration, we should also check the calibrated value of the soil erodibility and conservation practice factors against the actual ones on the ground. This is because their product effect is reflected in the MUSLE rather than their individual effect during the calibration of sediment yield. Unless otherwise, we can not reach a certain conclusion that how these factors are really affecting the soil erosion process. For a given uniform watershed, the temporal variation of the soil erodibility, cover and conservation practice factors is expected. As the temporal variation of these factors is difficult to measure in a large watershed, we may estimate them through calibration. But, it is highly preferable if these factors are measured and studied at a temporal and spatial scale to understand their effect on soil erosion in a particular field. Any change in these factors affects the coefficient of the MUSLE, this is because only a product effect of the coefficient and these factors is reflected in the MUSLE rather than their individual effect during the calibration of sediment yield. As compared to the other parameters of the MUSLE, the

individual effect of the exponent of the MUSLE is reflected during the calibration of sediment yield. Therefore, estimating the exponent of the MUSLE through calibration is more feasible than other parameters of the MUSLE. For a given uniform watershed, the topographic factor does not change with time (i.e it has a constant effect), the effect of the topographic factor can be seen when the MUSLE is applied at different watersheds. From this explanation, the independent effect of the exponent and topographic factor of the MUSLE can be seen by applying the model at different watersheds. In general, runoff and sediment data reflect hydro-climatic conditions of a particular area, which independently affect the overall calibration process.

3.4 Regionalizing the MUSLE under the Hydro-climatic Conditions of Ethiopia

To regionalize the MUSLE under the hydro-climatic conditions of Ethiopia, we estimate the best exponent of the MUSLE, and we estimate the best combination of the exponent and topographic factor of the MUSLE by applying the model at different watersheds of Ethiopia. For the sake of the calibration procedure, the main factors of the MUSLE which directly affect the soil erosion process such as cover, conservation practice, soil erodibility, and topographic factors are estimated based on past experiences from literature and comparative approaches, whereas the parameters which do not directly affect the soil erosion process or which have no direct physical meaning (i.e coefficient **a** and exponent **b**) are estimated through calibration.

3.4.1 Estimating the Factors of the MUSLE

The original factors of the USLE represent the average value to estimate the annual sediment yield. The unit plot (Wischmeier and Smith, 1978) represents the worst case for the maximum soil erosion at a given rainfall event. It is practically impossible to directly measure each field slope, slope length, the temporal variation of soil erodibility, instantaneous runoff, cover change, and conservation practice for a large watershed. In the actual field, the field slope and length are not uniform, which means they are irregular. The topographic, soil erodibility, and cover and conservation practice factors depend on the spatial resolution of the DEM, soil, and land use maps, respectively.

Therefore, in the actual sediment modeling, average field slope length (Desmet and Govers, 1996) and slope steepness or simply topographic factor (Pongsai et al., 2010), average runoff, average soil erodibility factor (Gwapedza et al., 2018), and average cover and conservation practice factors are taken.

a) Estimation of the runoff factor

To estimate the runoff factor, the peak runoff rate and/or volume of runoff can be obtained by direct measurement of the runoff on a storm-event basis, as well as using indirect methods, such as the Soil Conservation Service Curve Number (SCS CN) method, Rational method, flood routing, unit hydrograph, etc. In our case, we used the daily average discharge to estimate the annual total runoff volume and yearly peak runoff rate for the annual sediment yield estimation. The reasons for why we use directly measured flow

data and why we estimate the annual sediment yield are addressed above.

b) Estimation of the soil erodibility factor

To choose the soil erodibility equations on the basis of the original definition of the soil erodibility by Wischmeier and Smith (1978), the following conditions should be fulfilled. From the MUSLE,

$$K = \frac{y}{a(Qq)^b * LSCP} \tag{3.6}$$

where K represents the worst condition for the maximum erosion case when the slope-field length is 22.13 m and the slope angle is 9%. In this case, no cover and conservation practices are employed in the field to give protection against soil erosion; the land is tilled up and down the slope, and therefore the maximum erosion is expected. In the above equation, K represents the maximum erosion case when the observed sediment yield (y) is due to soil erosion from a field with a specified slope length, slope angle, cover, and conservation practice.

If we take $C = P = 1$, K represents the maximum erosion from the field with the specified slope length and angle. However, our observed sediment yield does not represent the worst conditions for the maximum erosion case; we have some magnitude of the cover and soil conservation practice to give protection against soil erosion, and land is not tilled up and down the slope. Therefore, in this case, K represents the minimum value as compared to the actual value that will be obtained from the soil erodibility equation for the worst conditions for the maximum soil erosion case (K_{eq})

$$K_{min} = \frac{y}{aQ^bLS} << K_{eq.} \tag{3.7}$$

For our watersheds, the minimum K value is calculated by replacing the annual sediment load, outflow volume, and topographic factor (the reasons why we use the annual erodibility factor are given in section 3.3). However, at this point, the coefficient and exponent of the model are not known for our watersheds; therefore, the minimum reference value (K_{min}) is set. Based on the soil data we have, the actual soil erodibility factor is calculated using the soil erodibility equations that were proposed by David (1988); Wawer et al. (2005), and Williams and Renard (1983) as cited by Chen et al. (2011). Accordingly, the graphs of the K-factor are shown in figure 3.28.

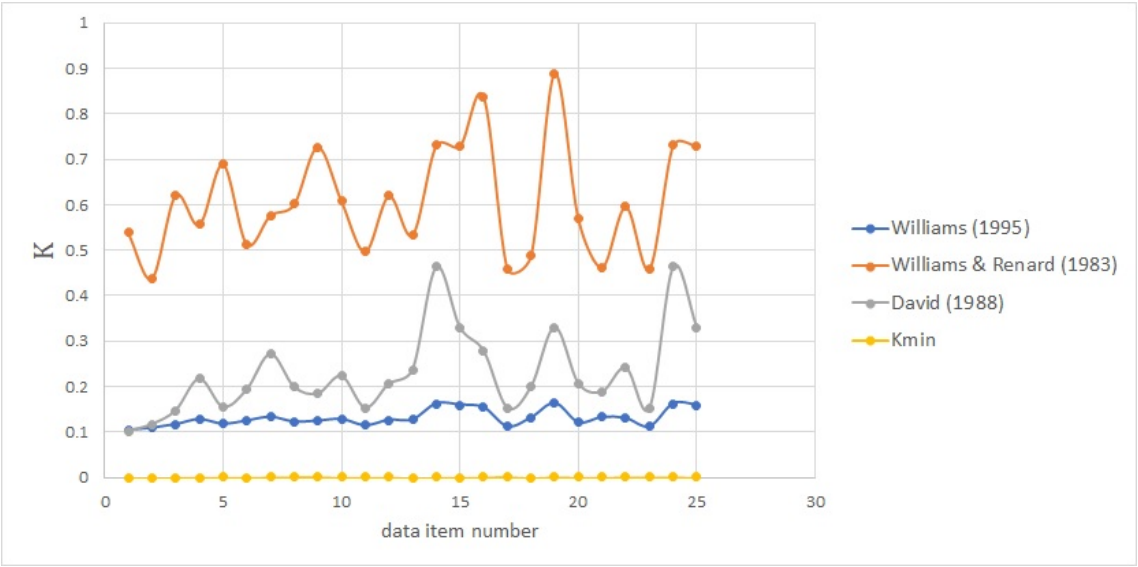

Figure 3.28: The K-factor graphs of different soil types, which represent any of the four watersheds under our consideration.

From the graph, a reasonable actual erodibility graph for our watersheds lies between the minimum K-factor graph and the calculated K-factor using Williams's (1995) equation as cited by Wawer et al. (2005). To proceed with Williams's (1995) equation as cited by Wawer et al. (2005), Williams's sub-K-factors are calculated and compared based on the silt and sand content, clay and silt content, and organic carbon content of our soil data. Comparatively speaking, the soil erodibility increases if the silt content increases, and the sand and clay content decreases. This is because the interaction between soil particles ranges from the loose interaction for silt soil to the strong interaction for clay soil. Humus, manure, organic matter, and the organic carbon content decreases soil erodibility as it binds the soil particles together, or it provides protective cover for the soil particles.

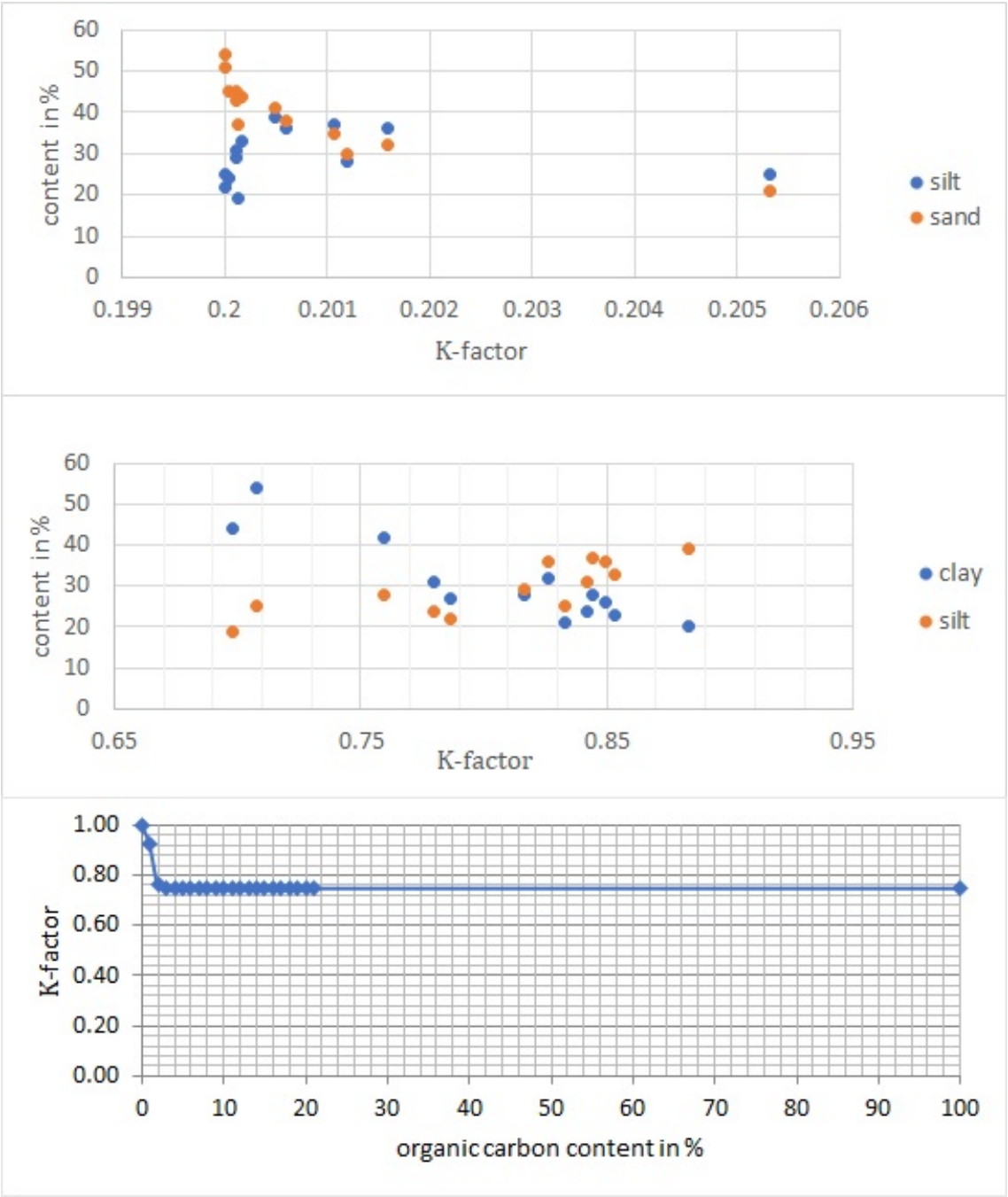

Figure 3.29: Comparison of sub-K-factors based on soil data, which represent any of the four watersheds under our consideration.

From figure 3.29, the soil erodibility factors conform to the general comparisons stated above. Therefore, we use Williams's (1995) equation as cited by Wawer et al. (2005) to calculate the soil erodibility factor using soil data of the watersheds under our consideration and watersheds of Ethiopia in general.

c) Estimation of the topographic factor

To estimate the topographic factor (LS-factor) for our watersheds, the SWAT+ model

is used to define as many HRU as possible to consider an areal distribution of the slope steepness and slope length. In the TxtInOut folder of the SWAT+ model, area and topography information of each HRU are stored in the hru.con and topography.hyd files, respectively. These files are exported to an excel spreadsheet for analysis.

The area, slope, and slope length of each HRU are used to estimate the LS-factor for each HRU using the equations of the topographic factor in section 2.1.2.1 and equations (3.8) and (3.9) in section 3.4.2. The weighted average of the LS-factors is taken to represent the watershed (at this point, it is important to note that the sediment or flow routing techniques in the SWAT+ model are not employed due to one or more reasons are stated above). The best-fit methods are chosen during the calibration of the annual sediment yield (see the calibration stage below).

d) Estimation of the cover factor (C-factor)

Although the C-factor value can be taken from the literature or determined in situ, an extensive literature review compiling the potential soil loss rates of different crop and forest covers compared to likely soil loss rates of bare soil can be used to determine likely C-factor values of a particular site (Benavidez et al., 2018). The published guidelines (Renard et al., 2011; Wischmeier and Smith, 1978), the revised C-factor (Cai et al., 2000) as cited by Luo et al. (2016) and the Normalized Difference Vegetation Index (Liu et al., 2020; van der Knijff et al., 2000) can be used to compute the C-factor. In our case, the annual or average annual cover factor for each land use category is adopted based on the assessment of the literature.

Benavidez et al. (2018) reviewed C-factors for the general types of land use and land cover. For our watersheds, the adopted cover factor for each land use is shown in table 3.1. To estimate an areal weighted average of the cover factor for our watersheds, SWAT+ model is used to define as many HRU as possible to consider the areal distributions of land use and land cover. In the TxtInOut folder of the SWAT+ model, the area of each HRU is stored in the hru.con file, and the HRU's land use data files are stored in the HRU-data.hru file.

These files are exported to an excel spreadsheet for analysis and calculation of the areal weighted average. We can use the shapefile of each land use map (see figures 3.7 – 3.14) to estimate the areal coverage of each land use classes in QGIS, and then the corresponding C and P-factors can be assigned.

Table 3.1: The assigned cover and conservation practice factors for each land use of the watersheds under our consideration.

Land use category	C**-Factor**	P**-Factor**
Acacia	0.01	1
Acacia Bushland/Thicket	0.01	1
Acacia Shrubland/Grassland	0.01	1
Agricultural land	0.525	0.52
Bare Land	1	1
Dispersed Acacia	0.01	1

Dispersed Shrub	0.01	1
Eucalyptus	0.001	1
Fir/Cedar Forest	0.001	1
Forest	0.001	1
Forest; Montane broadleaf	0.001	1
Grassland	0.01	1
Grassland, Herbaceous Wetland	0.01	1
Grassland; unstocked (woody plant)	0.01	1
Herbaceous Wetlands	0.01	1
Montane Broadleaf Evergreen Woodland	0.001	1
Rocky Bare Land	1	1
Secondary Semi-deciduous Forest/Woodland	0.001	1
Semi-Desert Grassland with Shrubland	0.01	1
Shrubland	0.01	1
Tropical Forest	0.001	1
Plantations	0.001	1
Tropical Plantations	0.001	1
Urban	0	1
Water Bodies	0	0
Wetland	0.01	1
Woodland	0.01	1

e) Estimation of soil conservation or erosion control practice factor (P-factor)

The soil conservation or erosion control practice factor can be estimated with the help of available tables (Wischmeier and Smith, 1978), using land use and land cover maps (Gwapedza et al., 2018; Jang et al., 2015; Luo et al., 2016), and through field measurement (refer the literature review report by Sadeghi et al. (2014)). For our case, the annual soil conservation practice factor for each land use category is adopted based on the assessment of the literature. Benavidez et al. (2018) reviewed the P factors for general types of land use and land cover. The adopted P factor for the land use and land cover category of each watershed is shown in table 3.1. The areal weighted average of the P factor was found in the same manner as the cover factor.

3.4.2 Estimating the Coefficient and Exponent of the MUSLE Through Calibration

For a chosen value of the exponent b, the best-fit corresponding value of the coefficient a is estimated through calibration. The selection of the best exponent and the best equation among listed above and below (see equations (3.8) and (3.9)) for the topographic factor is done after calibration of observed and simulated sediment (i.e., the MUSLE is used to estimate sediment load). Figure 3.30 shows sample graphs of the calibrated sediment when the topographic factor is calculated using the equation that was proposed by Wischmeier and Smith (1978).

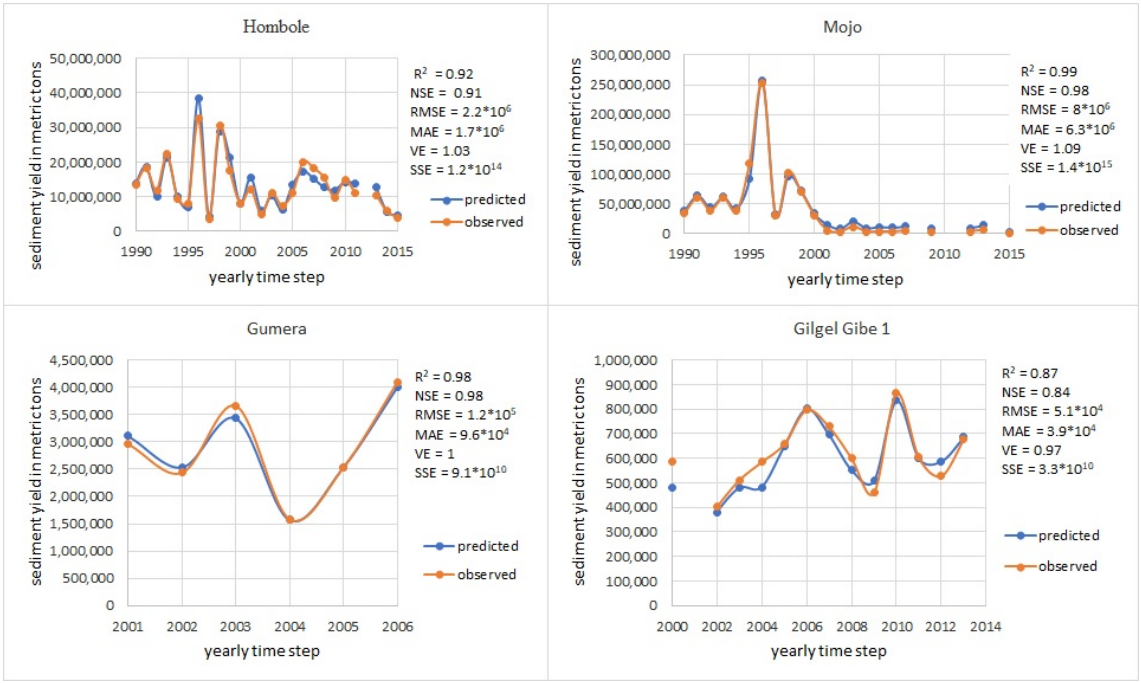

Figure 3.30: Sample graphs of observed and predicted sediment yield.

During calibration, the Nash-Sutcliffe efficiency corresponds to each LS-factor, the exponent b and the coefficient a is evaluated, and graphs of the exponent b versus the Nash-Sutcliffe efficiency, and graphs of the coefficient a versus exponent b are drawn for each watershed, as shown in figures 3.31 – 3.37. For a chosen value of b, we test seven different equations of the topographic factor for each watershed. Therefore, we can have as many graphs as possible.

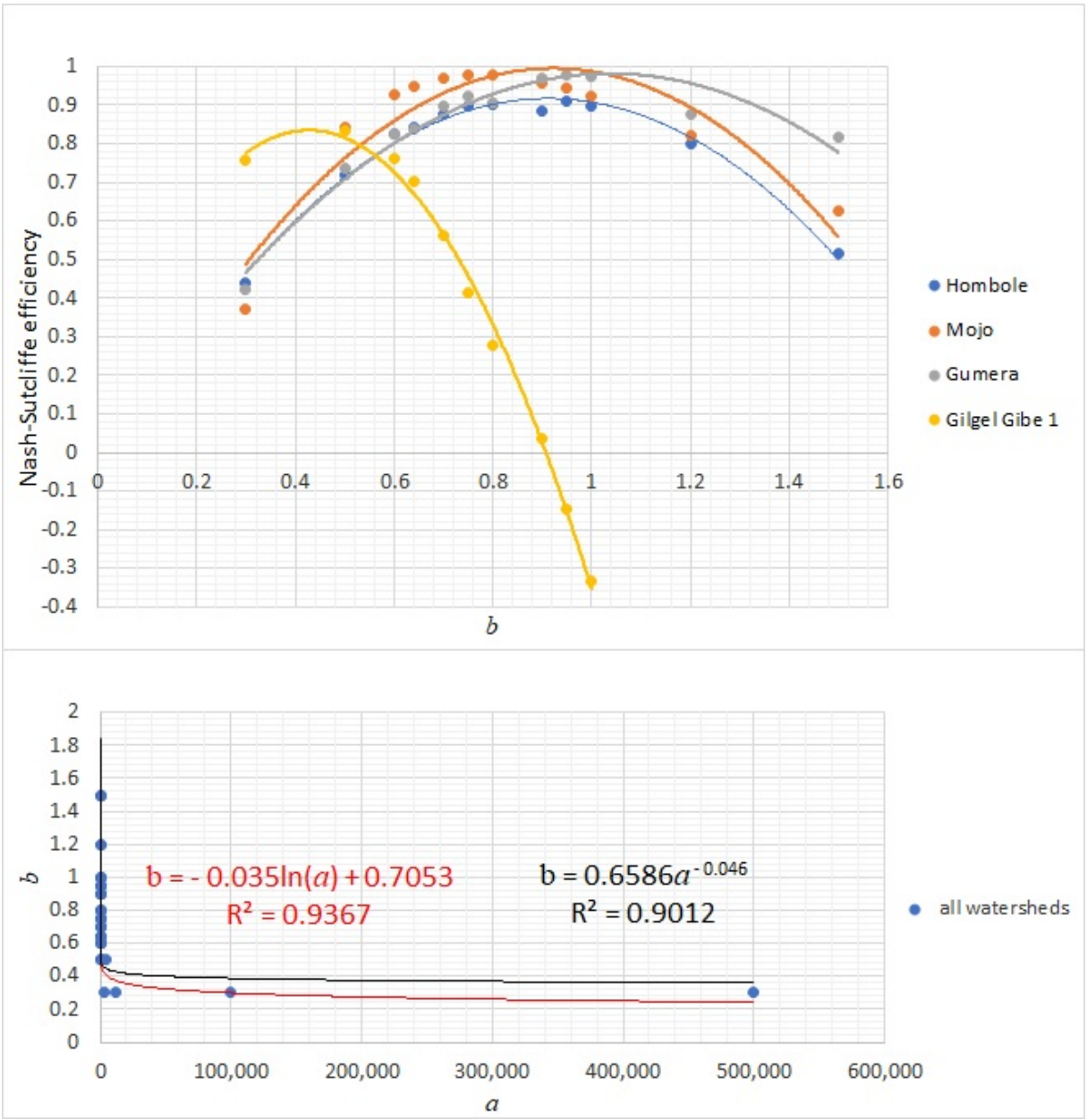

Figure 3.31: Therelationship between the exponent b versus the Nash–Sutcliffe efficiency as well as the coefficient a versus the exponent b when the topographic factor is calculated using the equation that was proposed by Wischmeier and Smith (1978).

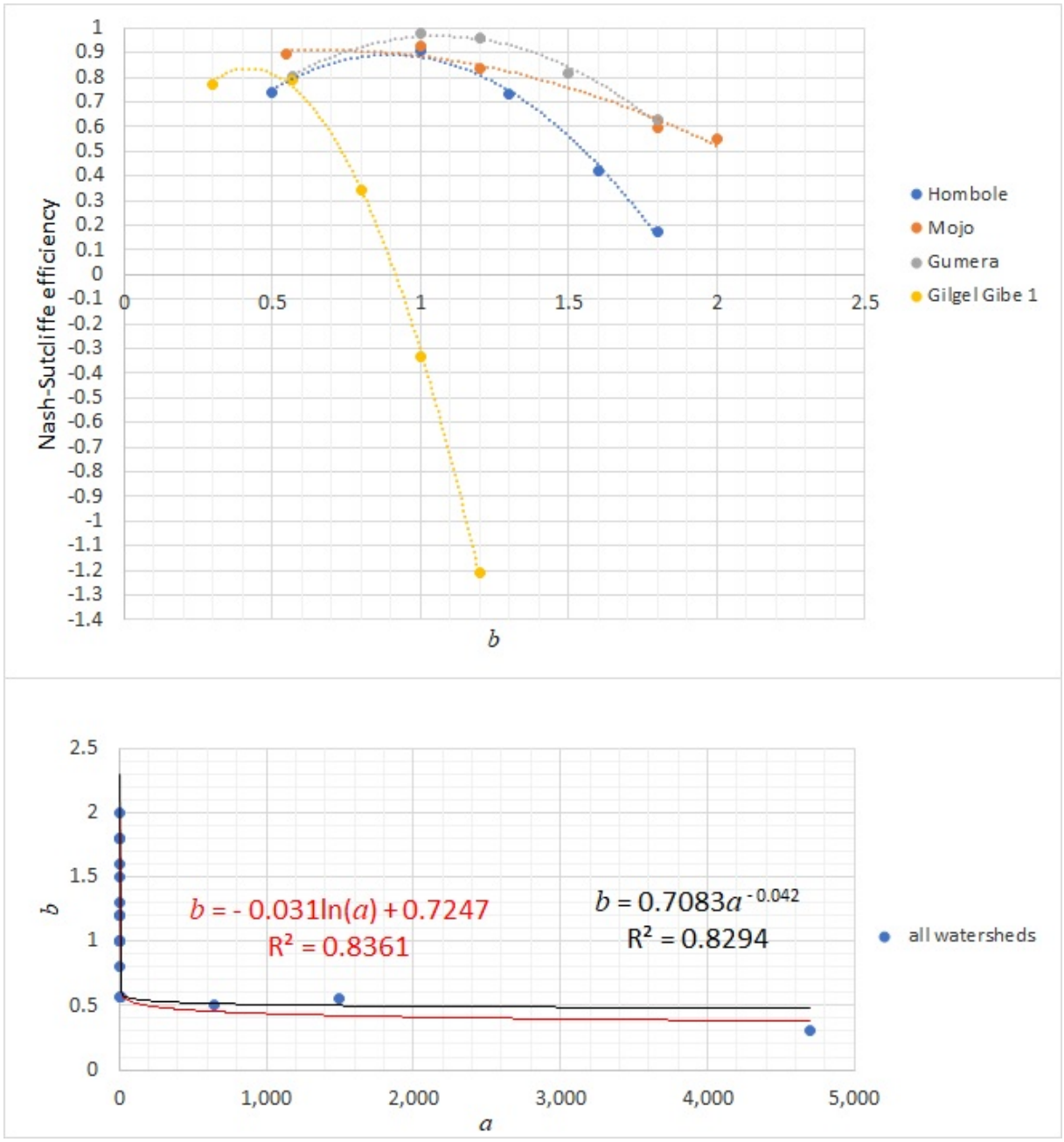

Figure 3.32: The relationship between the exponent b versus the Nash-Sutcliffe efficiency as well as the coefficient a versus the exponent b when the topographic factor is calculated using the equations that were proposed by Foster et al., (1977) and McCool et al., (1987, 1989), as cited by Renard et al. (1997).

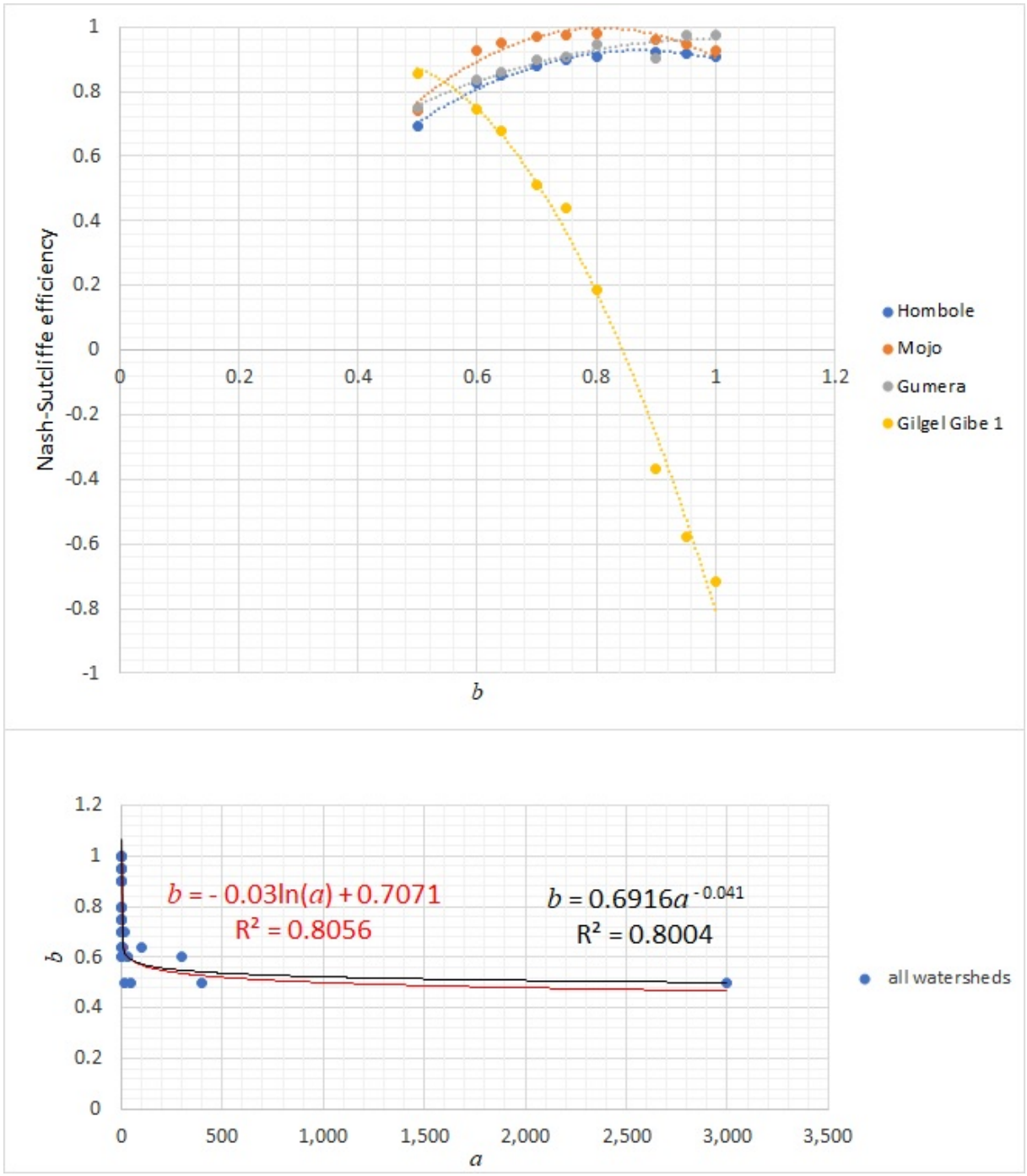

Figure 3.33: The relationship between the exponent b versus the Nash-Sutcliffe efficiency as well as the coefficient a versus the exponent b when the topographic factor is calculated using the equation that was proposed by Morgan (2005).

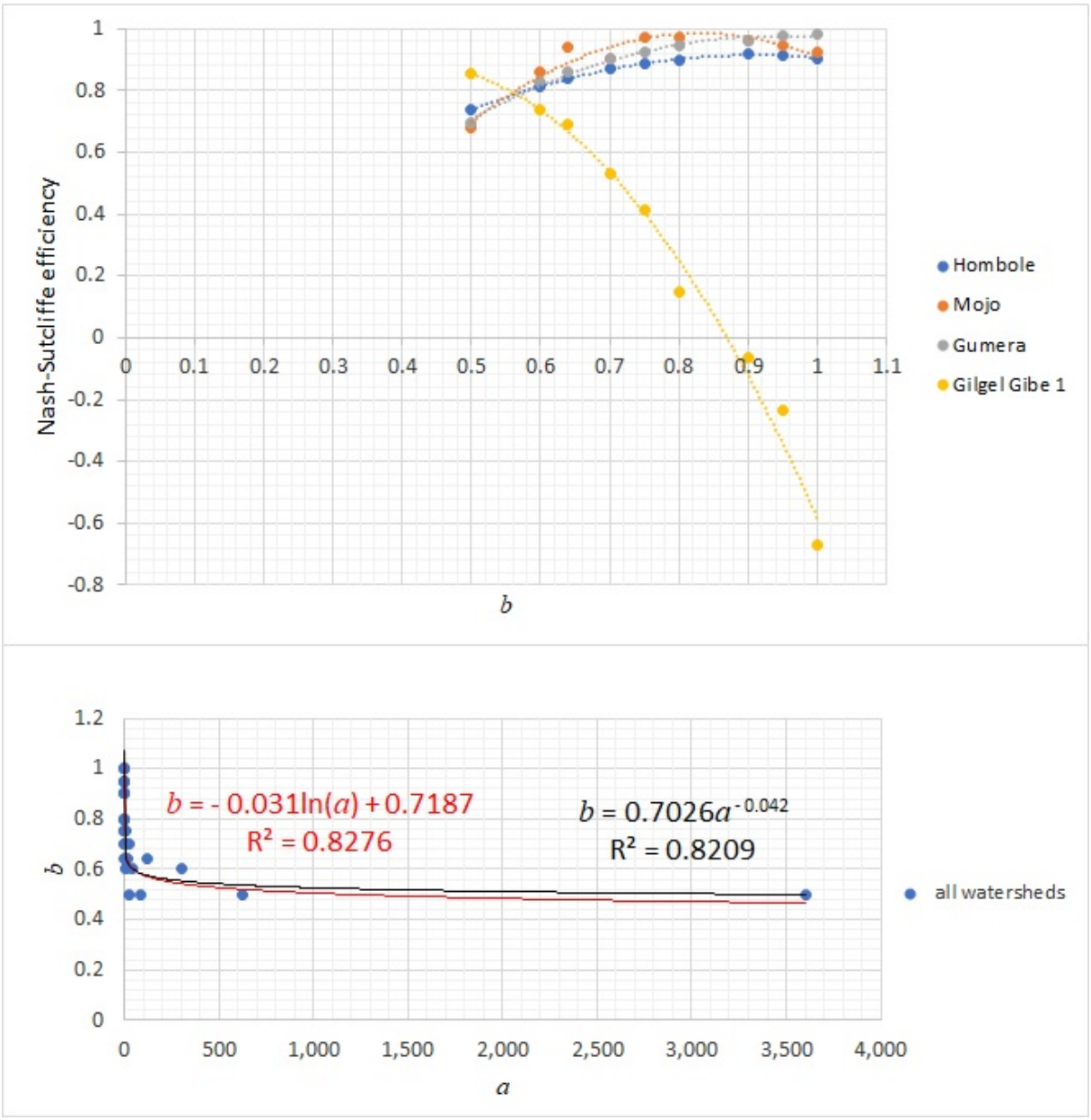

Figure 3.34: The relationship between the exponent b versus the Nash-Sutcliffe efficiency as well as the coefficient a versus the exponent b when the topographic factor is calculated using the equation that was proposed by McCool et al., (1987), as cited by Pongsai et al. (2010).

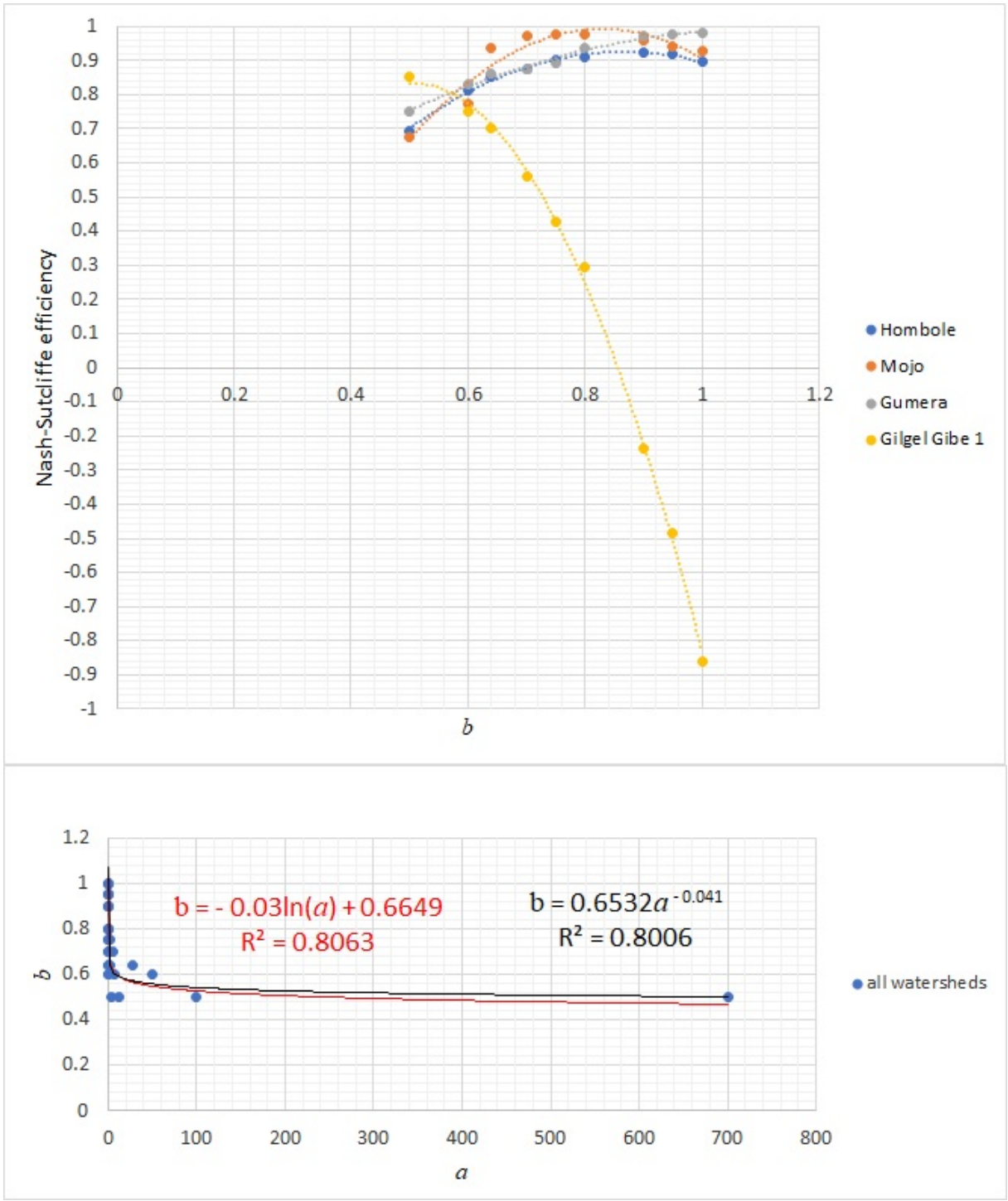

Figure 3.35: The relationship between the exponent b versus the Nash-Sutcliffe efficiency as well as the coefficient a versus the exponent b when the topographic factor is calculated using the equation that was proposed by David (1988).

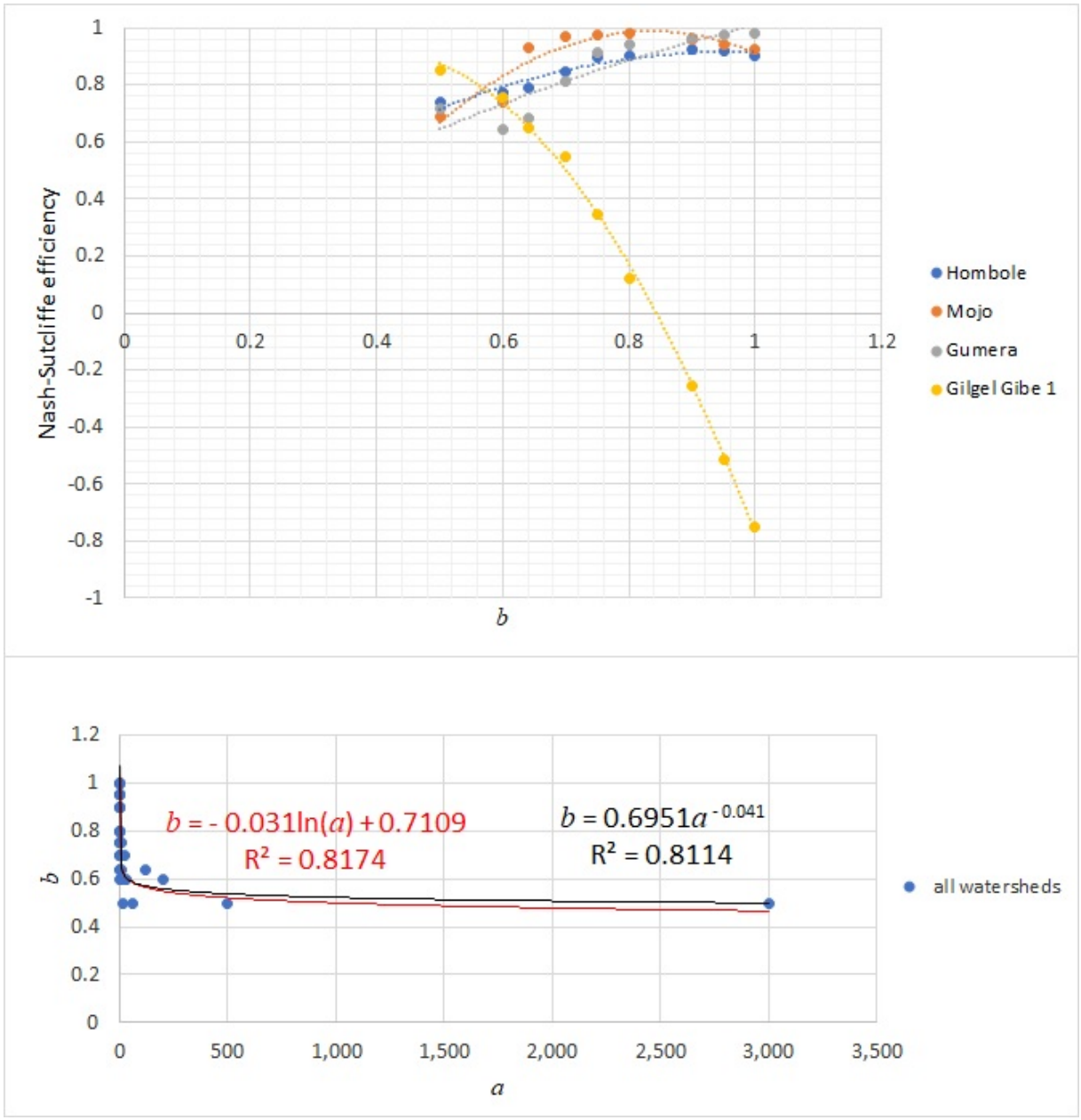

Figure 3.36: The relationship between the exponent b versus the Nash-Sutcliffe efficiency as well as the coefficient a versus the exponent b when the topographic factor is calculated using the Chines equation.

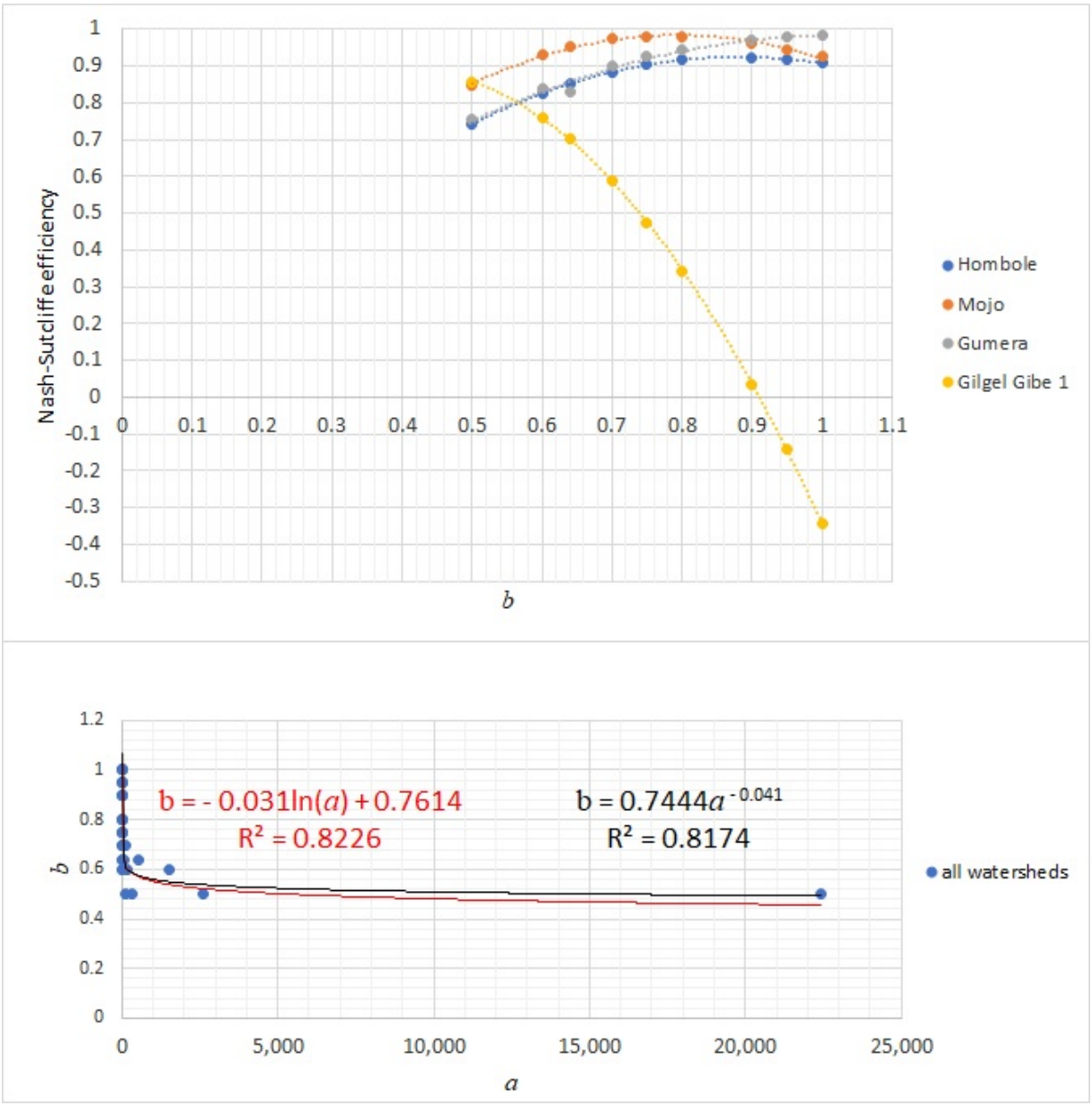

Figure 3.37: The relationship between the exponent b versus the Nash-Sutcliffe efficiency as well as the coefficient a versus the exponent b when the topographic factor is calculated using equations (3.8) and (3.9).

$$LS = (0.02222J^{1.5} + 0.03231J + 0.1004) * 0.2901 \triangle y^{0.4002} \text{ for } J < 5\% \quad (3.8)$$

$$LS = (0.02222J^{1.5} + 0.03231J + 0.1004) * 0.2105 \triangle y^{0.5004} \text{ for } J > 5\% \quad (3.9)$$

where$J$ is the slope in %, and $\triangle y$ is the slope length. For further description, readers are encouraged to watch the video at `https://www.youtube.com/watch?v=w6w8jxbTJfo` (accessed on 25 February 2021). For the case of the watersheds under our consideration, we take $\triangle y/22.1$ as the field slope length.

3.4.3 Verifying the Best Exponent of the MUSLE

As explained in section 3.3, the yearly simulation time step is preferred to address the gradual processes of soil erosion and sediment transport. It is important to prove whether a change in the simulation time step changes the coefficient and the exponent of the MUSLE or not. This approach leads us to find the best exponent of the MUSLE.

Proof

If we consider the small simulation time step and the small simulation period, we can maintain the temporal variation of the factors, which directly affects the soil erosion process. For a given field, no change in the cover, conservation practice, and soil erodibility factors of the MUSLE will be expected at the small simulation period. At the end of the simulation period, only in variation of the coefficient and the exponent of the MUSLE with the simulation time step affect sediment yield output (see the proof steps below for a change in runoff and the peak runoff rate).

If the variations of the coefficient and the exponent of the MUSLE with a small change in the simulation time step are detected, then the variations of the coefficient and the exponent with any other simulation time step are confirmed. For the sake of starting, let us consider one and two unit simulation time steps and two unit simulation period; no change in the factors of the MUSLE will be expected for about two unit simulation period. Therefore, soil loss from a field at the one unit simulation time step for about two unit simulation period, is equal to the sum of soil loss at the end of the first and next one unit time;

$$a_1(Q_1q_1)^{b_1}KLSCP + a_1(Q_2q_2)^{b_1}KLSCP \tag{3.10}$$

where suffixes 1 and 2 correspond to the runoff volume (Q), and the peak runoff rate (q) indicate the first and second simulation at the one unit simulation time step or interval. We note that K, L, S, C, and P are the same for the two unit simulation period, and the coefficient and the exponent are the same at the one unit simulation time step. Soil loss from the field at the two unit simulation time step for about a two unit simulation period;

$$a_2\left((Q_1+Q_2)q_1\right)^{b_2}KLSCP \text{ if the peak runoff rate is } q_1 \tag{3.11}$$

$$a_2\left((Q_1+Q_2)q_2\right)^{b_2}KLSCP \text{ if the peak runoff rate is } q_2 \tag{3.12}$$

where a_2 and b_2 indicate a value of the coefficient (a) and exponent (b) at the two unit simulation time step. We note that the total runoff volume (Q) at the end of the two unit simulation period, is equal to the sum of the runoff volumes at the end of the first and next one unit time; the peak runoff rate will be expected before one unit time or between 1 and 2 unit time.

In either case, sediment yield is the same. Therefore,

If the peak runoff rate is q_1

$$a_1(Q_1q_1)^{b_1}KLSCP + a_1(Q_2q_2)^{b_1}KLSCP = a_2\left((Q_1+Q_2)q_1\right)^{b_2}KLSCP \tag{3.13}$$

$$a_1(Q_1q_1)^{b_1} + a_1(Q_2q_2)^{b_1} = a_2\left((Q_1+Q_2)q_1\right)^{b_2} \tag{3.14}$$

If there is no variation of the coefficient and exponent with small variation in simulation time step, then $a_1 = a_2 = a$ and $b_1 = b_2 = b$

$$(Q_1 q_1)^b + (Q_2 q_2)^b = ((Q_1 + Q_2) q_1)^b \tag{3.15}$$

In the same way

If the peak runoff rate is q_2

$$a_1 (Q_1 q_1)^{b_1} KLSCP + a_1 (Q_2 q_2)^{b_1} KLSCP = a_2 \left((Q_1 + Q_2) q_2\right)^{b_2} KLSCP \tag{3.16}$$

$$a_1 (Q_1 q_1)^{b_1} + a_1 (Q_2 q_2)^{b_1} = a_2 ((Q_1 + Q_2) q_2)^{b_2} \tag{3.17}$$

If there is no variation of the coefficient with small variation in simulation time step, then $a_1 = a_2 = a$ & $b_1 = b_2 = b$

$$(Q_1 q_1)^b + (Q_2 q_2)^b = ((Q_1 + Q_2) q_2)^b \tag{3.18}$$

Equations (3.15) and (3.18) are false for a given value of the exponent b. In this case, the coefficient and the exponent of the MUSLE change as a change in simulation time step for a given total simulation period. Equations (3.15) and (3.18) hold true when $b = 1$ and $q_1 = q_2$, and for other values of the exponent b and $q_1 = q_2$, it is false. This implies that only one peak runoff rate is possible per storm event (i.e., from the beginning of runoff to the end of the runoff from a slope-field). This means that sediment is transported from the beginning of runoff to the end of the runoff; the objective of the MUSLE is to estimate the total sediment load transported from the beginning of runoff to the end of the runoff.

Therefore, the best theoretical exponent of the MUSLE is 1. This is a theoretical exponent because the left and right sides of equations (3.15) and (3.18) represent the theoretical linked expressions without knowledge of observed sediment. The actual exponent of the MUSLE is estimated by applying the model at selected watersheds. From all graphs (see figures 3.31 – 3.37), the best actual exponent of the MUSLE is 1, which results in a Nash-Sutcliffe efficiency of approximately 1 irrespective of the topographic factor and the three watershed sizes (i.e., the Hombole, Mojo, and Gumera Watersheds). Therefore, the best exponent of the MUSLE is 1.

3.5 Improving the MUSLE by Physical Interpretation of its Factors

The assumption of the USLE and RUSLE is that the rainfall intensity is uniformly distributed over a slope field area. Likewise, in the case of the MUSLE, the runoff is uniformly distributed over the slope field area. The total runoff volume is considered for sediment yield modeling. In both cases, the slope length represents the worst condition for the maximum erosion case, and therefore, the slope length is the shortest distance from the origin of the runoff to the bottom of the slope. The underlying physical assumption to improve the MUSLE is that the amount of potential energy of the runoff is proportional

to the shear stress for sediment transport from a slope field and the kinetic energy of the runoff at the bottom of the slope field for gully formation. The potential energy of an object due to its position is given by

$$PE = mgh = \rho vgh \tag{3.19}$$

where PE is the potential energy, m is the mass of the object, g is the acceleration due to gravity, h is the height referring to the position of the object from a reference point, ρ is the density of the object, and v is the volume of the object.

In the process of all of the rainfall in the slope field area, the total potential energy of the runoff is given by (Li et al., 2017)

$$PE = \frac{\rho g}{4} BL^2 sin2\theta * Q \tag{3.20}$$

where PE is the total potential energy of the runoff (J), ρ is the density of water (kgm^{-3}), g is the acceleration due to gravity (ms^{-2}), B is the slope width (m), L is the slope length (m), θ is the slope angle, and Q is the runoff volume (m).

Equation (3.20) can be applied when the runoff volume flows down from the top of the slope field to the bottom of the slope field, and a temporal variation of the runoff volume is considered. However, this equation does not consider every other runoff volume that will begin at every slope height and flows down simultaneously to the bottom of the slope (i.e., the runoff that will start from any point on the entire slope surface due to the uniform distribution of rainfall on the entire slope field), and it also does not consider a temporal variation of every other runoff volume. Therefore, let us assume that every runoff volume due to raindrops on the entire slope length flows down to the bottom of the slope. Let us say the position of first runoff volume, as well as those of the second, third, and so on along the length of the slope are at the slope heights h, h_1, h_2, and so on from the bottom of the slope, respectively. One runoff volume takes over the position of another runoff volume as it flows down to the bottom of the slope.

The total potential energy of the first runoff volume due to its changes in position as it flows down from the height h to the bottom of the slope is equal to E_1:

$$E_1 = \int_0^h \rho vghdh \tag{3.21}$$

The total potential energy of the second runoff volume due to its changes in position as it flows down from the height h_1 (let us say just immediately after the first runoff volume) to the bottom of the slope is equal to E_2:

$$E_2 = \int_0^{h_1} \rho vghdh \tag{3.22}$$

The total potential energy of the third runoff volume due to its changes in position as it flows down from the height h_2 (let us say just immediately after the second runoff volume) to the bottom of the slope is equal to E_3, and so on:

$$E_3 = \int_0^{h_2} \rho vghdh \tag{3.23}$$

Therefore, the total potential energy of all runoff volumes due to their change in position along the length of the slope to the bottom of the slope is equal to E_t:

$$E_t = E_1 + E_2 + E_3 + \cdots + E_n \tag{3.24}$$

Then, we can substitute equations (3.21–3.23) into equation (3.24):

$$E_t = \int_0^h \rho v g h dh + \int_0^{h_1} \rho v g h dh + \int_0^{h_2} \rho v g h dh + \cdots + E_n \tag{3.25}$$

$$\int_0^h \rho v g h dh + \int_0^{h_1} \rho v g h dh + \int_0^{h_2} \rho v g h dh + \cdots + E_n = \int_0^h \left(\int \rho v g h dh \right) dh \tag{3.26}$$

where h_1 and h_2 are the heights of the slope just immediately after heights h and h_1, respectively, and so on.

$$E_t = \int_0^h \left(\int \rho v g h dh \right) dh \tag{3.27}$$

Each runoff volume (dv) in a very small area (dA) changes in time (dt) with the rainfall intensity (i_{rain}) and soil infiltration rate (i_{soil}):

$$dv = h_{runoff} * dA \tag{3.28}$$

where h_{runoff} is the runoff depth:

$$h_{runoff} = (i_{rain} - i_{soil}) * dt \tag{3.29}$$

Then, we can substitute equation (3.29) into equation (3.28):

$$dv = (i_{rain} - i_{soil}) dt * dA \tag{3.30}$$

It is noteworthy that only the depth of the runoff volume changed with a small change in time. If it rained continuously for some duration of time, then the runoff volume increased at every point of the slope length. Therefore, the total runoff volume at a particular point of the slope field is a function of the runoff depth changing with time, where the bottom area of the runoff volume does not change with time:

$$v = \int dv = \int_0^t (dA * (i_{rain} - i_{soil}))\, dt \tag{3.31}$$

Substituting equation (3.31) into equation (3.27) yields

$$E_t = \int_0^h \left(\int \rho g h \left(\int_0^t (dA * (i_{rain} - i_{soil})) dt \right) dh \right) dh \tag{3.32}$$

For our case, the total potential energy per a unit area (e_t) is important parameter for soil erosion and sediment transport along the length of the slope, and therefore

$$e_t = \frac{E_t}{dA} \tag{3.33}$$

Substituting equation (3.32) into equation (3.33) yields

$$e_t = \frac{\int_0^h \left(\int \rho g h \left(\int_0^t (dA * (i_{rain} - i_{soil}))dt \right) dh \right) dh}{dA} \tag{3.34}$$

The bottom area of each runoff volume is constant, and therefore

$$\int_0^t (dA * (i_{rain} - i_{soil}))dt = dA \int_0^t (i_{rain} - i_{soil})dt = dA * Q \tag{3.35}$$

where Q is the runoff volume in m

Substituting equation (3.35) into equation (3.34) yields

$$e_t = \frac{\int_0^h \left(\int \rho g h (dA * Q) dh \right) dh}{dA} \tag{3.36}$$

We can evaluate the integral as follows:

$$e_t = Q \frac{\rho g h^3}{6} \tag{3.37}$$

The trigonometric relationship between the slope length, slope angle, and height is given by

$$h = L \sin\theta \tag{3.38}$$

Substituting equation (3.38) into equation (3.37) yields

$$e_t = Q * \frac{\rho g (L \sin\theta)^3}{6} \tag{3.39}$$

We should note that as every runoff volume flows down simultaneously to the bottom of the slope, the runoff concentrates at the bottom of the slope, and it is proportional to the rainfall intensity. The runoff concentration leads to gully formation at the bottom of the slope. The total potential energy of the runoff is proportional to the rainfall intensity.

We can compare the total potential energy of the runoff per unit area (equation (3.39)) with the MUSLE:

$$Q * \frac{\rho g (L \sin\theta)^3}{6} \sim a(Qq)^b KLSCP \tag{3.40}$$

From the relationship in equation (3.40), we can reveal the following.

In the MUSLE, $a(Qq)^b LS$ is the term which contributes to the energy of the runoff, whereas K, C, and P are the coefficients which contribute to the energy dissipation (i.e., K, C and P can be taken as friction resistances against the flow, and the values of K, C, and P vary from 0 – 1).

Therefore, we can use $Q * \frac{\rho g (L \sin\theta)^3}{6}$ in place of $a(Qq)^b LS$ in the MUSLE:

$$y \sim Q * \frac{\rho g (L \sin\theta)^3 KCP}{6} \tag{3.41}$$

For a given watershed, the topography does not change over time (i.e., the slope length (L) and slope angle (θ) are constant). Therefore, the runoff volume (Q) is proportional

to the sediment yield by defining the proportionality constants:

$$y = aQ^b * \frac{\rho g(L\sin\theta)^3 KCP}{6} \tag{3.42}$$

The topographic factor of the MUSLE is proportional to the field slope length and angle (i.e., the topographic factor is calculated based on a field slope length and angle). If the topographic factor of the MUSLE is considered, then

$$LS \sim \frac{\rho g(L\sin\theta)^3}{6} \tag{3.43}$$

where on the left side of the equation, L and S represent the slope length factor and slope steepness factor of the MUSLE respectively, whereas on the right side of the equation, L and θ represent a field length and slope angle respectively, and $\frac{\rho * g}{6}$ is the constant.

By defining an increasing function f for the proportionality,

$$\frac{\rho g(L\sin\theta)^3}{6} = f(LS) \tag{3.44}$$

Let $f(LS) = LS$

$$\frac{\rho g(L\sin\theta)^3}{6} = LS \tag{3.45}$$

Substitute equation 3.45 into 3.42

$$y = aQ^b KLSCP \tag{3.46}$$

Therefore, we call equation (3.46) the improved MUSLE.

3.5.1 Estimating the Theoretical Exponent of the Improved MUSLE

As explained in section 3.3, the yearly simulation time step is preferred to address the gradual processes of soil erosion and sediment transport. It is important to prove whether a change in the simulation time step changes the coefficient and the exponent of the improved MUSLE or not. This approach led us to estimate the theoretical exponent of the improved MUSLE.

Proof

If we consider the small simulation time step and the small simulation period, we can maintain the temporal variation of the factors which directly affect the soil erosion process. For a given field, no change in the cover, conservation practice, or soil erodibility factors of the improved MUSLE will be expected in the small simulation period. At the end of the simulation period, only variation of the coefficient and the exponent of the improved MUSLE with the simulation time step affects the sediment yield output (see the proof steps below for a change in the runoff volume (Q). If the variations of the coefficient and the exponent of the improved MUSLE with a small change in the simulation time step are detected, then the variations of the coefficient and the exponent with any other simulation time step are confirmed. For the sake of the start, let us consider 1 and 2 unit simulation time steps and a 2-unit simulation period. No change in the factors of

the improved MUSLE will be expected for about a 2-unit simulation period. Therefore, the soil loss from a field at the 1-unit simulation time step for about a 2-unit simulation period is equal to the sum of the soil loss at the end of the first and next 1-unit time:

$$a_1(Q_1)^{b_1}KLSCP + a_1(Q_2)^{b_1}KLSCP \tag{3.47}$$

where suffixes 1 and 2 correspond to the runoff volume (Q), indicating the first and second simulation at the 1-unit simulation time step or interval. It is noteworthy that K, L, S, C, and P are the same for the 2-unit simulation period. The coefficient and the exponent are the same at the 1-unit simulation time step.

The soil loss from the field at the 2-unit simulation time step for about a 2-unit simulation period is expressed as

$$a_2(Q_1 + Q_2)^{b_2}KLSCP \tag{3.48}$$

where a_2 and b_2 indicate a value of the coefficient (a) and exponent (b) at the 2-unit simulation time step. It is noteworthy that the total runoff volume (Q) at the end of the 2-unit simulation period is equal to the sum of the runoff volumes at the end of the first and next 1-unit time.

In either case, the sediment yield is the same, and therefore

$$a_1(Q_1)^{b_1}KLSCP + a_1(Q_2)^{b_1}KLSCP = a_2(Q_1 + Q_2)^{b_2}KLSCP \tag{3.49}$$

$$a_1(Q_1)^{b_1} + a_1(Q_2)^{b_1} = a_2(Q_1 + Q_2)^{b_2} \tag{3.50}$$

If there is no variation in the coefficient or exponent with small variation in the simulation time step, then

$$a_1 = a_2 = a \text{ and } b_1 = b_2 = b \tag{3.51}$$

$$(Q_1)^b + (Q_2)^b = (Q_1 + Q_2)^b \tag{3.52}$$

Equation (3.52) is false if $b > 1$ or $b < 1$. In this case, the coefficient and the exponent of the improved MUSLE change with a change in the simulation time step for a given total simulation period. Equation (3.52) holds true when $b = 1$. This implies that we consider the total runoff volume per storm event (i.e., from the beginning of runoff to the end of the runoff from a slope field) to estimate the total sediment load. The objective of the improved MUSLE is to estimate the total sediment load transported from the beginning of runoff to the end of the runoff from the slope field. Therefore, the theoretical exponent of the improved MUSLE is one. It is a theoretical exponent because the left and right sides of equation (3.52) represent the theoretical linked expressions without knowledge of the observed sediment. With knowledge of the observed sediment, the actual exponent of the improved MUSLE can be obtained by applying the model at the selected watersheds of Ethiopia.

3.5.2 Estimating the Factors of the Improved MUSLE

In the MUSLE, the runoff factor is the product of the total runoff volume and peak runoff rate. In the improved MUSLE, the peak runoff rate is eliminated. We used the daily average discharge to estimate the annual total runoff volume for the annual sediment yield estimation. The reasons for why we used directly measured flow data and why

we estimated the annual sediment yield are addressed in section 2.1.2. We estimate topographic, soil erodibility, cover and conservation practice factors in the same way as the MUSLE.

3.5.3 Estimating the Coefficient and Exponent of the Improved MUSLE Through Calibration

For a chosen value of the exponent b, the best fit corresponding value of coefficient a was estimated through calibration. The selection of the best exponent and the best equation of the topographic factor was performed after calibration of the observed and simulated sediment (i.e., the improved MUSLE was used to estimate the sediment load). Figure 3.38 shows sample graphs of the calibrated sediment when the topographic factor was calculated using the equation that was proposed by Wischmeier and Smith (1978).

During calibration, the Nash-Sutcliffe efficiency corresponds to each LS factor, exponent b and coefficient a are evaluated, and graphs of exponent **b** versus the Nash-Sutcliffe efficiency and coefficient a versus exponent b are drawn for each watershed, as shown in figures 3.39 – 3.45. For a chosen value of **b**, we tested seven different equations of the topographic factor for each watershed. Therefore, we could have as many graphs as possible.

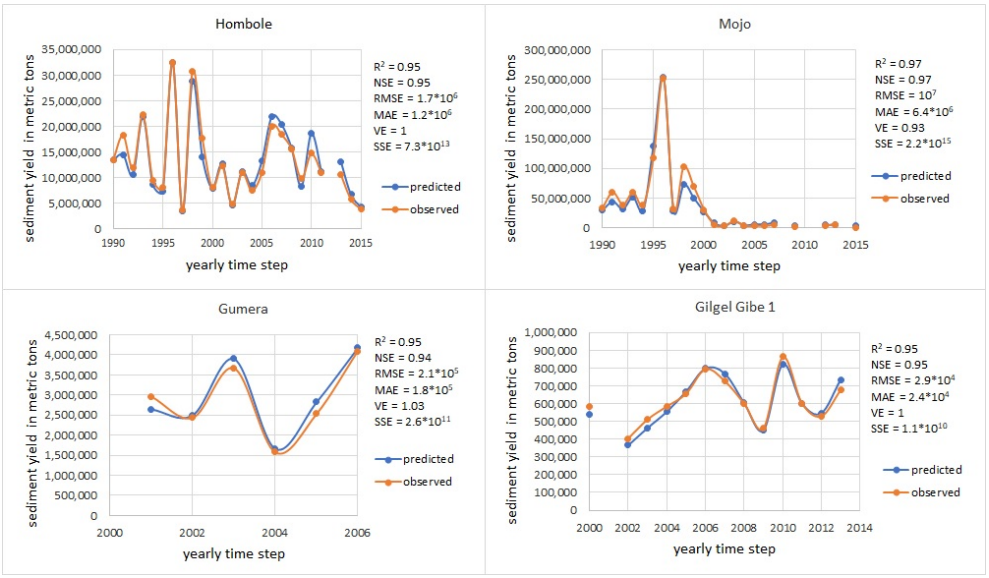

Figure 3.38: Sample graphs of observed and predicted sediment yield

.

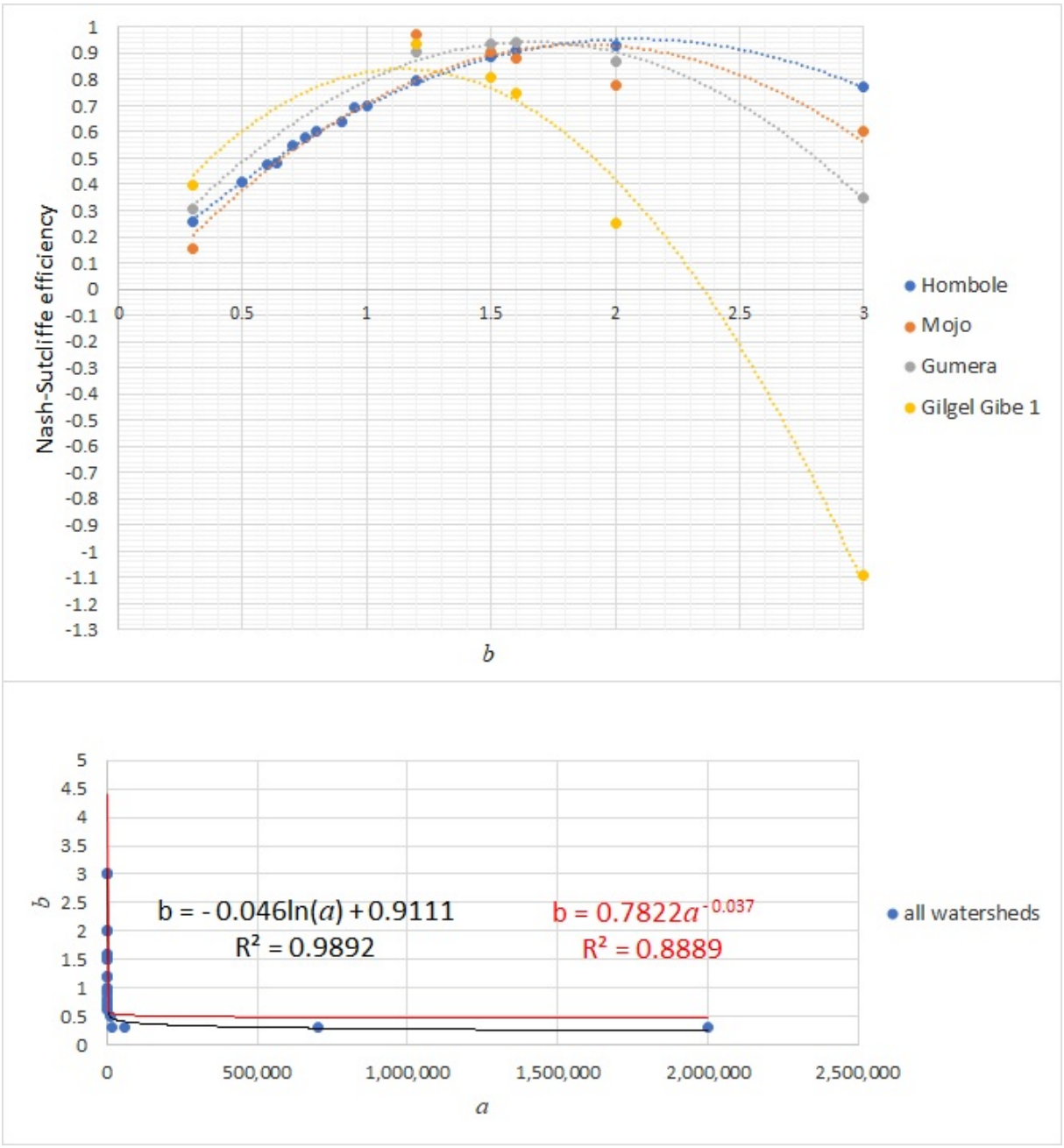

Figure 3.39: The relationship between the exponent b and the Nash-Sutcliffe efficiency as well as the coefficient a versus the exponent b when the topographic factor is calculated by using the equation that was proposed by Wischmeier and Smith (1978).

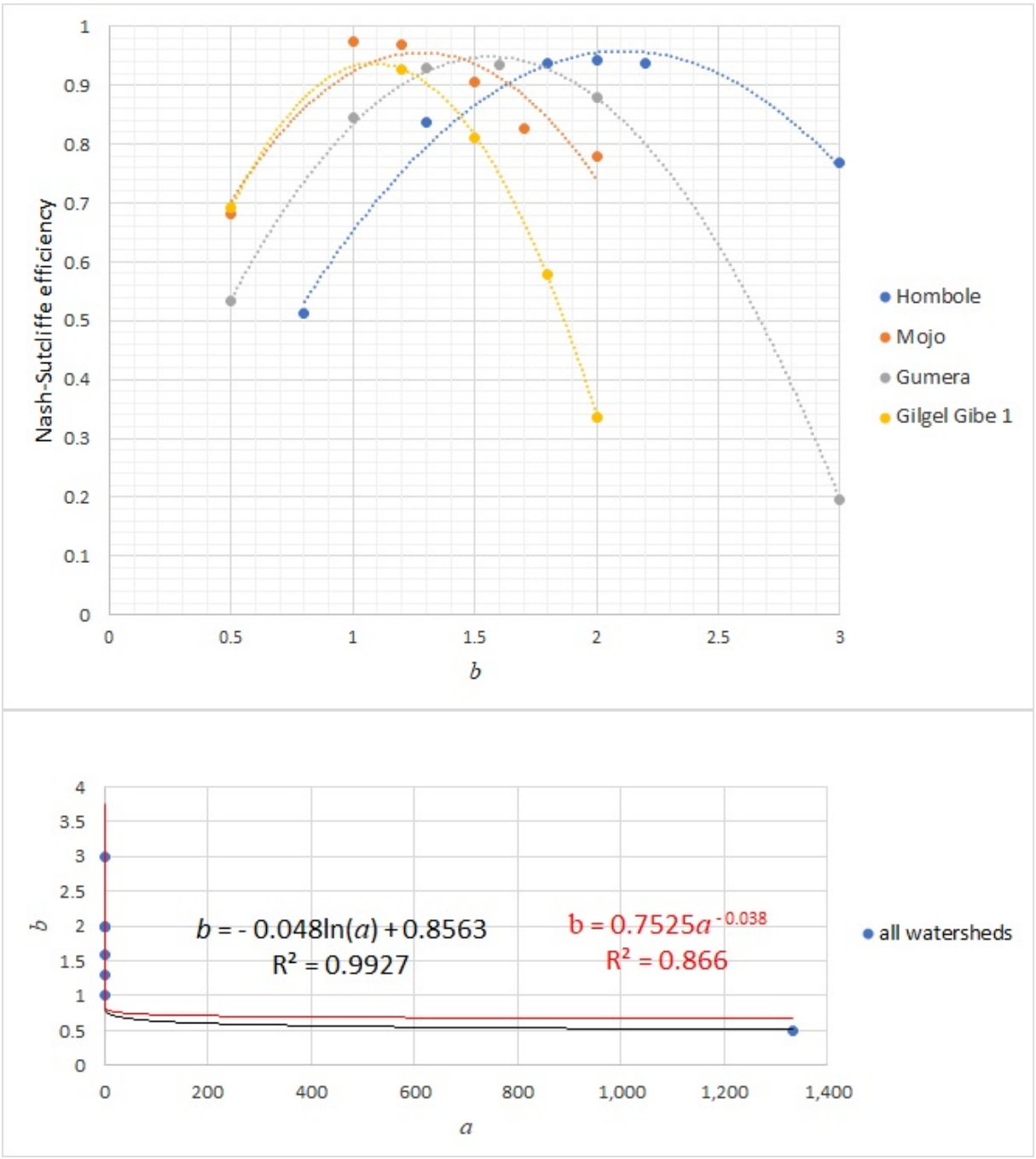

Figure 3.40: The relationship between the exponent b versus the Nash-Sutcliffe efficiency as well as the coefficient a versus the exponent b when the topographic factor is calculated by using the equations that were proposed by Foster et al., (1977) and McCool et al., (1987, 1989), as cited by Renard et al. (1997).

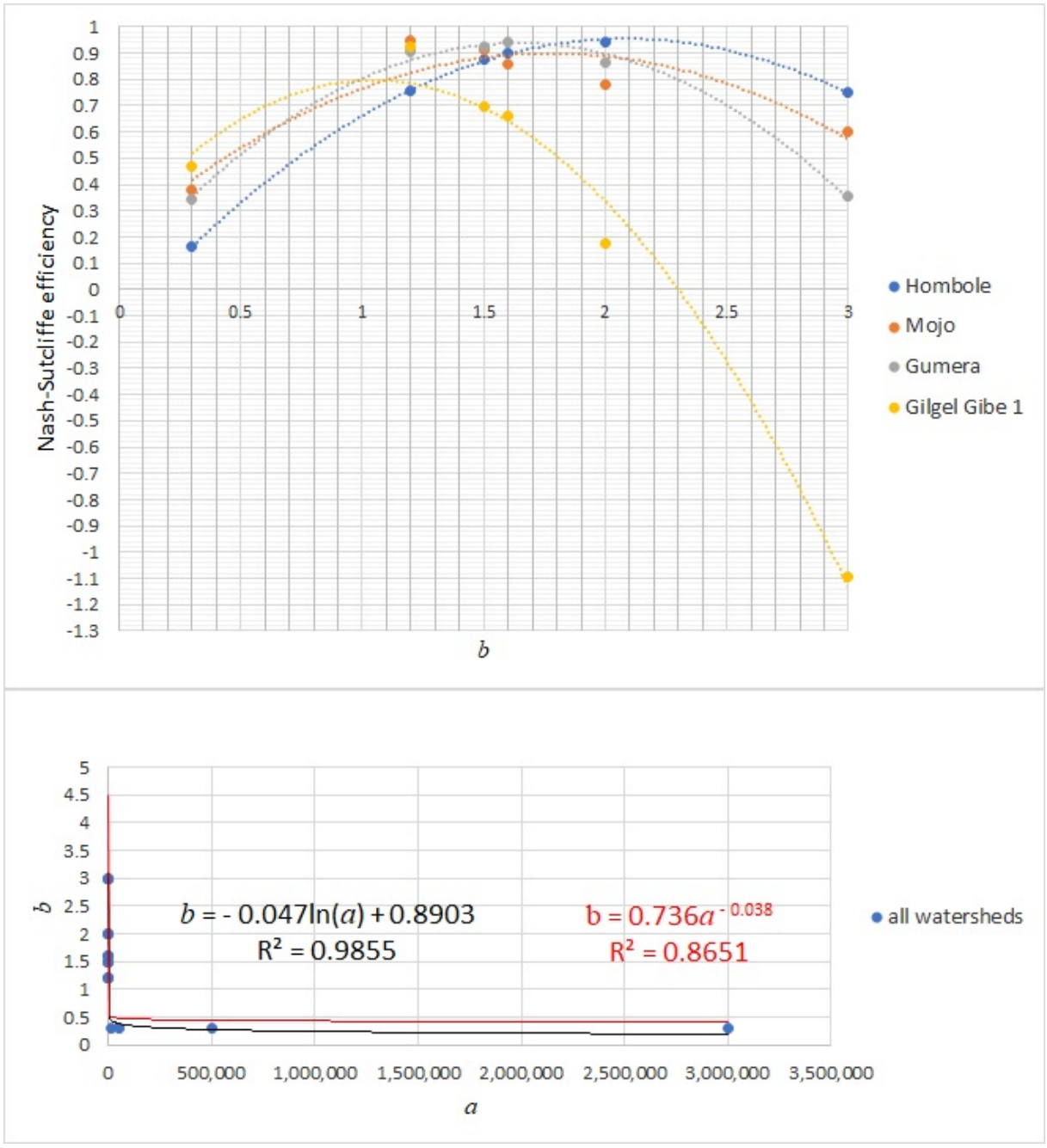

Figure 3.41: The relationship between the exponent b versus the Nash-Sutcliffe efficiency as well as the coefficient a versus the exponent b when the topographic factor is calculated by using the equation that was proposed by Morgan (2005).

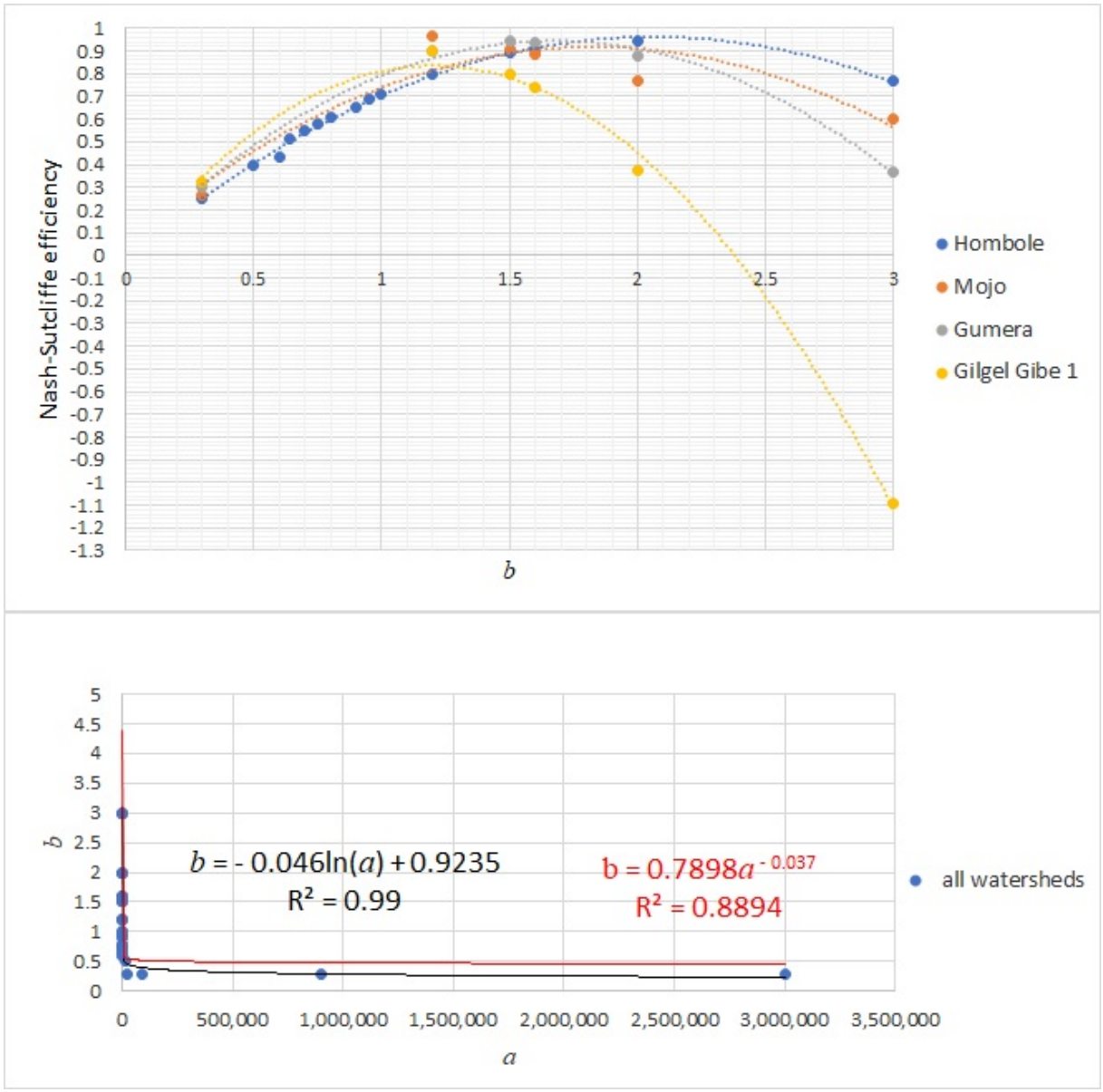

Figure 3.42: The relationship between exponent b versus the Nash-Sutcliffe efficiency as well as the coefficient a versus the exponent b when the topographic factor is calculated by using the equation that was proposed by McCool et al. (1987), as cited by Pongsai et al. (2010).

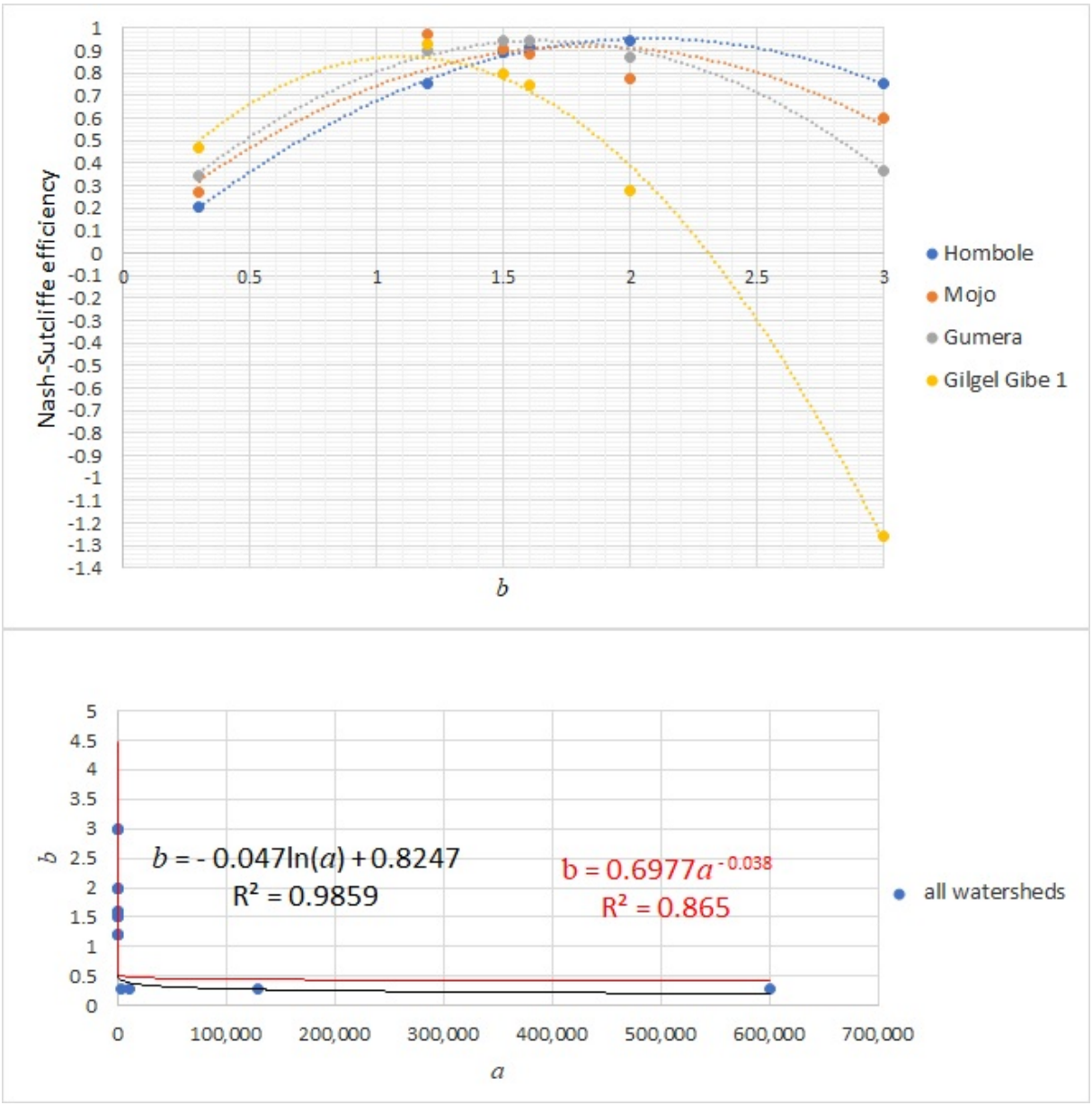

Figure 3.43: The relationship between the exponent b versus the Nash-Sutcliffe efficiency as well as the coefficient a versus the exponent b when the topographic factor is calculated by using the equation that was proposed by David (1988).

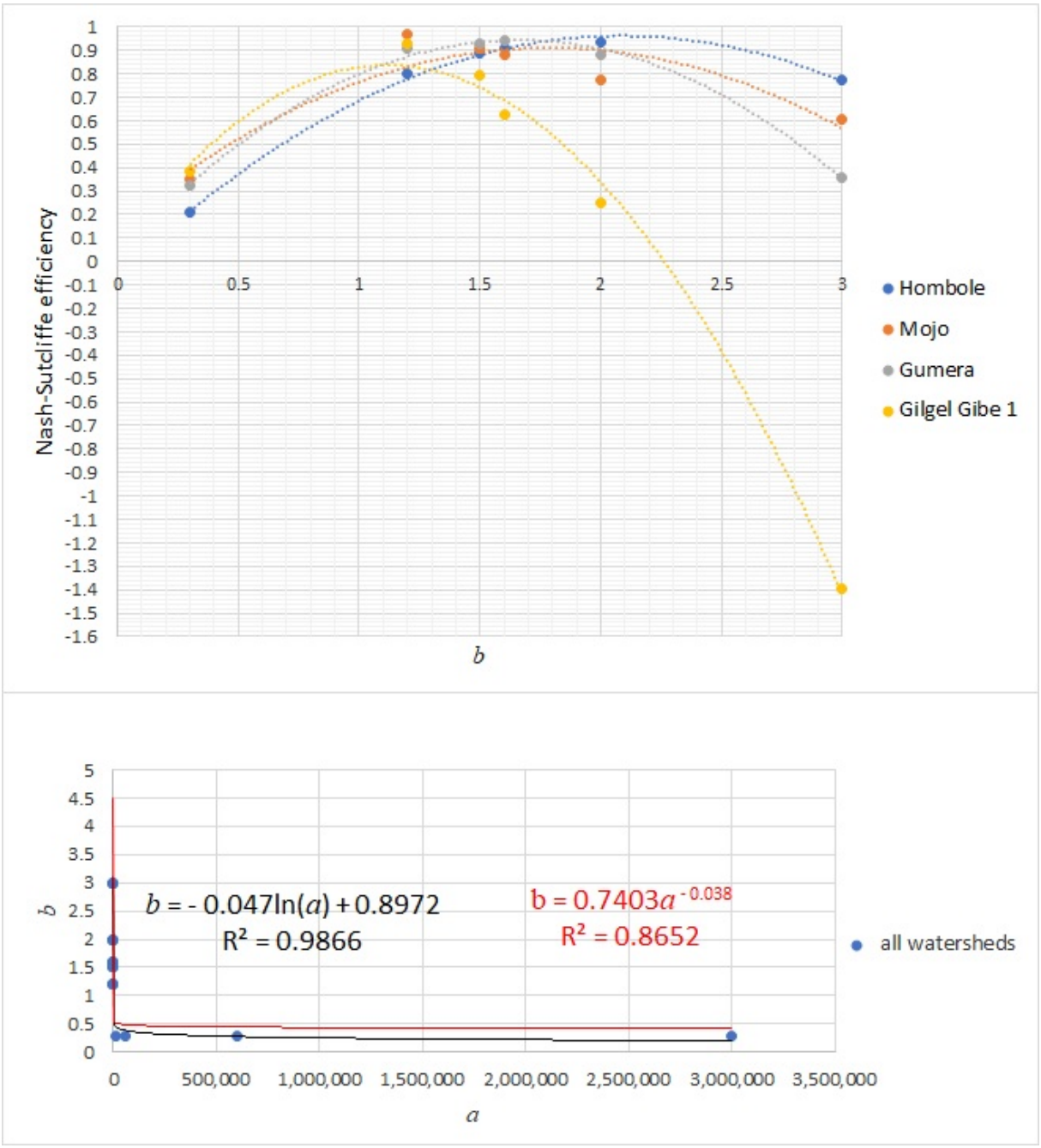

Figure 3.44: The relationship between the exponent b versus the Nash-Sutcliffe efficiency as well as the coefficient a versus the exponent b when the topographic factor is calculated using the Chines equation.

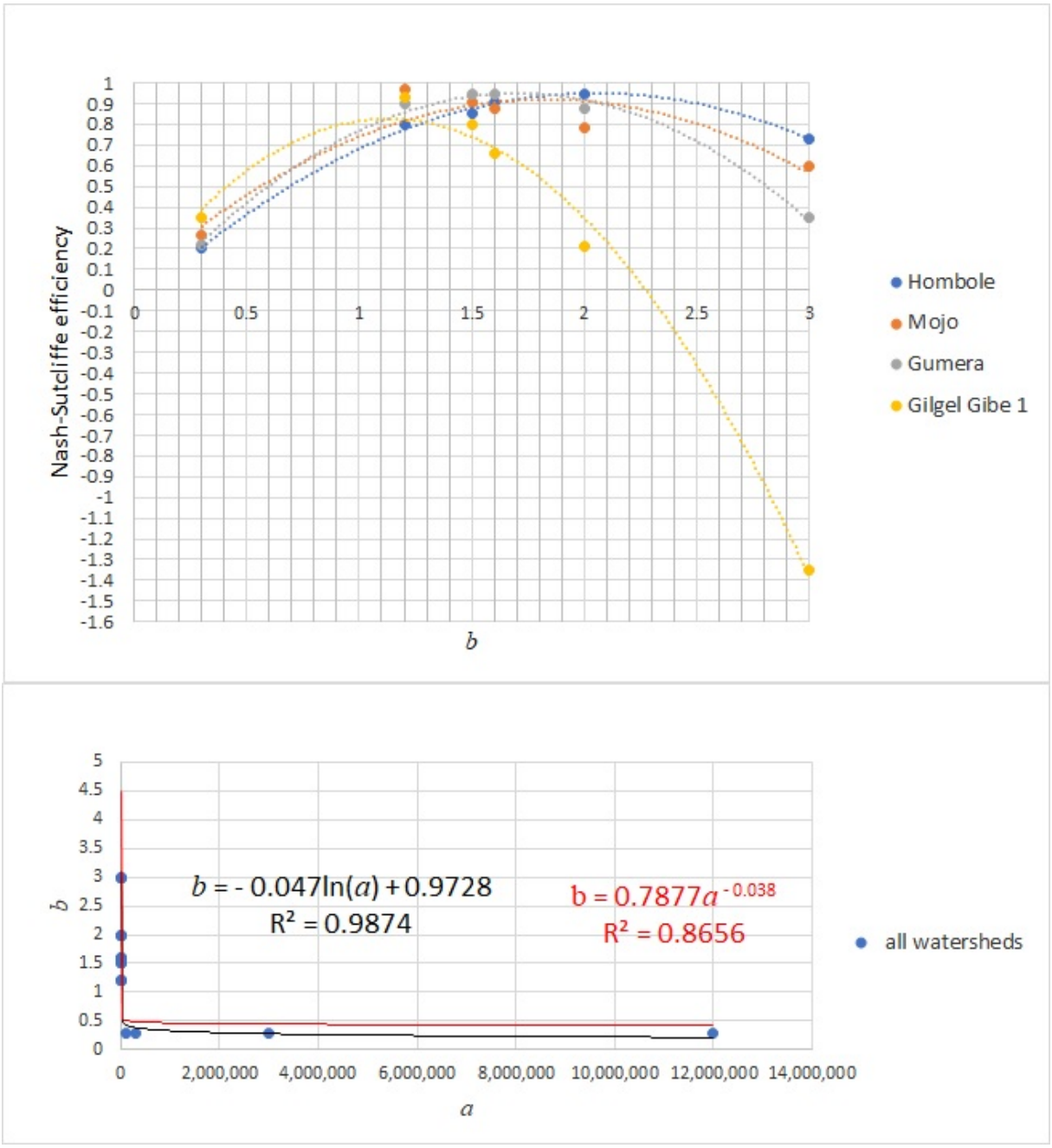

Figure 3.45: The relationship between the exponent b versus the Nash-Sutcliffe efficiency as well as the coefficient a versus exponent b when the topographic factor is calculated using equations (3.8) and (3.9).

3.6 Deriving a Soil Loss Equation for Sediment Yield Estimation

From section 3.5, the total potential energy of the first runoff volume due to its changes in position as it flows down from the height h to the bottom of the slope is equal to E_1. Therefore, consider equation 3.21

$$E_1 = \int_0^h \rho v g h dh \tag{3.53}$$

From equations 3.31 and 3.35, $v = QdA$. If the energy of the runoff volume along the length of the slope (i.e., energy per a unit area) is considered, $v = Q$. Therefore,

$$E_1 = \int_0^h \rho Q g h dh \tag{3.54}$$

Evaluate integral

$$E_1 = \frac{\rho g Q h^2}{2} \tag{3.55}$$

Consider equation 3.38

$$h = Lsin\theta \tag{3.56}$$

Substitute equation 3.56 into 3.55

$$E_1 = \frac{\rho g Q (Lsin\theta)^2}{2} \tag{3.57}$$

Let us consider the following explanations in the context of runoff energy for sediment yield estimation.

As we explained in the previous section to improve the MUSLE, the slope and slope length factors of the MUSLE contribute to the energy of runoff whereas the soil erodibility, cover, and conservation practice factors of the MUSLE contribute to resistance to the runoff. This is because soil conservation practice blocks and at the same time stores the runoff volume up to some level to break its energy and reduce its velocity, which mainly increases sediment deposition by reducing sediment transport. As there more soil protection works are in a field, more dissipation of the energy of the runoff, and less soil loss from the slope area and the bottom of the slope are expected. A soil cover doesn't store the runoff volume but it blocks the runoff to break its energy, which mainly reduces soil erosion. However, the soil cover may play less importance in facilitating sediment deposition. As dense the soil cover or vegetation becomes, more dissipation of energy of the runoff, and less soil loss from the slope area and the bottom of the slope are expected. It is obvious that soil erodibility contributes to the energy dissipation of the runoff. However, its effect on soil erosion and sediment transport should be explained.

As soil becomes more compacted and smooth, less dissipation of the energy of the runoff, and less soil loss from the slope area, but more soil loss is expected from the bottom of the slope due to the concentrated flow. In this case, the fraction of soil shear resistance against the flow is high (i.e., its soil erodibility property is low) along the length of the

slope. The runoff volume will have high kinetic energy at the bottom of the slope as the potential energy of the runoff converts to the kinetic energy at the bottom of the slope. Due to the high kinetic energy at the bottom of the slope, the runoff will have high speed and momentum to scour the soil surface and leads to the gully formation at the bottom of the slope. As soil becomes more loose or rough, more dissipation of the energy of the runoff, more soil loss from the upper parts of the slope area, less sediment transport or more sediment deposition, and less soil loss from the bottom of the slope are expected. This is because the runoff loses its most of energy at the upper part of the slope. In this case, the fraction of soil shear resistance against the runoff is low (i.e., its erodibility property is high) along the length of the slope.

Based on the above explanations, if a fraction of soil shear resistance (S_r) against the runoff is zero, then its soil erodibility factor (K) is one. Therefore,

$$S_r = 1 - K \tag{3.58}$$

As slope of the field increases, the energy of the runoff increase, and more soil erosion is expected. As the slope length decreases, obstacles or friction resistance against the runoff decreases, and more erosion due to the energy of the runoff is expected. As the slope length increases, the energy of the runoff decreases as resistance against flow increases along the length of the slope, and its shear force decreases. Therefore, sediment deposition is expected at the lower parts of the slope. Based on this explanation, a coefficient of the energy dissipation should be taken into account for the energy loss of the runoff volume due to the length of the slope, for sediment yield estimation.

Equation 3.57 shows the total potential energy of the first runoff. Based on the above explanations if the energy loss due to friction is taken into account, the available total energy of the first runoff volume is equal to $\triangle E_1$.

$$\triangle E_1 = \frac{\rho g Q (L sin\theta)^2 (1-K) C P L_{f1}}{2} \tag{3.59}$$

where L_{f1} is the coefficient of the energy dissipation due to the length of the slope

Work done by the first runoff volume is equal to W_1

$$W_1 = F_1 * L \tag{3.60}$$

where F_1 is the force due to the runoff volume, and L is the slope length

The first runoff volume has energy available $\triangle E_1$, therefore

$$W_1 = \triangle E_1 \tag{3.61}$$

Substitute equation 3.61 into 3.60

$$\triangle E_1 = F_1 L \tag{3.62}$$

Rearrange equation 3.62

$$F_1 = \frac{\triangle E_1}{L} \tag{3.63}$$

Substitute equation 3.59 into 3.63

$$F_1 = \frac{\rho g Q (L sin\theta)^2 (1-K) C P L_{f1}}{2L} \tag{3.64}$$

Simplify equation 3.64

$$F_1 = \frac{\rho g Q (L sin^2\theta)(1-K) C P L_{f1}}{2} \tag{3.65}$$

From section 3.5, the total potential energy of the second runoff volume due to its changes in position as it flows down from the height h_1 (let us say just immediately after the first runoff volume) to the bottom of the slope is equal to E_2. Therefore, consider equation 3.22

$$E_2 = \int_0^{h_1} \rho v g h dh \tag{3.66}$$

Since $v = Q$ (see the explanation above), therefore

$$E_2 = \int_0^{h_1} \rho Q g h dh \tag{3.67}$$

Evaluate integral

$$E_2 = \frac{\rho g Q h_1^2}{2} \tag{3.68}$$

The trigonometric relationship between the slope length, slope angle, and height is given by

$$h_1 = L_1 sin\theta \tag{3.69}$$

Substitute equation 3.69 into 3.68

$$E_2 = \frac{\rho g Q (L_1 sin\theta)^2}{2} \tag{3.70}$$

Equation 3.70 shows the total potential energy of the second runoff volume. If the energy loss due to friction is taken into account, the available total energy of the second runoff volume is equal to $\triangle E_2$.

$$\triangle E_2 = \frac{\rho g Q (L_1 sin\theta)^2 (1-K) C P L_{f2}}{2} \tag{3.71}$$

Work done by the second runoff volume is given by

$$W_2 = F_2 * L_1 \tag{3.72}$$

The second runoff volume has energy available $\triangle E_2$, therefore

$$W_2 = \triangle E_2 \tag{3.73}$$

Substitute equation 3.73 into 3.72

$$\triangle E_2 = F_2 L_1 \tag{3.74}$$

Rearrange equation 3.74

$$F_2 = \frac{\triangle E_2}{L_1} \tag{3.75}$$

Substitute equation 3.71 into 3.75

$$F_2 = \frac{\rho g Q (L_1 sin\theta)^2 (1-K) C P L_{f2}}{2L_1} \tag{3.76}$$

Simplify equation 3.76

$$F_2 = \frac{\rho g Q (L_1 sin^2\theta)(1-K) C P L_{f2}}{2} \tag{3.77}$$

From section 3.5, the total potential energy of the third runoff volume due to its changes in position as it flows down from the height h_2 (let us say just immediately after the second runoff volume) to the bottom of the slope is equal to E_3, and so on. Therefore, consider equation 3.23

$$E_3 = \int_0^{h_2} \rho v g h dh \tag{3.78}$$

Since $v = Q$ (see the explanation above), therefore,

$$E_3 = \int_0^{h_2} \rho Q g h dh \tag{3.79}$$

Evaluate integral

$$E_3 = \frac{\rho g Q h_2^2}{2} \tag{3.80}$$

The trigonometric relationship between the slope length, slope angle, and height is given by

$$h_2 = L_2 sin\theta \tag{3.81}$$

Substitute equation 3.81 into 3.80

$$E_3 = \frac{\rho g Q (L_2 sin\theta)^2}{2} \tag{3.82}$$

Equation 3.82 shows the total potential energy of the third runoff volume. If the energy loss due to friction is taken into account, the available total energy of the third runoff volume is equal to $\triangle E_3$.

$$\triangle E_3 = \frac{\rho g Q (L_2 sin\theta)^2 (1-K) C P L_{f3}}{2} \tag{3.83}$$

Work done by the third runoff volume is given by

$$W_3 = F_3 * L_2 \tag{3.84}$$

The third runoff volume has energy available $\triangle E_3$, therefore,

$$W_3 = \triangle E_3 \tag{3.85}$$

Substitute equation 3.85 into 3.84

$$\triangle E_3 = F_3 L_2 \tag{3.86}$$

Rearrange equation 3.86

$$F_3 = \frac{\triangle E_3}{L_2} \tag{3.87}$$

Substitute equation 3.83 into 3.87

$$F_3 = \frac{\rho g Q (L_2 sin\theta)^2 (1-K) C P L_{f3}}{2 L_2} \tag{3.88}$$

Simplify equation 3.88

$$F_3 = \frac{\rho g Q (L_2 sin^2\theta)(1-K) C P L_{f3}}{2} \tag{3.89}$$

Therefore, determine the sum of all runoff forces

$$F = F_1 + F_2 + F_3 ... + F_n \tag{3.90}$$

Substitute equation 3.65, 3.77, 3.89, and so on into 3.90.

$$\begin{aligned} F = \frac{\rho g Q (L sin^2\theta)(1-K) C P L_{f1}}{2} + \frac{\rho g Q (L_1 sin^2\theta)(1-K) C P L_{f2}}{2} + \\ \frac{\rho g Q (L_2 sin^2\theta)(1-K) C P L_{f3}}{2} + ... + F_n \end{aligned} \tag{3.91}$$

where L_1 and L_2 are the lengths of the slope corresponding to the heights of the slope h_1 and h_2 respectively provided that h_1 and h_2 are the heights of the slope just immediately after heights h and h_1 respectively, and so on. Therefore, equation 3.91 is written as

$$F = \int_0^L \frac{\rho g Q (L sin^2\theta)(1-K) C P L_f}{2} dL \tag{3.92}$$

Simplify equation 3.92

$$F = \frac{\rho g Q sin^2\theta * (1-K) * C P \int_0^L (L * L_f) dL}{2} \tag{3.93}$$

Next, we define soil shear resistance (shear force) which acts against the runoff direction parallel to the slope length.

Soil shear resistance which acts at slope height h_1 parallel to the length of the slope is equal to f_1

$$f_1 = m_1 g cos\theta \tag{3.94}$$

where m_1 is the mass of soil, g is the acceleration due to gravity

Soil shear resistance which acts at slope height h_2 parallel to the length of the slope is equal to f_2

$$f_2 = m_2 g cos\theta \tag{3.95}$$

Soil shear resistance which acts at slope height h_3 parallel to the length of the slope is equal to f_3

$$f_3 = m_3 g cos\theta \tag{3.96}$$

Soil shear resistance which acts at slope height h_n parallel to the length of the slope is equal to f_n

$$f_n = m_n g cos\theta \tag{3.97}$$

Sum all shear resistances (shear forces) which act against the runoff direction is equal to F_s

$$F_s = F_1 + F_2 + F_3 + ... + F_n \tag{3.98}$$

Substitute equations 3.94 – 3.97, and so on into equation 3.99

$$F_s = m_1 g cos\theta + m_2 g cos\theta + m_3 g cos\theta + ... + m_n g cos\theta \tag{3.99}$$

Simplify equation 3.99

$$F_s = mg cos\theta \tag{3.100}$$

where m is the total mass of sediment

At equilibrium, where sediment deposition takes place or sediment sinks into a channel at the end of the slope field, the runoff force (F) is taken to be counterbalanced by the soil shear resistance (F_s).

$$F = F_s \tag{3.101}$$

Substitute equations 3.93 and 3.100 into 3.101

$$\frac{\rho g Q sin^2\theta * (1 - K) * CP \int_0^L (L * L_f) dL}{2} = mg cos\theta \tag{3.102}$$

Rearrange equation 3.102

$$m = \frac{\rho Q (1 - K) CP sin^2\theta}{2 cos\theta} \int_0^L (L * L_f) dL \tag{3.103}$$

Next, let us consider the rainfall impact energy for soil erosion (refer to figure A5). If the free fall velocity (terminal velocity) of a raindrop is considered, then the kinetic energy (KE) of the raindrop that causes soil erosion on the slope field is given by

$$KE = \frac{1}{2} m v^2 cos\theta \tag{3.104}$$

where m is the mass of the raindrop, and u is the terminal velocity of the raindrop

But $m = \rho * V$, therefore

$$KE = \frac{1}{2} \rho V u^2 cos\theta \tag{3.105}$$

where ρ is the density of the raindrop, and V is the volume of the raindrop

The total kinetic energy (KE_{total}) of the raindrops on the entire slope field is given by

$$KE_{total} = \frac{1}{2} \rho V_t u^2 cos\theta \tag{3.106}$$

where V_t is the total volume of the raindrop

Let us assume that the raindrop is uniformly distributed over the entire slope field, therefore, the total volume of the raindrops (V_t) is given by

$$V_t = Ah \tag{3.107}$$

where A is the area of the slope field, and h is the height of the raindrop

Substitute equation 3.107 into 3.106

$$KE_{total} = \frac{1}{2}\rho Ahu^2 cos\theta \tag{3.108}$$

where KE_{total} is the total kinetic energy of the raindrops

The area of the slope field is given by

$$A = Lw \tag{3.109}$$

where L is the length of the slope field, and w is the width of the slope field

Substitute equation 3.109 into 3.108

$$KE_{total} = \frac{1}{2}\rho Lwhu^2 cos\theta \tag{3.110}$$

Consider equation 3.110

The total kinetic energy per a unit width of the slope is given by

$$KE_{total} = \frac{1}{2}\rho Lhu^2 cos\theta \tag{3.111}$$

The total amount of soil loss (m) is proportional to the total kinetic energy of the raindrops, soil resistance against the rainfall impact, and soil cover. The soil shear resistance can be taken as the soil erodibility factor of the USLE. Since the soil cover reduces soil erosion by reducing the raindrop impact energy, it can be taken as the cover factor of the USLE. Since the soil conservation practice factor has no role in reducing the rainfall impact energy, we will not consider it in the context of the rainfall energy for soil erosion. Therefore,

$$m \sim KE_{total} * KC \tag{3.112}$$

Substitute equation 3.111 into 3.112

$$m \sim \frac{1}{2}\rho Lhu^2 cos\theta * KC \tag{3.113}$$

where K is the soil erodibility factor, and C is the cover factor of the USLE

Equation 3.103 is based on runoff energy whereas equation 3.113 is based on rainfall energy for estimation of the amount of soil loss from a slope field. As runoff is directly proportional to rainfall, the amount of soil loss due to the runoff is directly proportional to the amount of soil loss due to the rainfall. Therefore, correlate equation 3.103 and 3.113.

$$\frac{\rho Q(1-K)CPsin^2\theta}{2cos\theta}\int_0^L (L * L_f)dL \sim \frac{1}{2}\rho Lhu^2 cos\theta * KC \tag{3.114}$$

Rearrange equation 3.114

$$\int_0^L (L * L_f)dL \sim \frac{hu^2 K cos^2\theta}{Q(1-K)Psin^2\theta} L \tag{3.115}$$

Equation 3.115 can be written as

$$\int_0^L (L * L_f)dL \sim \int_0^L \frac{hu^2 K cos^2\theta}{Q(1-K)Psin^2\theta} dL \tag{3.116}$$

Simplify equation 3.116

$$L * L_f \sim \frac{hu^2 K cos^2\theta}{Q(1-K)Psin^2\theta} \tag{3.117}$$

Rearrange equation 3.117

$$L_f \sim \frac{hu^2 K cos^2\theta}{Q(1-K)Psin^2\theta} * \frac{1}{L} \tag{3.118}$$

Since the effect of the slope length on soil erosion can be seen while keeping other variables constant. Therefore,

$$L_o = \frac{hu^2 K cos^2\theta}{Q(1-K)Psin^2\theta} \tag{3.119}$$

where L_o is the constant

Substitute equation 3.119 into 3.118

$$L_f \sim \frac{L_o}{L} \tag{3.120}$$

By defining the proportionality constant c and v

$$L_f = c\frac{L_o}{L^v} \tag{3.121}$$

We expect sediment transport by a runoff volume if $0 < L_f \leq 1$. As a slope length increases, L_f decreases to zero. As a slope length becomes smaller and smaller, L_f approaches one. Since L_f is inversely proportional to L, a value of v should be a positive value. If $cL_o > 1$ and $L < 1$, there is no a positive value of v such that $0 < L_f \leq 1$. For a given value of cL_o, there is a possible value of v such that $0 < L_f \leq 1$ if $L \geq 1$. Therefore, the minimum slope length is defined to be 1m (i.e., $L \geq 1$m) from which soil erosion and sediment transport take place.

Let $v = 1$

$$L_f = c\frac{L_o}{L} \tag{3.122}$$

Substitute equation 3.122 into 3.103

$$m \sim \frac{\rho Q(1-K)CPsin^2\theta}{2cos\theta} \int_0^L (L * c\frac{L_o}{L})dL \tag{3.123}$$

Evaluate integral

$$m \sim \frac{\rho Q(1-K)CPsin^2\theta}{2cos\theta} L * cL_o \tag{3.124}$$

For a particular field with slope angle and length, soil cover, soil erodibility, and conservation practice can be controlled. Runoff due to rainfall determines hydro-climatic conditions of the field, and it independently affects soil loss from the field. Therefore, by defining the proportionality constants a_o and b

$$m = \frac{a_o \rho Q^b (1-K) CP sin^2\theta}{2cos\theta} L * cL_o \tag{3.125}$$

Since a_0, ρ, c, L_0 are all constants, let $a = \frac{1}{2} a_o \rho c L_o$. Therefore, equation 3.125 is given as

$$m = \frac{a Q^b (1-K) CP sin^2\theta}{cos\theta} L \tag{3.126}$$

We call equation 3.126 the SLESYE

To take into account soil loss from a horizontal field (i.e., the field slope is zero), we can consider the topographic factor (LS) of the MUSLE. The topographic factor of the MUSLE is proportional to the field slope length and angle (i.e., the topographic factor is calculated based on a field slope length and angle). From equation 3.126,

$$\frac{sin^2\theta}{cos\theta} L \sim LS \tag{3.127}$$

where, on the left side of the proportionality, L and θ represent a field slope length and angle respectively, whereas, on the right side, L and S represent the slope length factor and slope steepness factor of the MUSLE respectively.

By defining an increasing function f for the proportionality,

$$\frac{sin^2\theta}{cos\theta} L = f(LS) \tag{3.128}$$

Let $f(LS) = LS$

$$\frac{sin^2\theta}{cos\theta} L = LS \tag{3.129}$$

Substitute equation 3.129 into 3.126

$$m = a Q^b (1-K) CPLS \tag{3.130}$$

We call equation 3.130 the RSLESYE-v1

3.6.1 Evaluating the SLESYE

We evaluate the coefficient and exponent of the SLESYE following a similar calibration procedure as that of the MUSLE or improved MUSLE (see section 3.5.3). For the sake of calibration procedure, we estimate the soil erodibility, soil cover, and conservation practice factors of the SLESYE in the same ways as the soil erodibility, soil cover, and conservation practice factors of the improved MUSLE (see section 3.5.2). Runoff volume, slope angle, and slope length are taken directly. Thus, figure 3.46 shows sample graphs of the calibrated sediment, and figure 3.47 shows graphs of exponent b versus the Nash-Sutcliffe efficiency as well as coefficient a versus exponent b.

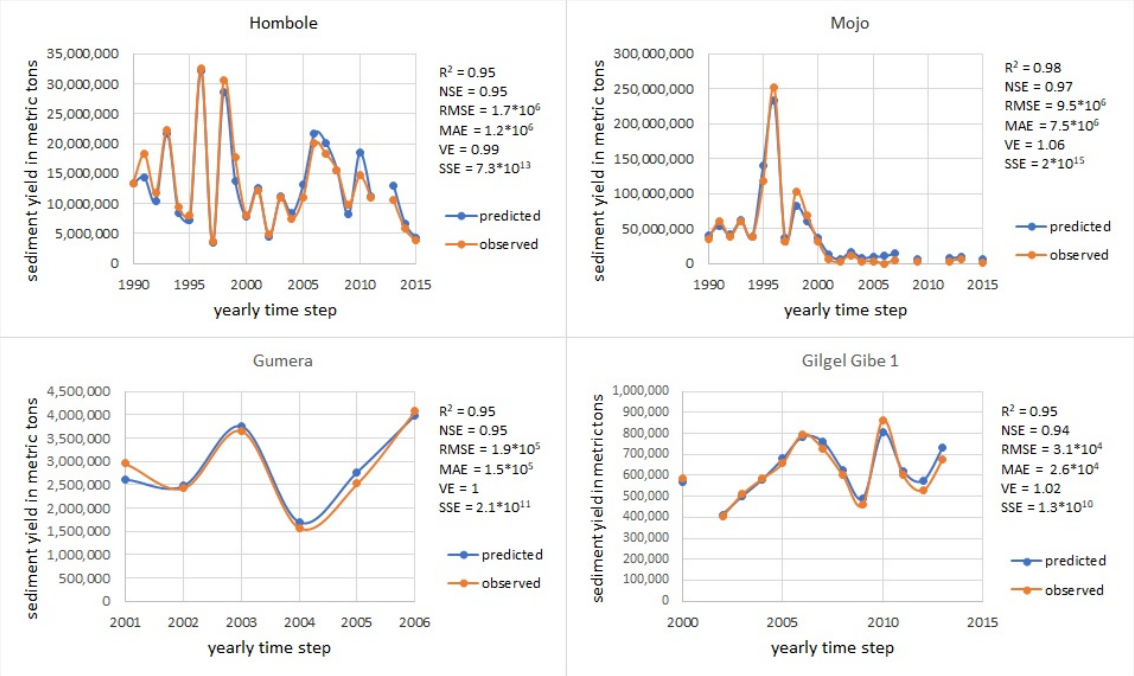

Figure 3.46: Sample graphs of observed and predicted sediment yield

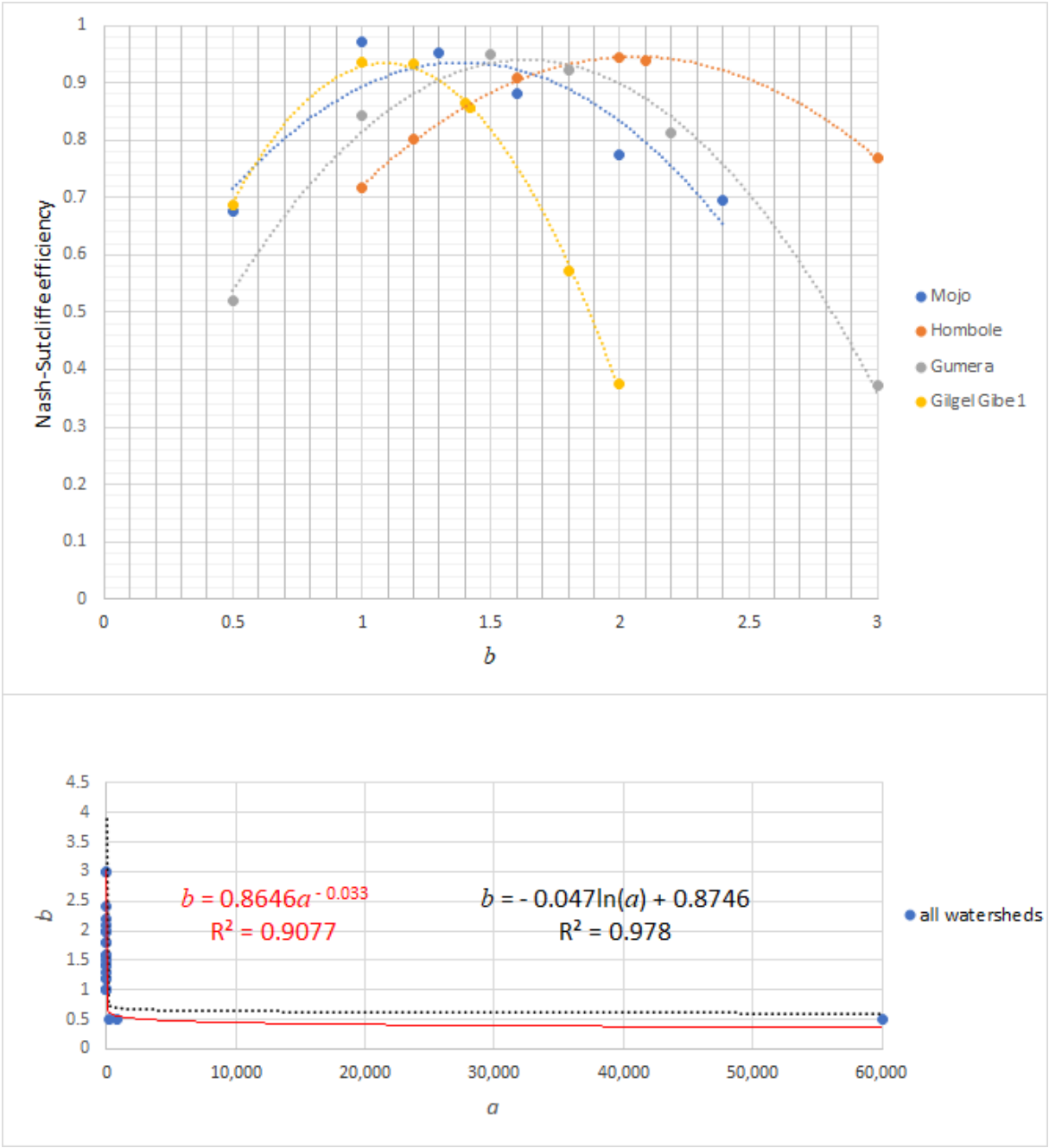

Figure 3.47: The relationship between the exponent b and the Nash-Sutcliffe efficiency as well as the coefficient a versus the exponent b.

3.6.2 Estimating the Theoretical Exponent and the Factors of the RSLESYE-v1

To estimate theoretical exponent of the RSLESYE-v1, we follow a similar procedure to that of the improved MUSLE (see section 3.5.1). Since the structure or mathematical form of the RSLESYE-v1 is similar to the improved MUSLE, the theoretical exponent of the RSLESYE-v1 is the same as the improved MUSLE. We also estimate the factor of the RSLESYE-v1 in the same way as the improved MUSLE (see section 3.5.2).

3.6.3 Estimating the Coefficient and Exponent of the RSLESYE-v1 Through Calibration

For the sake of comparison purposes, we evaluate equation 3.130 following a similar evaluation procedure as that of the MUSLE or improved MUSLE (see section 3.5.3). Figure 3.48 shows sample graphs of the calibrated sediment when the topographic factor was calculated using the equation that was proposed by Wischmeier and Smith (1978).

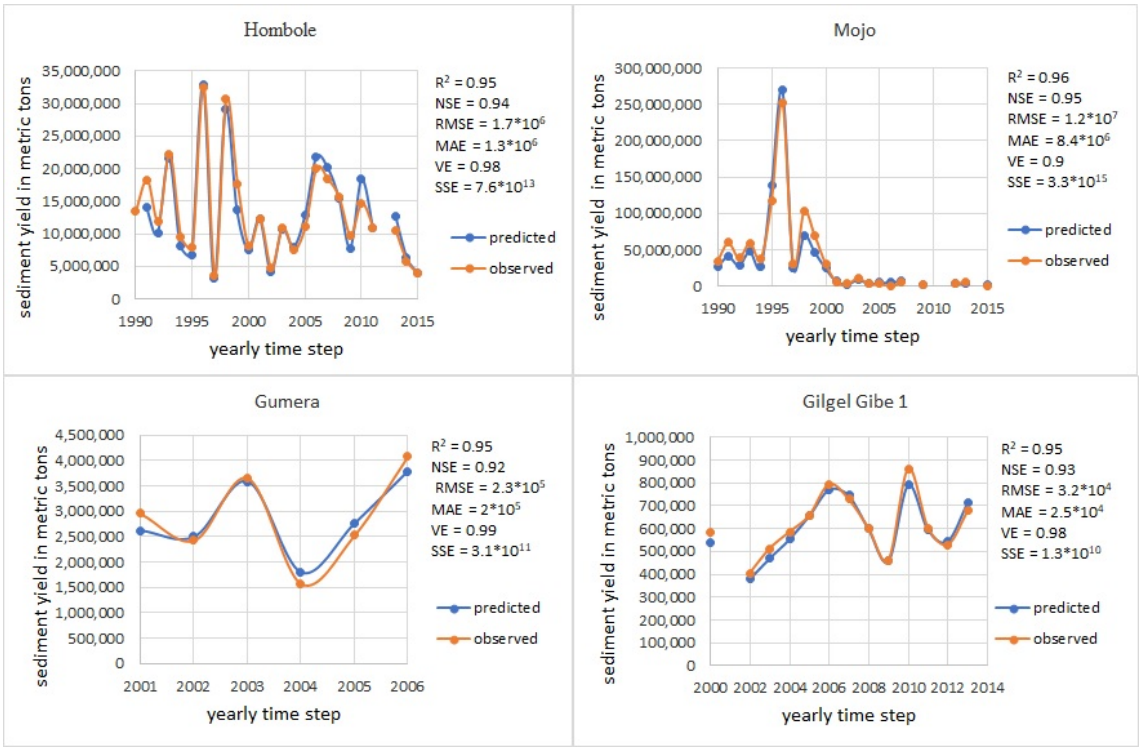

Figure 3.48: Sample graphs of observed and predicted sediment yield

Graphs of exponent b versus the Nash-Sutcliffe efficiency and coefficient a versus exponent b are drawn for each watershed, as shown in figure 3.49 – 3.55.

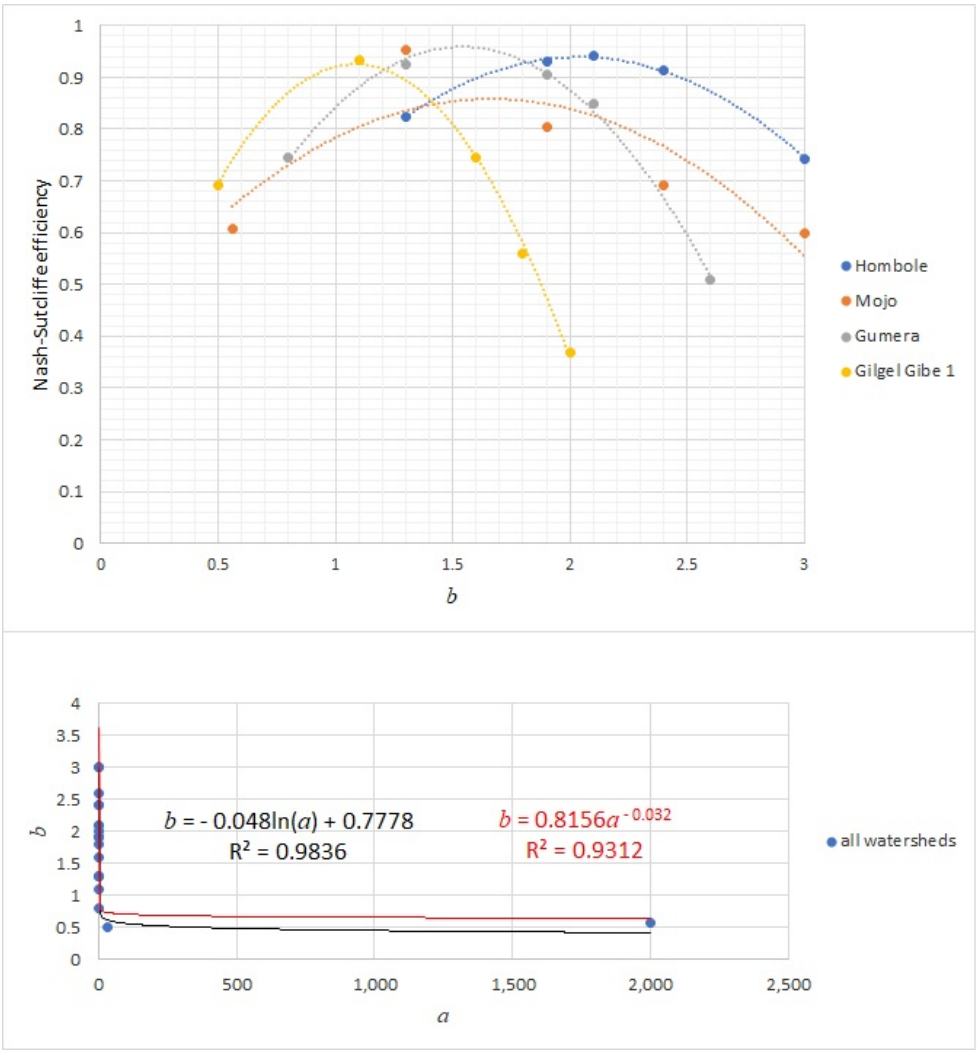

Figure 3.49: The relationship between the exponent b and the Nash-Sutcliffe efficiency as well as the coefficient a versus the exponent b when the topographic factor is calculated by using the equation that was proposed by Wischmeier and Smith (1978).

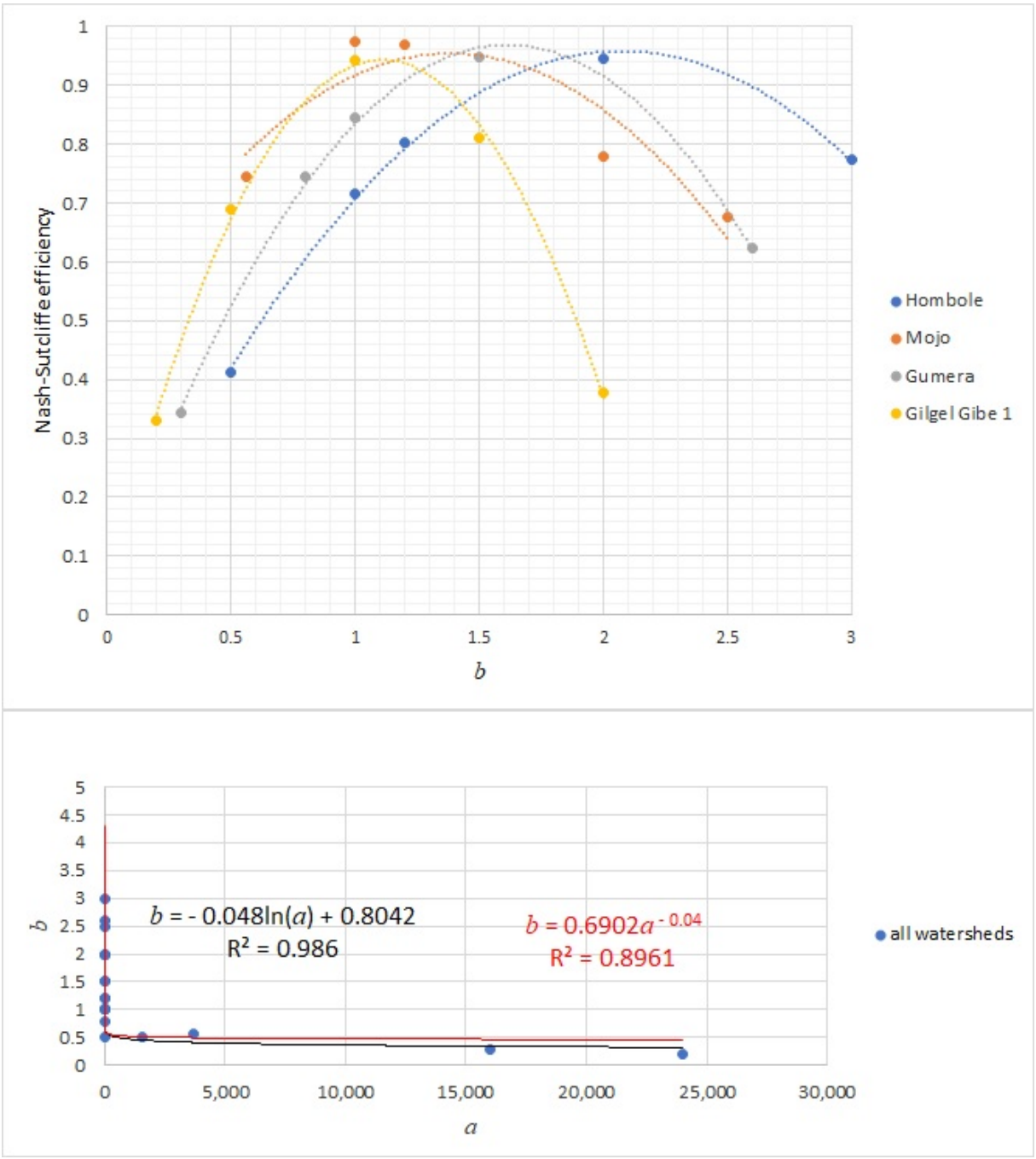

Figure 3.50: The relationship between the exponent b versus the Nash-Sutcliffe efficiency as well as the coefficient a versus the exponent b when the topographic factor is calculated by using the equations that were proposed by Foster et al., (1977) and McCool et al., (1987, 1989), as cited by Renard et al. (1997).

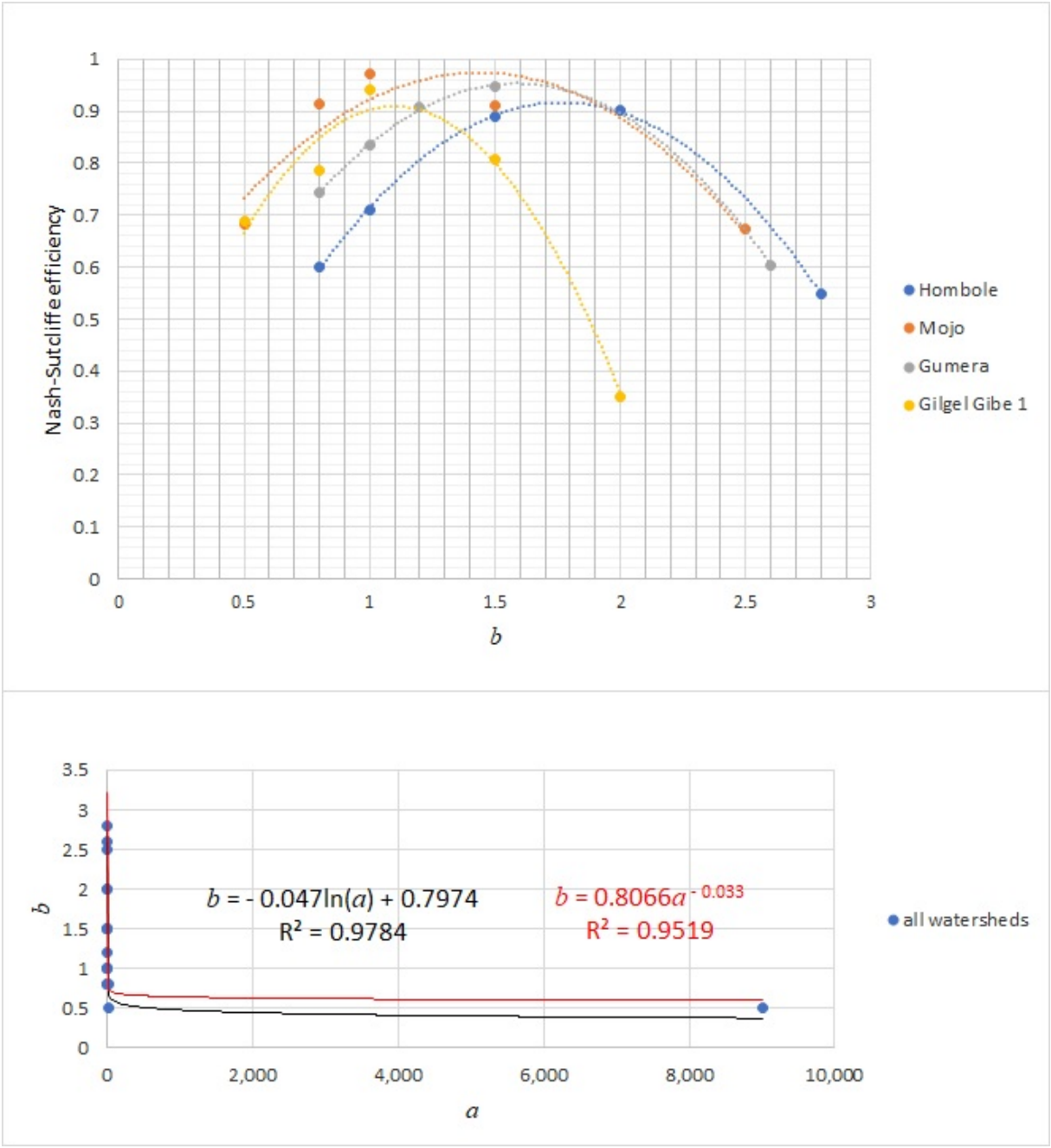

Figure 3.51: The relationship between the exponent b versus the Nash-Sutcliffe efficiency as well as the coefficient a versus the exponent b when the topographic factor is calculated by using the equation that was proposed by Morgan (2005).

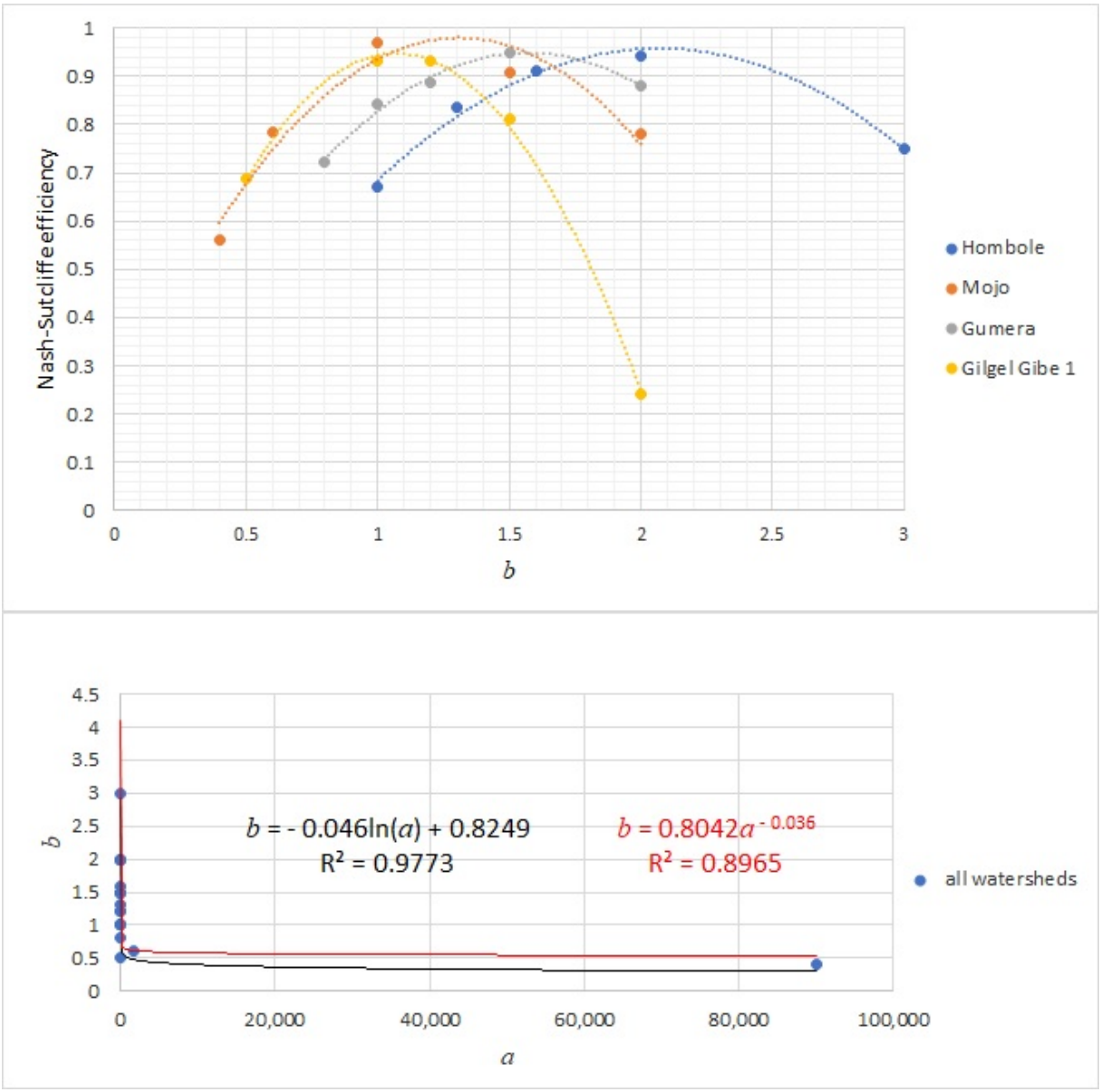

Figure 3.52: The relationship between the exponent b versus the Nash-Sutcliffe efficiency as well as the coefficient a versus the exponent b when the topographic factor is calculated by using the equation that was proposed by McCool et al. (1987), as cited by Pongsai et al. (2010).

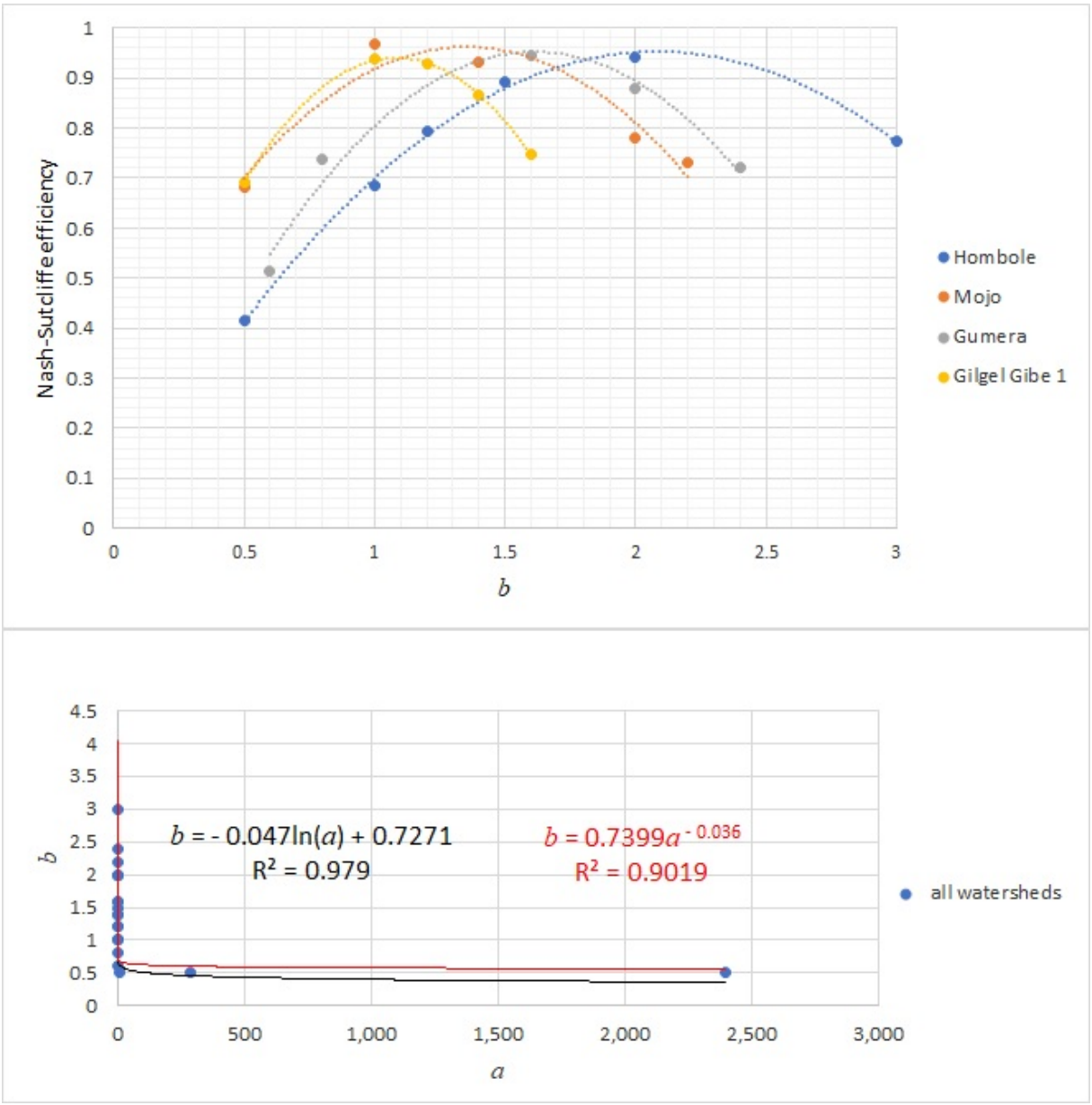

Figure 3.53: The relationship between the exponent b versus the Nash-Sutcliffe efficiency as well as the coefficient a versus the exponent b when the topographic factor is calculated by using the equation that was proposed by David (1988).

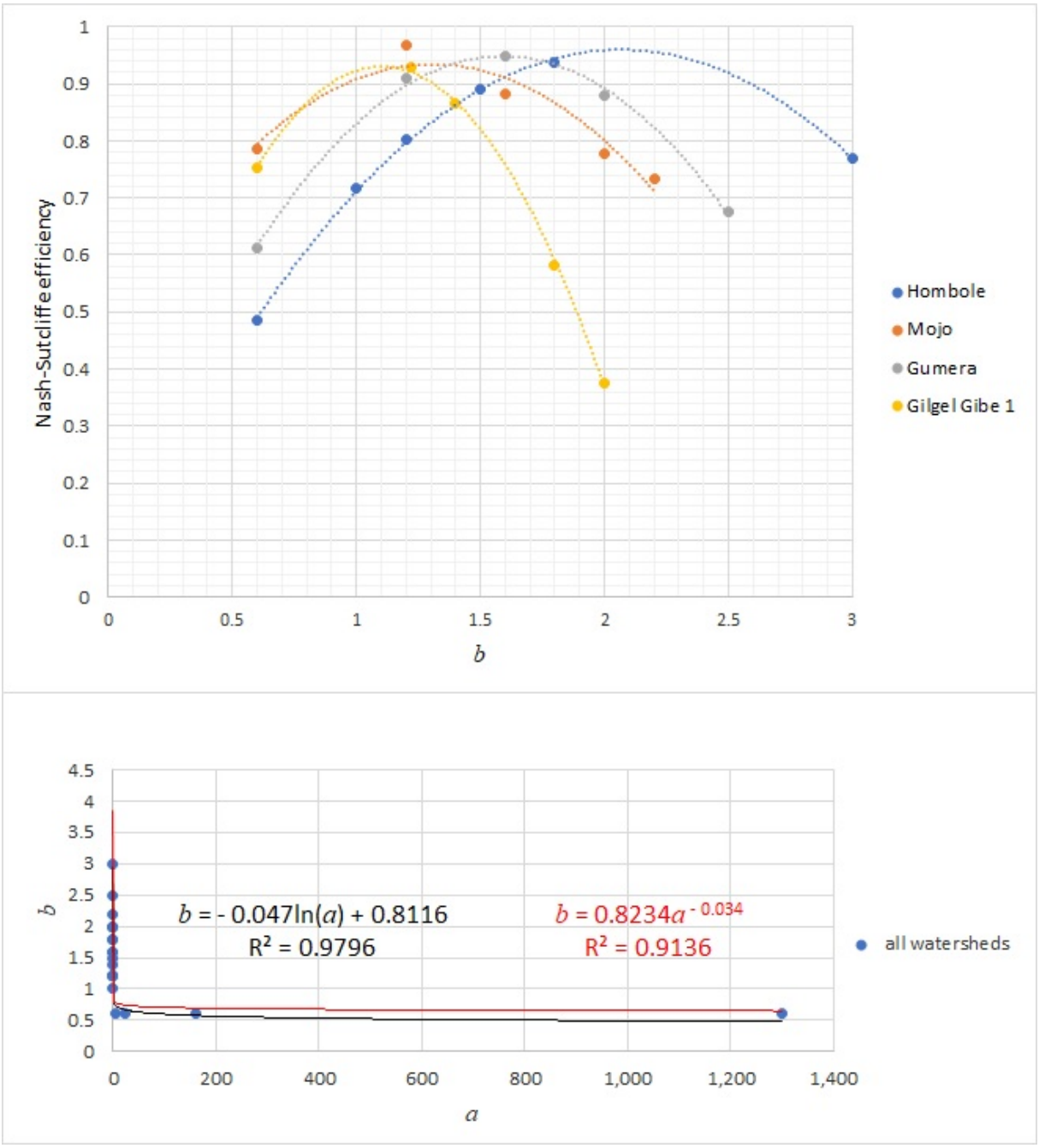

Figure 3.54: The relationship between the exponent b versus the Nash-Sutcliffe efficiency as well as the coefficient a versus the exponent b when the topographic factor is calculated using the Chines equation.

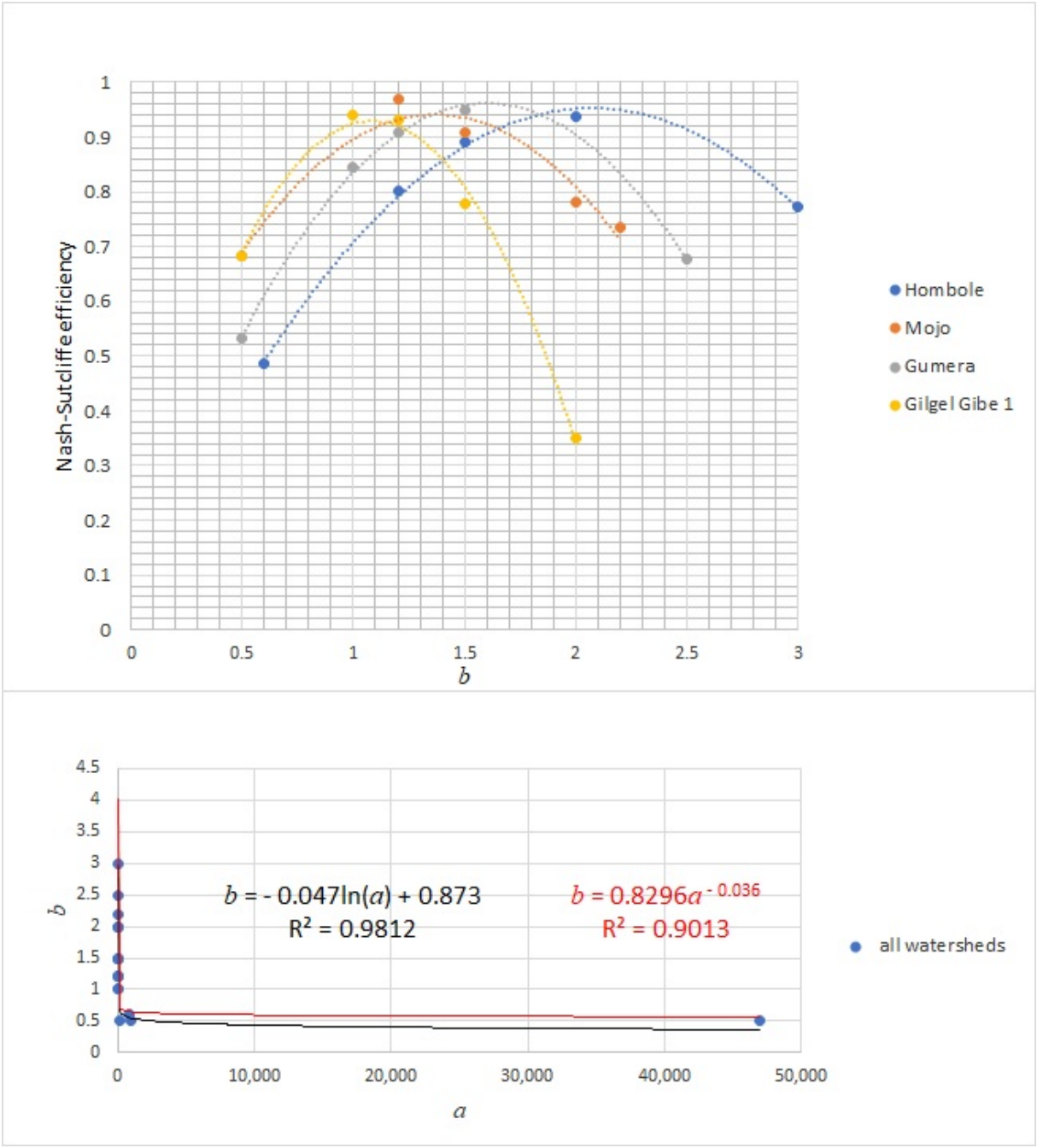

Figure 3.55: The relationship between the exponent b versus the Nash-Sutcliffe efficiency as well as the coefficient a versus the exponent b when the topographic factor is calculated using equations (3.8) and (3.9).

3.7 Improving the Accuracy of a Model by Modifying its Mathematical Form

In this case, we consider the Nash–Sutcliffe efficiency equation to modify the mathematical form of a given model. The Nash–Sutcliffe efficiency is one of the commonly used statistical tools to measure the performance of the model. For the same observed

data but different simulated values, if a Nash-Sutcliffe efficiency of the correlated values shows an improvement, then it is the premise that the other statistical measures also show an improvement. The performance of the model can be improved by minimizing the overestimation and underestimation of the model.

For measured sediment yield (let us say x) and predicted sediment yield (let us say y), the Nash-Sutcliffe efficiency is given by

$$E = 1 - \frac{\sum (x-y)^2}{\sum (x-\bar{x})^2} \tag{3.131}$$

where E represents the Nash-Sutcliffe efficiency (for this case only), and $\bar{x}$ is the average of the measured values.

Expand equation 3.131

$$E = 1 - \frac{\sum (x^2 - 2xy + y^2)}{\sum (x^2 - 2x\bar{x} + \bar{x}^2)} \tag{3.132}$$

$$E = 1 - \frac{\sum x^2 - \sum 2xy + \sum y^2}{\sum x^2 - \sum 2x\bar{x} + \sum \bar{x}^2} \tag{3.133}$$

For continuously measured and predicted values, express equation 3.133 in integral form

$$E = 1 - \frac{\int x^2 dx - \int 2xy? + \int y^2 dy}{\int x^2 dx - \int 2x\bar{x} dx + \int \bar{x}^2 dx} \tag{3.134}$$

where question mark ? represents dx or dy, which will be decided latter in this document.

To solve integrals $\int 2x\bar{x}dx$ and $\int \bar{x}^2 dx$ in equation 3.134, we consider a graph of a function $f(x) = x$ as shown in figure 3.56.

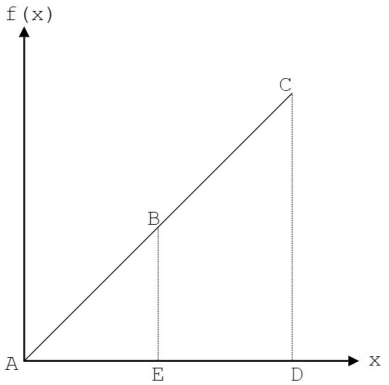

Figure 3.56: The graph of the function $f(x)$

In figure 3.56, consider right angle triangles $\triangle ACD$ and $\triangle ABE$. Let the lengths of line segments from point A to B is L_1, from point B to C is L_2, from point A to E is x_1, and from point A to D is x. Based on the Angle-Angle Triangle Similarity Theorem, triangles $\triangle ACD$ and $\triangle ABE$ are similar triangles. Therefore, based on this similarity theorem:

$$\frac{x_1}{x} = \frac{L_1}{L_1 + L_2} \tag{3.135}$$

Let point B indicates an average or mid point of line segment AC, then

$$L_1 = L_2 \tag{3.136}$$

Substitute equation 3.136 into 3.135

$$\frac{x_1}{x} = \frac{L_1}{L_1 + L_1} = \frac{1}{2} \tag{3.137}$$

Rearrange equation 3.137

$$x_1 = \frac{x}{2} \tag{3.138}$$

The average of values that will be returned by the function $f(x)$ is obtained at $x_1 = \frac{x}{2}$. Therefore, the average of values that will be returned by the function $f(x)$ is $\frac{x}{2}$. Let $\bar{x}$ is the average of values that will be returned by the function $f(x)$, therefore,

$$\bar{x} = \frac{x}{2} \tag{3.139}$$

The average of values that will be returned by the function $f(x)$ is given by

$$\bar{x} = \frac{\int x dx}{n} \tag{3.140}$$

where n denotes a number of continuous values that will be returned by the function at equal intervals.

Substitute equation 3.139 into 3.140

$$\frac{x}{2} = \frac{\int_0^x x dx}{n} \tag{3.141}$$

Solve equation 3.141

$$n = x + \frac{2c_o}{x} \tag{3.142}$$

where c_o is the constant

The value of the constant (c_o) is determined by considering the discrete number of values that will be returned by the function $f(x)$ at equal intervals. Accordingly, the value of c_o is determined to be 0.

Rearrange equation 3.140

$$n = \frac{\int x dx}{\bar{x}} \tag{3.143}$$

Substitute equation 3.143 into 3.142, and note that $c_o = 0$. Therefore,

$$x = \frac{\int x dx}{\bar{x}} \tag{3.144}$$

Rearrange equation 3.144

$$\bar{x} = \frac{1}{x} \int_0^x x dx \tag{3.145}$$

Therefore, the average of values that will be returned by the function $f(x)$ is $\frac{1}{x}\int_0^x xdx$

Substitute equation 3.145 into 3.134

$$E = 1 - \frac{\int x^2dx - \int 2xy? + \int y^2dy}{\int x^2dx - \int 2x(\frac{1}{x}\int_0^x xdx)dx + \int(\frac{1}{x}\int_0^x xdx)^2dx} \tag{3.146}$$

Simplify equation 3.146 (for the time being, let us leave out integral constant)

$$E = 1 - \frac{\frac{x^3}{3} - \int 2xy? + \frac{y^3}{3}}{\frac{x^3}{12}} \tag{3.147}$$

Consider equation 3.147

If y is expressed in terms of x, $? = dx$

If the measured and predicted values are equal (i.e., $y = x$), then

$$E = 1 - \frac{\frac{x^3}{3} - \int 2x^2dx + \frac{x^3}{3}}{\frac{x^3}{12}} \tag{3.148}$$

Simplify equation 3.148 (for the time being, leave out integral constant)

$$E = 1 \tag{3.149}$$

Equation 3.149 shows that the Nash–Sutcliffe efficiency (E) is equal to 1 if the measured values are exactly equal to the predicted values, which is true. Therefore, in equations 3.147 and 3.149, consideration of constants of integral is not important.

Consider equation 3.147

If the measured and predicted values are not equal (i.e., $y \neq x$ and $E < 1$), let $y = x + c$ where c is the correction constant that maximize the Nash–Sutcliffe efficiency. Therefore,

$$E = 1 - \frac{\frac{x^3}{3} - \int 2x(x+c)dx + \frac{y^3}{3}}{\frac{x^3}{12}} \tag{3.150}$$

Simplify equation 3.150 (consideration of a constant of integral is not important, therefore, leave out the constant of integral).

$$E = 1 - \frac{\frac{x^3}{3} - \frac{2x^3}{3} - cx^2 + \frac{y^3}{3}}{\frac{x^3}{12}} \tag{3.151}$$

Rearrange equation 3.151

$$y = \left(\frac{5-E}{4}x^3 + 3cx^2\right)^{\frac{1}{3}} \tag{3.152}$$

Consider equation 3.152

If a value of y is unknown, then the value of y is estimated based on given values of x, E, and c. Therefore, in equation 3.152, y and x are variables whereas E and c are constants

or calibration parameters that independently affect the calibration of the equation. From our derivation step, $E \leq 1$. However, the best value of E corresponding to a value of c, which maximize the prediction accuracy of the equation can fall outside this range (i.e., it can have a value greater than one). Therefore, based on equation 3.152, the general recommended value of E is less than or equal to 5.

Consider equation 3.152

Let us say variable y stands for the mass of soil loss, and variable x stands for the variables or factors that affect soil loss. Therefore, we apply equation 3.152, for instance, to modify the mathematical form of equation 3.130. Accordingly,

$$y = m \tag{3.153}$$

$$x = aQ^b(1-K)CPLS \tag{3.154}$$

Therefore, substitute equations 3.153 and 3.154 into equation 3.152

$$m = \left(\frac{5-E}{4}\left(aQ^b(1-K)CPLS\right)^3 + 3c\left(aQ^b(1-K)CPLS\right)^2\right)^{\frac{1}{3}} \tag{3.155}$$

We call equation 3.155 the RSLESYE-v2

Except for the constants c and E of the RSLESYE-v2, its other parameters are the same as that of the RSLESYE-v1.

3.7.1 Evaluating the RSLESYE-v2

Since RSLESYE-v1 is an integral part of the RSLESYE-v2, we can first evaluate the RSLESYE-v1 to determine its best parameters. The best exponent and topographic factor of the RSLESYE-v1 are determined by the procedure in section 3.6.3. We have already evaluated RSLESYE-v1, and we found its best exponent and topographic factor for all watersheds under our consideration (see section 4.5). For this best exponent (i,e., 1.42) and topographic factor (see section 4.5), the coefficient of the RSLESYE-v1 is estimated through calibration for the maximum performance of the RSLESYE-v1, as shown in figure 3.57.

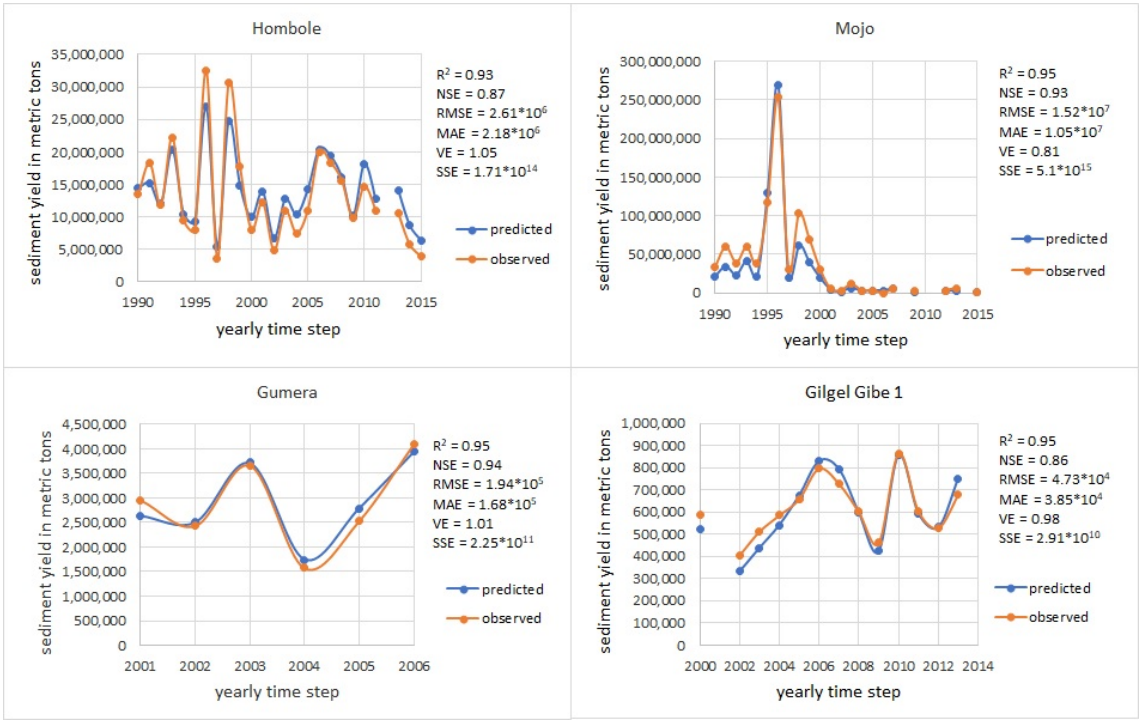

Figure 3.57: The performance of the calibrated RSLESYE-v1 when its exponent is 1.42 and its topographic factor is calculated using the equations that were proposed by Foster et al., (1977) and McCool et al., (1987, 1989), as cited by Renard et al. (1997).

Then, to evaluate the RSLESYE-v2, we use the calibrated values of RSLESYE-v1, and we estimate values of E and c through calibration. Figure 3.58 shows sample graphs of calibrated sediment yield. During calibration, a Nash-Sutcliffe efficiency corresponding to each value of E is evaluated, and a graph of E versus Nash-Sutcliffe efficiency, as well as a graph of c versus E are drawn for each watershed, as shown in figures 3.59 and 3.60.

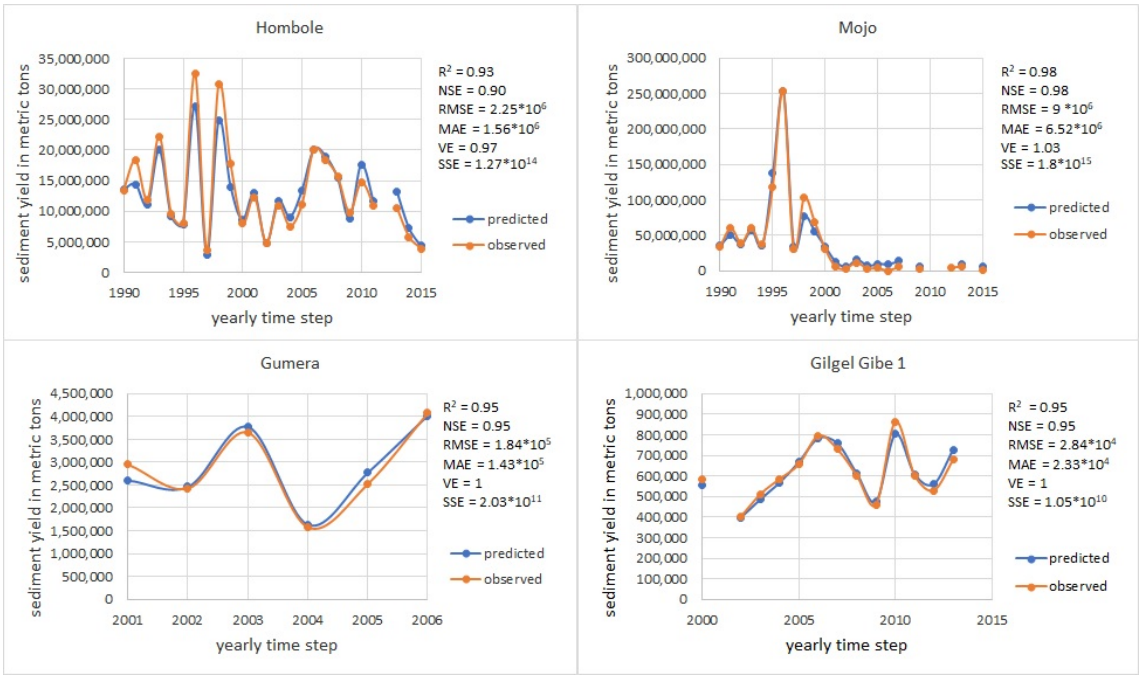

Figure 3.58: Sample graphs of observed and predicted sediment yield

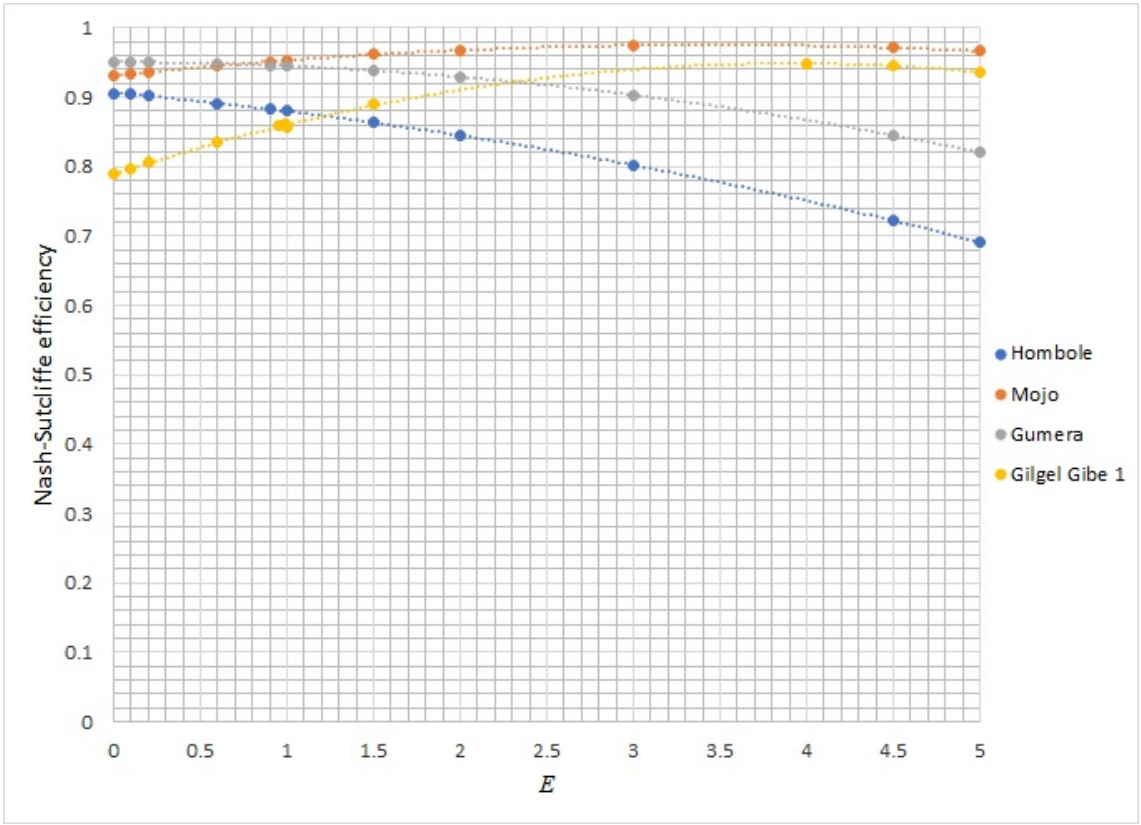

Figure 3.59: The relationship between the Nash-Sutcliffe efficiency and the calibration parameter E

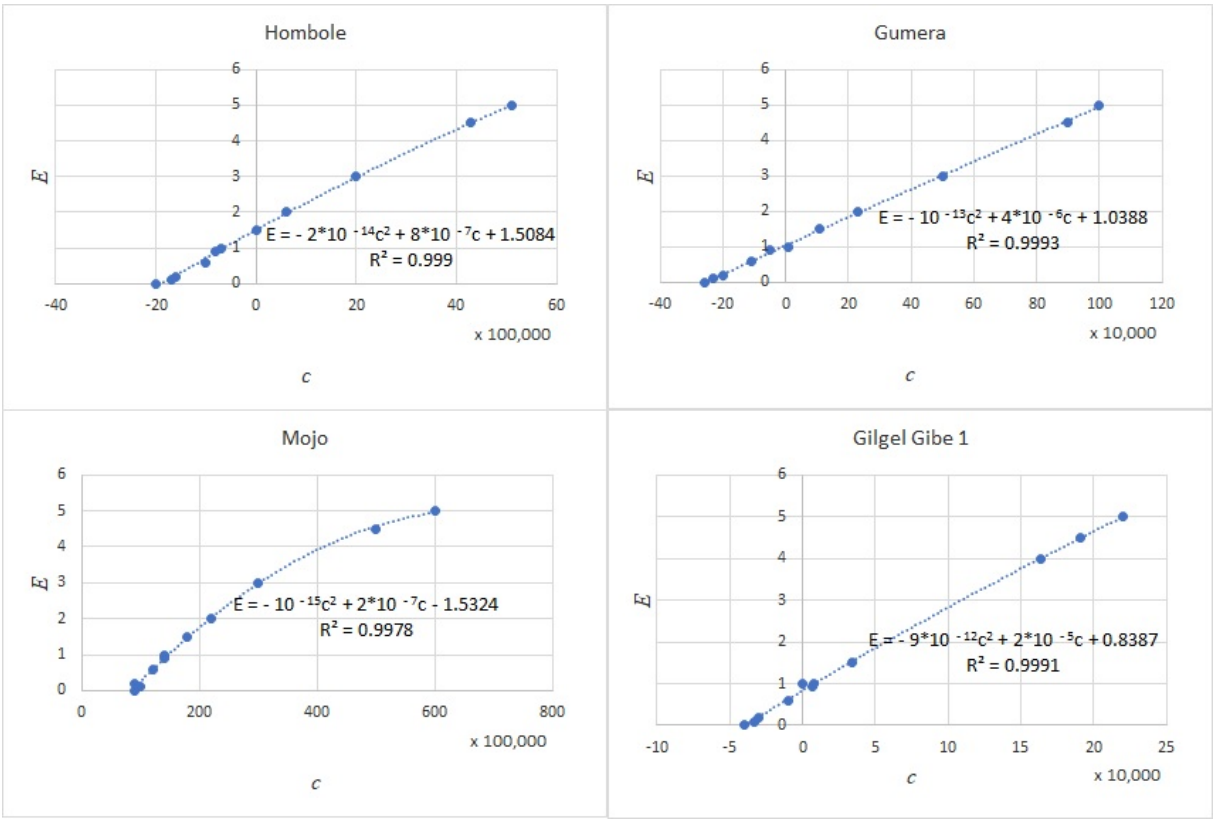

Figure 3.60: The relationship between the calibration parameters E and c

3.8 Checking the Performance of the Original SWAT+ Model

In the previous sections, we regionalized the MUSLE under the hydro-climatic conditions of Ethiopia, we improved the MUSLE, and we proposed the SLESYE and its revised versions by taking the observed flow as direct input data. However, if rainfall is taken as direct input data for sediment yield estimation, we apply the SWAT+ model for sediment yield estimation. This is because the model generates runoff by taking climatic data as its input data.

3.8.1 Selection of a Suitable Watershed

Selecting a suitable watershed based on the quality and quantity perspective of input data is important to apply the SWAT+ model. Compared with the other watersheds, we could see a sufficient number of climatic stations and a logical relationship between rainfall, flow, sediment, and impact of land use change for the Hombole Watershed (see section 3.2.4). And also, the performance of the sediment rating curve for the Hombole Watershed is good. Therefore, the Hombole Watershed is suitable for the implementation of the SWAT+ model, which is the largest watershed among the others. For a large watershed, applying the SWAT+ model is an appropriate approach to divide the watershed into sub-watersheds so as to consider spatial variation.

3.8.2 Preparation of Input Data for the SWAT+ Model

The required initial input data to run the SWAT+ model are DEM, stream network in the shape file, a geographic location of an outlet point, maps and tabular data of land use and soil, and tabular data of urban, plant, and climate data. The climate data includes precipitation, minimum and maximum temperature, wind speed, relative humidity, and solar radiation. We have prepared the maps (see sections 3.2.1 – 3.2.3), and the tabular data according to the input data format of the SWAT+ model. For a good reason, as the SWAT+ model had been demonstrated at Robit Watershed in Ethiopia, we used the standard urban and plant data of the SWAT+ model for our modeling.

Based on the initial input data, we can use the recommended land use management data (such as conservation practice, curve numbers, etc) in the SWAT+ model. The SWAT+ editor provides options to modify the initial input and the land use management data. As the calibration of the model determines the value of the input data parameters, the final value of the input data and model parameters can be decided based on the calibration and validation results of the model.

3.8.3 Estimation of the QSWAT+ Model Parameters

In the QSWAT+ model, the expression for calculating a channel width or depth (in meters) is given by $mult * A^{exp}$ where A is the drainage area, $mult$ and exp are the constants that depend on the channel width and depth. The channel width and depth affect the flow and sediment routing in the SWAT+ model, and they can be estimated through calibration. For the initial input values, the SWAT+ model assumes the default values for the constants. The initial default values may not be the same for all watersheds. Therefore, to estimate the values of the constants for the Hombole watershed, we considered four points on the mainstream of the watersheds; we estimate the channel width (w) based on a satellite image, and the channel depth (d) is estimated by considering maximum flow, and by applying the continuity equation or mass balance equation. Accordingly, the width and depth of the channel for the Hombole watershed can be determined by $w = 0.3A^{0.6}$ and $d = 0.00151A$
where A is the drainage area of the watershed

In this section, we considered a physical background to estimate the channel width and depth. However, we have to check whether this approach improves the initial performance of the model in the section 3.8.5.

3.8.4 Selection of Modelling Approaches in the SWAT+ Model

Among the SWAT+ modeling approaches, we focus on the modeling approaches which directly or indirectly affect sediment yield. The sediment yield is affected by surface runoff which in turn is affected by potential evapotranspiration and infiltration. The SWAT+ model uses different empirical equations to estimate each of these interrelated processes. Therefore, we select a suitable method based on the input data and modeling approach.

The SWAT+ model provides three alternative methods such as the Penman/Monteith, Priestley-Taylor, and Hargreaves methods to estimate potential evapotranspiration. It

also provides options to upload ET values directly. The Penman/Monteith method is intended to correctly predict ET under variate of locations and climate conditions and can be applied in case of data shortages (Wu et al., 2021). It is used to calculate potential evapotranspiration when temperature, wind speed and relative humidity data are available. The Priestley-Taylor equation, a simplification of the Penman/Monteith equation (Flint and Childs, 1991; Shekar and Hemalatha, 2021). The Hargreaves method is advantageous in regions where solar radiation, humidity, and wind data are lacking or are of low or questionable quality (Hargreaves and Allen, 2003). For our modeling approach, we selected the Penman/Monteith method.

The SWAT+ model provides two alternative methods for flow routing, such as variable storage and Muskingum methods. For the variable storage method, Shekar and Hemalatha (2021) reported that SWAT-2012 model did not perform a transformation of the outflow compared to the inflow. For the Muskingum method, Shekar and Hemalatha (2021) reported that the calculated evaporation in a reach for each sub-daily time step in SWAT-2009 and SWAT-2012 models was taken as daily evaporation, and the calculated transmission losses were not summed up during each time step to have the total amount of transmission losses during a day. Therefore, for flow routing in SWAT+ model, we can select the Muskingum method for daily time step. However, we can check that the model performance in either of the cases is the same for the watershed under our consideration (i.e., the Hombole Watershed).

The SWAT+ model provides three options to estimate runoff. These involve the calculation of daily curve number value as a function of soil moisture, daily CN value as a function of plant evapotranspiration, and using the traditional SWAT method that bases CN on soil moisture but retention is adjusted for mildly-slope field-drained watersheds. According to the traditional SWAT method, the retention should be adjusted as watersheds in Ethiopia are characterized by a hilly slope. The calculation of the daily CN value as the function of plant evapotranspiration may not be suitable due to limited daily temperature, relative humidity, and watershed management data. Since the SWAT+ provides the option to consider the warm-up period that determines initial soil moisture, we selected the daily CN values as the function of soil moisture.

The SWAT+ model provides two options for event codes. The first event code is daily/ rainfall/ curve number runoff/ daily routing, and the other event code is sub-daily rainfall/ Green and Ampt infiltration/sub-daily routing. Since we have daily rainfall data, we selected the first event code for our modeling approach.

The SWAT+ model provides three methods for sediment routing. These methods are the Bagnold model, Brownlie model, and Yang model. We can check that the model performance in all cases is the same for the selected watershed. There is a possibility that sediment transport equations yield similar sediment yields (Yen et al., 2017).

The SWAT+ model provides two methods to calculate the cover factor of the MUSLE. The first method is cover factor calculation using the minimum cover factor of a land cover, the total mass of the plant community, and surface residues. The other method is a new cover factor calculation without using the minimum cover factor of the land cover but the calculation is based on the total mass of the plant community above ground, total surface residues, and plant biomass. As there is no significant difference between these

two methods, we selected the first method for our modeling approaches.

3.8.5 Sensitivity Analysis, Calibration and Validation of the Original SWAT+ Model

Before we do sensitivity analysis, calibrate and validate the model, we first check the initial performance of the model. The initial performance of the model relates to the quality of input data, selected time steps, and modeling approaches of the SWAT+ model. Since we have observed flow and sediment data from 1990 – 2015 and four land use maps that show land use changes (see section 3.2.2), we check the initial performance of the model from 1990 – 2000. To calibrate sediment yield, we should first calibrate flow. Therefore, checking the initial performance of the model for daily, monthly, and yearly average flow is an important task. For evaluation, we use statistical performance measures such as R^2, NSE, RMSE, MAE, VE, and SSE, and we also use graphs to evaluate the performance of the model.

If we use all or a large number of the calibration parameters, we require a long time to calibrate the model as the model needs to be rerun several times, in this case, we may not easily calibrate the model. Sensitivity analysis is a technique to minimize the size of the calibration parameters by choosing the appropriate parameters that have a significant effect on flow or sediment yield. As compared to the other parameters, a change in the values of the appropriate parameters results in a higher value of the flow or sediment yield. We can do a manual or automatic sensitivity analysis. The result of the automatic sensitivity analysis depends on the number of times the model should be rerun and the algorithms it uses for sensitivity analysis. For example, the current version of the automatic sensitivity analysis and calibration tool like the SWAT+ Toolbox v1.0 supports four algorithms for the sensitive analysis, such as the Sobol, Fourier Amplitude, Random Balance Designs Fourier Amplitude, and Delta Moment-Independent Measure. We can check that the SWAT+ Toolbox v1.0 is not successful for a large watershed, as it takes more than a week for a few simulations runs.

Basically, the selection of the calibration parameters depends on the structure or mathematical form of the model (for example, see explanation in the section 3.3). To directly calibrate the model, we choose the following parameters which affect the flow. These are one of the sensitivity parameters which have been reported in the literature many times. We use the SWAT+ Toolbox v1.0 to calibrate the model, which uses Dynamically Dimensioned Search algorithms for the calibration. We use the following current best value of the parameters (in percent change) for the evaluation of the model, which were estimated using the SWAT+ Toolbox v1.0 at chosen 120 iterations.

Table 3.2: Automatically calibrated value of the selected flow calibration parameters, using the SWAT+ Toolbox v1.0.

Selected calibration parameters	Selected types of change	Selected range	Current best value
perco	percent change	-60 – 60	26.096

alpha	percent change	-60 – 60	59.736
flo_min	percent change	-60 – 60	-26.266
awc	percent change	-60 – 60	26.796
ovn	percent change	-60 – 60	-34.143
cn3_swf	percent change	-60 – 60	-16.226
epco	percent change	-60 – 60	51.905
esco	percent change	-60 – 60	47.492
cn2	percent change	-60 – 60	-57.468

For the validation of the model in the context of flow estimation, we use observed flow data from 2001 – 2015 provided that missing flow records on August 21, 2012, August 25, 2012, September 3, 2012, and September 6, 2012, are not considered for the comparison against the simulated flow. Since we want to minimize uncertainty, we prefer not to fill data using statistical approaches rather than we prefer not to consider the missing observed flow data. We check the performance of the calibrated model by changing the land use maps for the periods 2001 – 2008, 2009 – 2012, and 2013 – 2015, and without changing the land use map (i.e., the land use map of 1989 – 2000 is used for both calibration and validation periods).

As flow and sediment transport are interrelated processes, the calibration parameters which affect flow also affect sediment yield. It is important to note here that the flow calibration parameters which have less effect on flow may have much effect on sediment yield. We selected the following calibration parameters that only affect the sediment yield. These parameters are one of the sensitivity parameters which have been reported in literature many times. Due to the same reason mentioned above, the SWAT Toolbox v1.0 is not successful in the sensitivity analysis and calibration of sediment yield. We use the SWAT+ Editor to do sensitivity analysis manually. For the analysis, we take the minimum, maximum and intermediate values for one parameter while keeping the other parameters constant. We use the most sensitive parameter to calibrate the model. In the actual case, parameters usle_p and usle_k have equal sensitivity effect (for an explanation, see section 3.3). Therefore, one of these parameters is an unnecessary calibration parameter. The values of these parameters were assigned based on the explanations given in the section 3.3. To control the calibration parameters while considering the future evaluation of the model, we also assigned the values of the parameters which did not show a significant effect on sediment yield.

Table 3.3: The assigned and manually calibrated values of the sediment calibration parameters

Selected parameters	test range	sensitivity	assigned or calibrated value
lat_sed	0 – 5000	no significant changes were seen	0
spcon	0.0001 – 0.01	no significant changes were seen	1
spexp	1 – 1.50	no significant changes were seen	1
prf	0 – 2	no significant changes were seen	1
adj_pkr	0.5 – 2	no significant changes were seen	1
usle_p	0 – 1	no significant changes were seen	0.583
usle_k	0 – 1	no significant changes were seen	0.113
bedldcoef	0 – 1	significant changes were seen	0.055

For the validation of the model in the context of sediment yield estimation, we use sediment data generated by the sediment rating equation. Since there are missing flow records on August 21, 2012, August 25, 2012, September 3, 2012, and September 6, 2012, we do not have sediment data in these periods to compare against the simulated sediment.

3.9 Modifying the SWAT+ Model for Sediment Yield Estimation

In this section, we modify the source code of the SWAT+ model rev.60.5.4 in three different types for sediment yield estimation. To evaluate these three types of the SWAT+ models, we use the same calibration parameters, data, and approach as the original SWAT+ model.

3.9.1 Type One

Compared to the other parameters of the MUSLE, the parameter whose value can be estimated through calibration is the exponent (see explanation in the section 3.3). In the previous section, we determined the best exponent and the best equation of the topographic factor of the MUSLE under the hydro-climatic condition of Ethiopia. Therefore, to modify the source code of the SWAT+ model rev.60.5.4 for sediment yield estimation, we replace the best exponent ($b = 0.57$) and the following best equation of the topographic factor in the source code, i.e., in the subroutine ero_ysed and subroutine

hru_lte_read respectively.

$$LS = (0.02222J^{1.5} + 0.03231J + 0.1004) * 0.2901 \triangle y^{0.4002} \text{ for } J < 5\% \quad (3.156)$$

$$LS = (0.02222J^{1.5} + 0.03231J + 0.1004) * 0.2105 \triangle y^{0.5004} \text{ for } J > 5\% \quad (3.157)$$

where L is the slope length factor, S is the slope steepness factor, J is the slope in %, $\triangle y = \lambda/22.1$, and λ is the slope length.

a) Before modification

The original source code of the SWAT+ model rev.60.5.4, in the subroutine ero_ysed, which require modifications are provided below.

```
sedyld(j) = (10. * surfq(j) * qp_cms * hru(j)%area_ha) ** .56 * cklsp(j)
qp_cms = qp_cms * 3.6 / hru(j)%km !cms–> mm/h
sedyld(j) = 1.586 * rock * (surfq(j) * qp_cms) ** .56 * (hru(j)%area_ha) ** 0.12 * &
usle_cfac(j) * soil(j)%ly(1)%usle_k * hru(j)%lumv%usle_p * hru(j)%lumv%usle_ls
```

The original source code of the SWAT+ model rev.60.5.4, in the subroutine hru_lte_read, which require modifications are provided below.

```
xm = 0.
xm = .6 * (1. - EXP(-35.835 * hlt_db(idb)%slope))
sin_sl = SIN(Atan(hlt_db(idb)%slope))
hlt_db(idb)%uslels = (hlt_db(idb)%slopelen/22.128)**xm * &
(65.41 * sin_sl * sin_sl + 4.56 * sin_sl + .065)
```

b) After modification

The modified source code of the SWAT+ model rev.60.5.4, in the subroutine ero_ysed, are given below.

```
sedyld(j) = (surfq(j) * qp_cms * hru(j)%area_ha) ** .57 * 4000. * cklsp(j) * rock
```

The modified source code of the SWAT+ model rev.60.5.4, in the subroutine hru_lte_read, are given below.

```
sin_sl = hlt_db(idb)%slope *100.
if(sin_sl < 5.0) then
hlt_db(idb)%uslels = (hlt_db(idb)%slopelen/22.1)**0.4002 * 0.2901 * & (0.02222 *
sin_sl**1.5 + 0.03231*sin_sl + 0.1004)
else
hlt_db(idb)%uslels = (hlt_db(idb)%slopelen/22.1)**0.5004 * 0.2105 * & (0.02222 *
sin_sl**1.5 + 0.03231*sin_sl + 0.1004)
end if
```

We call this type the SYEt1-SWAT+ model

3.9.2 Type Two

The SWAT+ model provides calibration parameters like peak rate adjustment factor for sediment routing in the subbasin (tributary channels) (adj_pkr) and peak rate adjustment factor for sediment routing in the main channel (prf), their values can be estimated

during the calibration of sediment yield. There is uncertainty that how likely the SWAT+ model estimates the actual peak runoff rate. To minimize uncertainty, in our previous section, the peak runoff rate is eliminated in the improved MUSLE. Therefore, we improve the SWAT+ model by replacing the improved MUSLE ($aQ^{1.44}KLSCP$) in the place of the MUSLE in the source code, i.e., in the subroutine ero_ysed. The following best equation of the topographic factor corresponding to the improved MUSLE is also replaced in place of the topographic factor of the MUSLE in the source code, i.e., in the subroutine hru_lte_read.

$$L = \left(\frac{\lambda}{22.13}\right)^{m} \tag{3.158}$$

$$m = \frac{\beta}{1+\beta} \tag{3.159}$$

$$\beta = \frac{\frac{\sin\theta}{0.0896}}{3\left(\sin\theta\right)^{0.8} + 0.56} \tag{3.160}$$

$$S = 10.8\sin\theta + 0.03 \text{ if the slope is less than } 9\% \tag{3.161}$$

$$S = 16.8sin\theta - 0.5 \text{ if the slope is greater than or equal to } 9\% \tag{3.162}$$

where λ is the slope length (m), and θ is the angle of the slope in degree.

a) Before modification

The original source code of the SWAT+ model, in the subroutine ero_ysed, which require modifications are provided in section 3.9.1. The original source code of the SWAT+ model, in the subroutine hru_lte_read, which require modifications are provided below.

```
 xm = .6 * (1. - EXP(-35.835 * hlt_db(idb)%slope))
hlt_db(idb)%uslels = (hlt_db(idb)%slopelen/22.128)**xm * &
(65.41 * sin_sl * sin_sl + 4.56 * sin_sl + .065)
```

b) After modification

The modified source code of the SWAT+ model rev.60.5.4, in the subroutine ero_ysed, are given below.

```
 sedyld(j) = (surfq(j)) ** 1.44 * cklsp(j) * rock
```

The modified source code of the SWAT+ model rev.60.5.4, in the subroutine hru_lte_read, are given below.

```
betha4_imusle = sin_sl / 0.0896* (3.0 * sin_sl ** 0.8 + 0.56)
xm = betha4_imusle / (betha4_imusle +1)
if (hlt_db(idb)%slope < 0.09) then
hlt_db(idb)%uslels = (hlt_db(idb)%slopelen/22.13)**xm * &
(10.8 * sin_sl + .003)
else
hlt_db(idb)%uslels = (hlt_db(idb)%slopelen/22.13)**xm * &
(16.8 * sin_sl - .5)
end if
```

We call this type the SYEt2-SWAT+ model

3.9.3 Type Three

In this case, we modify the SWAT+ model by replacing the RSLESYE-v1 ($aQ^{1.42}(1-K)LSCP$) in the place of the MUSLE in the source code, i.e., in the subroutine ero_ysed. The best equation of the topographic factor corresponding to the RSLESYE-v1 is also replaced in the place of the topographic factor of the MUSLE in the source code, i.e., in the subroutine hru_lte_read.

a) Before modification

The original source code of the SWAT+ model, in the subroutine ero_ysed, which require modifications are provided in section 3.9.1. The original source code of the SWAT+ model, in the subroutine hru_lte_read, which require modifications are provided in section 3.9.2.

b) After modification

The modified source code of the SWAT+ model rev.60.5.4, in the subroutine ero_ysed, are given below.

```
sedyld(j) = (surfq(j)) ** 1.42 * cklsp(j) * rock
```

! note the value of K is replaced by the value of $1-K$ in user soil table. The modified source code of the SWAT+ model rev.60.5.4, in the subroutine hru_lte_read, are given below.

```
betha4_imusle = sin_sl / 0.0896* (3.0 * sin_sl ** 0.8 + 0.56)
xm = betha4_imusle / (betha4_imusle +1)
if (hlt_db(idb)%slope < 0.09) then
hlt_db(idb)%uslels = (hlt_db(idb)%slopelen/22.13)**xm * &
(10.8 * sin_sl + .003)
else
hlt_db(idb)%uslels = (hlt_db(idb)%slopelen/22.13)**xm * &
(16.8 * sin_sl - .5)
end if
```

We call this type the SYEt3-SWAT+ model

3.10 Compiling the SWAT+ Editor

After compiling source code for both debug and release versions, we will obtain executable applications. We pack these two applications with SWAT+ Editor files, and we follow the following steps to compile SWAT+ Editor (these steps are taken from the original SWAT+ Editor's 'README' file).

1. Install Python 3 and up from https://www.python.org/
2. Install required Python packages
    - From command prompt, go to source code '/api' directory
    - Run 'pip install -r requirements.txt'
3. Update the 'appsettings.json' file in the root of the source code directory with your

python PATH variable (typically 'python' on Windows)

4. Install Node.js from https://nodejs.org/en/
5. Install required Node.js packages
    - From command prompt, go to the root directory of the source code
    - Run 'npm install'
6. If needed, adjust the 'pythonPath' setting in 'appsettings.json'; change to 'python' (Windows)
7. From command prompt, go to the root directory of the source code
8. Run 'npm run serve'
9. In another prompt, run 'npm run electron'

3.11 An Iterative Approach for Deriving and Solving an Accurate Regression Equation

In actual modelling, the underlying processes are generally complex and not well understood, this means that we have little or no idea about the form of the relationship (Seber and Wild, 2003). For example, different authors indicate that the power function is a commonly used nonlinear regression approach to model the sediment rating curve (eg.,Asselman (2000); Hapsari et al. (2019); Heng and Suetsugi (2014)). However, the error of the regression equation is very large. In this section, we provide a method to derive an accurate regression equation for sediment rating.

3.11.1 An Iterative Approach to Derive an Accurate Regression Equation

To arrive at iteration steps, let us begin from the following definition.

Definition: for given values of paired variables S and Q, variables x and y are defined by

$$y = i(bS)^{1/u} + jQ \tag{3.163}$$

$$x = k(hQ)^{1/w} + t \tag{3.164}$$

where i, b, u, j, k, h, w and t are constants.

Let $y \approx y(x)$

Since a polynomial function can accommodate negative or positive value, let us consider a polynomial function $y(x)$

$$y(x) = a_n x^n + a_{n-1}x^{n-1} + a_{n-2}x^{n-2} + ... + c \tag{3.165}$$

$$y = y(x) + e \tag{3.166}$$

where e is the error value

Substitute equation 3.163 into 3.166

$$i(bS)^{1/u} + jQ = y(x) + e \tag{3.167}$$

Rearrange equation 3.167

$$S = \frac{1}{bi^u}\left(y(x) - jQ + e\right)^u \tag{3.168}$$

In equation 3.168, variables $y(x)$, Q and e are connected by plus and minus sign. It shows that values of variables $y(x)$, Q or e have an individual effect on a value of variable S. This is a reason why we defined x and y in the above way to arrive at equation 3.168.

Let

$$e = e_1 + e_2 + e_3 + ... + e_{p-1} + e_p \tag{3.169}$$

Substitute equation 3.169 into 3.168

$$S = \frac{1}{bi^u}\left(y(x) - jQ + e_1 + e_2 + e_3 + ...e_{p-1} + e_p\right)^u \tag{3.170}$$

Equation 3.170 represents an actual value of variable S. In equation 3.170, if a value of error e_p is the minimum tolerable error that could be ignored, then the sum of error values e_1, e_2, e_3,....e_{p-1} represents an approximate value of the total error e. Therefore, the predicted value of variable S (let us say S_p) is given by

$$S_p = \frac{1}{bi^u}\left(y(x) - jQ + e_1 + e_2 + e_3 + ... + e_{p-1}\right)^u \tag{3.171}$$

Therefore, the difference between S and S_p is an error, which is equal to E_p (i.e., $E_p = S - S_p$), where $p-1$ refers to the number values of error e should be required to derive an accurate regression equation at p number of iteration steps. If there are $p-1$ number of values of error e (i.e., e_1, e_2, $e_3...e_{p-1}$), there are also $p-1$ number of values of corresponding error E (i.e., E_1, E_2, $E_3...E_{p-1}$).

Logic is now if we are able to express error e as a function of error E, we can derive an accurate regression equation. This is because of both errors (i.e., e and E) is the function of variables Q and S. Therefore, we define an iterative procedure to approximate a value of error e based on a value of the corresponding error E. Let an approximate value of error e_1, e_2, $e_3...e_{p-1}$ be equal to r_1, r_2, $r_3...r_{p-1}$ respectively. Therefore, the following iteration steps are defined based on equation 3.171 and the explanations above.

For the first iteration step ($p = 1$), $e_0 = 0$, $E_0 = 0$ and $r_0 = 0$. Therefore, the first predicted value of variable S (i.e., S_1) is determined by

$$S_1 = \frac{1}{bi^u}\left(y(x) - jQ\right)^u \tag{3.172}$$

If $S_1 \approx S$, no need to proceed to the next iteration step. If $S_1 \not\approx S$, we proceed to the next iteration step.

For the second iteration step ($p = 2$), e_1, E_1 and r_1 is determined by

$$e_1 = y - y(x) \tag{3.173}$$

$$E_1 = S - S_1 \tag{3.174}$$

$$r_1 = f_1(E_1) \tag{3.175}$$

where f_1 is the polynomial regression function between the values of e_1 and E_1. Therefore, at the second iteration step, the second predicted value of variable S (i.e., S_2) is determined by

$$S_2 = \frac{1}{bi^u} \left(y(x) - jQ + r_1\right)^u \tag{3.176}$$

If $S_2 \approx S$, no need to proceed to the next iteration step. If $S_2 \not\approx S$, we proceed to the next iteration step.

For the third iteration step ($p = 3$), e_2, E_2 and r_2 is determined by

$$e_2 = y - \left(y(x) + r_1\right) \tag{3.177}$$

$$E_2 = S - S_2 \tag{3.178}$$

$$r_2 = f_2(E_2) \tag{3.179}$$

where f_2 is the polynomial regression function between the values of e_2 and E_2. Therefore, at the third iteration step, the third predicted value of variable S (i.e., S_3) is determined by

$$S_3 = \frac{1}{bi^u} \left(y(x) - jQ + r_1 + r_2\right)^u \tag{3.180}$$

If $S_3 \approx S$, no need to proceed to the next iteration step. If $S_3 \not\approx S$, we proceed to the next iteration step.

For the fourth iteration steps ($p = 4$), e_3, E_3 and r_3 is determined by

$$e_3 = y - \left(y(x) + r_1 + r_2\right) \tag{3.181}$$

$$E_3 = S - S_3 \tag{3.182}$$

$$r_3 = f_3(E_3) \tag{3.183}$$

where f_3 is the polynomial regression function between the values of e_3 and E_3. Therefore, at the fourth iteration step, the fourth predicted value of variable S (i.e., S_4) is determined by

$$S_4 = \frac{1}{bi^u} \left(y(x) - jQ + r_1 + r_2 + r_3\right)^u \tag{3.184}$$

If $S_4 \approx S$, no need to proceed to the next iteration step. If $S_4 \not\approx S$, we proceed to the next iteration step.

For the $(p-1)$th iteration step, e_{p-2}, E_{p-2} and r_{p-2} is determined by

$$e_{p-2} = y - \left(y(x) + r_1 + r_2 + r_3 + ... + r_{p-3}\right) \tag{3.185}$$

$$E_{p-2} = S - S_{p-2} \tag{3.186}$$

$$r_{p-2} = f_{p-2}(E_{p-2}) \tag{3.187}$$

where f_{p-2} is the polynomial regression function between the values of e_{p-2} and E_{p-2}. Therefore, at the $(p-1)$th iteration step, the $(p-1)$th predicted value of variable S (i.e., S_{p-1}) is determined by

$$S_{p-1} = \frac{1}{bi^u}\left(y(x) - jQ + r_1 + r_2 + r_3 + ... + r_{p-2}\right)^u \tag{3.188}$$

For the pth iteration step, e_{p-1}, E_{p-1} and r_{p-1} is determined by

$$e_{p-1} = y - \left(y(x) + r_1 + r_2 + r_3 + ... + r_{p-2}\right) \tag{3.189}$$

$$E_{p-1} = S - S_{p-1} \tag{3.190}$$

$$r_{p-1} = f_{p-1}(E_{p-1}) \tag{3.191}$$

where f_{p-1} is the polynomial regression function between the values of e_{p-1} and E_{p-1}. Therefore, at the pth iteration step, the pth predicted value of variable S (i.e., S_p) is determined by

$$S_p = \frac{1}{bi^u}\left(y(x) - jQ + r_1 + r_2 + r_3 + ...r_{p-2} + r_{p-1}\right)^u \tag{3.192}$$

3.11.2 Determining the Final Form of the Accurate Regression Equation

Suppose at the pth iteration step, $S \approx S_P$. Then, the final form of an accurate regression equation is obtained through substitutions.

Substitute equation 3.172 into 3.174

$$E_1 = S - \frac{1}{bi^u}\left(y(x) - jQ\right)^u \tag{3.193}$$

Substitute equation 3.176 into 3.178

$$E_2 = S - \frac{1}{bi^u}\left(y(x) - jQ + r_1\right)^u \tag{3.194}$$

Substitute equation 3.180 into 3.182

$$E_3 = S - \frac{1}{bi^u}\left(y(x) - jQ + r_1 + r_2\right)^u \tag{3.195}$$

Substitute equation 3.188 into 3.190

$$E_{p-1} = S - \frac{1}{bi^u}\left(y(x) - jQ + r_1 + r_2 + r_3... + r_{p-2}\right)^u \tag{3.196}$$

Substitute equation 3.193 into 3.175

$$r_1 = f_1\left(S - \frac{1}{bi^u}(y(x) - jQ)^u\right) \tag{3.197}$$

Substitute equation 3.194 into 3.179

$$r_2 = f_2\left(S - \frac{1}{bi^u}(y(x) - jQ + r_1)^u\right) \tag{3.198}$$

Substitute equation 3.195 into 3.183

$$r_3 = f_2\left(S - \frac{1}{bi^u}(y(x) - jQ + r_1 + r_2)^u\right) \tag{3.199}$$

Substitute equation 3.196 into 3.191

$$r_{p-1} = f_{p-1}\left(S - \frac{1}{bi^u}(y(x) - jQ + r_1 + r_2 + r_3... + r_{p-2})^u\right) \tag{3.200}$$

Substitute equation 3.197 into 3.198; equations 3.197 and 3.198 into 3.199; equations 3.197, 3.198 and 3.199 into 3.200 and so on. After all substitutions have been done one after the other, then the final resulting equation is very long. But, we can see that r_1, r_2, $r_3...r_p$ is the function of variables Q and S. For given values of paired variables, i, b, u, j, k, h, w and t are all constants. Therefore,

$$r_1 + r_2 + r_3 + ... + r_{p-1} = f_1(Q,S) + f_2(Q,S) + f_3(Q,S)... + f_{p-1}(Q,S) \tag{3.201}$$

Substitute equation 3.201 into 3.192

$$S_p = \frac{1}{bi^u}\left(y(x) - jQ + f_1(Q,S) + f_2(Q,S) + f_3(Q,S)... + f_{p-1}(Q,S)\right)^u \tag{3.202}$$

Substitute equation 3.164 into 3.165

$$y(x) = a_n\left(k(hQ)^{1/w} + t\right)^n + a_{n-1}\left(k(hQ)^{1/w} + t\right)^{n-1} + a_{n-2}(k(hQ)^{1/w} + t)^{n-2} + ... + c \tag{3.203}$$

From equation 3.203, $y(x)$ is the function of variable Q. Therefore,

$$y(x) = f(Q) \tag{3.204}$$

Substitute equation 3.204 into 3.202

$$S_p = \frac{1}{bi^u}\left(f(Q) - jQ + f_1(Q,S) + f_2(Q,S) + f_3(Q,S)... + f_{p-1}(Q,S)\right)^u \tag{3.205}$$

Suppose at the pth iteration step, $S \approx S_P$. Therefore, equation 3.205 is given by

$$S \approx \frac{1}{bi^u}\left(f(Q) - jQ + f_1(Q,S) + f_2(Q,S) + ... + f_{p-1}(Q,S)\right)^u \tag{3.206}$$

Equation 3.206 is the shorthand form of a very long equation. The substituting equations' power constants u, w, and n make the equation complex and difficult to simplify. However, the substituting equations that form the complex equation are easily interconnected in an Excel spreadsheet or programmed in Matlab. As we can see from equation 3.206, there are only two variables Q and S. Therefore, we can solve this equation for a given value of Q or S. A procedure to solve the equation is provided in section 3.11.5.

3.11.3 Determining Initial Values for Deriving an Accurate Regression Equation

In sections 3.11.1 and 3.11.2, we showed the steps to derive and determine the final form of the accurate regression equation based on values of paired variables S and Q. To start deriving the equation based on the values of the paired variables S and Q, we should have to first determine the constants (see equations 3.163 and 3.164). The polynomial function (see equation 3.165) directly describes the relationship between variables x and y, but it indirectly describes the relationship between variables S and Q. Therefore, for given values of paired variables S and Q, we find values of constants i, b, u, j, k, h, w, and t for equations 3.163 and 3.164 such that plots of x versus y yield a smooth curve of a polynomial function. Accordingly, once all values of constants are known, the initial and final values of variables will be determined by following the iteration steps above.

3.11.4 Deriving an Accurate Sediment Rating Equation

In above sections, we indicated the general directions showing how to derive and determine the final form of the accurate regression equation, and we also indicated the direction showing how to determine the initial values to start deriving the equation. For a practical example, we use sediment concentration and corresponding river or streamflow data (see table 3.4) to derive an accurate sediment rating equation. In the table, suspended sediment concentration data is represented by variable S whereas flow data is represented by variable Q.

Table 3.4: Sediment concentration versus river or streamflow data

S	Q	S	Q	S	Q	S	Q	S	Q	S	Q
0.14	4.45	0.38	20.12	2.36	94.00	1.39	0.17	1.49	31.02	0.69	199.26
1.28	6.25	1.32	15.30	0.32	17.68	1.03	1.53	0.55	25.32	0.90	189.28
0.16	2.21	12.49	149.06	3.93	42.80	0.44	21.83	0.77	17.64	0.57	198.42
0.24	37.89	0.28	15.04	4.07	119.92	1.12	93.23	0.44	3.15	0.53	319.65
0.21	33.19	14.66	37.81	2.42	6.09	1.30	74.07	1.33	12.06	0.77	110.63
0.14	30.44	1.98	167.03	0.74	0.49	0.92	1.60	1.26	14.15	0.67	104.23
0.19	37.09	4.62	114.72	2.67	57.20	1.18	24.21	0.74	5.39	0.51	153.16
0.26	40.82	2.58	59.48	1.00	56.88	0.62	17.47	1.01	53.83	0.35	159.87
0.15	1.51	3.67	152.82	1.29	52.23	4.95	144.55	4.32	39.80	0.25	135.77
0.24	2.51	1.15	238.53	10.35	57.74	5.58	108.34	1.63	13.08	0.17	3.12
2.14	54.81	1.91	58.37	25.17	49.32	0.81	9.69	24.41	2.40	0.18	29.89
0.67	23.65	0.89	4.79	1.81	108.29	0.76	9.72	28.09	0.63	0.23	3.64
1.18	30.74	0.61	5.10	36.73	159.62	11.86	15.58	2.37	39.32	0.76	12.60
0.43	32.12	1.41	32.37	51.81	179.98	1.40	93.23	1.88	17.10	0.53	113.22
0.75	38.05	0.58	24.74	90.85	69.49	5.28	105.25	2.81	25.48	0.43	97.20
0.32	20.44	2.24	11.55	4.96	128.92	1.16	104.70	19.72	1.30	0.80	50.24

3.53	55.26	1.42	13.48	4.11	104.01	0.48	36.19	23.65	1.51	0.17	1.28
0.41	21.89	13.49	40.42	2.22	82.63	1.37	38.07	19.66	0.99	0.37	0.31
2.49	35.16	6.76	43.20	0.42	5.31	1.81	42.83	0.16	0.29	10.07	37.64
1.21	63.67	2.70	75.92	0.33	6.18	0.56	37.75	0.52	2.53	0.54	0.45
0.65	37.58	1.33	130.30	0.33	5.18	1.49	37.75	17.00	5.25	0.29	35.88
0.41	22.34	11.75	176.14	0.20	2.21	0.42	48.70	0.30	0.23	3.11	117.10
2.83	44.08	5.42	111.82	0.16	2.48	0.43	48.70	0.80	0.31	5.37	207.80
1.48	24.09	2.94	98.13	0.28	3.08	0.42	35.76	23.20	32.44	5.04	95.13
0.63	22.51	3.83	99.30	0.95	5.64	0.78	48.92	0.43	0.43	3.36	146.50
6.73	133.89	1.35	168.55	0.68	6.99	7.12	95.55	31.05	50.11	3.87	152.71
0.45	31.28	1.24	20.22	0.34	3.72	0.60	54.25	20.31	10.16	2.63	50.12
0.48	31.03	1.78	62.43	0.19	5.43	0.78	56.13	0.32	0.22	5.95	62.99
0.44	57.53	3.43	71.05	1.38	53.34	2.79	13.58	0.36	0.44	3.26	73.70
0.20	34.61	2.63	38.20	1.31	67.62	3.78	10.14	14.60	228.98	3.23	129.79
0.28	32.44	3.13	39.30	2.18	8.69	3.30	5.27	30.02	127.80	2.07	122.71
0.37	26.92	0.93	48.68	3.16	44.75	0.65	41.22	7.70	10.93	0.65	73.37
0.20	2.70	0.38	28.72	0.38	12.68	2.85	47.26	33.64	28.16	3.04	129.32
2.58	93.17	0.36	34.10	4.97	31.55	0.39	41.71	27.86	30.54	2.19	152.27
0.15	1.21	2.87	151.57	3.24	44.48	0.30	39.25	2.58	2.54	4.74	180.53
0.38	33.75	7.17	33.49	4.64	45.20	1.27	65.49	9.56	12.85	1.55	118.12
0.34	30.32	0.57	16.89	39.48	56.21	3.44	271.87	3.57	21.47	0.17	3.19
0.19	3.98	4.71	37.33	0.34	6.30	1.74	208.40	4.75	16.66	7.24	225.41
0.36	4.61	3.49	40.91	59.70	61.38	0.39	29.66	1.63	2.89	5.13	176.56
1.39	102.17	1.34	33.79	13.36	148.11	1.80	85.73	37.06	22.19	5.27	221.30
1.11	59.16	3.86	74.78	0.63	4.54	3.33	108.97	0.33	0.23	2.47	171.11
0.52	33.87	0.48	24.69	0.40	0.57	0.85	69.59	0.27	1.72	3.94	276.35
0.27	152.47	7.52	75.00	0.30	0.13	5.34	127.63	0.47	1.56	1.08	110.00
18.53	78.29	1.28	16.81	0.19	0.48	2.48	77.18	0.36	0.75	2.52	137.09
0.38	2.89	0.97	27.20	0.63	0.60	12.29	98.50	37.66	36.81	0.28	17.58
0.27	11.05	1.08	59.65	1.08	1.01	3.42	110.31	11.92	214.26	0.21	17.16
0.54	14.02	2.94	66.77	1.25	23.21	4.41	70.46	23.07	67.11	0.24	19.31
0.79	19.02	1.57	66.74	0.35	14.29	8.77	108.26	2.89	6.26	0.63	101.23
1.29	58.66	0.23	32.58	5.50	31.05	0.29	46.20	9.81	9.92	2.68	274.87
0.60	4.56	2.93	66.22	0.36	1.30	0.69	35.27	0.39	0.17	2.01	140.60
0.23	24.35	3.61	23.95	0.24	1.83	6.14	60.28	0.29	1.85	0.94	148.94
0.30	29.23	0.58	15.38	0.27	1.83	7.78	82.47	3.20	7.15	3.40	179.02
0.36	23.58	4.46	119.18	2.61	46.23	5.45	72.37	0.33	1.27	4.83	181.19

0.73	226.44	1.53	16.09	2.30	107.37	1.80	72.65	0.50	0.88	2.76	175.82
1.04	231.54	4.27	30.15	5.80	355.23	6.28	144.50	8.06	6.52	4.44	214.76
0.71	173.97	0.54	30.39	18.50	133.38	0.76	13.54	0.48	1.13	1.76	115.29
1.59	50.64	0.51	26.49	4.67	148.95	0.72	12.26	19.58	85.06	4.95	177.35
4.82	99.40	0.28	12.27	1.87	132.59	0.82	11.28	0.30	0.72	1.48	101.10
2.82	18.86	0.33	61.50	3.57	113.26	0.80	12.24	1.16	1.21	6.10	145.92
0.61	72.30	0.32	38.59	6.87	118.23	0.73	9.70	0.39	1.14	6.09	152.61
1.17	84.22	1.28	23.90	5.27	121.66	0.81	10.55	0.36	0.64	4.34	142.45
0.41	12.03	0.24	49.53	0.25	1.50	0.75	10.38	0.46	0.36	3.20	153.48
0.46	16.91	8.39	232.91	0.27	1.80	0.86	11.69	0.23	0.64	6.96	263.48
1.50	16.62	0.20	0.42	0.31	0.78	0.76	11.85	0.33	1.38	1.77	127.29
0.62	17.65	0.18	6.47	2.19	0.76	55.67	103.16	0.26	0.97	2.00	88.42
0.42	10.38	0.76	11.92	11.84	0.77	40.87	56.90	0.35	1.63	3.36	108.43
0.38	62.83	0.30	10.18	4.26	0.74	20.17	25.76	11.58	18.41	4.12	109.92
0.48	44.38	0.54	4.93	5.77	0.32	11.20	16.43	0.21	1.97	0.91	93.72
0.29	25.15	31.76	55.98	4.50	0.44	9.71	19.69	14.76	12.43	2.84	94.94
0.27	2.72	7.66	197.55	6.59	0.43	3.03	37.75	45.57	9.86	4.59	129.44
1.62	11.78	1.38	134.05	0.92	11.76	11.27	26.97	8.05	3.37	2.51	139.24
5.35	53.47	1.17	22.75	31.40	1.60	69.93	34.78	13.44	5.32	2.58	144.18
0.29	4.23	1.19	195.35	8.40	0.93	6.13	21.76	15.25	23.31	5.72	171.62
7.07	200.33	0.97	193.68	5.20	0.44	39.35	117.00	34.20	16.55	3.96	207.69
0.57	7.86	1.37	201.84	12.68	0.44	27.25	37.75	15.01	16.64	2.13	146.80
1.05	9.04	1.69	205.97	0.71	9.93	21.58	30.66	18.28	24.10	3.31	148.29
0.68	53.32	1.11	139.99	4.39	0.72	18.56	23.01	8.58	10.44	4.87	187.62
0.45	66.91	1.30	168.31	36.95	0.72	11.80	19.02	0.21	0.43	2.62	118.57
0.60	51.73	2.25	264.60	0.71	13.37	6.45	22.07	14.17	10.15	1.38	94.30
0.35	5.62	1.14	233.50	10.20	361.08	3.67	97.29	0.88	0.65	7.70	208.42
0.53	6.71	1.71	18.52	2.47	254.38	1.12	86.98	25.65	29.16	5.50	112.99
0.25	8.90	2.14	236.63	2.19	245.57	2.98	83.68	12.38	10.89	5.11	184.17
7.06	18.77	3.22	17.85	2.87	51.24	5.70	119.69	35.03	6.75	5.17	154.67
1.19	50.21	0.76	17.13	8.82	154.82	3.23	124.85	2.94	1.35	3.95	127.96
1.58	111.47	2.74	13.87	2.64	235.94	4.67	126.00	5.16	4.97	4.78	176.35
3.37	76.86	25.59	97.91	3.74	289.75	4.78	140.53	2.11	1.16	6.53	212.73
0.99	62.46	2.24	66.73	2.03	246.12	5.83	84.36	0.18	9.62	1.82	139.40
0.30	24.61	0.98	98.90	0.86	43.60	2.74	41.96	0.15	114.51	3.48	200.64
0.34	26.30	1.00	73.00	14.64	43.91	0.45	38.08	0.12	3.72	5.06	153.94
3.59	87.21	3.23	296.16	11.77	75.13	0.42	42.77	0.28	3.37	6.85	190.77

0.49	24.87	2.43	285.66	4.13	413.23	1.03	41.25	0.28	3.37	2.29	116.25
3.57	29.98	0.56	5.42	2.65	170.43	0.43	24.19	0.73	4.92	7.65	259.50
0.88	30.47	0.59	5.76	3.10	410.41	1.94	90.56	0.20	6.88	2.97	153.25
4.95	64.42	1.60	0.37	0.30	1.91	1.32	108.50	0.31	2.99	2.53	122.99
1.30	28.83	0.73	27.55	0.29	0.95	3.50	38.88	0.17	2.30	2.32	161.80
										5.10	258.24

To make it clear, we use the following steps to derive an accurate sediment rating equation based on the above pairs of sediment concentration and river or streamflow data.

Step 1. For given values of paired variables S and Q, estimate constants i, b, u, j, k, h, w, and t such that plots of x versus y yields a smooth curve of polynomial function (refer to equations 3.163 and 3.164)

Step 2. Choose a polynomial regression function that fits the plots of x versus y

Step 3. From the regression equation in step 2, find the constants of equation 3.165

Step 4. Calculate y by using equation 3.163

Step 5. Calculate x by using equation 3.164

Step 6. Calculate $y(x)$ based on steps 3 and 5

Step 7. Calculate S_1 by using equation 3.172, where S_1 represents the first predicted value. Plot graphs of measured (S) and predicted (S_1) values. If the graphs do not match each other, then we proceed to the next iteration step.

Step 8. Calculate e_1 by using equation 3.173

Step 9. Calculate E_1 by using equation 3.174

Step 10. Consider a polynomial regression function to correlate e_1 and E_1

Step 11. Calculate r_1 by using the regression equation from step 10 (i.e., refer to equation 3.197)

Step 12. Replace the calculated value of r_1 from step 11 in equation 3.176

Step 13. Calculate S_2 by using equation 3.176, where S_2 represents the second predicted value. Plot graphs of measured (S) and predicted (S_2) values. If the graphs do not match each other, then proceed to the next iteration step.

Step 14. Replace the calculated value of r_1 from step 11 in equation 3.177

Step 15. Then, calculate e_2 by using equation 3.177

Step 16. Calculate E_2 by using equation 3.178

Step 17. Consider a polynomial regression function to correlate e_2 and E_2

Step 18. Calculate r_2 by using the regression equation from step 17 (i.e., refer to equation 3.198)

Step 19. Replace the calculated value of r_1 from step 11, and the calculated value of r_2 from step 18 in equation 3.180

Step 20. Then, calculate S_3 by using equation 3.180, where S_3 represents the third predicted value. Plot graphs of measured (S) and predicted (S_3) values. If the graphs do not match each other, then we proceed to the next iteration step, and so on.

We repeat the same procedure to calculate a value of S_p by using equation 3.192, where subscript p stands for number of iteration steps. During each iteration step, we plot graphs of the measured (S) and predicted (S_p) values. Our iteration procedure ends when the graphs almost match each other.

Based on the paired data given in the table 3.4, the values of the required constants (i.e., i, b, u, j, k, h, w, and t) and variables (i.e., $y(x)$, r_1, r_2, r_3, r_4....r_{14}) had been determined by following the above steps. The values of these constants and variables are given below. Figure 3.61 shows the graph of the original river or streamflow (Q) versus sediment concentration (S) data, and the graph of the transformed data (x versus y) (see section 3.11.3).

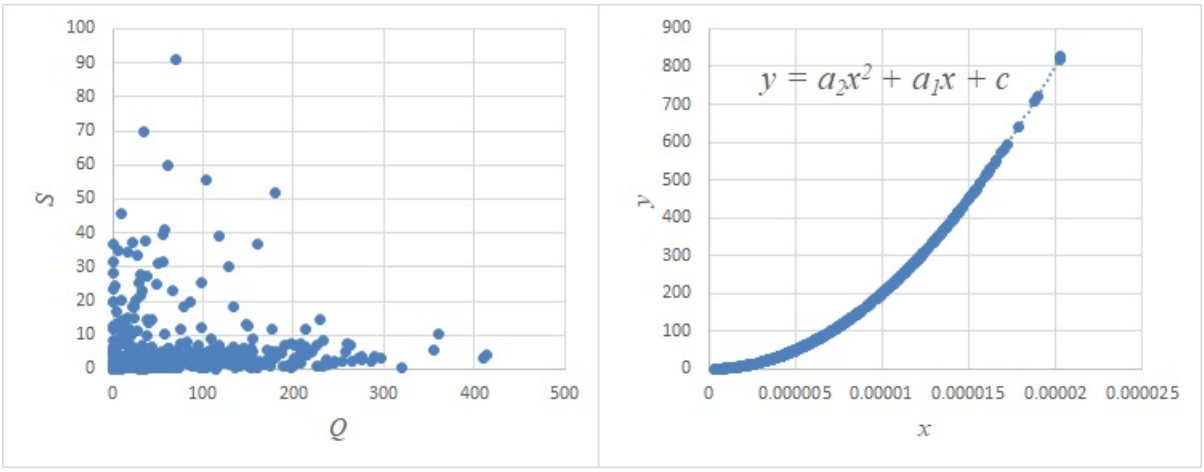

Figure 3.61: The original and transformed data according to step one

$$k = 0.000001 \tag{3.207}$$

$$h = 1 \tag{3.208}$$

$$w = 2 \tag{3.209}$$

$$t = 0 \tag{3.210}$$

$$i = 0.0000111 \tag{3.211}$$

$$b = 0.0022 \tag{3.212}$$

$$u = 2 \tag{3.213}$$

$$j = 2 \tag{3.214}$$

$$y(x) = 1999999995091.56x^2 + 0.10499849x + 0.0000001 \tag{3.215}$$

$$r_1 = (-0.00008E_1^2 + 1.011E_1 + 0.004 - E_1) * 10^{-5} \tag{3.216}$$

$$r_2 = (1.052E_2 + 0.006 - E_2) * 10^{-6} \tag{3.217}$$

$$r_3 = (0.002E_3^2 + 1.089E_3 - 0.018 - E_3) * 10^{-6} \tag{3.218}$$

$$r_4 = (1.042E_4 - E_4) * 10^{-6} \tag{3.219}$$

$$r_5 = (0.007E_5^2 + 1.096E_5 - 0.006 - E_5) * 10^{-6} \tag{3.220}$$

$$r_6 = (0.001E_6^2 + 1.047E_6 - E_6) * 10^{-6} \tag{3.221}$$

$$r_7 = (0.02E_7^2 + 1.143E_7 - 0.004 - E_7) * 10^{-6} \tag{3.222}$$

$$r_8 = (0.005E_8^2 + 1.066E_8 - E_8) * 10^{-6} \tag{3.223}$$

$$r_9 = (0.013E_9^2 + 1.075E_9 - E_9) * 10^{-6} \tag{3.224}$$

$$r_{10} = (0.026E_{10}^2 + 1.09E_{10} - 0.001 - E_{10}) * 10^{-6} \tag{3.225}$$

$$r_{11} = (0.026E_{11}^2 + 1.102E_{11} - E_{11}) * 10^{-6} \tag{3.226}$$

$$r_{12} = (-0.001E_{12}^2 + 1.04E_{12} - E_{12}) * 10^{-6} \tag{3.227}$$

$$r_{13} = (0.115E_{13}^2 + 1.139E_{13} - E_{13}) * 10^{-6} \tag{3.228}$$

$$r_{14} = (0.007E_{14}^2 + 1.048E_{14} - E_{14}) * 10^{-6} \tag{3.229}$$

As the values of the above constants and variables were already determined, the final form of the accurate regression equation is obtained by direct substitutions (refer to section 3.11.2). Therefore, the final form of the accurate sediment rating equation is given by

$$S \approx \frac{1}{bi^u} \left(f(Q) - jQ + f_1(Q,S) + f_2(Q,S) + ... + f_{14}(Q,S)\right)^u \tag{3.230}$$

For the final form of the equation, the graphs of measured (S)and predicted sediment concentration (S_p) matched each other (see figure 3.62).

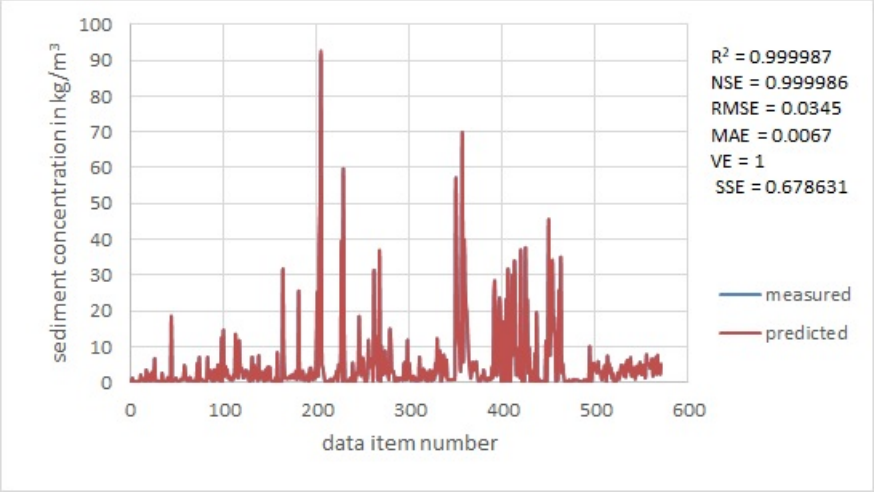

Figure 3.62: Graphs of measured (S) and predicted (S_p) sediment concentration

Since the final form of the equation is a very large and complex equation, the above values of the variables are easily interconnected in an excel spreadsheet or programmed in Matlab. A separate Excel spreadsheet and video presentation are provided at `https://1drv.ms/f/s!AtNG51Vlt6XqhwNVMPn1cOaJrGgd?e=d3RJhe`

3.11.5 Solving the Accurate Sediment Rating Equation

In the above section, we showed the procedures to derive the accurate sediment rating equation. For the paired suspended sediment concentration (S) and flow data (Q), we calculated each value of E_1, E_2, E_3...E_{14}, and the corresponding value of e_1, e_2, e_3...e_{14} respectively. At the fifteenth iteration step, at the values of E_{14} and e_{14}, $S \approx S_{15}$. Therefore, the last remaining errors are E_{15} and e_{15}. According to the steps above or section 3.11.1, a value of E_{15} is determined by

$$E_{15} = S - S_{15} \tag{3.231}$$

Based on equation 3.205

$$S_{15} = \frac{1}{bi^u}\left(f(Q) - jQ + f_1(Q,S) + f_2(Q,S) + f_3(Q,S)... + f_{14}(Q,S)\right)^u \tag{3.232}$$

Therefore,

$$E_{15} = S - \frac{1}{bi^u}\left(f(Q) - jQ + f_1(Q,S) + f_2(Q,S) + f_3(Q,S)... + f_{14}(Q,S)\right)^u \tag{3.233}$$

Based on equations 3.163, 3.189 and 3.201

$$e_{15} = f_0(Q,S) - \left(f(Q) + f_1(Q,S) + f_2(Q,S) + f_3(Q,S) + ... + f_{14}(Q,S)\right) \tag{3.234}$$

For each paired values of S and Q, there are corresponding values of E_{15} and e_{15}. Now, we take the values of E_{15} and e_{15} as paired input data to derive another equation that relates E_{15} and e_{15} by following the above steps, and so on. To derive the equation based on paired values of E_{15} and e_{15}, we calculate another values of E_p and e_p (see the steps above). To avoid confusion, let us express these other values of E_p and e_p in terms of E_p^* and e_p^* respectively. Therefore, we define the following relationship.

$$\text{If } \lim_{E_p^* \to\ 0}(E_1^* + E_p^*) = E_1^*, \text{ then } E_{14} + E_p^* \approx E_{14} \tag{3.235}$$

For the given paired data (S and Q), at the value of E_{14}, $S \approx S_{15}$. According to steps above or section 3.11.1, the value of E_{14} is determined by

$$E_{14} = S - S_{14} \tag{3.236}$$

Consider equation 3.205

$$S_{14} = \frac{1}{bi^u}\left(f(Q) - jQ + f_1(Q,S) + f_2(Q,S) + f_3(Q,S)... + f_{13}(Q,S)\right)^u \tag{3.237}$$

Therefore,

$$E_{14} = S - \frac{1}{bi^u}\left(f(Q) - jQ + f_1(Q,S) + f_2(Q,S) + f_3(Q,S)... + f_{13}(Q,S)\right)^u \tag{3.238}$$

For each paired value of S and Q, there is a corresponding value of E_{14}, which is a unique value. It is to mean that, let's us say for a given value of Q, there is only one value of S which results in a corresponding value, minimum value, or zero value of E_{14} (i.e., there

is no possibility to have two different values of E_{14} for the same values of paired data). From the relationship to approximate a value of E_{14} for an unknown value of suspended sediment concentration or flow data, we keep on deriving a series of equations until a value of E_p^* is approximately zero or it is far apart from a value of E_1^*. In this case, the value of E_p^* determines the accuracy of the approximation. Therefore, to estimate an unknown value of suspended sediment concentration for a given value of flow data, a value of suspended sediment concentration that results in the minimum value of E_P^* is the solution.

Since the systems of equations forming the complex equation are very long, the separate Excel spreadsheet and video presentation on deriving and solving the accurate sediment rating equation are provided at `https://1drv.ms/f/s!AtNG51Vlt6XqhwNVMPn1cOaJrGgd?e=d3RJhe`

4. RESULTS

4.1 The Input Data

The first input tasks for our main research works were data preparation, review, and analysis. The prepared land use maps are given in figures 3.7 – 3.14; soil maps are given in figures 3.4 – 3.6; stream network for the Hombole Watershed is given in figure 3.15. The pictorial representations of selected land use categories are given in figures A1 – A4.

The distributions of climatic stations are given in figures 3.16 – 3.18. Compared with the other watersheds under our consideration, the Hombole Watershed has a sufficient number of climatic stations.

The relationships between daily or monthly average rainfall, flow and sediment are given in figures 3.19 – 3.26. For all watersheds under consideration, there were direct relationships between monthly average rainfall and flow. The data review shows that flow and sediment yield estimation in monthly time step was the convenient approach for all watersheds under our considerations. Compared with the other watersheds under our consideration, we could see a logical relationship between rainfall, flow, sediment, and the impact of land use change for the Hombole Watershed.

The sediment rating curves for each watershed are given in figure 3.27. Compared with the other watersheds under our consideration, the performance of the sediment rating curve for the Hombole Watershed was good. The expression to calculate a channel width and depth for the Hombole Watershed is given in section 3.8.3.

4.2 The Regionalized MUSLE

We confirmed that the best exponent of the MUSLE was 1 irrespective of the topographic factor, which resulted in the maximum performance of the MUSLE (i.e., approximately 100%). From all graphs (see figures 3.31 – 3.37), if we considered one watershed, we took the exponent and topographic factor, which resulted in the maximum Nash-Sutcliffe efficiency; however, if we considered two or more watersheds, we took the exponent and topographic factor, which resulted in the minimum Nash-Sutcliffe efficiency.

Accordingly, the best exponent of the MUSLE was 0.57, which resulted in a Nash-Sutcliffe efficiency of approximately 0.8 if the topographic factor was calculated using equations (3.8) and (3.9). Therefore, this was the best combination of the exponents and topographic factors of the MUSLE under the hydro-climatic conditions of all watersheds under our consideration.

To determine the best combination of the exponent and topographic factor of the MUSLE, the important relationships between the coefficient a and exponent b, the exponent b and the Nash-Sutcliffe efficiency are drawn for the future evaluation of the MUSLE at any watershed. As we can see from the graphs (see figures 3.31 – 3.37), for observed and simulated sediment, as the relationship between the coefficient a and exponent b approaches to power or logarithmic function; the relationship between the exponent b and the Nash-Sutcliffe efficiency approaches to a quadratic function. This relationship can be

used to find the best performance of the MUSLE during the calibration of the model.

4.3 The Improved MUSLE

We called equation (3.46) the improved MUSLE. The input data requirement of the MUSLE was changed for calculation of its runoff factor, for possible application of the model using only the runoff volume, and the topographic, soil erodibility, cover, and conservation practice factors. From all graphs (see figures 3.39 – 3.45), the best actual exponent b of the improved MUSLE was 1.2, which resulted in a Nash-Sutcliffe efficiency of approximately 1 irrespective of the topographic factor, whereas the theoretical exponent of the improved MUSLE was 1. Therefore, the best exponent of the improved MUSLE was obtained only through calibration of the observed and predicted sediment.

From all the graphs (see figures 3.39 – 3.45), if we considered one watershed, we took the exponent and topographic factor which resulted in the maximum Nash-Sutcliffe efficiency, but if we considered two or more watersheds, we took the exponent and topographic factor which resulted in the minimum Nash-Sutcliffe efficiency. Accordingly, the best exponent of the improved MUSLE was 1.44, which resulted in a Nash-Sutcliffe efficiency of approximately 0.84 if the topographic factor was calculated by using the equations that were proposed by Foster et al., (1977) and McCool et al., (1987, 1989), as cited by Renard et al. (1997). Therefore, this was the best combination of the exponent and topographic factor of the improved MUSLE under the hydroclimatic conditions of all watersheds under our consideration. Compared with the original MUSLE, the improved MUSLE showed better performance (i.e., the minimum performance was 84%) over the original MUSLE (i.e., the minimum performance was 80%).

To determine the best combination of the exponent and topographic factor of the improved MUSLE, the important relationships between the coefficient a and exponent b, the exponent b and the Nash-Sutcliffe efficiency are drawn for the future evaluation of the improved MUSLE at any watershed. As we can see from the graphs (see figures 3.39 – 3.45), for observed and simulated sediment, as the relationship between the coefficient a and exponent b approaches to power or logarithmic function; the relationship between the exponent b and the Nash-Sutcliffe efficiency approaches to a quadratic function. This relationship can be used to find the best performance of the improved MUSLE during the calibration of the model.

4.4 The SLESYE

We called equation 3.126 the SLESYE. From figure 3.47, if we considered one watershed, we took the exponent which resulted in the maximum Nash-Sutcliffe efficiency, but if we considered two or more watersheds, we took the exponent which resulted in the minimum Nash-Sutcliffe efficiency. Accordingly, the best actual exponent of the SLESYE was 1.4, which resulted in a Nash-Sutcliffe efficiency of 0.86.

To determine the best exponent of the SLESYE, the important relationships between coefficient a and exponent b as well as exponent b and the Nash-Sutcliffe efficiency are drawn for the future evaluation of the SLESYE at any watershed. As we can see from the graphs (see figure 3.47), for observed and simulated sediment, as the relationship

between the coefficient a and exponent b approaches to power or logarithmic function; the relationship between the exponent b and the Nash-Sutcliffe efficiency approaches to a quadratic function. This relationship can be used to find the best performance of the SLESYE during the calibration of the model.

4.5 The First Revised Version of the SLESYE

We called equation 3.130 the RSLESYE-v1. From all graphs (see figures 3.49 – 3.55), the best actual exponent b of the RSLESYE-v1 was 1, which resulted in a Nash-Sutcliffe efficiency of 0.98. The best actual exponent of the RSLESYE-v1 was equal to its theoretical exponent.

From all the graphs (see figures 3.49 – 3.55), if we considered one watershed, we took the exponent and topographic factor which resulted in the maximum Nash-Sutcliffe efficiency, but if we considered two or more watersheds, we took the exponent and topographic factor which resulted in the minimum Nash-Sutcliffe efficiency. Accordingly, the best exponent of the RSLESYE-v1 was 1.42 which resulted in a Nash-Sutcliffe efficiency of approximately 0.86 if the topographic factor was calculated by using the equations that were proposed by Foster et al., (1977) and McCool et al., (1987, 1989), as cited by Renard et al. (1997). Therefore, this was the best combination of the exponent and topographic factor of the RSLESYE-v1 under the hydroclimatic conditions of all watersheds under our consideration. Compared with the original MUSLE and the improved MUSLE, the RSLESYE-v1 showed the best performance (i.e., the minimum performance was 86 %) over the regionalized MUSLE (i.e., the minimum performance was 80%) and the improved MUSLE (i.e., the minimum performance was 84%).

To determine the best combination of the exponent and topographic factor of the RSLESYE-v1, the important relationships between the coefficient a and exponent b, the exponent b and the Nash-Sutcliffe efficiency are drawn for the future evaluation of the RSLESYE-v1 at any watershed. As we can see from the graphs (see figures 3.49 – 3.55), for observed and simulated sediment, as the relationship between the coefficient a and exponent b approaches to power or logarithmic function; the relationship between the exponent b and the Nash-Sutcliffe efficiency approaches to a quadratic function. This relationship can be used to find the best performance of the RSLESYE-v1 during the calibration of the model.

4.6 The Second Revised Version of the SLESYE

We called equation 3.155 the RSLESYE-v2. The values of the best exponent and topographic factor of the RSLESYE-v2 were the same as that of the RSLESYE-v1 (see section 4.5). As compared with the RSLESYE-v1 (see figure 3.57), the RSLESYE-v2 increased the accuracy of sediment yield prediction from 0.87 to 0.90 for the Hombole Watershed, from 0.93 to 0.98 for the Mojo Watershed, from 0.94 to 0.95 for the Gumera Watershed, from 0.86 to 0.95 for the Gilgel Gibe 1 Watershed (see figure 3.58). From figures 3.59 and 3.60, the relationship between the Nash-Sutcliffe efficiency and calibration parameter E, as well as the relationship between the calibration parameters E and c approach to a quadratic function. These relationships help to determine the best values of E and c for

the maximum possible performance of the RSLESYE-v2.

4.7 The Performance of the Original SWAT+ Model

Before calibration and validation of the SWAT+ model, we checked the initial performance of the SWAT+ model by considering the density of weather gauging stations and the simulation time steps. As compared with the available twenty-five national weather gauging stations, we checked that the performance of the model was better when thirty-three gauging stations (i.e., twenty-five national weather gauging stations, and eight stations from global weather data) had been considered. The performance of the model for daily, monthly, and yearly simulation time steps are given in figures A8, A6 and A7 respectively. The initial performance before calibration of the model for the monthly average flow and thirty-three gauging stations was very good, and there were also direct relationships between the observed monthly average rainfall and flow for all watersheds under our consideration. Therefore, we considered the monthly simulation time step and thirty-three gauging stations for the calibration and validation of the model.

At the current best value of the flow calibration parameters, as shown in table 3.2, calibration results of the original SWAT+ model are given in figure 4.1.

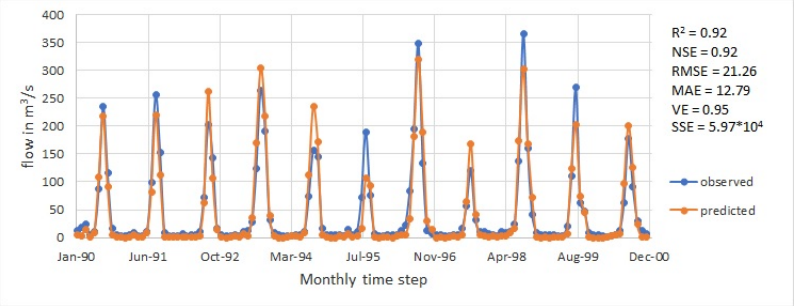

Figure 4.1: The calibrated original SWAT+ model rev.60.5.4 for the monthly average flow

For the validation of the model, we considered two cases to evaluate the performance of the calibrated model. When the land use maps were changed for the simulation periods 2001 – 2008, 2009 – 2012, and 2013 – 2015, the performance of the original SWAT+ model is given in figures A9, A10 and A11 respectively. When the land use map was not changed (i.e., the land use map of 1989 – 2000 was used) for the simulation periods 2001 – 2008, 2009 – 2012, and 2013 – 2015, the performance of the model is given in figure A12, A13 and A14 respectively. For the simulation periods 2001 – 2008 and 2009 – 2012, the performance of the model for the latter case was very good. However, for the simulation period 2013 – 2015, the performance of the model for the latter case decreased but it was not huge difference. Therefore, there was no need to change the land use map as the calibrated values of the calibration parameters better-captured flow in the validation period 2001 – 2015 for the same land use map. Therefore, for the validation period 2001 – 2015, the performance of the validated model is given in figure 4.2.

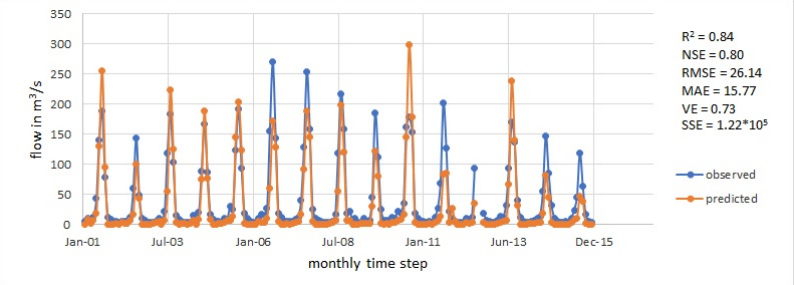

Figure 4.2: The validated original SWAT+ model rev.60.5.4 for the monthly average flow

For the validated model, the basin annual average water balance is given in figure A15. The difference between precipitation and loses (i.e., surface runoff + lateral flow + percolation + evapotranspiration) was 17.33 mm.

Since the SWAT+ model gives daily, monthly, or yearly total sediment load in metric tons, we used the observed monthly total sediment load in metric tons to evaluate the model. We found that the parameter 'bedldcoef' is the most sensitive parameter for sediment calibration. The sediment calibration and validation results of the original SWAT+ model are given in figures 4.3 and 4.4 respectively.

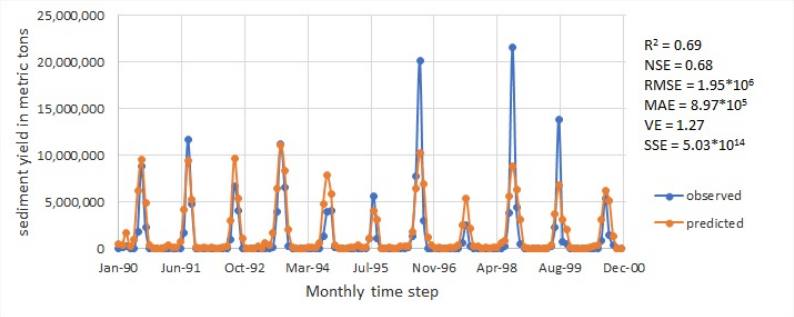

Figure 4.3: The calibrated original SWAT+ model rev.60.5.4 for the monthly total sediment yield

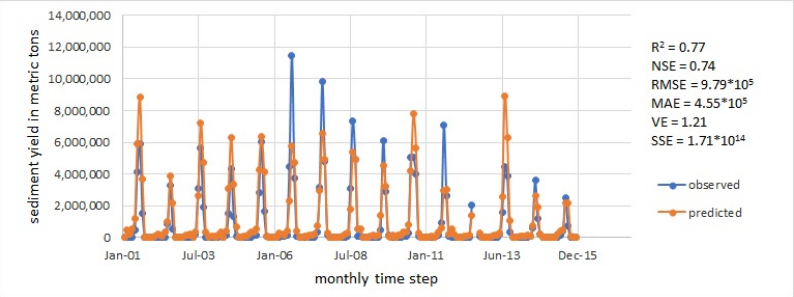

Figure 4.4: The validated original SWAT+ model rev.60.5.4 for the monthly total sediment yield

The performance of the model was evaluated using six statistical indicators as shown in figures 4.1 – 4.4. Overall, the original SWAT+ model prediction of the monthly average flow was very good, whereas the SWAT+ model prediction of the monthly total sediment yield was fairly good.

4.8 The Modified SWAT+ models for Sediment Yield Estimation

The original SWAT+ rev.60.5.4 model was modified in three different types for sediment yield estimation. The SWAT+ editors were compiled for each of the modified SWAT+.

4.8.1 The First Type of the Modified SWAT+ Model for Sediment Yield Estimation

We called the first type of the modified SWAT+ model the SYEt1-SWAT+ model. Since the runoff components of the original SWAT+ model were not changed in the SYEt1-SWAT+ model, the flow calibration and validation results were the same for both models. The sediment yield calibration and validation results of the SYEt1-SWAT+ model are given in figures 4.5 and 4.6 respectively.

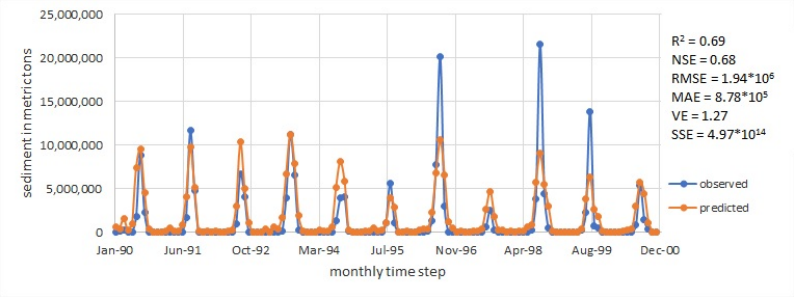

Figure 4.5: The calibrated SYEt1-SWAT+ model for the monthly total sediment yield

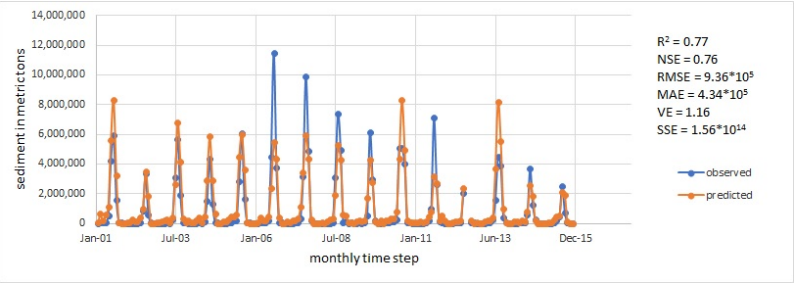

Figure 4.6: The validated SYEt1-SWAT+ model for the monthly total sediment yield

For sediment yield estimation, the SYEt1-SWAT+ model showed better performance than the original SWAT+ model.

4.8.2 The Second Type of the Modified SWAT+ Model for Sediment Yield Estimation

We called the second type of the modified SWAT+ model the SYEt2-SWAT+ model. Similar to the previous type, the runoff components of the original SWAT+ model were not changed in the SYEt2-SWAT+ model. Therefore, the flow calibration and validation results of the SYEt2-SWAT+ model were the same as the original SWAT+ model or SYEt1-SWAT+ model. The sediment yield calibration and validation results of the SYEt2-SWAT+ model are given in figures 4.7 and 4.8 respectively.

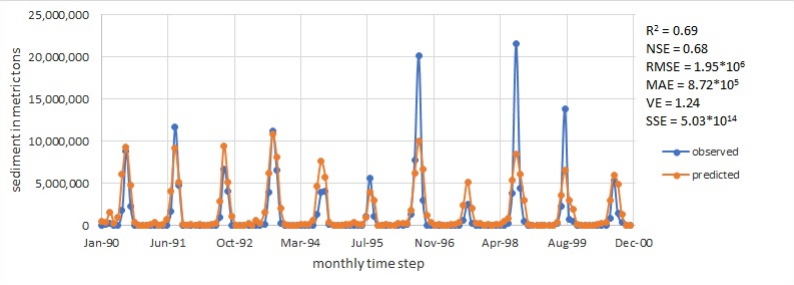

Figure 4.7: The calibrated SYEt2-SWAT+ model for the monthly total sediment yield

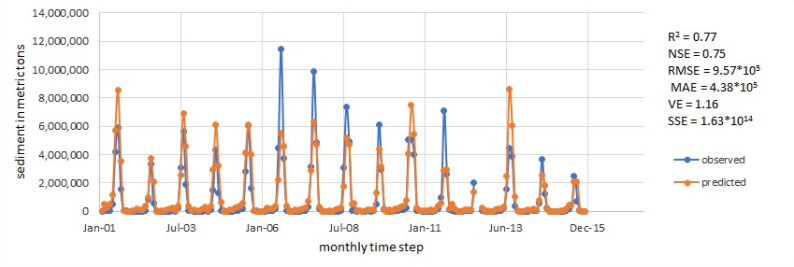

Figure 4.8: The validated SYEt2-SWAT+ model for the monthly total sediment yield

For sediment yield estimation, the SYEt2-SWAT+ model showed better performance than the original SWAT+ model.

4.8.3 The Third Type of the Modified SWAT+ Model for Sediment Yield Estimation

We called the third type of the modified SWAT+ model the SYEt3-SWAT+ model. In this type too the runoff components of the original SWAT+ model were not changed. Therefore, the flow calibration and validation results of the SYEt3-SWAT+ model were the same as the above SWAT+ models. The sediment yield calibration and validation results of the SYEt3-SWAT+ model are given in figures 4.9 and 4.10 respectively.

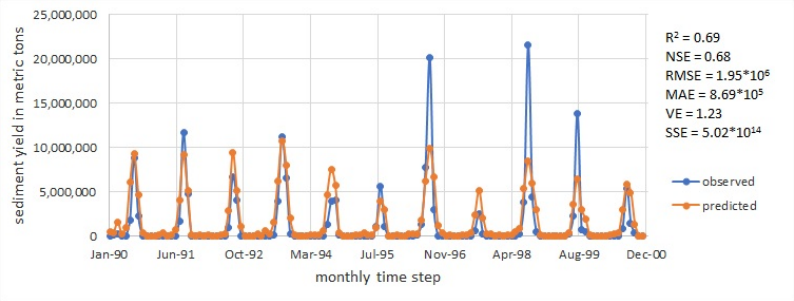

Figure 4.9: The calibrated SYEt3-SWAT+ model for the monthly total sediment yield

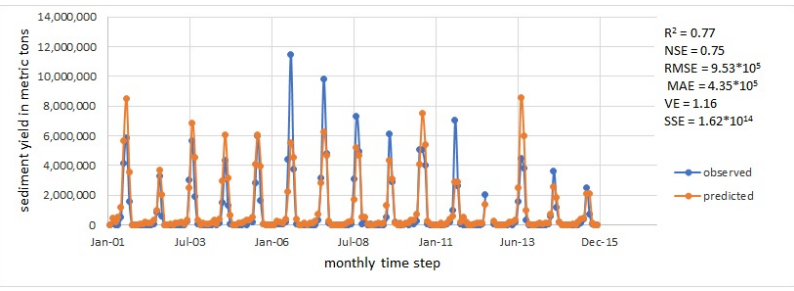

Figure 4.10: The validated SYEt3-SWAT+ model for the monthly total sediment yield

For sediment yield estimation, the SYEt3-SWAT+ model showed better performance than the original SWAT+.

4.9 The Iterative Approach for Deriving and Solving the Accurate Sediment Rating Equation

The iterative approach for deriving an accurate regression equation based on values of paired variables is given in section 3.11.1. The procedures to determine the final form of the accurate regression equation are given in section 3.11.2. Accordingly, the shorthand form of the final accurate regression equation is given by

$$S \approx \frac{1}{bi^u}\left(f(Q) - jQ + f_1(Q,S) + f_2(Q,S) + ... + f_{p-1}(Q,S)\right)^u \tag{4.1}$$

where, S and Q are variables, b, i, u and j are constants for given values of paired data.

The accurate sediment rating equation which was derived based on five hundred seventh one number of records of suspended sediment concentration and flow data is given by

$$S \approx \frac{1}{bi^u}\left(f(Q) - jQ + f_1(Q,S) + f_2(Q,S) + ... + f_{14}(Q,S)\right)^u \tag{4.2}$$

The graphs of measured and predicted suspended sediment concentration matched each other (see figure 3.62), and statistical measures for the data correlation are given in figure 3.62. The procedures to solve the accurate regression equation are given in section 3.11.5.

The separate Excel spreadsheet and video presentation on deriving and solving the accurate sediment rating equation are provided at
`https://1drv.ms/f/s!AtNG51Vlt6XqhwNVMPn1cOaJrGgd?e=d3RJhe`

5. DISCUSSIONS

5.1 Discussions on the Regionalized MUSLE

Based on our evaluation of the soil erodibility equations, we found that the best equation to estimate the soil erodibility factor was the Williams' (1995) equation, as cited by Wawer et al. (2005). We considered the land use maps to assign a value for the cover and conservation practice factors from the past experiences from the literature, and the coefficient a was estimated through calibration. Since only a product effect of the coefficient, soil erodibility, cover, and conservation practice factors are reflected in the MUSLE rather than their individual effect during the calibration of the sediment yield, any change in these factors affects the coefficient of the MUSLE.

Therefore, we do not like to suggest strict procedures to estimate these factors. It is highly preferable if these factors are measured and studied at a temporal and spatial scale to understand their effect on soil erosion in a particular field. This is because the soil erodibility, cover, and conservation practice factors of the MUSLE reflect site-specific conditions. For example, we can talk about the density and pattern of land cover, nature and extent of soil conservation and flood protection work, and the temporal variation of soil properties.

For all watersheds under our consideration, the best exponent of the MUSLE was 0.57, which resulted in a Nash-Sutcliffe efficiency of 0.8 if the topographic factor was calculated using equations (3.8) and (3.9). In this case, the proposed exponent of the model was different from its original exponent (0.56), while for other exponents and topographic factors, the performance of the model decreased. For example, the best exponent of the model was 0.56, which resulted in a Nash-Sutcliffe efficiency of 0.78 if the topographic factor was calculated using the equation that was proposed by McCool et al. (1987), as cited by Pongsai et al. (2010). In this case, the proposed exponent was the same as the original exponent of the MUSLE (0.56); however, the performance of the MUSLE decreased as compared with the previous one. Therefore, the performance of the MUSLE was very good for the previous case.

The performance of the MUSLE was tested at a watershed scale using directly measured flow data; it showed good performance (i.e., the performance of the MUSLE is greater than or equal to 80%) for all four watersheds under our consideration provided that the exponent and topographic factor of the original MUSLE were changed. This result supports the literature review report that the model shows better performance at a watershed scale than a plot scale and if it is applied using directly measured runoff data (Sadeghi et al., 2014).

This also supports the conclusions of some authors as the MUSLE has been observed to give good results in various applications in some parts of tropical Africa (Ndomba, 2007), as cited by Adegede and Mbajiorgu (2019). The MUSLE has also been successfully demonstrated in sub-Saharan Africa (Adegede and Mbajiorgu, 2019). In addition, it also supports the experimental plot result of sheet erosion at the Enerta study site in Ethiopia, where the MUSLE was better at estimating soil loss from a cultivated field than

the USLE (Muche et al., 2013).

5.2 Discussions on the Improved MUSLE

To improve the MUSLE, we assumed that the amount of potential energy of the runoff was proportional to the shear stress for sediment transport from a slope field and the kinetic energy of the runoff at the bottom of the slope field for gully formation. Li et al. (2017) underestimated the total potential energy of the runoff that would be available for soil erosion and sediment transport (compare equations (3.20) and (3.39)). Based on the physical assumption, the peak runoff rate was eliminated from the variables of the MUSLE. This improvement had an advantage for the possible application of the model in data-scarce areas and not use indirect methods to estimate the peak runoff rate.

To compare the improved MUSLE with the regionalized MUSLE, we followed a similar evaluation procedure to evaluate the improved MUSLE versus the original MUSLE. The improved MUSLE showed better performance (i.e., the minimum performance was 84%) over the regionalized MUSLE (i.e., the minimum performance was 80%) for all watersheds under consideration. This improvement may be linked to the uncertainty in the peak runoff rate (i.e., uncertainty in the interpretation of the daily flow data for the yearly peak runoff rate) or other unknown reasons. As all variables of the improved MUSLE are parts of the original MUSLE, there is no indication to say gully erosion is considered in the improved MUSLE, as per the physical assumption that we made to improve the MUSLE.

5.3 Discussions on the SLESYE and its Revised Versions

In the SLESYE and its revised versions, the slope steepness factor (S) is given by

$$S = \frac{\sin^2 \theta}{\cos \theta} \tag{5.1}$$

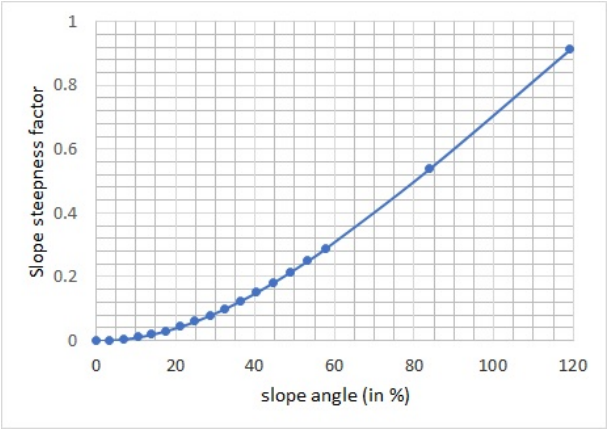

Figure 5.1: The relationship between slope angle and slope steepness factor of the SLESYE

As slope angle increases slope steepness factor increases. As the slope steepness factor increases more soil erosion and sediment transport are expected. From figure 5.1, there is a direct relationship between slope angle and slope steepness factor of the SLESYE. Therefore, the derived equation of the slope steepness factor is appropriate.

In the SLESYE, the runoff volume, soil cover factor, soil conservation practice factor, slope steepness factor, and slope length are directly proportional to sediment yield, and the soil erodibility is indirectly proportional to the sediment yield. This proportionality can be explained by considering three cases.

a) Case one: how is sediment yield affected if runoff volume is constant in given periods but soil erodibility increases ?

The SLESYE estimates the total sediment load based on the total runoff volume. It was derived while considering the effect of an individual runoff volume and soil erodibility on sediment transport.

For the same runoff volume (i.e., for the same rainfall distribution in given periods), as soil erodibility increases from period to period, the runoff volume gets concentrated with sediment particles. This action reduces sediment transport and facilitates sediment deposition along the length of the slope, which eventually leads to mud concentration at the lower parts of the slope. Therefore, sediment yield at the bottom end of the slope or an outlet of a watershed is expected to decrease as soil erodibility increases. For example, if we consider silt and clay soil, silt soil is easily erodible soil as compared with clay soil. This is because of the cohesive force between soil particles, clay soil has a higher cohesive force than silt soil. Therefore, for the same runoff volume, sediment yield is expected to decrease for silt soil due to deposition. One reason for the deposition can be the settling velocity of soil particles; silt soil settles first as compared with clay soil. Actually, soil erodibility expresses highly erodible soil to non-erodible soil (rocky or paved soil). In the SLESYE, if $K = 1$, it shows mud or high shear stress. In this case, no sediment transport is expected. If $K = 0$, it shows a rocky or paved area. In this case, the cover factor is zero, and therefore, no soil erosion is expected. This shows that soil erosion and sediment transport are expected in the range of these two extremes. Based on these explanations, the SLESYE considers the sediment deposition process. Therefore, the SLESYE is an appropriate model for the sediment yield estimation.

b) Case two: how is sediment yield affected if runoff volume increases in given periods but soil erodibility is constant ?

For the same soil erodibility, as runoff volume increases from period to period, soil erosion and sediment transport are expected to increase and sediment deposition is expected to decrease due to the scouring power of the runoff volume. In this case, how soil erosion can be increased if soil erodibility is constant? Since soil erodibility refers to the property of soil which indicates how a given soil is erodible or susceptible to erosion or it refers to the degree of ease in eroding a given soil, it does not tell us the mass of the soil. For example, soil erodibility tells us how easy to erode silt soil compared with clay soil, but it does not directly tell us the mass of silt soil available in a given field. In this context, more runoff volume erodes and caries more silt soil or another type of soil having constant erodibility.

Therefore, based on above explanations, the SLESYE hold true.

c) Case three: how is sediment yield affected if both runoff volume and soil erodibility increase simultaneously in given periods ?

Depending on the magnitude of runoff volume and soil erodibility factor, soil erosion and sediment deposition processes are not easy to define.

5.4 Discussions on the Performance of the SWAT+ model

The initial performance of the original SWAT+ model for the monthly average flow was very good as shown in figure A6. This might be linked to the data quality (for example, there was the direct relationship between the observed monthly average rainfall and flow as shown in figure 3.19) and the predetermined parameters of the QSWAT+ model like the channel width and depth (see section 3.8.3). The performance of the calibrated SWAT+ model was very good when the single land use map was used for the entire simulation periods (compare figures A9, A10, A11 with figures A12, A13 and A14 respectively). This was linked to the values of the calibration parameters that directly or indirectly affect the value of the input data parameters. It would be also linked to the uncertainty in the temporal and spatial resolution of the land use and soil data. Furthermore, it depends on dominant land use and soil that form a HRU in the SWAT+ model (i.e., in the HRU only dominant land use and soil are considered).

The SWAT+ model showed very good performance for the flow but it showed fairly good performance for the sediment yield. These might be linked to the quality and quantity of the available data. To compare the simulated flow against the observed flow data, we had sufficient and continuous records of the observed flow data in daily or monthly time step. However, we did not have sufficient and continuous records of the observed sediment data to compare against the simulated sediment. Since we had had very limited and non-continuous records of the sediment data, we used sediment rating curves to generate sediment data. Therefore, the sediment data were subject to the error of the sediment rating curves.

5.5 Discussions on the Accurate Sediment Rating Equation

The relationship between the sediment concentration and flow was given by the complex equation (it was not polynomial or other kinds of known function). This equation may reflect the complex relationship between the dynamic behavior of flow and sediment transport.

A power function is a commonly used non-linear regression approach for predicting sediment from a given flow data. However, a regression error is very large. The comparison of sediment prediction accuracy of the proposed regression equation and power function are given in figures 5.2 – 5.5. The proposed regression equation is very accurate. We can minimize a regression error as small as possible by increasing iteration steps.

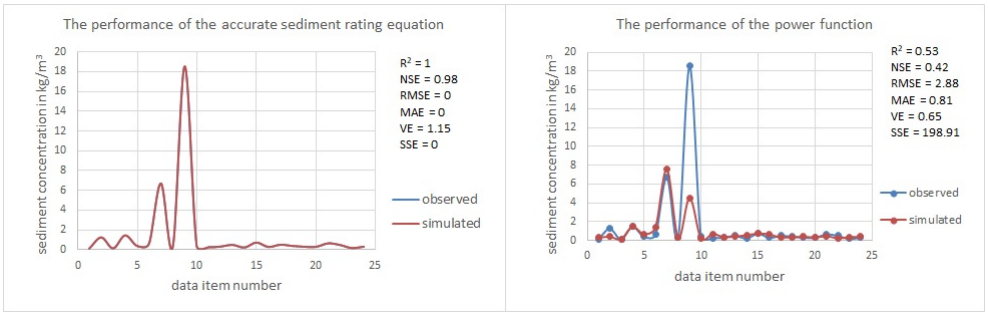

Figure 5.2: Comparison of sediment prediction accuracy of the proposed regression equation and the power function ($S = 0.069Q^{0.9576}$) for the Hombole Watershed

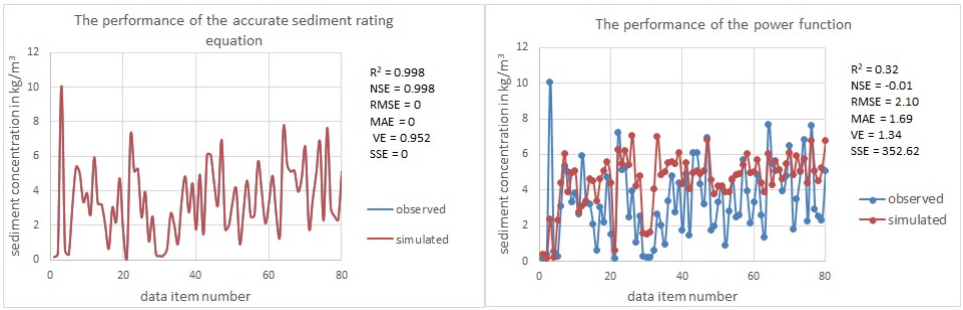

Figure 5.3: Comparison of sediment prediction accuracy of the proposed regression equation and the power function ($S = 0.2036Q^{0.5475}$) for the Gumera Watershed, provided that all data records were taken into account without any preconditions.

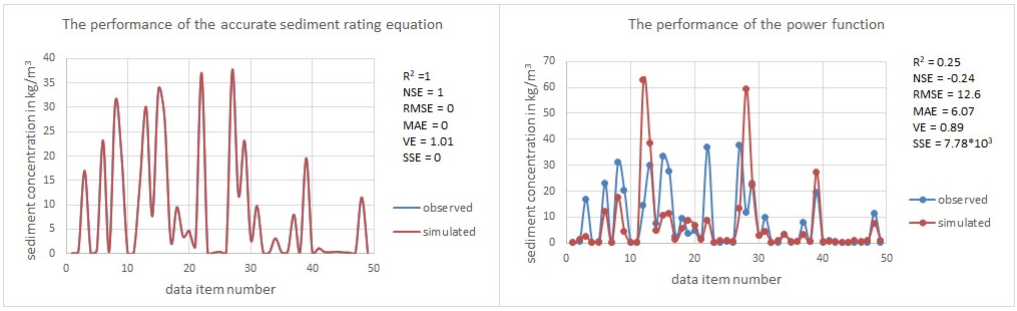

Figure 5.4: Comparison of sediment prediction accuracy of proposed regression equation and the power function ($S = 0.659Q^{0.839}$) for the Mojo Watershed, provided that all data records were taken into account without any preconditions.

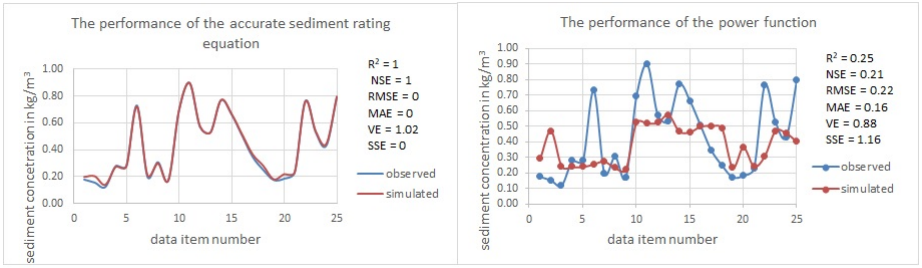

Figure 5.5: Comparison of sediment prediction accuracy of the proposed regression equation and the power function ($S = 0.1901Q^{0.1916}$) for the Gilgel Gibe 1 Watershed, provided that all data records were taken into account without any preconditions.

Model calibration and validation are challenging tasks to apply a model for a particular purpose, even for further improvement of the model. For example, if we consider the MUSLE or the improved MUSLE, finding the coefficient, soil erodibility, cover, and conservation practice factors of the MUSLE or the improved MUSLE through calibration is not a feasible approach. This is because only a product effect of the coefficient and these factors is reflected in the MUSLE or the improved MUSLE rather than their individual effect during the calibration of sediment yield. Therefore, the individual effect of model variables rather than their product effect on the engaged physical processes is important. Therefore, expressing the relationship between model variables in such a way that their individual effects can be seen on the engaged physical process is essential. The proposed regression method may play a significant role in this regard.

6. CONCLUSIONS AND RECOMMENDATIONS

6.1 Conclusions and Recommendations on the Regionalized MUSLE

We verified that the best exponent of the MUSLE was 1, which resulted in the maximum performance of the MUSLE. The performance of the MUSLE was greater than or equal to 80% for all four watersheds under our consideration. We expect the same for other watersheds of Ethiopia provided that the exponent of the model is 0.57 and that its topographic factor is calculated using the following equations (`https://www.youtube.com/watch?v=w6w8jxbTJfo` (accessed on 25 February 2021)).

$$LS = (0.02222J^{1.5} + 0.03231J + 0.1004) * 0.2901 \triangle y^{0.4002} \text{ for } J < 5\% \tag{6.1}$$

$$LS = (0.02222J^{1.5} + 0.03231J + 0.1004) * 0.2105 \triangle y^{0.5004} \text{ for } J > 5\% \tag{6.2}$$

where L is the slope length factor, S is the slope steepness factor, J is the slope in %, $\triangle y = \lambda/22.1$, and λ is the slope length.

The above value of the exponent and the equations of the topographic factor can be taken as the best combination of the exponent and topographic factor under the hydro-climatic conditions of Ethiopia. We recommend further investigation of the best combination of the exponent and topographic factors by applying the MUSLE at different watersheds of Ethiopia.

We suggested the best equations of the topographic factor for the conditions of Ethiopia. In the MUSLE, the topographic factor is directly proportional to the soil erosion and sediment yield. However, as the slope length becomes increasingly larger, there is a possibility that soil erosion from the upper part of the slope becomes deposited at the lower part of the slope. Therefore, more research works are required to understand the effect of the slope length on soil erosion and sediment transport.

6.2 Conclusions and Recommendations on the Improved MUSLE

The improved MUSLE is given by

$$y = aQ^bKLSCP \tag{6.3}$$

where y is the sediment yield in metric tons, a is the coefficient, Q is the runoff volume in m^3, b is the exponent, K is the soil erodibility factor, L is the slope length factor, S is the slope steepness factor, C is the soil cover factor, and P is the soil conservation practice factor. The improved MUSLE showed better performance (i.e., the minimum performance was 84%) over the regionalized MUSLE (i.e., the minimum performance was 80%) for all four watersheds under consideration. The performance of the improved MUSLE was

greater than or equal to 84% for all four watersheds under our consideration, provided that the exponent of the model was 1.44, and its topographic factor was calculated by using the equations that were proposed by Foster et al., (1977) and McCool et al., (1987, 1989) as cited by Renard et al. (1997):

$$L = \left(\frac{\lambda}{22.13}\right)^{m} \tag{6.4}$$

$$m = \frac{\beta}{1+\beta} \tag{6.5}$$

$$\beta = \frac{\frac{\sin\theta}{0.0896}}{3\left(\sin\theta\right)^{0.8} + 0.56} \tag{6.6}$$

$$S = 10.8\sin\theta + 0.03 \text{ if the slope is less than } 9\% \tag{6.7}$$

$$S = 16.8sin\theta - 0.5 \text{ if the slope is greater than or equal to } 9\% \tag{6.8}$$

where λ is the slope length (m), and θ is the angle of the slope in degree.

The above value of the exponent and the equations of the topographic factor can be taken as the best combination of the exponent and topographic factor under the hydroclimatic conditions of Ethiopia. We recommend further investigation of the best combination of the exponent and topographic factor by applying the improved MUSLE at different watersheds of Ethiopia.

As per our discussion above, we cannot exactly tell whether gully erosion is considered in the improved MUSLE or not. As part of the comparison between the original MUSLE and the improved MUSLE, what different effect does the peak runoff rate have on soil erosion and sediment transport compared with the runoff volume? As far as the lumped model is concerned, the individual effect of the runoff and peak runoff rate on soil erosion and sediment transport should be explicitly shown. This helps us to put a physical demarcation between the peak runoff rate and runoff volume. Therefore, better explanation and further improvement of the MUSLE may become necessary to address soil erosion and sediment transport problems. In the improved MUSLE (the same for the original MUSLE), the topographic factor is directly proportional to the soil erosion and sediment yield. However, as the slope length becomes larger and larger, there is a possibility that soil erosion from the upper part of the slope gets deposited at the lower part of the slope. Therefore, more research is required to understand the effect of the slope length on soil erosion and sediment transport.

The improved MUSLE considers the topographic factor of the original MUSLE. Equation (3.42) does not consider the topographic factor of the original MUSLE; therefore, this equation should also be tested.

6.3 Conclusions and Recommendations on the SLESYE and the Revised Versions of the SLESYE

The SLESYE is given by

$$y = aQ^{b}(1-K)CPL\frac{\sin^{2}\theta}{\cos\theta} \tag{6.9}$$

The RSLESYE-v1 is given by

$$y = aQ^b(1-K)CPLS \tag{6.10}$$

The RSLESYE-v2 is given by

$$y = \left(\frac{5-E}{4}\left(aQ^b(1-K)CPLS\right)^3 + 3c\left(aQ^b(1-K)CPLS\right)^2\right)^{\frac{1}{3}} \tag{6.11}$$

where y is the sediment yield in metric tons, a is the coefficient, b is the exponent, Q is the runoff volume in m^3, K is the soil erodibility factor, L is the slope length in the case of the SLESYE, L is slope length factor in the case of the RSLESYE-v1 and RSLESYE-v2, θ is the angle of slope in degree, $\frac{\sin^2\theta}{\cos\theta}$ is the slope steepness factor (S) of the SLESYE, C is the soil cover factor, P is the soil conservation practice factor, and E and c are calibration parameters.

The performance of the SLESYE, RSLESYE-v1, and RSLESYE-v2 is greater than or equal to 86%, 86%, and 90% respectively for all watersheds under our consideration. Therefore, the performance of the SLESYE and its revised versions was better than the regionalized MUSLE (i.e., the minimum performance was 80%) or improved MUSLE (i.e. the minimum performance was 84%). The best exponent of the SLESYE, RSLESYE-v1, and RSLESYE-v2 was 1.4, 1.42, and 1.42 respectively. The best topographic factor of the RSLESYE-v1 and RSLESYE-v2 was calculated by using the equations that were proposed by Foster et al., (1977) and McCool et al., (1987, 1989) as cited by Renard et al. (1997) (these equations are given in section 6.2).

We evaluated the performance of the RSLESYE-v2 by considering positive values of the calibration parameter E. However, the performance of the RSLESYE-v2 will be further improved by considering negative values of E, this is true for the case of the Hombole and Gumera Watersheds (see figure 3.59). We changed the mathematical form of the RSLESYE-v1, and we called the resulting forms of the equation the RSLESYE-v2. The mathematical form of the MUSLE, the improved MUSLE, the SLESYE or any other model will be changed by the following similar procedure that we followed to change mathematical form of the RSLESYE-v1.

Physically speaking, the SLESYE and its revised versions are more appropriate than the original MUSLE or improved MUSLE for sediment yield estimation. The SLESYE and its revised versions do not consider peak runoff rate, and therefore, it is advantageous to the data-scarce area. However, if we include the peak runoff rate in the SLESYE or revised versions, the physical meaning for sediment estimation is still appropriate. Therefore, we recommend the SLESYE and its revised versions for sediment yield estimation at data-scarce areas, and we also recommend including the peak runoff rate in the RSLESYE-v1 (i.e., $a(Qq)^b(1-K)CPLS$), SLESYE, and RSLESYE-v2, and test their performance if the peak runoff data are available.

6.4 Conclusions and Recommendations on the Modified SWAT+ models

The modified SWAT+ models showed the better performance than the original SWAT+ model. Therefore, we recommend the modified SWAT+ models for sediment yield esti-

mation. If we want to apply $a(Qq)^b(1-K)CPLS$ in the SWAT+ model environment, we can adjust the soil erodibility factor in the user soil table of the SWAT+ model or simply K is the calibration parameter.

6.5 Conclusions and Recommendations on the Iterative Approach for Deriving and Solving the Accurate Sediment Rating Equation

The accurate sediment rating equation was derived by following the proposed iteration steps. For the paired values of suspended sediment concentration (S) and flow (Q) data, the shorthand form of the final accurate sediment rating equation is given by

$$S \approx \frac{1}{bi^u}\left(f(Q) - jQ + f_1(Q,S) + f_2(Q,S) + ... + f_{14}(Q,S)\right)^u \tag{6.12}$$

where, b, i, u and j are constants for given values of paired data

In this dissertation, the polynomial regression functions were considered to derive very long and complex accurate regression equation. However, we can use any other known functions. And also, variables x and y were defined in such a way that individual effects of other variables can reflect on variable S (refer to section 3.11.1). However, we can define variables x and y in another way, and we follow the proposed iterative approach to derive an accurate regression equation.

The proposed iterative approach can be used to derive an accurate regression equation based on given values of paired variables. Therefore, the iterative approach can be used to model any processes, and any calibration and validation processes can be addressed.

In this dissertation, the iterative procedure is provided to solve the accurate regression equation. For further research, the analytical solution of the equation is recommended.

APPENDICES

Table A1: Climatic stations of the Upper Awash River Basin. Data source: National Meteorology Agency of Ethiopia

station name	station's location	available data type	record period
Abebe Keranso	8.978056°N 38.169167°E	daily rainfall	1999 – 2020
Addis Ababa	9.01891°N 38.7475°E	daily rainfall	1986 – 2020
		daily maximum and minimum relative humidity	1986 – 1987
Enselale (Hidosokoke)	8.937°N 38.44°E	daily rainfall	1986 – 2019
Ginchi	9.01667°N 38.1333°E	daily rainfall	1986 – 2015
Guranda Meta	8.912°N 38.593°E	daily rainfall	1986 – 2018
Hombole	8.368167°N 38.78°E	daily rainfall	1986 – 2020
Kimoye	9.013°N 38.341°E	daily rainfall	1986 – 2020
		daily maximum and minimum temperature	1986 – 2020
Koka Dam	8.471°N 39.157°E	daily rainfall	1986 – 2020
		daily maximum and minimum temperature	1986 – 2020
Mojo	8.609°N 39.114°E	daily rainfall	1986 – 2020
		daily maximum and minimum temperature	1986 – 2020
Sebeta	8.915°N 38.629°E	daily rainfall	2015 – 2020
		daily maximum and minimum temperature	2015 – 2020
Sendafa	9.152167°N 39.0215°E	daily rainfall	1986 – 2020
Tefki	8.846°N 38.494°E	daily rainfall	2007 – 2020
		daily maximum temperature	2007 – 2020
		daily minimum temperature	2009 – 2020
Teji	8.836°N 38.375°E	daily rainfall	1986 – 2020
Tulu Bolo	8.658°N 38.211°E	daily rainfall	1987 – 2020
		daily maximum and minimum temperature	1987 – 2020
Zequala	8.86667°N 38.866667°E	daily rainfall	1986 – 2017
Addis Alem	9.042°N 38.38333°E	daily rainfall	1987 – 2019
		daily maximum and minimum temperature	1997 – 2019

Alem Tena	8.29°N 38.90783°E	daily rainfall	1987 – 2019
		daily maximum and minimum temperature	1987 – 2019
Arbuchulele	8.47°N 38.25133°E	daily rainfall	2004 – 2019
Asgori	8.79°N 38.3342°E	daily rainfall	1987 – 2018
		daily maximum and minimum temperature	1987 – 2018
Bantuliben	8.6185°N 38.357°E	daily rainfall	1987 – 2018
Boneya	8.7845°N 38.64167°E	daily rainfall	1987 – 2019
		daily maximum temperature	2010 – 2014
		daily minimum temperature	2010 – 2016
chefedonsa	8.97°N 39.1232°E	daily rainfall	1987 – 2019
		daily maximum temperature	1998 – 2019
		daily minimum temperature	1996 – 2019
Debrezeit	8.733333°N 38.95°E	daily rainfall	1987 – 2018
		daily maximum temperature	1987 – 2013
		daily minimum temperature	1988 – 2018
		daily maximum and minimum relative humidity	1994 – 2012
		daily maximum wind speed	1994 – 2005
		daily maximum sun hour duration	1994 – 2013
Dilela	8.63583°N 38.04083°E	daily rainfall	1987 – 2019
Dire Gidib	9.15783°N 38.943°E	daily rainfall	2000 – 2018
		daily maximum and minimum temperature	2000 – 2018
Ejersa Lele	8.2432°N 38.686°E	daily rainfall	1987 – 2019
Welenkomi	9.001833°N 38.254667°E	daily rainfall	1987 – 2019

Table A2: Climatic stations of the Gumera Watershed. Data source: National Meteorology Agency of Ethiopia

station name	station's location	available data type	record period
Amed Ber	11.9135°N 37.8858°E	daily rainfall	1986 – 2020

		daily maximum and minimum temperature	1986 – 2019
Debre Tabor	11.8666°N 37.9954°E	daily rainfall	1988 – 2020
		daily maximum and minimum temperature	1988 – 2019
		daily maximum and minimum relative humidity	1988 – 2019
		daily maximum wind speed	1988 – 2018
		daily maximum sun hour duration	1993 – 2019
Gassay	11.7971°N 38.134497°E	daily rainfall	2004 – 2019
		daily maximum and minimum temperature	2004 – 2019
Lewaye	11.72°N 38.07194°E	daily rainfall	1987 – 2020
Licha	11.651°N 37.885°E	daily rainfall	2008 – 2018
Mekaneyesus	11.6076°N 38.05422°E	daily rainfall	1987 – 2020
		daily maximum and minimum temperature	1994 – 2019
Wanzaye	11.7862°N 37.67503°E	daily rainfall	1986 – 2020
		daily maximum and minimum temperature	1986 – 2019

Table A3: Climatic stations of the Gilgel Gibe 1 Watershed. Data source: National Meteorology Agency of Ethiopia

station name	station's location	available data type	record period
Ako	8.032117°N 37.20255°E	daily rainfall	2010 – 2020
		daily maximum and minimum temperature	2010 – 2020
Assendabo	7.7605°N 37.231117°E	daily rainfall	1986 – 2020
		daily maximum and minimum temperature	1986 – 2020
Chekorsa	7.616667°N 36.733333°E	daily rainfall	1986 – 2019
Dedo	7.504233°N 36.879717°E	daily rainfall	1986 – 2020
		daily maximum temperature	1986 – 2020
		daily minimum temperature	1986 – 2005
Busa	8.7725°N 38.1382°E	daily rainfall	1987 – 2019

		daily maximum and minimum temperature	2015 – 2019
Dimtu	7.85°N 37.2333°E	daily rainfall	1987 – 2019
Jiren Abajifar	7.700117°N 36.706367°E	daily rainfall	2008 – 2017
Serbo	7.7°N 36.966667°E	daily rainfall	1998 – 2018
Yebu	7.68333°N 36.816667°E	daily rainfall	1987 – 2019
		daily maximum and minimum temperature	1987 – 2019

Table A4: Global weather data for SWAT model 1979 – 2014 (maximum and minimum temperature, rainfall, wind, relative humidity and solar radiation of the Upper Awash River Basin)

	name of weather data location	period
weatherdata-86381	8.58633271°N 38.12720908°E	1979 – 2014
weatherdata-86384	8.586290359°N 38.4375°E	1979 – 2014
weatherdata-86388	8.586290359°N 38.75°E	1979 – 2014
weatherdata-89381	8.89852047°N 38.125°E	1979 – 2014
weatherdata-89384	8.89852047°N 38.4375°E	1979 – 2014
weatherdata-89388	8.89852047°N 38.75°E	1979 – 2014
weatherdata-89391	8.89852047°N 39.0625°E	1979 – 2014
weatherdata-92384	9.210749626°N 38.4375°E	1979 – 2014

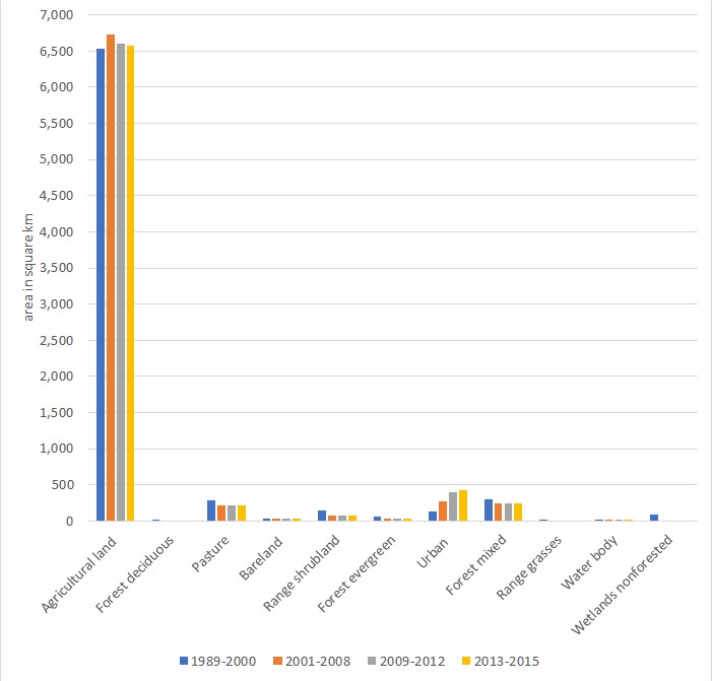

Figure A1: The pictorial representation of land use change for the Hombole Watershed

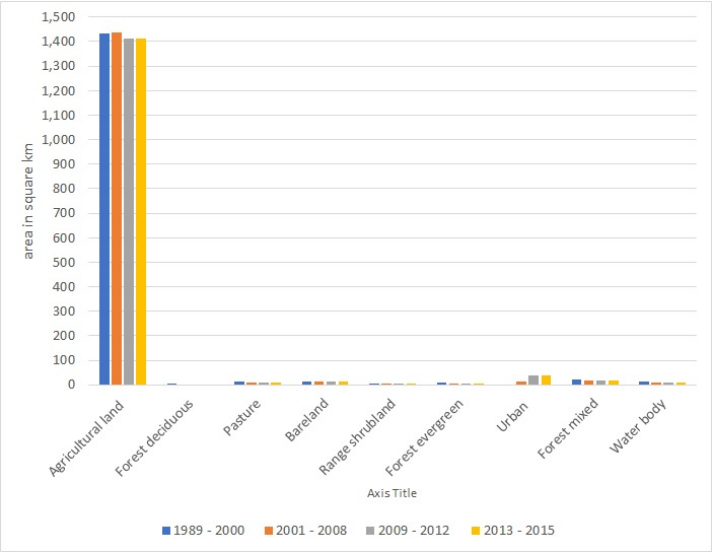

Figure A2: The pictorial representation of land use change for the Mojo Watershed

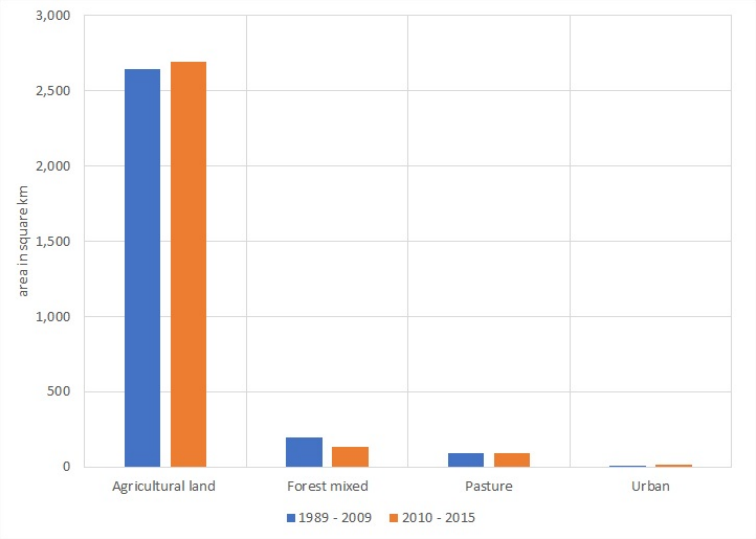

Figure A3: The pictorial representation of land use change for the Gilgel Gibe 1 Watershed

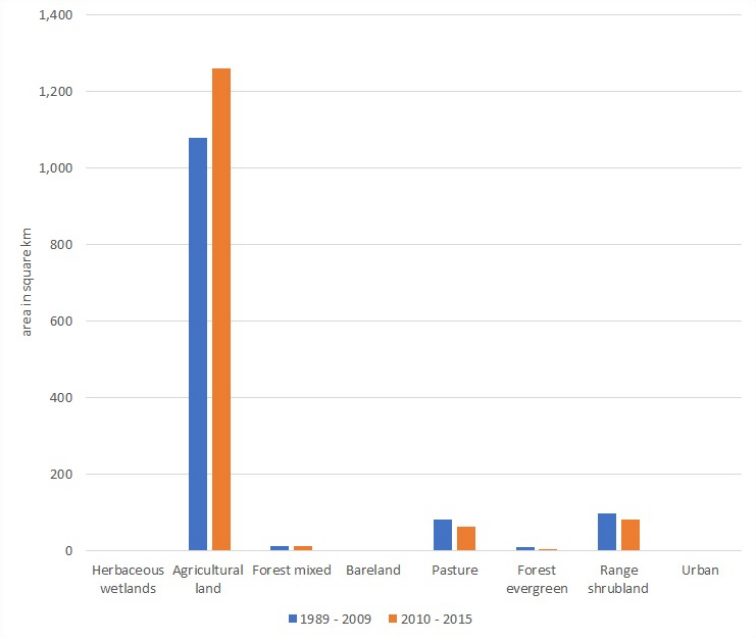

Figure A4: The pictorial representation of land use change for the Gumera Watershed

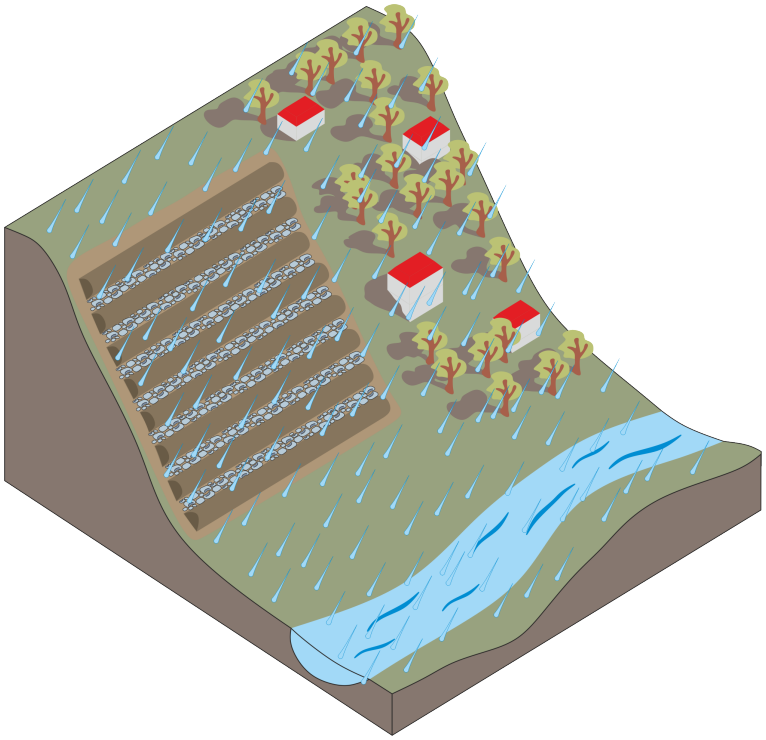

Figure A5: The main variables affecting soil erosion (I Acknowledge my colleague Julia who helped me to draw this figure)

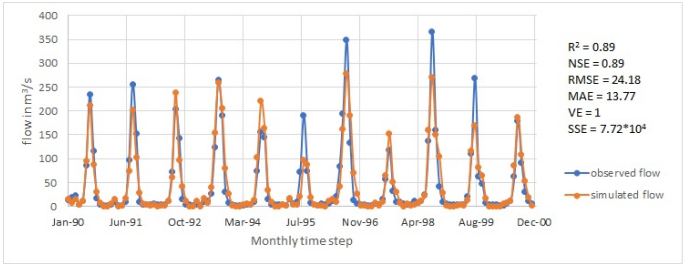

Figure A6: The initial performance of the Original SWAT+ model at monthly time step

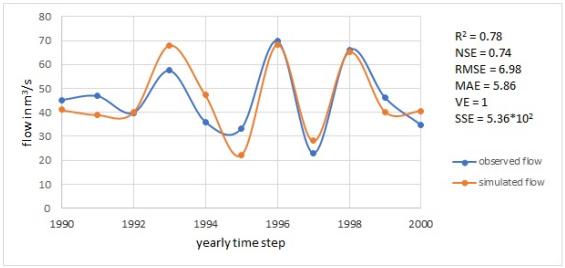

Figure A7: The initial performance of the Original SWAT+ model at yearly time step

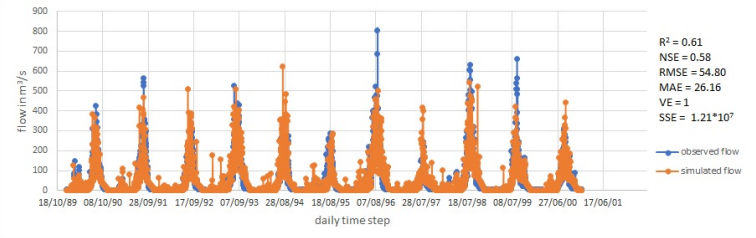

Figure A8: The initial performance of the Original SWAT+ model at daily time step

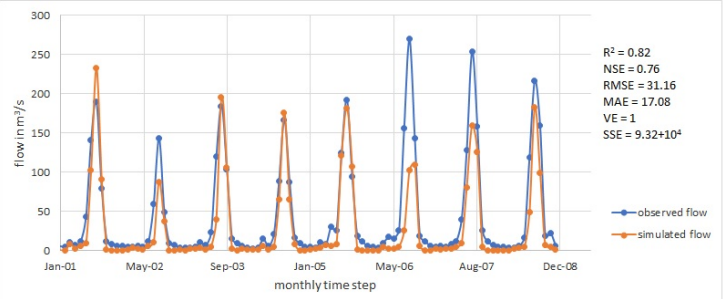

Figure A9: The performance of the calibrated original SWAT+ model when the land use map of 2001 – 2008 was used for the simulation period 2001 – 2008

.

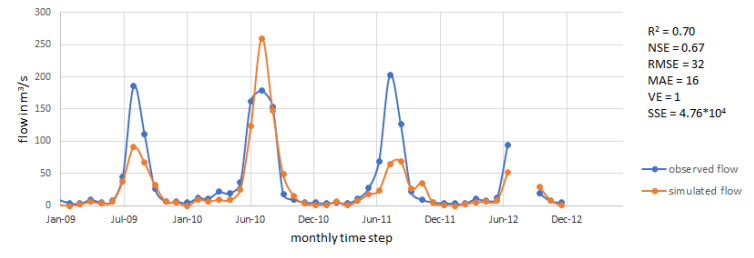

Figure A10: The performance of the calibrated original SWAT+ model when the land use map of 2009 – 2012 was used for the simulation period 2009 – 2012

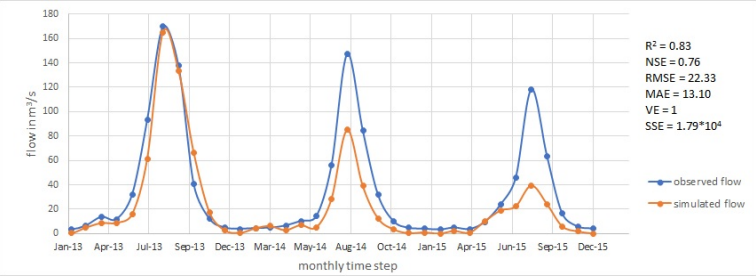

Figure A11: The performance of the calibrated original SWAT+ model when the land use map of 2013 – 2015 was used for the simulation period 2013 – 2015

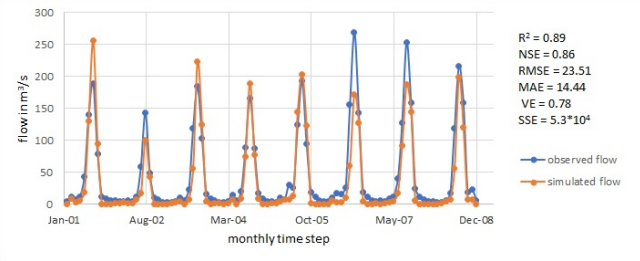

Figure A12: The performance of the calibrated original SWAT+ model when the land use map of 1989 – 2000 was used for the simulation period 2001 – 2008

.

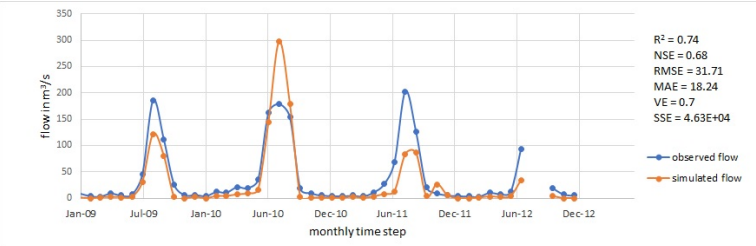

Figure A13: The performance of the calibrated original SWAT+ model when the land use map of 1989 – 2000 was used for the simulation period 2009 – 2012

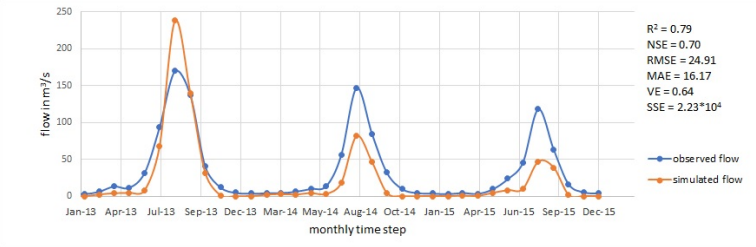

Figure A14: The performance of the calibrated original SWAT+ model when the land use map of 1989 – 2000 was used for the simulation period 2013 – 2015

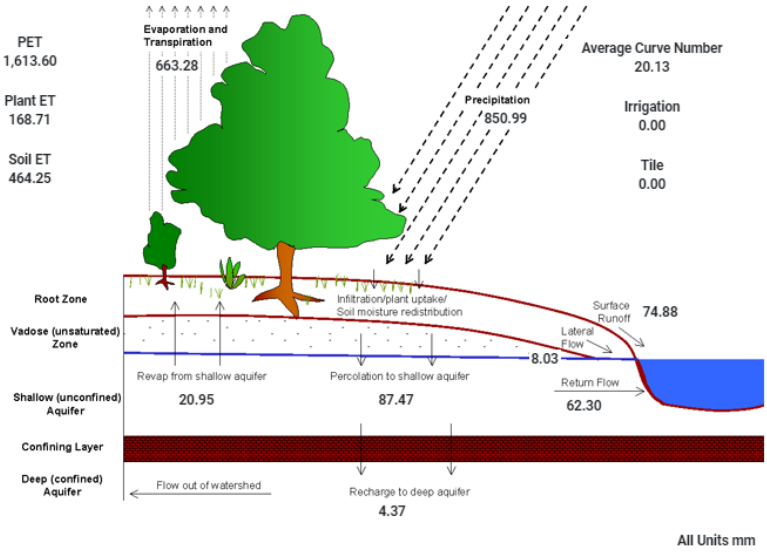

Figure A15: The basin average annual water balance of the Hombole Watershed. This figure is an output of the SWAT+ editor.

REFERENCES

Ad, d. R., Victor, J., Cees, W. and Coen, R. (1998). LISEM: A Physically-Based Hydrologic and Soil Erosion Catchment Model. In Boardman, J. and Favis-Mortlock, D. (eds), *Modelling Soil Erosion by Water*. Berlin, Heidelberg: Springer Berlin Heidelberg, 429–440.

Adegede, A. P. and Mbajiorgu, C. C. (2019). Event-based sediment yield modelling using MUSLE in North-central Nigeria. *Agricultural Engineering International: CIGR Journal* 21: 7–17.

Adu, J. and Kumarasamy, M. (2018). Assessing Non-Point Source Pollution models: a review. *Pol. J. Environ. Stud* 27: 1913–1922, doi:10.15244/pjoes/76497.

Aga, A. O., Chane, B. and Melesse, A. M. (2018). Soil erosion modelling and risk assessment in data scarce Rift Valley Lake regions, Ethiopia. *Water* 10, doi:10.3390/w10111684.

Amare, S., Langendoen, E., Keesstra, S., Ploeg, M., Gelagay, H., Lemma, H. and Zee, S. (2021). Susceptibility to gully erosion: Applying Random Forest (rf) and Frequency Ratio (fr) approaches to a small catchment in Ethiopia. *Water* 13, doi:10.3390/w13020216.

An, L. S., Liao, K. H., Zhou, B. H., Pan, W. and Chen, Q. (2016). Global sensitivity analysis of the parameters of the Modified Universal Soil Loss Equation. *Applied Ecology and Environmental Research* 14: 505–514, doi:10.15666/aeer/1404_505514.

Arekhi, S., Shabani, A. and Rostamizad, G. (2012). Application of the Modified Universal Soil Loss Equation (musle) in prediction of sediment yield (case study: Kengir watershed, Iran). *Arab J. Geosci.* 5: 1259–1267, doi:10.1007/s12517-010-0271-6.

Arnold, J. G., Moriasi, D. N., Gassman, P. W., Abbaspour, K. C., White, M. J., Srinivasan, R., Santhi, C., Harmel, R. D., van Griensven, A., Van, L. M. W., Kannan, N. and Jha, M. K. (2012). SWAT: Model use, calibration, and validation. *American Society of Agricultural and Biological Engineers* 55: 1491–1508.

Asselman, N. E. M. (2000). Fitting and interpretation of sediment rating curves. *Journal of Hydrology* 234: 228–248, doi:10.1016/S0022-1694(00)00253-5.

Balabathina, V. N., Raju, R. P., Mulualem, W. and Tadele, G. (2020). Estimation of soil loss using remote sensing and GIS-based Universal Soil Loss Equation in Northern catchment of Lake Tana sub-basin, Upper Blue Nile basin, Northwest Ethiopia. *Environmental Systems Research* 9, doi:10.1186/s40068-020-00203-3.

Balamurugan, G. (1989). The use of suspended sediment rating curves in malaysia: Some preliminary considerations. *Pertanika* 12: 367–376.

Baoyuan, L., Keli, Z. and Yun, X. (2002). An empirical soil loss equation : 21–25.

Bárdossy, A., Bogárdi, I. and Duckstein, L. (1993). Theory and methodology: Fuzzy nonlinear regression analysis of dose-response relationships. *European Journal of Operational Research* 66: 36–51.

Barnes, T. J. (1998). A history of regression: Actors, networks, machines, and numbers. *Environment and Planning* 30: 203–223.

Beasley, D. B., Huggins, L. F. and Monke, E. J. (1980). ANSWERS: A model for watershed planning. *Transactions of the ASAE* 23, doi:10.13031/2013.34692.

Bekele, B. and Gemi, Y. (2021). Soil erosion risk and sediment yield assessment with Universal Soil Loss Equation and GIS: In Dijo watershed, Rift Valley basin of Ethiopia. *Modeling Earth Systems and Environment* 7: 273–291, doi:10.1007/s40808-020-01017-z.

Belay, A., Claassens, A. S. and Wehner, F. C. (2002). Effect of direct nitrogen and potassium and residual phosphorus fertilizers on soil chemical properties, microbial components and maize yield under long-term crop rotation. *Biol Fertil Soils* 35: 420–427, doi:10.1007/s00374-002-0489-x.

Benavidez, R., Jackson, B., Maxwell, D. and Norton, K. (2018). A review of the (Revised) Universal Soil Loss Equation ((R)USLE): With a view to increasing its global applicability and improving soil loss estimates. *Hydrology and Earth System Sciences* 22: 6059–6086, doi:10.5194/HESS-22-6059-2018.

Betrie, G. D., Griensven, A., Mohamed, Y. A., Popescu, I., Mynett, A. E. and Hummel, S. (2011). Linking SWAT and SOBEK using open modeling interface (openMI) for sediment transport simulation in the Blue Nile river basin. *Transactions of the ASABE* 54: 1749–1757, doi:10.13031/2013.39847.

Bieger, K., Arnold, J. G., Rathjens, H., White, M. J., Bosch, D. D., Allen, P. M., Volk, M. and Srinivasan, R. (2017). Introduction to SWAT+, a completely restructured version of the Soil and Water Assessment Tool. *Journal of the American Water Resources Association* 53, doi:10.1111/1752-1688.12482.

Blanco-Canqui, H. and Benjamin, J. G. (2013). Impacts of soil organic carbon on soil physical behavior. *Advances in Agricultural Systems Modeling* 3, doi:10.2134/advagricsystmodel3.c2.

Boekel, P. and Peerlkamp, P. (1956). Soil consistency as a factor determining the soil structure of clay soils. *Wageningen Journal of Life Sciences* 4, doi:10.18174/njas.v4i1.17792.

Bogale, A. (2020). Review, impact of land use/cover change on soil erosion in the Lake Tana basin, Upper Blue Nile, Ethiopia. *Applied Water Science* 10, doi:10.1007/s13201-020-01325-w.

Bonumá, N. B., Rossi, C. G., Arnold, J. G., Reichert, J. M., Minella, J. P., Allen, P. M. and Volk, M. (2014). Simulating landscape sediment transport capacity by using a modified SWAT model. *Journal of Environmental Quality* 43: 55–66, doi:10.2134/jeq2012.0217.

Brunori, F., Penzo, M. C. and Torri, D. (1989). Soil shear strength: Its measurement and soil detachability. *CATENA* 16: 59–71, doi:10.1016/0341-8162(89)90004-0.

Bunke, O., Droge, B. and Polzehl, J. (1999). Model selection, transformations and variance estimation in nonlinear regression. *Statistics: A Journal of Theoretical and Applied Statistics* 33: 197–240, doi:10.1080/02331889908802692.

Cai, P., Sun, X., Wu, Y., Gao, C., Mortimer, M., Holden, P. A., Redmile-Gordon, M. and Huang, Q. (2019). Soil biofilms: Microbial interactions, challenges, and advanced techniques for ex-situ characterization. *Soil Ecol. Lett* : 85–93doi:10.1007/s42832-019-0017-7.

Chen, L., Qian, X. and Shi, Y. (2011). Critical area identification of potential soil loss in a typical watershed of the three gorges reservoir region. *Water Resour Manage.* 25: 3445–3463, doi:10.1007/s11269-011-9864-4.

Chen, S.-C., Wu, C.-Y., Wu, Y.-L. and Wang, S.-H. (2009). Taiwan Universal Soil Loss Equation (TUSLE) based on revised factors and gis layers-an example from Shihmen reservoir watershed. *Chinese Journal of Soil and Water Conservation* 40, doi:10.29417/JCSWC.200906_40(2).0007.

Coffey, M. E., Workman, S. R., Taraba, J. L. and Fogle, A. W. (2004). Statistical procedures for evaluating daily and monthly hydrologic model predictions. *Biosystems and Agricultural Engineering Faculty Publications* 47: 59–68, doi:10.13031/2013.15870.

Cole, Cooley, Dyke, Favis-Mortlock, Foster, Hanson, Jones, Jones, O., Kiniry, Laflen, Lyles, Nicks, Onstad, Richardson, Robertson, Sharpley, Smith, Smith, F., Spanel, Springer, Steiner and williams (1990). *EPIC—Erosion/Productivity Impact Calculator*, *Technical Bulletin Number 1768*. United States Department of Agriculture, Agricultural Research Service.

Cyco n, M., Mrozik, A. and Piotrowska-Seget, Z. (2019). Antibiotics in the soil environment—degradation and their impact on microbial activity and diversity. *Frontiers in Microbiology* 10: 338, doi:10.3389/fmicb.2019.00338.

David, W. P. (1988). Soil and water conservation planning: Policy issues and recommendations. *Journal of Philippine Development* XV: 47–84.

Degife, A., Worku, H. and Gizaw, S. (2021). Environmental implications of soil erosion and sediment yield in Lake Hawassa watershed, South-central Ethiopia. *Environmental Systems Research* 10, doi:10.1186/s40068-021-00232-6.

Desmet, P. and Govers, G. (1996). A GIS procedure for automatically calculating the USLE LS factor on topographically complex landscape units. *Journal of Soil and Water Conservation* 51.

Devi, G., Ganasri, B. and Dwarakish, G. (2015). A review on hydrological models. *Aquatic Procedia* 4: 1001–1007, doi:10.1016/j.aqpro.2015.02.126, international Conference on Water Resources, Coastal and Ocean Engineering (ICWRCOE'15).

Devi, R., Tesfahune, E., Legesse, W., Deboch, B. and Beyene, A. (2008). Assessment of siltation and nutrient enrichment of Gilgel Gibe dam, Southwest Ethiopia. *Bioresource Technology* 99: 975–979, doi:10.1016/j.biortech.2007.03.013.

Dile, Y., Daggupati, P., George, C., Srinivasan, R. and Arnold, J. (2016). Introducing a new open source GIS user interface for the SWAT model. *Environmental Modelling & Software* 85: 129–138, doi:10.1016/j.envsoft.2016.08.004.

Dlapa, P., Hrinlk, D., Hrabovsky, A., Simkovic, I., Zarnovican, H., Sekucia, F. and Kollar, J. (2020). The impact of land-use on the hierarchical pore size distribution and water retention properties in loamy soils. *Water* 12, doi:10.3390/w12020339.

Donigian, A. S. J., Bicknell, B. R. and Imhoff, J. C. (1995). *Hydrological Simulation Program - FORTRAN (HSPF)*. Water Resource Publications, Colorado, USA.

Doomen, A. M. C., Wijma, E., Zwolsman, J. J. G. and Middelkoop, H. (2008). Predicting suspended sediment concentrations in the Meuse river using a supply-based rating curve. *Hydrological Processes* 22: 1846–1856, doi:10.1002/hyp.6767.

Du, K.-L. and Swamy, M. N. S. (2014). *Neural Networks and Statistical Learning*. Springer, doi:10.1007/978-1-4471-5571-3.

Easton, Z. M., Fuka, D. R., Walter, M. T., Cowan, D. M., Schneiderman, E. M. and Steenhuis, T. S. (2008). Re-conceptualizing the Soil and Water Assessment Tool (SWAT) model to predict runoff from variable source areas. *Journal of Hydrology* 348: 279–291, doi:10.1016/j.jhydrol.2007.10.008.

Efthimiou, N. (2019). The role of sediment rating curve development methodology on river load modeling. *Environmental Monitoring and Assessment* 191, doi:10.1007/s10661-018-7167-4.

Ekwue, E. (1990). Organic-matter effects on soil strength properties. *Soil & Tillage Research* : 289–297.

Engel, B., Storm, D., White, M., Arnold, J. and Arabi, M. (2007). A hydrologic/water quality model application protocol. *Journal of the American Water Resources Association* 43: 1223–1236, doi:10.1111/j.1752-1688.2007.00105.x.

Fagbohun, B. J., Anifowose, A. Y. B., Odeyemi, C., Aladejana, O. O. and Aladeboyeje, A. I. (2016). GIS-based estimation of soil erosion rates and identification of critical areas in Anambra sub-basin, Nigeria. *Modeling Earth Systems and Environment* 2, doi:10.1007/s40808-016-0218-3.

Fang, K., Kou, D., Wang, G., Chen, L., Ding, J., Li, F., Yang, G., Qin, S., Liu, L., Zhang, Q. and Yang, Y. (2017). Decreased soil cation exchange capacity across Northern China's grasslands over the last three decades. *Journal of Geophysical Research: Biogeosciences* 122: 3088–3097, doi:10.1002/2017JG003968.

Fenta, A. A., Tsunekawa, A., Haregeweyn, N., Tsubo, M., Yasuda, H., Kawai, T., Ebabu, K., Berihun, M. L., Belay, A. S. and Sultan, D. (2021). Agroecology-based soil erosion assessment for better conservation planning in Ethiopian river basins. *Environmental Research* 195: 110786, doi:10.1016/j.envres.2021.110786.

Fernandez-Delgado, M., Sirsat, M., Cernadas, E., Alawadi, S., Barro, S. and Febrero-Bande, M. (2019). An extensive experimental survey of regression methods. *Neural Networks* 111: 11–34, doi:10.1016/j.neunet.2018.12.010.

Finney, D. J. (1996). A note on the history of regression. *Journal of Applied Statistics* 23: 555–557, doi:10.1080/02664769624099.

Flanagan, D. and Nearing, M. (1995). USDA–water erosion prediction project hillslope profile and watershed model documentation.

Flint, A. L. and Childs, S. W. (1991). Use of the Priestley-Taylor evaporation equation for soil water limited conditions in a small forest clearcut. *Agricultural and Forest Meteorology* 56: 247–260, doi:10.1016/0168-1923(91)90094-7.

Francipane, A., Ivanov, Y., Noto, L., Istanbulluoglu, E., Arnone, E. and Bras, R. L. (2012). tRIBS-erosion: A parsimonious physically-based model for studying catchment hydro-geomorphic response. *CATENA* 92: 216–231, doi:10.1016/j.catena.2011.10.005.

Frankl, A., Deckers, J., Moulaert, L., Damme, A. V., Haile, M., Poesen, J. and Nyssen, J. (2014). Integrated solutions for combating gully erosion in areas prone to soil piping: Innovations from the drylands of Northern Ethiopia. *Land Degradation & Development* doi:10.1002/ldr.2301.

Gabet, E. J., Reichman, O. and Seabloom, E. W. (2003). The effects of bioturbation on soil processes and sediment transport. *Annu. Rev. Earth Planet. Sci.* 31: 249–73, doi:10.1146/annurev.earth.31.100901.141314.

Ganasri, B. P. and Ramesh, H. (2016). Assessment of soil erosion by RUSLE model using remote sensing and GIS - a case study of Nethravathi basin. *Geoscience Frontiers* 7: 953–961, doi:10.1016/J.GSF.2015.10.007.

Gashaw, T., Tulu, T. and Argaw, M. (2017). Erosion risk assessment for prioritization of conservation measures in Geleda watershed, Blue Nile basin, Ethiopia. *Environmental Systems Research* doi:10.1186/s40068-016-0078-x.

Gelagay, H. S. and Minale, A. S. (2016). Soil loss estimation using GIS and remote sensing techniques: A case of Koga watershed, Northwestern Ethiopia. *International Soil and Water Conservation Research* 4: 126–136, doi:10.1016/j.iswcr.2016.01.002.

Glad, I. K. (1998). Parametrically guided non-parametric regression. *Scandinavian Journal of Statistics* 25: 649–668.

Gupta, H., Sorooshian, S. and Yapo, P. (1999). Status of automatic calibration for hydrologic models: Comparison with multilevel expert calibration. *Journal of Hydrologic Engineering* 4: 135–143, doi:10.1061/(ASCE)1084-0699(1999)4:2(135).

Gwapedza, D., Slaughter, A., Hughes, D. and Mantel, S. (2018). Regionalising MUSLE factors for application to a data-scarce catchment 377: 19–24, doi:10.5194/PIAHS-377-19-2018.

Haile, G. W. and Fetene, M. (2012). Assessment of soil erosion hazard in Kilie catchment, East Shoa, Ethiopia. *land degradation & development* 23: 293–306, doi:10.1002/ldr.1082.

Hao, P. and Chiang, J. (2008). Fuzzy regression analysis by support vector learning approach. *IEEE Transactions on Fuzzy Systems* 16: 428–441.

Hapsari, D., Onishi, T., Imaizumi, F., Noda, K. and Senge, M. (2019). The use of sediment rating curve under its limitations to estimate the suspended load. *Reviews in Agricultural Science* 7: 88–101, doi:10.7831/ras.7.0$_$88.

Haregeweyn, N., Melesse, B., Tsunekawa, A., Tsubo, M., Meshesha, D. and Balana, B. B. (2012). Reservoir sedimentation and its mitigating strategies: A case study of Angereb reservoir (NW Ethiopia). *Journal of Soils and Sediments* : 12:291–305doi:10.1007/s11368-011-0447-z.

Haregeweyn, N., Poesen, J., Nyssen, J., Wit, J. D., Haile, M., Govers, G. and Deckers, S. (2006). Reservoirs in Tigray (Northern Ethiopia): Characteristics and sediment deposition problems. *Land Degradation & Development* : 17:211–230doi:10.1002/ldr.698.

Haregeweyn, N., Tsunekawa, A., Nyssen, J., Poesen, J., Tsubo, M., Meshesha, D. T., Sch'utt, B., Adgo, E. and Tegegne, F. (2015). Soil erosion and conservation in Ethiopia: A review. *Progress in Physical Geography* : 750–774doi:10.1177/0309133315598725.

Haregeweyn, N., Tsunekawa, A., Poesen, J., Tsubo, M., Meshesha, D. T., Fenta, A. A., Nyssen, J. and Adgo, E. (2017). Comprehensive assessment of soil erosion risk for better land use planning in river basins: Case study of the Upper Blue Nile river. *Science of The Total Environment* 574: 95–108, doi:10.1016/j.scitotenv.2016.09.019.

Hargreaves, G. H. and Allen, R. G. (2003). History and evaluation of Hargreaves evapotranspiration equation. *J. Irrig. Drain Eng* 129: 53–63, doi:10.1061/(ASCE)0733-9437(2003)129:1(53).

Heng, S. and Suetsugi, T. (2014). Comparison of regionalization approaches in parameterizing sediment rating curve in ungauged catchments for subsequent instantaneous sediment yield prediction. *Journal of Hydrology* 512: 240–253, doi:10.1016/j.jhydrol.2014.03.003.

Hoang, L., Schneiderman, E., Moore, K., Mukundan, R., Owens, E. and Steenhuis, T. (2017). Predicting saturation-excess runoff distribution with a lumped hillslope model:SWAT-HS. *Hydrological Processes* 31: 2226–2243, doi:10.1002/hyp.11179.

Hope, J. A., Paterson, D. M. and Thrush, S. F. (2020). The role of microphytobenthos in soft-sediment ecological networks and their contribution to the delivery of multiple ecosystem services. *Journal of Ecology* 108: 815–830, doi:10.1111/1365-2745.13322.

Horowitz, A. J. (2003). An evaluation of sediment rating curves for estimating suspended sediment concentrations for subsequent flux calculations. *Hydrological Processes* 17: 3387–3409, doi:10.1002/hyp.1299.

Hurni, K., Zeleke, G., Kassie, M., B.Tegegne, Kassawmar, T., Teferi, E., Moges, A., Tadesse, D., Ahmed, M., Degu, Y., Kebebew, Z., Hodel, E., Amdihun, A., Mekuriaw, A., Debele, B., Deichert, G. and Hurni, H. (2015). Soil degradation and sustainable land management in the rainfed agricultural areas of Ethiopia: An assessment of the economic implications.

Jain, R. K. and Kothyari, U. C. (2009). Cohesion influences on erosion and bed load transport. *Water Resources Research* 45, doi:10.1029/2008WR007044.

Jang, C., Shin, Y., Kum, D., Kim, R., Yang, J. E., Kim, S. C., Hwang, S. I., Lim, K. J., Yoon, J., Park, Y. S. and Jung, Y. (2015). Assessment of soil loss in South Korea based on land-cover type. *Stochastic Environmental Research and Risk Assessment* 29: 2127–2141, doi:10.1007/s00477-015-1027-3.

Jeloudar, F. T., Sepanlou, M. G. and Emadi, S. (2018). Impact of land use change on soil erodibility. *Global J. Environ. Sci. Manage* 4: 59–70, doi:10.22034/gjesm.2018.04.01.006.

Jepsen, R., Roberts, J. and Lick, W. (1997). Effects of bulk density on sediment erosion rates. *Water, Air and Soil Pollution* 99: 21–31.

Jien, S. and Wang, C. (2013). Effects of biochar on soil properties and erosion potential in a highly weathered soil. *CATENA* 110: 225–233, doi:10.1016/j.catena.2013.06.021.

Jin, X., Jin, Y. and Mao, X. (2019). Land use/cover change effects on river basin hydrological processes based on a Modified Soil and Water Assessment Tool: A case study of the Heihe river basin in Northwest China's arid region. *Sustainability* 11, doi:10.3390/su11041072.

Jing, H., Chen, G., Wang, W. and Li, G. (2018). Effects of concentration-dependent settling velocity on nonequilibrium transport of suspended sediment. *Environmental Earth Sciences* 77, doi:10.1007/s12665-018-7731-9.

Kaba£a, C. and £ABAZ, B. (2018). Relationships between soil ph and base saturation – conclusions for polish and international soil classifications. *Soil Science Annual* 69: 206–214, doi:10.2478/ssa-2018-0021.

Kidane, M., Bezie, A., Kesete, N. and Tolessa, T. (2019). The impact of land use and land cover (lulc) dynamics on soil erosion and sediment yield in Ethiopia. *Heliyon* 5: e02981, doi:10.1016/j.heliyon.2019.e02981.

Kim, J.-G., Park, Y., Yoo, D., Kim, N.-W., Engel, B. A., Kim, S., Kim, K.-S. and Lim, K. J. (2009). Development of a SWAT patch for better estimation of sediment yield in steep sloping watersheds. *JOURNAL OF THE AMERICAN WATER RESOURCES ASSOCIATION* 45: 963–972, doi:10.1111/j.1752-1688.2009.00339.x.

Kinnell, P. I. A. (2005). Why the Universal Soil Loss Equation and the revised version of it do not predict event erosion well. *Hydrological Processes* 19: 851–854, doi:10.1002/hyp.5816.

Kinnell, P. I. A. (2010). Event soil loss, runoff and the Universal Soil Loss Equation family of models: A review. *Journal of Hydrology* 385: 384–397, doi:10.1016/J.JHYDROL.2010.01.024.

Kinnell, P. I. A. (2019). A review of the science and logic associated with approach used in the Universal Soil Loss Equation family of models. *Soil systems* doi:10.3390/soilsystems3040062.

Knisel, W. G. (1980). CREAMS: A field scale model for chemicals, runoff, and erosion from agricultural management systems.

Kopal, I., Labaj, I., Vršková, J., Harničárová, M., Valíček, J., Ondrušová, D., Krmela, J. and Palková, Z. (2022). A generalized regression neural network model for predicting the curing characteristics of carbon black-filled rubber blends. *Polymers* 14, doi:10.3390/polym14040653.

Kropaček, J., calogero Schillaci, riccardo Salvini and M'arKer, M. (2016). Assessment of gully erosion in the Upper Awash, Central Ethiopian highlands based on a comparison of archived aerial photographs and very high resolution satellite images. *Geogr. Fis. Dinam. Quat.* : 161–170doi:10.4461/GFDQ2016.39.15.

Kruk, E. (2021). Use of chosen methods for determination of the usle soil erodibility factor on the example of loess slope. *Journal of Ecological Engineering* 22: 151—-161, doi:10.12911/22998993/128861.

Kuttah, D. and Sato, K. (2015). Review on the effect of gypsum content on soil behavior. *Transportation Geotechnics* 4: 28–37, doi:10.1016/j.trgeo.2015.06.003.

Lee, C., Low, Y. M. and Chiew, Y. (2016). Multi-dimensional rheology-based twophase model for sediment transport and applications to sheet flow and pipeline scour. *Phys. Fluids 28, 053305* doi:10.1063/1.4948987.

Lemma, H., Frankl, A., Dessie, M., Poesen, J., Adgo, E. and Nyssen, J. (2020). Consolidated sediment budget of Lake Tana, Ethiopia (2012–2016). *Geomorphology* 371: 107434, doi:10.1016/j.geomorph.2020.107434.

Li, G.-L., Zheng, T.-Z., Fu, Y., Li, B.-Q. and Zhang, T. (2017). Soil detachment and transport under the combined action of rainfall and runoff energy on shallow overland flow. *J. Mt. Sci.* 14: 1373–1383, doi:10.1007/s11629-016-3938-y.

Li, H. and Yin, G. (2009). Generalized method of moments estimation for linear regression with clustered failure time data. *Biometrika* 96: 293–306, doi:10.1093/biomet/asp005.

Li, J., Wang, W., Guo, M., Kang, H., Wang, Z., Huang, J., Sun, B., Wang, K., Zhang, G. and Bai, Y. (2020). Effects of soil texture and gravel content on the infiltration and soil loss of spoil heaps under simulated rainfall. *Journal of Soils and Sediments* 20, doi:10.1007/s11368-020-02729-6.

Linnet, K. (1998). Performance of deming regression analysis in case of misspecified analytical error ratio in method comparison studies. *Clinical Chemistry* 44: 1024–1031, doi:10.1093/clinchem/44.5.1024.

Liu, B., Xie, Y., Li, Z., Liang, Y., Zhang, W., Fu, S., Yin, S., Wei, X., Zhang, K., Wang, Z., Liu, Y., Zhao, Y. and Guo, Q. (2020). The assessment of soil loss by water erosion in China. *International Soil and Water Conservation Research* 8: 430–439, doi:10.1016/j.iswcr.2020.07.002.

Lolli, B. and Gasperini, P. (2012). A comparison among general orthogonal regression methods applied to earthquake magnitude conversions. *Geophysical Journal International* 190: 1135–1151, doi:10.1111/j.1365-246X.2012.05530.x.

Lu, C.-M. and Chiang, L.-C. (2019). Assessment of sediment transport functions with the modified SWAT-Twn model for a Taiwanese small mountainous watershed. *Water* 11, doi:10.3390/w11091749.

Luo, Y., Yang, S., Liu, X., Liu, C., Zhang, Y., Zhou, Q., Zhou, X. and Dong, G. (2016). Suitability of revision to MUSLE for estimating sediment yield in the Loess Plateau of China. *Stochastic Environmental Research and Risk Assessment* 30: 379–394, doi:10.1007/s00477-015-1131-4.

Masters, T. and Land, W. (1997). A new training algorithm for the general regression neural network, 1997 ieee international conference on systems, man, and cybernetics. *lEEE* : 1990–1994doi:10.1109/ICSMC.1997.635142.

Matsumoto, S., Ogata, S., Shimada, H., Sasaoka, T., Hamanaka, A. and Kusuma, G. J. (2018). Effects of ph-induced changes in soil physical characteristics on the development of soil water erosion. *Geosciences* 8, doi:10.3390/geosciences8040134.

Mitasova, H., Hofierka, J., Zlocha, M. and Iverson, L. R. (1996). Modelling topographic potential for erosion and deposition using GIS. *International Journal of Geographical Information Systems* 10: 629–641, doi:10.1080/02693799608902101.

Moges, M. M., Abay, D. and Engidayehu, H. (2018). Investigating reservoir sedimentation and its implications to watershed sediment yield: The case of two small dams in data-scarce Upper Blue Nile basin, Ethiopia. *Lakes & Reservoirs: Science, Policy & Management for Sustainable Use* 23: 217–229, doi:10.1111/LRE.12234.

Moore, I. D. and Wilson, J. P. (1992). Length-slope factors for the Revised Universal Soil Loss Equation: Simplified method of estimation. *Journal of Soil and Water Conservation* 47: 423–428.

Morala, P., Cifuentes, J. A., Lillo, R. E. and Ucar, I. (2021). Towards a mathematical framework to inform neural network modelling via polynomial regression. *Neural Networks* 142: 57–72, doi:10.1016/j.neunet.2021.04.036.

Morgan, R. and Duzant, J. (2008). Modified MMF (Morgan–Morgan–Finney) model for evaluating effects of crops and vegetation cover on soil erosion. *Earth Surface Processes and Landforms* 33: 90–106, doi:10.1002/esp.1530.

Morgan, R. P. C. (2005). *Soil Erosion and Conservation*. Blackwell Science Ltd.

Morgan, R. P. C., Quinton, J. N., Smith, R. E., Govers, G., Poesen, J. W. A., Chisci, G. and Torri, D. (1998). The EUROSEM Model. In Boardman, J. and Favis-Mortlock, D. (eds), *Modelling Soil Erosion by Water*. Berlin, Heidelberg: Springer Berlin Heidelberg, 389–398.

Msadala, V. C. and Basson, G. R. (2017). Revised Regional Sediment Yield Prediction Methodology for Ungauged Catchments in South Africa. *Journal of the South African Institution of Civil Engineering* 59: 28–36, doi:10.17159/2309-8775/2017/v59n2a4.

Muche, H., Temesgen, M. and Yimer, F. (2013). Soil loss prediction using USLE and MUSLE under conservation tillage integrated with 'fanya juus' in Choke mountain, Ethiopia. *International Journal of Agricultural Sciences* 3: 46–52.

Ndomba (2010). Modelling of sedimentation upstream of Nyumba Ya Mungu reservoir in Pangani river basin. *Nile Basin Water Science & Engineering Journal* 3: 25–38.

Neave, M. and Rayburg, S. (2006). Salinity and erosion: A preliminary investigation of soil erosion on a salinized hillslope. *Sediment Dynamics and the Hydromorphology of Fluvial Systems Proceedings of a symposium held in Dundee, UK, July. IAHS Publ. 306* .

Nguyen, T. V., Dietrich, J., Dang, T. D., Tran, D. A., Doan, B. V., Sarrazin, F. J., Abbaspour, K. and Srinivasan, R. (2022). An interactive graphical interface tool for parameter calibration, sensitivity analysis, uncertainty analysis, and visualization for the Soil and Water Assessment Tool. *Environmental Modelling & Software* 156: 105497, doi:10.1016/j.envsoft.2022.105497.

Noack, M., Gerbersdorf, S. U., Hillebrand, G. and Wieprecht, S. (2015). Combining field and laboratory measurements to determine the erosion risk of cohesive sediments best. *Water* 7: 5061–5077, doi:10.3390/w7095061.

Odongo, V., Onyando, J., Mutua, B., van Oel, P. and Becht, R. (2013). Sensitivity analysis and calibration of the Modified Universal Soil Loss Equation (MUSLE) for the Upper Malewa catchment, Kenya. *International Journal of Sediment Research* 28: 368–383, doi:10.1016/S1001-6279(13)60047-5.

Ogden, F., Downer, C. and Meselhe, E. (2003). U.S. Army Corps of Engineers Gridded Surface/Subsurface Hydrologic Analysis (GSSHA) model: Distributed-parameter, physically based watershed simulations. doi:10.1061/40685(2003)376.

Özsoy, V. S. and Örkçü, H. H. (2016). Estimating the parameters of nonlinear regression models through Particle Swarm optimization. *Gazi University Journal of Science* 29: 187–199.

Panagos, P., Meusburger, K., Ballabio, C., Borrelli, P. and Alewell, C. (2014). Soil erodibility in europe: A high-resolution dataset based on LUCAS. *Science of The Total Environment* 479-480: 189–200, doi:10.1016/j.scitotenv.2014.02.010.

Pandey, A., Chowdary, V. and Mal, B. C. (2009). Sediment yield modelling of an agricultural watershed using MUSLE, remote sensing and GIS. *Paddy Water Environment* 7: 105–113, doi:10.1007/s10333-009-0149-y.

Pao, H. (2008). A comparison of neural network and multiple regression analysis in modeling capital structure. *Expert Systems with Applications* 35: 720–727, doi:10.1016/j.eswa.2007.07.018.

Patil, S., Sivapalan, M., Hassan, M., Ye, S., Harman, C. and Xu, X. (2012). A network model for prediction and diagnosis of sedimentdynamics at the watershed scale. *Journal of Geophysical Research* 117, doi:10.1029/2012JF002400.

Pelletier, J. (2012). A spatially distributed model for the long-term suspended sediment discharge and delivery ratio of drainage basins. *Journal of Geophysical Research* 117, doi:10.1029/2011JF002129.

Pongsai, S., Vogt, D. S., Shrestha, R. P., Clemente, R. and Eiumnoh, A. (2010). Calibration and validation of the Modified Universal Soil Loss Equation for estimating sediment yield on sloping plots: A case study in Khun Satan catchment of Northern Thailand. *Canadian Journal of Soil Science* 90: 585–596, doi:10.4141/CJSS09076.

Powlson, D. S., Hirsch, P. R. and Brookes, P. C. (2001). The role of soil microorganisms in soil organic matter conservation in the tropics. *Nutrient Cycling in Agroecosystems* 61: 41–51.

Qian, S. S. and Reckhow, K. H. (2005). Nonlinear regression modeling of nutrient loads in streams: A Bayesian approach. *Water Resources Research* 41, doi:10.1029/2005WR003986.

Rahman, M. and Asadujjaman, M. (2021). Implementation of artificial neural network on regression analysis, 2021 5th annual systems modelling conference doi:10.1109/SMC53803.2021.9569881.

Razavian, S., Wenby, R., Fisher, T. and Meiselman, H. (1997). Determination of particle sedimentation rate by ultrasonic interferometry: Role of particle size, density and volume fraction. *Biorheology* 34: 349–362, doi:10.3233/BIR-1997-344-507.

Refsgaard, J. and Storm, B. (1995). *MIKE SHE*. Water Resource Publications, Colorado, USA.

Renard, K., Foster, G., Weesies, G., McCool, D. and Yoder, D. (1997). *Predicting Soil Erosion by Water: A Guide to Conservation Planning with the Revised Universal Soil Loss Equation*. USDA, Agriculture Handbook, No 703, 404pp.

Renard, K., Yoder, D., Lightle, D. and S.M., D. (2011). *Handbook of Erosion Modelling: Universal Soil Loss Equation and Revised Universal Soil Loss Equation*. Blackwell Publishing Ltd.

Rimmeri, D. L. and Greenland, D. J. (1976). Effects of calcium carbonate on the swelling behaviour of a soil clay. *Journal of Soil Science* .

Rousseva, S., Torri, D. and Pagliai, M. (2002). Effect of rain on the macroporosity at the soil surface. *European Journal of Soil Science* 53: 83–94, doi:10.1046/j.1365-2389.2002.00426.x.

Sadeghi, S. H., Mizuyama, T. and Vangah, B. G. (2007). Conformity of MUSLE estimates and erosion plot data for storm-wise sediment yield estimation. *Terr. Atmos. Ocean. Sci.* 18: 117–128.

Sadeghi, S. H. R., Gholami, L., Darvishan, A. K. and Saeidi, P. (2014). A review of the application of the MUSLE model worldwide. *Hydrological Sciences Journal* 59: 365–375, doi:10.1080/02626667.2013.866239.

Sanford, L. P. (2008). Modeling a dynamically varying mixed sediment bed with erosion, deposition, bioturbation, consolidation, and armoring. *Computers & Geosciences* 34: 1263–1283, doi:10.1016/j.cageo.2008.02.011.

Schmidt, S., Tresch, S. and Meusburger, K. (2019). Modification of the rusle slope length and steepness factor (LS-factor) based on rainfall experiments at steep alpine grasslands. *MethodsX* 6: 219–229, doi:10.1016/j.mex.2019.01.004.

Seal, H. L. (1967). Studies in the history of probability and statistics. XV: The historical development of the gauss linear model. *Biometrika* 54: 1–24.

Seber, G. A. F. and Wild, C. J. (2003). *Nonlinear Regression*. John Wiley & Sons.

Shawul, A. A., Chakma, S. and Melesse, A. M. (2019). The response of water balance components to land cover change based on hydrologic modeling and Partial Least Squares Regression (PLSR) analysis in the Upper Awash basin. *Journal of Hydrology: Regional Studies* 26: 100640, doi:10.1016/j.ejrh.2019.100640.

Shekar, N. C. S. and Hemalatha, H. N. (2021). Performance comparison of Penman–Monteith and Priestley–Taylor models using MOD16A2 remote sensing product. *Pure Appl. Geophys.* 178: 3153–3167, doi:10.1007/s00024-021-02780-5.

Sofo, A., Mininni, A. N. and Ricciuti, P. (2020). Soil macrofauna: A key factor for increasing soil fertility and promoting sustainable soil use in fruit orchard agrosystems. *Agronomy* 10, doi:10.3390/agronomy10040456.

Soil Conservation Service (1966). Geologic investigation for watershed planning.

Specht, D. F. (1991). A general regression neural network. *IEEE Transactions on Neural Networks* 2: 568–576, doi:10.1109/72.97934.

Stanchi, S., Zecca, O., Hudek, C., Pintaldi, E., Viglietti, D., D'Amico, M. E., Colombo, N., Goslino, D., Letey, M. and Freppaz, M. (2021). Effect of soil management on erosion in mountain vineyards (N-W Italy). *Sustainability* 13, doi:10.3390/su13041991.

Stanton, J. M. (2001). Galton, Pearson, and the Peas: A brief history of linear regression for statistics instructors. *Journal of Statistics Education* 9, doi:10.1080/10691898.2001.11910537.

Steenhuis, T. S., Schneiderman, E. M., Mukundan, R., Hoang, L., Moges, M. and Owens, E. M. (2019). Revisiting SWAT as a saturation-excess runoff model. *Water* 11, doi: 10.3390/w11071427.

Tadese, M., Kumar, L., Koech, R. and Kogo, B. K. (2020). Mapping of land-use/land-cover changes and its dynamics in Awash River basin using remote sensing and GIS. *Remote Sensing Applications: Society and Environment* 19: 100352, doi:10.1016/j.rsase.2020.100352.

Tadesse, A. and Dai, W. (2019). Prediction of sedimentation in reservoirs by combining catchment based model and stream based model with limited data. *International Journal of Sediment Research* doi:10.1016/j.ijsrc.2018.08.001.

Tadesse, L., Suryabhagavan, K., Sridhar, G. and Legesse, G. (2017). Land use and land cover changes and soil erosion in Yezat watershed, North Western Ethiopia. *International Soil and Water Conservation Research* 5: 85–94, doi:10.1016/j.iswcr.2017.05.004.

Talebia, A., Bahrami, A., Mardian, M. and Mahjoobi, J. (2015). Determination of optimized sediment rating equation and its relationship with physical characteristics of watershed in semiarid regions: A case study of Pol-Doab watershed, Iran. *Desert* 20: 135–144, doi:10.22059/JDESERT.2015.56477.

Tamene, L., Park, S., Dikau, R. and Vlek, P. (2006). Analysis of factors determining sediment yield variability in the highlands of Northern Ethiopia. *Geomorphology* 76: 76–91, doi:doi:10.1016/j.geomorph.2005.10.007.

Tan, Z., Leung, L., Li, H.-Y. and Tesfa, T. (2018). Modeling sediment yield in land surface and earth system models: Model comparison, development, and evaluation. *Journal of Advances in Modeling Earth Systems* 10: 2192–2213, doi:10.1029/2017MS001270.

Tessema, Y. M., Jasi nska, J., Yadeta, L. T., Switoniak, M., Puchałka, R. and Gebregeorgis, E. G. (2020). Soil loss estimation for conservation planning in the Welmel watershed of the Genale Dawa basin, Ethiopia. *Agronomy* 10, doi:10.3390/agronomy10060777.

Tilahun, S. A., Ayana, E. K., Guzman, C. D., Dagnew, D. C., Zegeye, A. D., Tebebu, T. Y., Yitaferu, B. and Steenhuis, T. S. (2016). Revisiting storm runoff processes in the Upper Blue Nile basin:the Debre Mawi watershed. *CATENA* : 47–56doi:10.1016/j.catena.2016.03.029.

Tomandl, D. and Schober, A. (2001). A modified general regression neural network (MGRNN) with new, efficient training algorithms as a robust 'black box'-tool for data analysis. *Neural Networks* 14: 1023–1034, doi:10.1016/S0893-6080(01)00051-X.

Torri, D., Poesen, J., Borselli, L., Bryan, R. and Rossi, M. (2012). Spatial variation of bed roughness in eroding rills and gullies. *CATENA* 90: 76–86, doi:10.1016/j.catena.2011.10.004.

Tully, T., Sullivan, C., Weil, R. and Sanchez, P. (2015). The state of soil degradation in Sub-Saharan Africa: Baselines, trajectories, and solutions. *Sustainability* 7: 6523–6552, doi:10.3390/su7066523.

Vaidya, G. S., Rillig, M. C. and Wallander, H. (2011). The role of glomalin in soil erosion. *Scientific World* 9: 82–85, doi:10.3126/sw.v9i9.5524.

van der Knijff, J. M., Jones, R. and Montanarella, L. (2000). *Soil Erosion Risk Assessment in Europe*. European Soil Bureau.

Wagari, M. and Tamiru, H. (2021). Rusle model based annual soil loss quantification for soil erosion protection:a case of Fincha catchment, Ethiopia. *Air, Soil and Water Research* doi:10.1177/117862212110462.

Wang and Liu (2014). Effects of land use changes on soil erosion in a fast developing area. *Int. J. Environ. Sci. Technol.* 11: 1549–1562, doi:10.1007/s13762-013-0341-x.

Wang, B., Zheng, F. and Guan, Y. (2016). Improved USLE-K factor prediction: A case study on water erosion areas in China. *International Soil and Water Conservation Research* 4: 168–176, doi:10.1016/j.iswcr.2016.08.003.

Wang, F. and Du, T. (2014). Implementing support vector regression with differential evolution to forecast motherboard shipments. *J. Amer. Math. Soc.* 41: 3850–3855, doi:10.1016/j.eswa.2013.12.022.

Wang, S. (1999). Nonlinear regression: a hybrid model. *Computers & Operations Research* 26: 799–817, doi:10.1016/S0305-0548(98)00088-4.

Wawer, R., Nowocie $\tilde{n}$, E. and Podolski, B. (2005). Real and calculated k_{USLE} erodibility factor for selected polish soils. *Polish Journal of Environmental Studies* 14: 655–658.

Wei, L., Zhang, B. and Wang, M. (2007). Effects of antecedent soil moisture on runoff and soil erosion in alley cropping systems. *Agricultural Water Management* 94: 54–62, doi:10.1016/j.agwat.2007.08.007.

White, E., Easton, Z., Fuka, D., Collick, A., Adgo, E., McCartney, M., Awulachew, S., Selassie, Y. and Steenhuis, T. (2011). Development and application of a physically based landscape water balance in the SWAT model. *Hydrol. Process.* 25: 915–925, doi:10.1002/hyp.7876.

Wiese, M. and Schaper, K.-J. (1993). Application of neural networks in the QSAR analysis of percent effect biological data: Comparison with adaptive least squares and nonlinear regression analysis. *SAR and QSAR in Environmental Research* 1: 137–152, doi:10.1080/10629369308028825.

Williams, H., J.R; Berndt (1977). Sediment yield prediction based on watershed hydrology. doi:10.13031/2013.35710.

Williams, J., Nicks, A. and Arnold, J. (1985). Simulator for water resources in rural basins. *J. Hydraul. Eng* 111: 970–986, doi:10.1061/(ASCE)0733-9429(1985)111:6(970).

Williams, J. R. (1975). Sediment routing for agricultural watersheds.

Wischmeier, W. H. and Mannering, J. V. (1969). Relation of soil properties to its erodibility. *Soil Sci. Soc. Amer. Proc* 33.

Wischmeier, W. H. and Smith, D. (1978). *Predicting Rainfall Erosion Losses: A Guide to Conservation Planning*. United States Department of Agriculture.

Wolka, K., Tadesse, H., Garedew, E. and Yimer, F. (2015). Soil erosion risk assessment in the Chaleleka wetland watershed, Central Rift Valley of Ethiopia. *Environmental Systems Research* 4, doi:10.1186/s40068-015-0030-5.

World Bank Group (2007). *The Cost of Land Degradation in Ethiopia: A Review of Past Studies*. Washington, D.C.

Wu, F. Y. and Yen., K. K. (1992). Applications of neural network in regression analysis. *Computers and Industrial Engineering* 23: 93–95.

Wu, H., Zhu, W. and Huang, B. (2021). Seasonal variation of evapotranspiration, Priestley-Taylor coefficient and crop coefficient in diverse landscapes. *Geography and Sustainability* 2: 224–233, doi:10.1016/j.geosus.2021.09.002.

Yang, M. and Lin, T. (2002). Fuzzy least-squares linear regression analysis for fuzzy input–output data. *Fuzzy Sets and Systems* 126: 389–399, doi:10.1016/S0165-0114(01)00066-5.

Yen, H., Lu, S., Feng, Q., Wang, R., Gao, J., Brady, D. M., Sharifi, A., Ahn, J., Chen, S., Jeong, J., White, M. J. and Arnold, J. G. (2017). Assessment of optional sediment transport functions via the complex watershed simulation model SWAT. *Water* 9, doi:10.3390/w9020076.

Yen, H., Park, S., Arnold, J. G., Srinivasan, R., Chawanda, C. J., Wang, R., Feng, Q., Wu, J., Miao, C., Bieger, K., Daggupati, P., Griensven, A., Kalin, L., Lee, S., Sheshukov, A. Y., White, M. J., Yuan, Y., Yeo, I., Zhang, M. and Zhang, X. (2019). Ipeat+: A built-in optimization and automatic calibration tool of SWAT+. *Water* 11, doi:10.3390/w11081681.

Yesuph, A. Y. and Dagnew, A. B. (2019). Soil erosion mapping and severity analysis based on RUSLE model and local perception in the Beshillo catchment of the Blue Nile basin, Ethiopia. *Environmental Systems Research* 8, doi:10.1186/s40068-019-0145-1.

Yong, L. (2014). Novel global harmony search algorithm for least absolute deviation. *Journal of Applied Mathematics* 2014, doi:10.1155/2014/632975.

Young, R., Onstad, C., Bosch, D. and Anderson, W. (1987). AGNPS, agricultural non-point-source pollution model: A watershed analysis tool.

Yu, D., Xie, P., Dong, X., Hu, X., Liu, J., Li, Y., Peng, T., Ma, H., Wang, K. and Xu, S. (2018). Improvement of the SWAT model for event-based flood simulation on a sub-daily timescale. *Hydrology and Earth System Sciences* 22: 5001–5019, doi:10.5194/hess-22-5001-2018.

Zhang, G., Patuwo, B. E. and Hu, M. Y. (1998). Forecasting with artificial neural networks: The state of the art. *International Journal of Forecasting* 14: 35–62, doi:10.1016/S0169-2070(97)00044-7.

Zhang, H., Wei, J., Yang, Q., Baartman, J. E. M., Gai, L., Yang, X., Li, S., Yu, J., Ritsema, C. J. and Geissen, V. (2017). An improved method for calculating slope length and the LS parameters of the Revised Universal Soil Loss Equation for large watersheds. *Geoderma* 308: 36–45, doi:10.1016/J.GEODERMA.2017.08.006.